SLOPE STABILITY ANALYSIS AND STABILIZATION

New Methods and Insight

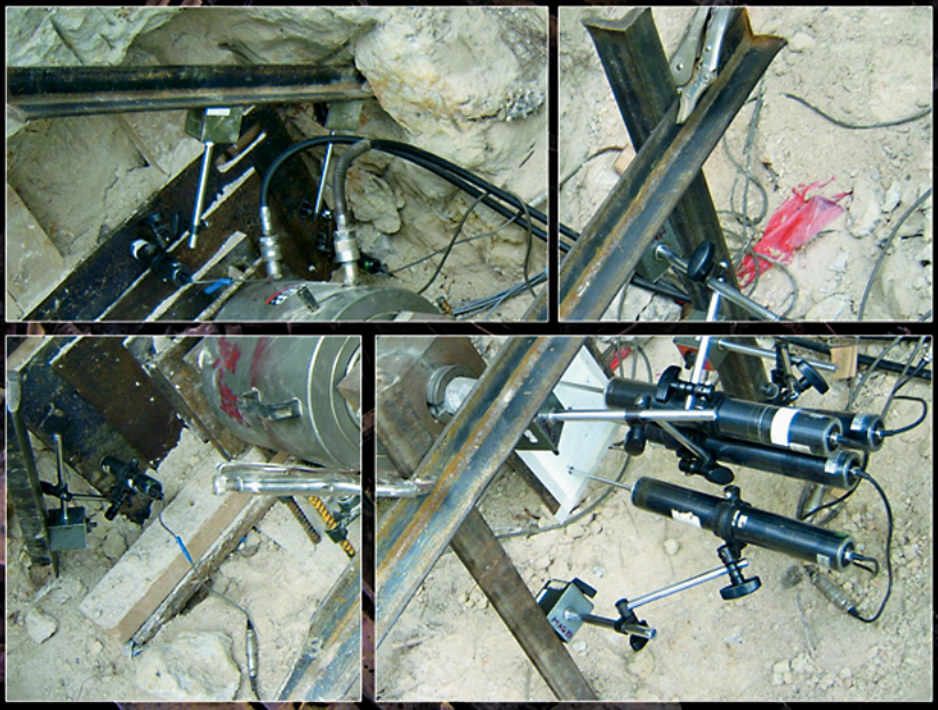

Y.M. Cheng and **C.K. Lau**

Slope Stability Analysis and Stabilization

Slope Stability Analysis and Stabilization

New methods and insight

Y.M. Cheng and C.K. Lau

Routledge
Taylor & Francis Group
LONDON AND NEW YORK

First published 2008
by Routledge
2 Park Square, Milton Park, Abingdon, Oxon OX14 4RN

Simultaneously published in the USA and Canada
by Routledge
270 Madison Ave, New York, NY 10016, USA

Routledge is an imprint of the Taylor & Francis Group, an informa business

This edition published in the Taylor & Francis e-Library, 2008.

"To purchase your own copy of this or any of Taylor & Francis or Routledge's collection of thousands of eBooks please go to www.eBookstore.tandf.co.uk."

British Library Cataloguing in Publication Data
A catalogue record for this book is available from the British Library

Library of Congress Cataloging in Publication Data
Cheng, Y.M.
Slope stability analysis and stabilization: new methods and insight Y.M. Cheng and C.K. Lau.
p. cm.
Includes bibliographical references and index.
1. Slopes (Soil mechanics) 2. Soil stabilization. I. Lau, C.K. II. Title.

TA749.C44 2008
624.1′51363—dc22 2007037813

ISBN 0-203-92795-8 Master e-book ISBN

ISBN10: 0–415–42172–1 (hbk)
ISBN10: 0–203–92795–8 (ebk)

ISBN13: 978–0–415–42172–0 (hbk)
ISBN13: 978–0–203–92795–3 (ebk)

Contents

Tables

Figures

Preface

To cope with the rapid development of Hong Kong, many slopes have been made for land development. Natural hillsides have been transformed into residential and commercial areas and used for infrastructural development. Hong Kong's steeply hilly terrain, heavy rain and dense development make it prone to risk from landslides. Hong Kong has a high rainfall, with an annual average of 2300 mm, which falls mostly in the summer months between May and September. The stability of man-made and natural slopes is of major concern to the Government and the public. Hong Kong has a history of tragic landslides. The landslides caused loss of life and a significant amount of property damage. For the 50 years after 1947, more than 470 people died, mostly as a result of failures associated with man-made cut slopes, fill slopes and retaining walls. Even though the risk to the community has been greatly reduced by concerted Government action since 1977, on average about 300 incidents affecting man-made slopes, walls and natural hillsides are reported to the Government every year.

There are various research works associated with the theoretical as well as practical aspects of slope stability in Hong Kong. This book is based on the research work by the authors as well as some of the teaching materials for the postgraduate course at Hong Kong Polytechnic University. The content in this book is new and some readers may find the materials arguable. A major part of the materials in this book is coded into the programs SLOPE 2000 and SLOPE 3D. SLOPE 2000 is now mature and has been used in many countries. The authors welcome any comment on the book or the programs.

The central core of SLOPE 2000 and SLOPE3D was developed mainly by Cheng while many research students helped in various works associated with the research results and the programs. The authors would like to thank Yip C.J., Wei W.B., Sandy Ng., Ling C.W., Li L. and Chen J. for help in preparing parts of the works and the preparation of some of the figures in this book.

1 Introduction

1.1 Introduction

The motive for writing this book is to address a number of issues in the current design and construction of engineered slopes. This book sets out to review critically the current situation and to offer alternative and, in our view, more appropriate approaches to the establishment of a suitable design model, the enhancement of basic theory, the locating of critical failure surfaces and the overcoming of numerical convergence problems. The latest developments in three-dimensional stability analysis and the finite element method will also be covered. This book will provide helpful practical advice in ground investigation, design and implementation on site. The objective is to contribute towards the establishment of best practice in the design and construction of engineered slopes. In particular, this book will consider the fundamental assumptions of both limit equilibrium and finite element methods in assessing the stability of a slope and give guidance in assessing their limitations. Some of the more up-to-date developments in slope stability analysis methods based on the authors' works will also be covered in this book.

Some salient case histories will also be given to illustrate how adverse geological conditions can have serious implications for slope design and how these can be dealt with. The last chapter touches on the implementation of design on site. The emphasis is on how to translate the conceptual design conceived in the design office into physical implementation on site in a holistic way, taking account of the latest developments in construction technology. Because of our background, a lot of cases and construction practices referred to in this book are related to experience gained in Hong Kong, but the engineering principles should nevertheless be applicable to other regions.

1.2 Background

Planet Earth has an undulating surface and landslides occur regularly. Early humans tried to select relatively stable ground for settlement. As populations grow and human life becomes more urbanized, terraces and corridors have to be created to make room for buildings and infrastructures such as quays, canals, railways and roads. Man-made cut and fill slopes have to be formed to

facilitate such developments. Attempts have been made to improve upon the rule-of-thumb approach of previous generations by mathematically calculating the stability of such cut and fill slopes. One of the earliest attempts was by the French engineer Alexander Collin (1846). In 1916, using the limit equilibrium method, K.E. Petterson (1955) mathematically back calculated the rotational stability of the Stigberg quay failure in Gothenburg, Sweden. A series of quay failures in Sweden provided the impetus for the Swedes to make one of the earliest attempts at quantifying slope stability using the method of slices and the limit equilibrium method. The systematical method has culminated in the establishment of the Swedish Method (or the Ordinary Method) of Slices (Fellenius, 1927). A number of subsequent refinements to the method were made: Taylor's stability chart (Taylor, 1937); Bishop's Simplified Method of Slices (Bishop, 1955) ensures the moments are in equilibrium; Janbu extended the circular slip to generalized slip surface (Janbu, 1973); Morgenstern and Price (1965) ensured moments and forces are simultaneously in equilibrium; Spencer's (1967) parallel inter-slice forces; and Sarma's (1973) imposed horizontal earthquake approach. These various methods have resulted in the modern Generalized Method of Slices (GMS) (e.g. Low *et al.*, 1998).

In the classical limit equilibrium approach, the user has to a priori define a slip surface before working out the stability. There are different techniques to ensure a critical slip surface can indeed be identified. A detailed discussion will be given in Chapter 3. As expected, the ubiquitous finite element method (Griffiths and Lane, 1999) or the equivalent finite difference method (Cundall and Strack, 1979), namely FLAC, can also be used to evaluate the stability directly using the strength reduction algorithm (Dawson *et al.*, 1999). Zhang (1999) has proposed a rigid finite element method to work out the factor of safety (FOS). The advantage of these methods is that there is no need to assume any inter-slice forces or slip surface, but there are also limitations to these methods which are covered in Chapter 4. On the other hand, other assumptions will be required for the classical limit equilibrium method that will be discussed in Chapter 2.

In the early days when computers were not as widely available, engineers preferred to use the stability charts developed by Taylor (1937), for example. Now that powerful and cheap computers are readily to hand, practitioners invariably use computer software to evaluate the stability in design. However, every numerical method has its own postulations and thus limitations. It is therefore necessary for the practitioner to be fully aware of them, so that the method can be used within its limitations in a real design situation. Apart from the numerical method, it is equally important for the engineer to have an appropriate design model for the design situation.

There is, however, one fundamental question that has been bothering us for a long time and this is that all observed failures are invariably 3D in nature but virtually all calculations for routine design assume the failure is in plane strain. Shear strengths in 3D and 2D (plane strain) are significantly different from each other. For example, typical sand can mobilize in plane strain up to

6° higher in frictional angle when compared with the shear strength in 3D or axi-symmetric strain (Bishop, 1972). It seems we have been conflating the two key issues: using 3D strength data but a 2D model, and thus rendering the existing practice highly dubious. However, the increase in shear strength in plane strain usually far outweighs the inherent higher FOS in a 3D analysis. This is probably the reason why in nature all slopes fail in 3D as it is easier for a slope to fail this way. Now that 3D slope stability analysis has been well established, there is no longer any excuse for practitioners not to do the analysis correctly, or at least take the 3D effect into account.

1.3 Closed-form solutions

For some simple and special cases, closed-form but non-trivial solutions do exist. These are very important results because apart from being academically pleasing, these should form the backbone of our other works presented in this book. Engineers, particularly younger ones, tend to rely heavily on code calculation using a computer and find it increasingly difficult to have a good feel for the engineering problems they face in their work. We hope that by looking at some of the closed-form solutions, we can put into our toolbox some very simple and reliable back-of-the-envelope-type calculations to help us develop a good feel for the stability of a slope and whether the computer code calculation is giving us a sensible answer. We hope that we can offer a little bit of help to engineers in avoiding the current tendency to over-rely on ready-made black box-type solutions and use instead simple but reliable engineering sense in their daily work so that design can proceed with greater understanding and fewer leaps in the dark.

For a circular slip failure with $c \neq 0$ and $\phi = 0$, if we take moment at the centre of rotation, the factor of safety will be obtained easily. This is the classical Swedish method that will be covered in Chapter 2. The factor of safety from the Swedish method should be exactly equal to that from the Bishop method for this case. On the other hand, the Morgenstern–Price method will fail to converge easily for this case while Sarma's method will give a result very close to that from the Swedish method. Apart from the closed-form solutions for the circular slip for $c \neq 0$ and $\phi = 0$ case which should already be very testing for the computer code to handle, the classical bearing capacity and earth pressure problem where closed-form solutions exist may also be used to calibrate and verify a code calculation. A bearing capacity problem can be seen as a slope with a very gentle slope angle but with substantial surcharge loading. The beauty of this classical problem is that it is relatively easy to extend the problem to the 3D or at least/axi-symmetric case where a closed-form solution also exists. For example, for an applied pressure of 5.14 Cu for the 2D case and 5.69 Cu for the axi-symmetric case (Shield, 1955), where Cu is the undrained shear strength of soil, the ultimate bearing capacity will be motivated. The computer code should yield FOS = 1.0 if the surcharge loadings are set to 5.14 Cu and 5.69 Cu, respectively. Likewise,

similar bearing capacity solutions also exist for frictional material in both plane strain and axi-symmetric strain (Cox, 1962 or Bolton and Lau, 1993). It is surprising to find that many commercial programs have difficulty in reproducing these classical solutions, and the limit of application of each computer program should be assessed by the engineers.

Similarly, the earth pressure problems, both active and passive, would also be a suitable check for the computer code. Here, the slope has a slope angle of 90°. By applying an active or passive pressure at the vertical face, the computer should yield FOS = 1.0 for both cases, which will be illustrated in Section 3.9. Likewise, the problem can be extended to the 3D, or more precisely axi-symmetric, case for a shaft stability problem (Kwong, 1991).

Our argument is that all codes should be benchmarked and validated through being required to solve the classical problems where 'closed-form' solutions exist for comparison. Hopefully, the comparison will reveal both their respective strengths and limitations so that users can put things into perspective when using the code for design in real life. More on this topic can be found in Chapter 2.

1.4 Engineering judgement

We all agree that engineering judgement is one of the most valuable assets of an engineer because engineering is very much an art as well as a science. In our view, however, the best engineers always use their engineering judgement *sparingly*. To us, engineering judgement is really a euphemism for a leap in the dark. So, in reality, the fewer leaps we make, the more comfortable we will be. We would therefore like to be able to use simple and understandable tools in our toolbox so that we can routinely do some back-of-the-envelope-type calculations to assist us in assessing and evaluating the design situations we are facing so that we can develop a good feel for the problem, thus enabling us to do slope stabilization on a more rational basis.

1.5 Ground model

Before we can set out to check the stability of a slope, we need to find out what it is like and what it consists of. From the topographical survey, or more usually an aerial photograph interpretation and subsequent ground-truthing, we can tell its height, its sloping angle and whether it has berms and is served by a drainage system or not. In addition, we also need to know its history, in terms of its geological past, whether it has suffered failure or distress and whether it has been engineered previously. In a nutshell, we need to build a geological model of the slope that features the key geological formations and characteristics. After some simplification and idealization in the context of the intended purpose of the site, a ground model can then be set up. Following the nomenclature of the Geotechnical Engineering Office in Hong Kong (GEO, 2007), a design model should finally be made, when the design parameters and boundary conditions are also delineated.

1.6 The status quo

A slope, despite being 'properly' designed and implemented, can still become unstable and collapse at an alarming rate. Wong's (2001) study suggests that the probability of an engineered slope failing in terms of major failures (defined as >50 m^3) is only about 50 per cent better than a non-engineered slope. Martin (2000) pointed out that the most important factor with regard to major failures is the adoption of an inadequate geological or hydrogeological model in the design of slopes. In Hong Kong, it is established practice for the Geotechnical Engineering Office to carry out a landslip investigation whenever there is a significant failure or when there is fatality. It is of interest to note that past failure investigations suggest the most usual causes of the failure are some 'unforeseen' adverse ground conditions and geological features in the slope. It is, however, widely believed that such 'unforeseen' adverse geological features, though unforeseen, really should be foreseeable if we set out to identify them at the outset. Typical unforeseen ground conditions are the presence of adverse geological features and adverse groundwater conditions.

(I) Examples of adverse geological features in terms of strength are the following:

1. adverse discontinuities, for example, relict joints;
2. relict instability caused by discontinuities: dilation of discontinuities with secondary infilling of low-frictional materials, that is, soft band, some time in the form of kaolin infill;
3. re-activation of pre-existing (relict) landslide, for example, slickensided joint;
4. faults.

(II) Examples of complex and unfavourable hydrogeological conditions are the following:

1. drainage lines;
2. recharge zones, for example, open discontinuities, dilated relict joints;
3. zones with large difference in hydraulic conductivity resulting in perched groundwater table;
4. a network of soil pipes and sinkholes;
5. damming of the drainage path of groundwater;
6. aquifer, for example, relict discontinuities;
7. aquitard, for example, basalt dyke;
8. tension cracks;
9. local depression;
10. depression of the rockhead;
11. blockage of soil pipes;
12. artesian conditions – Jiao *et al.* (2006) have pointed out that the normally assumed unconfined groundwater condition in Hong Kong is questionable. They have evidence to suggest that it is not

uncommon for a zone near the rockhead to have a significantly higher hydraulic conductivity resulting in artesian conditions;
13 time delay in the rise of the groundwater table;
14 faults.

It is not too difficult to set up a realistic and accurate ground model for design purposes using routine ground investigation techniques, but for the features mentioned above. In other words, in actuality, it is very difficult to identify and quantify the adverse geological conditions listed above. If we want to address the 'So what?' question, the adverse geological conditions may have two types of quite distinct impacts when it comes to slope design. We have to remember that we do not want to be pedantic but we still have a real engineering situation to deal with. The impacts boil down to two types: (1) the presence of zones and narrow bands of weakness and (2) the existence of complex and unfavourable hydrogeological conditions, that is, the transient ground porewater pressure is high and may even be artesian.

Although there is no hard-and-fast rule on how to identify adverse geological conditions, the mapping of the relict joints at the outcrops and the split continuous triple tube core (e.g. Mazier) samples may help to identify the existence of zones and planes of weakness so that these can be properly incorporated into the slope design. The existence of complex and unfavourable hydrogeological conditions may be a lot more difficult to identify as the impact would be more complicated and indirect. Detailed geomorphological mapping may be able to identify most of the surface features, such as drainage lines, open discontinuities, tension cracks, local depression and so on. More subtle features would be recharge zones, soil pipes, aquifer, aquitard, depression of the rockhead and faults. Such features may manifest as an extremely high-perched groundwater table and artesian conditions. It would be ideal to be able to identify all such hydrogeological features so that a proper hydrogeological model can be built up for some very special cases. However, under normal design situations, we would suggest a redundant number of piezometers are installed in the ground instead so that the transient perched groundwater table and artesian groundwater pressure, including any time delay in the rise of the groundwater table, can be measured directly using the compact and robust electronic proprietary groundwater pressure monitoring devices, for example, DIVERs developed by Van Essen. Such devices may cost a lot more than the traditional Halcrow buckets but can potentially provide the designer with the much needed transient groundwater pressure in order that a realistic design event can be built up for the slope design.

While the ground investigation should be planned with the identification of the adverse geological features firmly in mind, one must be aware that engineers have to deal with a large number of slopes and it may not be feasible to screen each and every slope thoroughly. One must accept, no matter what one does, some will inevitably be missed from our design. It is nevertheless still best practice to attempt to identify all potential adverse geological features so that these can be properly dealt with in the slope design.

As an example, a geological model could be a rock at various degrees of weathering resulting in the following geological sequence in a slope, that is, completely decomposed rock (saprolite) overlying moderately to slightly weathered rock. The slope may be mantled by a layer of colluvium. To get this far, the engineer has had to spend a lot of time and resources already. But this is probably still not enough. We know rock mass behaviour is strongly influenced by discontinuities. Likewise, when rock mass decomposes, they would still be heavily influenced by relict joints. An engineer has no choice, but has to be able to build a geological model with all the salient details for his design. It helps a lot if he also has a good understanding of the geological processes and this can assist him in finding the existence of any adverse geological features. Typically, such adverse features are the following: soft bands, internal erosion soil pipes and fault zones and so on, as listed previously. Such features may result in planes of weakness or create a very complicated hydrogeological system. Slopes often fail along such zones of weakness or as a result of the very high water table or even artesian water pressure, if these are not properly dealt with in the design through the installation of relief wells and sub-horizontal drains. With the assistance of a professional engineering geologist if required, the engineer should be able to construct a realistic geological model for his design. A comprehensive treatment of engineering practice in Hong Kong can be found in GEO Publication No. 1/2007 (GEO, 2007). This document may assist the engineer in recognizing when specialist engineering geological expertise should be sought.

1.7 Ground investigation

Ground investigation is defined here in the broadest possible sense as involving desk study, site reconnaissance, exploratory drilling, trenching and trial pitting, in situ testing, detailed examination during construction when the ground is opened up and supplementary investigation during construction planned, supervised and interpreted by a geotechnical specialist appointed at the inception of a project. It should be instilled in the minds of practitioners that a ground investigation does not stop when the ground investigation contract is completed but should be conducted throughout the construction period. In other words, mapping of the excavation during construction should be treated as an integral part of the ground investigation. Greater use of new monitoring techniques like differential Global Positioning Systems (GPS; Yin *et al.*, 2002) to detect ground movements should also be considered. In Hong Kong, ground investigation typically constitutes less than 1 per cent of the total construction costs of foundation projects but is mainly responsible for overruns in time (85 per cent) and budget (30 per cent) (Lau and Lau, 1998). The adage is that one pays for a ground investigation, irrespective of whether one is having one or not! That is, you either pay up front or else at the bitter end when things go wrong. So it makes good commercial sense to invest in a thorough ground investigation at the outset.

The geological model can be established by mapping the outcrops in the vicinity and the sinking of exploratory boreholes, trial pitting and trenching. A pre-existing slip surface of an old landslide where only residual shear strength is mobilized can be identified and mapped through the splitting and logging of a continuous Mazier sample (undisturbed sample) or even the sinking of an exploratory shaft.

In particular, Martin (2000) advocated the need to appraise relict discontinuities in saprolite and the more reliable prediction of a transient rise in the perched groundwater table through the following:

1 more frequent use of shallow standpipe piezometers sited at potential perching horizons;
2 splitting and examining continuous triple-tube drill hole samples, in preference to alternative sampling and standard penetration testing;
3 more extensive and detailed walkover surveys during ground investigation and engineering inspection especially natural terrain beyond the crest of cut slopes. Particular attention should be paid to drainage lines and potential recharge zones.

1.8 Design parameters

The next step would be to assign appropriate design parameters for the geological materials encountered. The key parameters for the geological materials are shear strength, hydraulic conductivity, density, stiffness and in situ stress. Stiffness and in situ stress are probably of less importance compared with the three other parameters. The boundary conditions are also important. The parameters can be obtained by index, triaxial, shear box and other in situ tests.

1.9 Groundwater regime

The groundwater regime would be one of the most important aspects for any slope design. As mentioned before, slope stability is very sensitive to the groundwater regime. Likewise, the groundwater regime is also heavily influenced by the intensity and duration of local rainfall and the drainage provision. Rainfall intensity is usually measured by rain gauges, and the groundwater pressure measured by standpipe piezometers installed in boreholes. Halcrow buckets or proprietary electronic groundwater monitoring devices, for example, DIVER by Van Essen and so on, should be used to monitor the groundwater conditions. The latter devices are essentially miniature pressure transducers (18 mm OD) complete with a datalogger and multi-years battery power supply so that they can be inserted into a standard standpipe piezometer (19 mm ID). They usually measure the total water pressure so that a barometric correction should be made locally to account for the changes in the atmospheric pressure. A typical device can measure the groundwater pressure once every 10 min. for 1 year with a battery lasting for a few years. The device has to be retrieved from the ground and connected to a computer to download the data. The device, for example, DIVER, is housed in a strong and watertight stainless steel housing. As the

metallic housing acts as a Faraday cage, the device is hence protected from stray electricity and lightning. More details on such devices can be found at the manufacturer's website (http://www.vanessen.com). One should also be wary of any potential damming of the groundwater flow as a result of underground construction work.

1.10 Design methodology

We have to tackle the problem from both ends: the probability of a design event occurring and the consequence should such a design event occur. Much more engineering input has to be given to cases with a high chance of occurring and a high consequence should such an event occur. For such sensitive cases, the engineer has to be more thorough in his identification of adverse geological features. In other words, he has to follow best practice for such cases.

1.11 Case histories

Engineering is both a science and an art. Engineers cannot afford to defer making design decisions until everything is clarified and understood as they need to make provisional decisions in order that progress can be made on site. It is expected that failures will occur whenever one is pushing further away from the comfort zone. Precedence is extremely important in helping the engineer know where the comfort zone is. Past success is obviously good for morale but, ironically, it is past failures that are equally, if not more, important. Past failures are usually associated with working at the frontier of technology or design based on extrapolating past experience. Therefore studying past mistakes and failures is extremely instructive and valuable. In Hong Kong, the GEO carries out detailed landslide investigations whenever there is a major landslide or landslide with fatality. We have selected some typical studies to illustrate some of the controlling adverse geological features mentioned in Section 1.6.

1.11.1 Case 1

The Shum Wan Road landslide occurred on 13 August 1995. Figure 1.1 shows a simplified geological section through the landslide. There is a thin mantle of colluvium overlying partially weathered fine-ash to coarse-ash crystallized tuff. Joints within the partially weathered tuff were commonly coated with manganese oxide and infilled with white clay of up to about 15 mm thick. An extensive soft yellowish brown clay seam typically 100–350 mm thick formed part of the base of the concave scar. Laboratory tests suggest that the shear strengths of the materials are as follows:

CDT: $c' = 5$ kPa; $\phi' = 38°$
Clay seam: $c' = 8$ kPa; $\phi' = 26°$
Clay seam (slickensided): $c' = 0$; $\phi' = 21°$

One of the principal causes of the failure is the presence of weak layers in the ground, that is, clay seams and clay-infilled joints. A comprehensive report on the landslide can be found in GEO's report (GEO, 1996b).

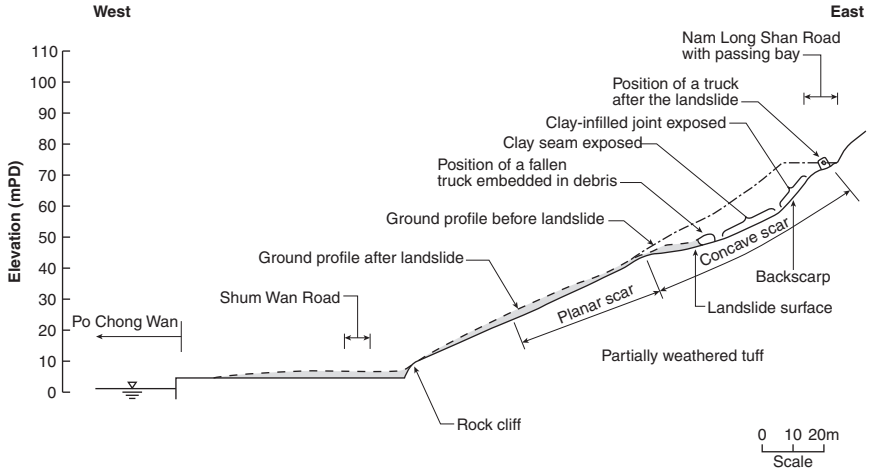

Figure 1.1 The Shum Wan Road landslide occurred on 13 August 1995 in Hong Kong.

Source: Reproduced by kind permission of the Hong Kong Geotechnical Engineering Office from GEO Report (1996b).

1.11.2 Case 2

The Cheung Shan Estate landslip occurred on 16 July 1993. Figure 1.2 shows the cross-section of the failed slope. The ground at the location of the landslip comprised colluvium of about 1 m thick over partially weathered granodiorite. The landslip appears to have taken place entirely within the colluvium. When rainwater percolated the colluvium and reached the less permeable partially weathered granodiorite, a 'perched water table' could have developed and caused the landslip. More details on the failure can be found in the GEO's report (GEO, 1996c).

1.11.3 Case 3

The three sequential landslides at milestone 14 $\frac{1}{2}$ Castle Peak Road occurred twice on 23 July and once on 7 August 1994.

The cross-section of the slope before failure is shown in Figure 1.3. The granite at the site was intruded by sub-vertical basalt dykes of about 800 mm thick. The dykes were exposed within the landslide scar. When completely decomposed, the basalt dykes are rich in clay and silt, and are much less permeable than the partially weathered granite. Hence, the dykes act as barriers to water flow. The groundwater regime was likely to be controlled by a number of decomposed dykes resulting in a damming of the groundwater flow and thus the raising of the groundwater level locally. The

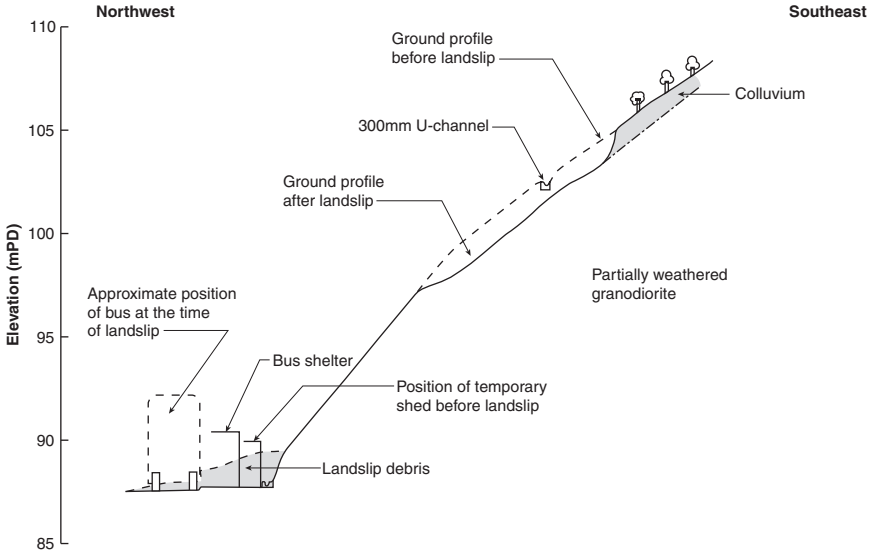

Figure 1.2 The Cheung Shan Estate landslip occurred on 16 July 1993 in Hong Kong.

Source: Reproduced by kind permission of the Hong Kong Geotechnical Engineering Office from GEO Report No. 52 (1996c).

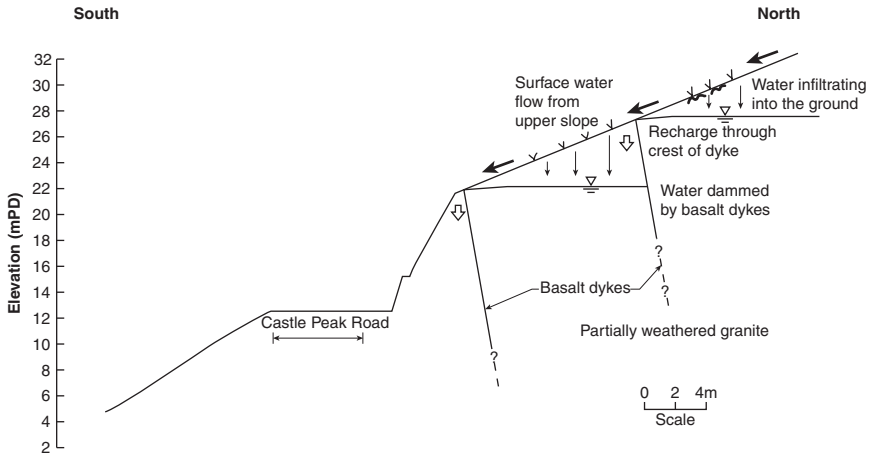

Figure 1.3 The landslide at Castle Peak Road occurred twice on 23 July and once on 7 August 1994 in Hong Kong.

Source: Reproduced by kind permission of the Hong Kong Geotechnical Engineering Office from GEO Report No. 52 (1996c).

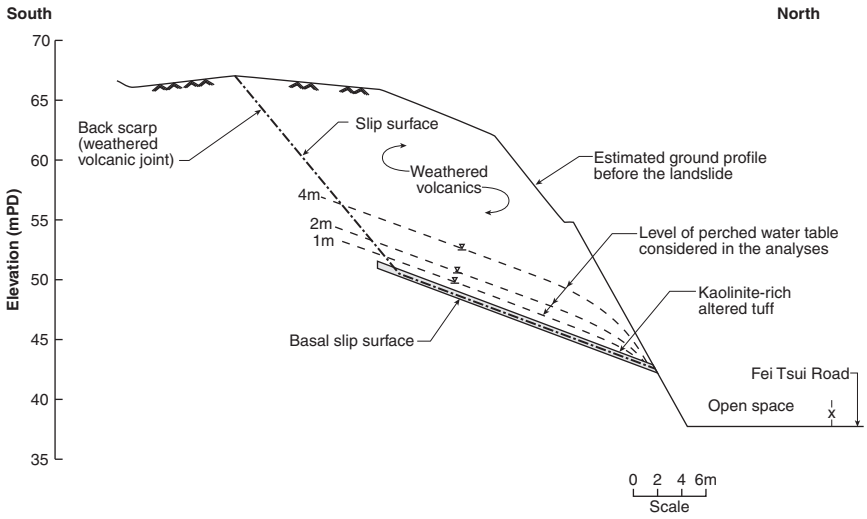

Figure 1.4 The Fei Tsui Road landslide occurred on 13 August 1995 in Hong Kong. *Source:* Reproduced by kind permission of the Hong Kong Geotechnical Engineering Office from the GEO Report (GEO, 1996a).

high local groundwater table was the main cause of the failure. More details can be found in the GEO's report (GEO, 1996c).

1.11.4 Case 4

The Fei Tsui Road landslide occurred on 13 August 1995. A cross-section through the landslide area comprises completely-to-slightly decomposed tuff overlain by a layer of fill of up to about 3 m thick as shown in Figure 1.4. A notable feature of the site is a laterally extensive layer of kaolinite-rich altered tuff. The shear strengths are

Altered tuff: $c' = 10$ kPa; $\phi' = 34°$
Altered tuff with kaolinite vein: $c' = 0$; $\phi' = 22–29°$

The landslide is likely to have been caused by the extensive presence of weak material in the body of the slope triggered by an increase in groundwater pressure following prolonged heavy rainfall. More details can be found in the GEO's report (GEO, 1996a).

1.11.5 Case 5

The landslides at Ching Cheung Road that involved a sequence of three successively larger progressive failures occurred on 7 July 1997 (500 m^3), 17

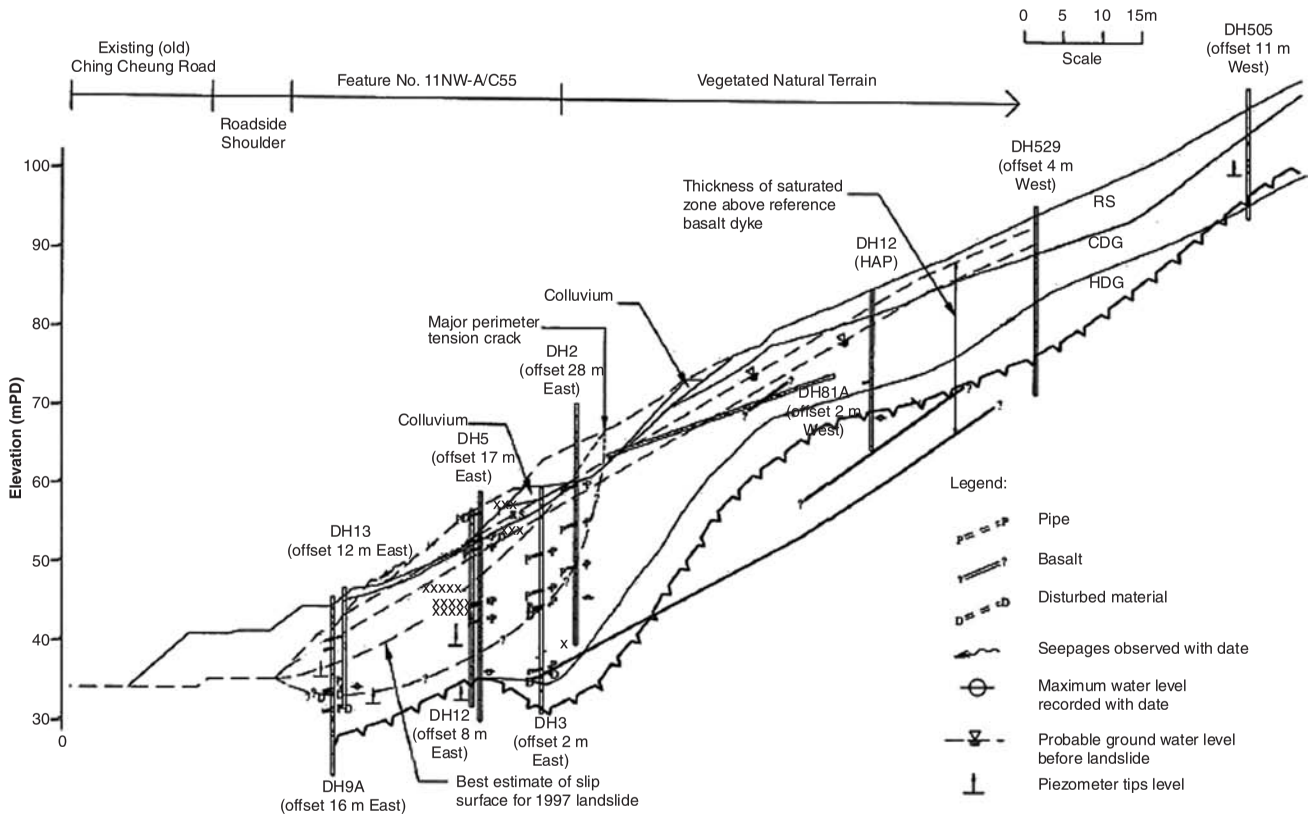

Figure 1.5 The landslides at Ching Cheung Road in 1997 (Hong Kong).

Source: Reproduced by kind permission of the Hong Kong Geotechnical Engineering Office from GEO Report No. 78 (GEO, 1998)

July 1997 (700 m^3) and 3 August 1997 (2000 m^3) (Figure 1.5). The cut slope was formed in 1967. Prior to its construction, the site was a borrow area and had suffered two failures in 1953 and 1963. A major landslide occurred during the widening of Ching Cheung Road (7500 m^3). Remedial works involved cutting back the slope and the installation of raking drains. Under the Landslip Preventive Measures (LPM) programme, the slope was trimmed back further between 1990 and 1992. Although this may have helped improve stability against any shallow failures, there would have been a significant reduction in the FOS of more deep-seated failures. In 1993, a minor failure occurred. In terms of geology, there is a series of intrusion of basalt dykes up to 1.2 m thick occasionally weathered to clayey silt. The hydraulic conductivity of the dykes would have been notably lower than the surrounding granite and therefore the dykes probably acted locally as aquitards, inhibiting the downward flow of the groundwater. There is also a series of erosion pipes of about 250 mm diameter at 6 m spacing. It seems likely that the first landslide occurred on 7 July 1997 and caused the blockage of natural pipes. The fact that the drainage line at the slope crest remained dry despite heavy rainfall may suggest that water recharged the ground upstream rather than ran off. There was a gradual building up of the groundwater table as a dual effect of recharging at the back and damming at the slope toe. The causes are likely to have been the reactivation of a pre-existing slip surface. Also it is likely that the initial failure caused the blockage of the raking drains and natural pipe system. The subsequent recharging from upstream and the blockage of the sub-soil drains, both natural and artificial, caused the final and most deep-seated third landslide. It is of interest to note that after the multiple failures at Ching Cheung Road, as a result of flattening of the slope and complex hydrogeology, the engineer put ballast back at the toe as an emergency measure to stabilize the slope. It seems the engineer knew intuitively that removing the toe weight would reduce the stability of the slope against deep-seated failure and the first solution that came to mind to stabilize the slope was to put dead weight back on the slope toe. More details on the landslide at Ching Cheung Road can be found in GEOs report No. 78 (GEO, 1998).

1.11.6 Case 6

The Kwun Lung Lau landslide occurred on 23 July 1994 (GEO, 1994). One of the key findings was that leakage from the defective buried foul-water and storm-water drains was likely to have been the principal source of sub-surface seepage flow towards the landslide location causing the failure.

In retrospect, standpipe piezometers should have been installed at the interface between the colluvium and underlying partially weathered granodiorite and within the zone blocked by aquitards, and the groundwater pressure monitored accordingly using devices such as DIVER for at least one wet season. The location of the weak zones ought also to have been found and taken into account in the design. The buried water-bearing services in the vicinity also need taking good care of.

2 Slope stability analysis methods

2.1 Introduction

In this chapter, the basic formulation of the two-dimensional (2D) slope stability method will be discussed. Presently, the theory and software for two-dimensional slope stability are rather mature, but there are still some important and new findings which will be discussed in this chapter. Most of the methods discussed in this chapter are available in the program SLOPE 2000 developed by Cheng, an outline of which is given in the Appendix.

2.1.1 Types of stability analysis

There are two different ways for carrying out slope stability analyses. The first approach is the *total stress approach* which corresponds to clayey slopes or slopes with saturated sandy soils under short-term loadings with the pore pressure not dissipated. The second approach corresponds to the *effective stress approach* which applies to long-term stability analyses in which drained conditions prevail. For natural slopes and slopes in residual soils, they should be analysed with the effective stress method, considering the maximum water level under severe rainstorms. This is particularly important for cities such as Hong Kong where intensive rainfall may occur over a long period, and the water table can rise significantly after a rainstorm.

2.1.2 Definition of the factor of safety (FOS)

The factor of safety for slope stability analysis is usually defined as the ratio of the ultimate shear strength divided by the mobilized shear stress at incipient failure. There are several ways in formulating the factor of safety F. The most common formulation for F assumes the factor of safety to be constant along the slip surface, and it is defined with respect to the force or moment equilibrium:

1 *Moment equilibrium*: generally used for the analysis of rotational landslides. Considering a slip surface, the factor of safety F_m defined with respect to moment is given by:

$$F_m = \frac{M_r}{M_d}, \tag{2.1}$$

where M_r is the sum of the resisting moments and M_d is the sum of the driving moment. For a circular failure surface, the centre of the circle is usually taken as the moment point for convenience. For a non-circular failure surface, an arbitrary point for the moment consideration may be taken in the analysis. It should be noted that for methods which do not satisfy horizontal force equilibrium (e.g. Bishop Method), the factor of safety will depend on the choice of the moment point as 'true' moment equilibrium requires force equilibrium. Actually, the use of the moment equilibrium equation without enforcing the force equilibrium cannot guarantee 'true' moment equilibrium.

2 *Force equilibrium*: generally applied to translational or rotational failures composed of planar or polygonal slip surfaces. The factor of safety F_f defined with respect to force is given by:

$$F_f = \frac{F_r}{F_d}, \tag{2.2}$$

where F_r is the sum of the resisting forces and F_d is the sum of the driving forces.

For 'simplified methods' which cannot fulfil both force and moment equilibrium simultaneously, these two definitions will be slightly different in the values and the meaning, but most design codes do not have a clear requirement on these two factors of safety, and a single factor of safety is specified in many design codes. A slope may actually possess several factors of safety according to different methods of analysis which are covered in the later sections.

A slope is considered as unstable if $F \leq 1.0$. It is however common that many natural stable slopes have factors of safety less than 1.0 according to the commonly adopted design practice, and this phenomenon can be attributed to:

1 application of additional factor of safety on the soil parameters is quite common;
2 the use of a heavy rainfall with a long recurrent period in the analysis;
3 three-dimensional effects are not considered in the analysis;
4 additional stabilization due to the presence of vegetation or soil suction is not considered.

An acceptable factor of safety should be based on the consideration of the recurrent period of heavy rainfall, the consequence of the slope failures, the knowledge about the long-term behaviour of the geological materials and the accuracy of the design model. The requirements adopted in Hong Kong

Table 2.1 Recommended factors of safety *F* (GEO, Hong Kong, 1984)

Risk of economic losses	*Risk of human losses*		
	Negligible	*Average*	*High*
Negligible	1.1	1.2	1.4
Average	1.2	1.3	1.4
High	1.4	1.4	1.5

Table 2.2 Recommended factor of safeties for rehabilitation of failed slopes (GEO, Hong Kong, 1984)

Risk of human losses	*F*
Negligible	>1.1
Average	>1.2
High	>1.3

Note: *F* for recurrent period of 10 years.

are given in Tables 2.1 and 2.2, and these values are found to be satisfactory in Hong Kong. For the slopes at the Three Gorges Project in China, the slopes are very high and steep, and there is a lack of previous experience as well as the long-term behaviour of the geological materials; a higher factor of safety is hence adopted for the design. In this respect, an acceptable factor of safety shall fulfil the basic requirement from the soil mechanics principle as well as the long-term performance of the slope.

The geotechnical engineers should consider the current slope conditions as well as the future changes, such as the possibility of cuts at the slope toe, deforestation, surcharges and excessive infiltration. For very important slopes, there may be a need to monitor the pore pressure and suction by tensiometer and piezometer, and the displacement can be monitored by the inclinometers, GPS or microwave reflection. Use of strain gauges or optical fibres in soil nails to monitor the strain and the nail loads may also be considered if necessary. For larges-scale projects, the use of the classical monitoring method is expensive and time-consuming, and the use of the GPS has become popular in recent years.

2.2 Slope stability analysis – limit equilibrium method

A slope stability problem is a statically indeterminate problem, and there are different methods of analysis available to the engineers. Slope stability analysis can be carried out by the limit equilibrium method (LEM), the limit analysis method, the finite element method (FEM) or the finite difference method. By far, most engineers still use the limit equilibrium method with which they are familiar. For the other methods, they are not commonly adopted in routine design, but they will be discussed in the later sections of this chapter and in Chapter 4.

Presently, most slope stability analyses are carried out by the use of computer software. Some of the early limit equilibrium methods are however simple enough that they can be computed by hand calculation, for example, the infinite slope analysis (Haefeli, 1948) and the $\phi_u = 0$ undrained analysis (Fellenius, 1918). With the advent of computers, more advanced methods have been developed. Most of limit equilibrium methods are based on the techniques of slices which can be vertical, horizontal or inclined. The first slice technique (Fellenius, 1927) was based more on engineering intuition than on a rigorous mechanics principle. There was a rapid development of the slice methods in the 1950s and 1960s by Bishop (1955); Janbu *et al.* (1956); Lowe and Karafiath (1960); Morgenstern and Price (1965); and Spencer (1967). The various 2D slice methods of limit equilibrium analysis have been well surveyed and summarized (Fredlund and Krahn, 1984; Nash, 1987; Morgenstern, 1992; Duncan, 1996). The common features of the methods of slices have been summarized by Zhu *et al.* (2003):

(a) The sliding body over the failure surface is divided into a finite number of slices. The slices are usually cut vertically, but horizontal as well as inclined cuts have also been used by various researchers. In general, the differences between different methods of cutting are not major, and the vertical cut is preferred by most engineers at present.
(b) The strength of the slip surface is mobilized to the same degree to bring the sliding body into a limit state. That means there is only a single factor of safety which is applied throughout the whole failure mass.
(c) Assumptions regarding inter-slice forces are employed to render the problem determinate.
(d) The factor of safety is computed from force and/or moment equilibrium equations.

The classical limit equilibrium analysis considers the ultimate limit state of the system and provides no information on the development of strain which actually occurs. For a natural slope, it is possible that part of the failure mass is heavily stressed so that the residual strength will be mobilized at some locations while the ultimate shear strength may be applied to another part of the failure mass. This type of progressive failure may occur in overconsolidated or fissured clays or materials with a brittle behaviour. The use of the finite element method or the extremum principle by Cheng *et al.* (2007c) can provide an estimation of the progressive failure.

Whitman and Bailey (1967) presented a very interesting and classical review of the limit equilibrium analysis methods, which can be grouped as:

1 *Method of slices*: the unstable soil mass is divided into a series of vertical slices and the slip surface can be circular or polygonal. Methods of analysis which employ circular slip surfaces include: Fellenius (1936); Taylor (1949); and Bishop (1955). Methods of analysis which employ non-circular slip surfaces include: Janbu (1973); Morgenstern and Price (1965); Spencer (1967); and Sarma (1973).

2 *Wedge methods*: the soil mass is divided into wedges with inclined interfaces. This method is commonly used for some earth dam (embankment) designs but is less commonly used for slopes. Methods which employ the wedge method include: Seed and Sultan (1967) and Sarma (1979).

The shear strength mobilized along a slip surface depends on the effective normal stress σ' acting on the failure surface. Frohlich (1953) analysed the influence of the σ' distribution on the slip surface on the calculated F. He suggested an upper and lower bound for the possible F values. When the analysis is based on the lower bound theorem in plasticity, the following criteria apply: equilibrium equations, failure criterion and boundary conditions in terms of stresses. On the other hand, if one applies the upper bound theorem in plasticity, the following alternative criteria apply: compatibility equations and displacement boundary conditions, in which the external work equals the internal energy dissipations.

Hoek and Bray (1977) suggested that the lower bound assumption gives accurate values of the factor of safety. Taylor (1948), using the friction method, also concluded that a solution using the lower bound assumptions leads to accurate F for a homogeneous slope with circular failures. The use of the lower bound method is difficult in most cases, so different assumptions to evaluate the factor of safety have been used classically. Cheng *et al.* (2007c,d) has developed a numerical procedure in Sections 2.8 and 2.9, which is effectively the lower bound method but is applicable to a general type of problem. The upper bound method in locating the critical failure surface will be discussed in Chapter 3.

In the conventional limiting equilibrium method, the shear strength τ_m which can be mobilized along the failure surface is given by:

$$\tau_m = \tau_f / F \tag{2.3}$$

where F is the factor of safety (based on force or moment equilibrium in the final form) with respect to the ultimate shear strength τ_f which is given by the Mohr–Coulomb relation as

$$\tau_f = c' + \sigma'_n \tan\phi' \text{ or } c_u \tag{2.4}$$

where c' is the cohesion, σ'_n is the effective normal stress, ϕ' is the angle of internal friction and c_u is the undrained shear strength.

In the classical stability analysis, F is usually assumed to be constant along the entire failure surface. Therefore, an average value of F is obtained along the slip surface instead of the actual factor of safety which varies along the failure surface if progressive failure is considered. There are some formulations where the factors of safety can vary along the failure surface. These kinds of formulations attempt to model the progressive failure in a simplified way, but the introduction of additional assumptions is not favoured by many engineers. Chugh (1986) presented a procedure for determining a variable factor of safety along the failure surface within the framework of the LEM. Chugh predefined a characteristic shape for the variation of the factor of safety along a failure surface, and this idea actually follows the idea of the variable inter-slice shear

force function in the Morgenstern–Price method (1965). The suitability of this variable factor of safety distribution is however questionable, as the local factor of safety should be mainly controlled by the local soil properties. In view of these limitations, most engineers prefer the concept of a single factor of safety for a slope, which is easy for the design of the slope stabilization measures. Law and Lumb (1978) and Sarma and Tan (2006) have also proposed different methods with varying factors of safety along the failure surface. These methods however also suffer from the use of assumptions with no strong theoretical background. Cheng *et al.* (2007c) has developed another stability method based on the extremum principle as discussed in Section 2.8 which can allow for different factors of safety at different locations.

2.2.1 Limit equilibrium formulation of slope stability analysis methods

The limit equilibrium method is the most popular approach in slope stability analysis. This method is well known to be a statically indeterminate problem, and assumptions on the inter-slice shear forces are required to render the problem statically determinate. Based on the assumptions of the internal forces and force and/or moment equilibrium, there are more than ten methods developed for slope stability analysis. The famous methods include those by Fellenius (1936), Bishop (1955), Janbu (1973), Janbu *et al.* (1956), Lowe and Karafiath (1960), Spencer (1967), Morgenstern and Price (1965) and so on.

Since most of the existing methods are very similar in their basic formulations with only minor differences in the assumptions on the inter-slice shear forces, it is possible to group most of the existing methods under a unified formulation. Fredlund and Krahn (1977) and Espinoza and Bourdeau (1994) have proposed a slightly different unified formulation to the more commonly used slope stability analysis methods. In this section, the formulation by Cheng and Zhu (2005) which can degenerate to many existing methods of analysis will be introduced.

Based upon the static equilibrium conditions and the concept of limit equilibrium, the number of equations and unknown variables are summarized in Tables 2.3 and 2.4.

From these tables it is clear that the slope stability problem is statically indeterminate in the order of $6n - 2 - 4n = 2n - 2$. In other words, we have to introduce additional $(2n - 2)$ assumptions to solve the problem. The locations of the base normal forces are usually assumed to be at the middle of the slice, which is a reasonable assumption if the width of the slice is limited. This assumption will reduce unknowns so that there are only $n - 2$ equations to be introduced. The most common additional assumptions are either the location of the inter-slice normal forces or the relation between the inter-slice normal and shear forces. That will further reduce the number of unknowns by $n - 1$ (n slice has only $n - 1$ interfaces), so the problem will become over-specified by 1. Based on different assumptions along the interfaces between slices, there are more than ten existing methods of analysis at present.

The limit equilibrium method can be broadly classified into two main categories: 'simplified' methods and 'rigorous' methods. For the simplified

Table 2.3 Summary of system of equations (n = number of slices)

Equations	*Condition*
n	Moment equilibrium for each slice
$2n$	Force equilibrium in X and Y directions for each slice
n	Mohr–Coulomb failure criterion
$4n$	Total number of equations

Table 2.4 Summary of unknowns

Unknowns	*Description*
1	Safety factor
n	Normal force at the base of slice
n	Location of normal force at base of slice
n	Shear force at base of slice
$n - 1$	Inter-slice horizontal force
$n - 1$	Inter-slice tangential force
$n - 1$	Location of inter-slice force (line of thrust)
$6n - 2$	Total number of unknowns

methods, either force or moment equilibrium can be satisfied but not both at the same time. For the rigorous methods, both force and moment equilibrium can be satisfied, but usually the analysis is more tedious and may sometimes experience non-convergence problems. The authors have noticed that many engineers have the wrong concept that methods which can satisfy both the force and moment equilibrium are accurate or even 'exact'. This is actually a wrong concept as all methods of analysis require some assumptions to make the problem statically determinate. The authors have even come across many cases where very strange results can come out from the 'rigorous' methods (which should be eliminated because the internal forces are unacceptable), but the situation is usually better for those 'simplified' methods. In this respect, no method is particularly better than others, though methods which have more careful consideration of the internal forces will usually be better than the simplified methods in most cases. Morgenstern (1992), Cheng as well as many other researchers have found that most of the commonly used methods of analysis give results which are similar to each other. In this respect, there is no strong need to fine tune the 'rigorous' slope stability formulations except for isolated cases, as the inter-slice shear forces have only a small effect on the factor of safety in general.

To begin with the generalized formulation, consider the equilibrium of force and moment for a general case shown in Figure 2.1. The assumptions used in the present unified formulation are:

1 The failure mass is a rigid body.
2 The base normal force acts at the middle of each slice base.
3 The Mohr–Coulomb failure criterion is used.

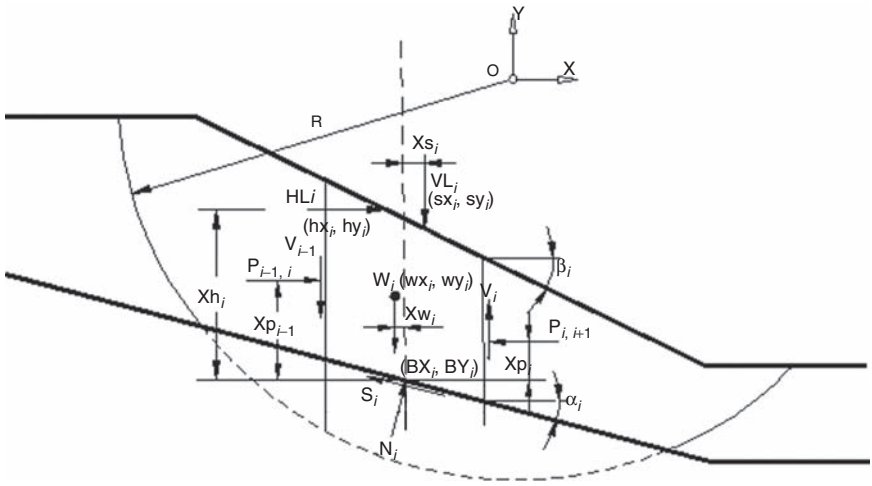

Figure 2.1 Internal forces in a failing mass.

2.2.1.1 Force equilibrium

The horizontal and vertical force equilibrium conditions for slice i are given by:

$$N_i \sin\alpha_i - S_i \cos\alpha_i + HL_i = P_{i,i+1} - P_{i-1,i} \tag{2.5}$$

$$W_i + VL_i - N_i \cos\alpha_i - S_i \sin\alpha_i = P_{i,i+1} \tan\phi_{i,i+1} - P_{i-1,i} \tan\phi_{i-1,i} \tag{2.6}$$

The Mohr–Coulomb relation is applied to the base normal force N_i and shear force S_i as

$$S_i = \frac{N_i \tan\phi_i + c_i l_i}{F} \tag{2.7}$$

The boundary conditions to the above three equations are the inter-slice normal forces, which will be 0 for the first and last ends:

$$P_{0,1} = 0; \quad P_{n,n+1} = 0. \tag{2.8}$$

When $i = 1$ (first slice), the base normal force N_1 is given by eqs (2.5)–(2.7) as

$$N_1 = \frac{A_1 \times F + C_i}{H_1 + E_1 \times F}, \quad P_{1,2} = \frac{L_1 + K_1 \times F + M_1}{H_1 + E_1 \times F} \tag{2.9}$$

$P_{1,2}$ is a first order function of the factor of safety F. For slice i the base normal force is given by

$$N_i = \frac{(\tan\phi_{i-1,i} - \tan\phi_{i,i+1})F \times P_{i-1,i} + A_i \times F + C_i}{H_i + E_i \times F} \tag{2.10}$$

$$P_{i,i+1} = \frac{(J_i \times f_i + G_i \times F)P_{i-1,i} + L_i + K_i \times F + M_i}{H_i + E_i \times F} \tag{2.11}$$

When $i = n$ (last slice), the base normal force is given by

$$N_n = \frac{AA_n \times F + D_n}{J_n + G_n \times F}, \quad P_{n-1,n} = -\frac{L_n + K_n \times F + M_n}{J_n + G_n \times F} \tag{2.12}$$

Eqs (2.11) and (2.12) relate the left and right inter-slice normal forces of a slice, and the subscript $i,i+1$ means the internal force between slice i and $i+1$. Definitions of symbols used in the above equations are:

$$A_i = W_i + VL_i - HL_i \tan\phi_{i,i+1}, \qquad AA_i = W_i + VL_i - HL_i \tan\phi_{i-1,i}$$
$$C_i = (\sin\alpha_i + \cos\alpha_i \tan\phi_{i,i+1})c_i A_i, \qquad D_i = (\sin\alpha_i + \cos\alpha_i \tan\phi_{i-1,i})c_i A_i$$
$$E_i = \cos\alpha_i + \tan\phi_{i,i+1} \sin\alpha_i, \qquad G_i = \cos\alpha_i + \tan\phi_{i-1,i} \sin\alpha_i$$
$$H_i = (-\sin\alpha_i - \tan\phi_{i,i+1} \cos\alpha_i)f_i, \qquad J_i = (-\sin\alpha_i - \tan\phi_{i-1,i} \cos\alpha_i)f_i$$
$$K_i = (W_i + VL_i)\sin\alpha_i + HL_i \cos\alpha_i \qquad V_i = P_{i,i+1} \tan\Phi_{i,i+1}$$
$$L_i = (-(W_i + VL_i)\cos\alpha_i - HL_i \sin\alpha_i)f_i, \quad M_i = (\sin^2\alpha_i - \cos^2\alpha_i)c_i A_i$$
$$A_i = W_i + VL_i - HL_i \tan\phi_{i,i+1}, \qquad B_i = W_i + VL_i - HL_i \tan\phi_{i-1,i}$$

where

α – base inclination angle, clockwise is taken as positive;
β – ground slope angle, counter-clockwise is taken as positive;
W – weight of slice; VL – external vertical surcharge;
HL – external horizontal load; P – inter-slice normal force;
V – inter-slice shear force; N – base normal force;
S – base shear force; F – factor of safety;
c, f – base cohesion c' and $\tan\phi'$;
l – base length l of slice, $\tan\boldsymbol{\Phi} = \lambda f(x)$;

{BX, BY}, coordinates of the mid-point of base of each slice; {wx, wy}, coordinates for the centre of gravity of each slice; {sx, sy}, coordinates for point of application of vertical load for each slice; {hx, hy} coordinates for the point of application of the horizontal load for each slice; Xw, Xs, Xh, Xp are lever arm from middle of base for self weight, vertical load, horizontal load and line of thrust, respectively, where $Xw = BX - wx$; $Xs = BX - sy$; $Xh = BY - hy$.

2.2.1.2 Moment equilibrium equation

Taking moment about any given point O in Figure 2.1, the overall moment equilibrium is given:

$$\sum_{i=1}^{n} [W_i wx_i + VL_i sx_i + HL_i hy_i + (N_i \sin\alpha_i - S_i \cos\alpha_i)BY_i - (N_i \cos_i - S_i \sin\alpha_i)BX_i] = 0 \tag{2.13}$$

It should be noted that most of the 'rigorous' methods adopt the overall moment equilibrium instead of the local moment equilibrium in the formulation, except for the Janbu rigorous method and the extremum method by Cheng *et al.* (2007c) which will be introduced in Section 2.8. The line of thrust can be back-computed from the internal forces after the stability analysis. Since the local moment equilibrium equation is not adopted explicitly, the line of thrust may fall outside the slice which is clearly unacceptable, and it can be considered that the local moment equilibrium cannot be maintained under this case. The effects of the local moment equilibrium are however usually not critical towards the factor of safety, as the effect of the inter-slice shear force is usually small in most cases. The engineers should however check the location of the thrust line as a good practice after performing those 'rigorous' analyses. Sometimes, the local moment equilibrium can be maintained by fine tuning of the inter-slice force function $f(x)$, but there is no systematic way to achieve this except by manual trial and error or the lower bound method by Cheng *et al.* (2007d) as discussed in Section 2.9.

2.2.2 Inter-slice force function

The inter-slice shear force V is assumed to be related to the inter-slice normal force P by the relation $V = \lambda f(x)P$. There is no theoretical basis to determine $f(x)$ for a general problem, as the slope stability problem is statically indeterminate by nature. More detailed discussion about $f(x)$ by the lower bound method will be given in Section 2.9. There are seven types of $f(x)$ commonly in use:

Type 1: $f(x) = 1.0$. This case is equivalent to the Spencer method and is commonly adopted by many engineers. Consider the case of a sandy soil with $c' = 0$. If the Mohr–Coulomb relation is applied to the inter-slice force relation, $V = P \tan\phi'$, then $f(x) = 1.0$ and $\lambda = \tan\phi$. Since there is no strong requirement to apply the Mohr–Coulomb relation for the inter-slice forces, $f(x)$ should be different from 1.0 in general. It will be demonstrated in Section 2.9 that $f(x) = 1.0$ is actually not a realistic relation.

Type 2: $f(x) = \sin(x)$. This is a relatively popular alternative to $f(x) = 1.0$. This function is adopted purely because of its simplicity.

Type 3: $f(x)$ = trapezoidal shape shown in Figure 2.2. Type 3 $f(x)$ will reduce to type 1 as a special case, but it is seldom adopted in practice.

Type 4: $f(x)$ = error function or the Fredlund–Wilson–Fan force function (1986) which is in the form of $f(x) = \Psi \exp(-0.5c^n\eta^n)$, where Ψ, c and n have to be defined by the user. η is a normalized dimensional factor which has a value of -0.5 at left exit end and $=0.5$ at right exit end of the failure surface. η varies linearly with the x-ordinates of the failure surface. This error function is actually based on an elastic finite element stress analysis by Fan *et al.* (1986). Since the stress state in the limit equilibrium analysis is the ultimate condition and is different from the elastic stress analysis by Fan *et al.* (1986), the suitability of this inter-slice force function cannot be

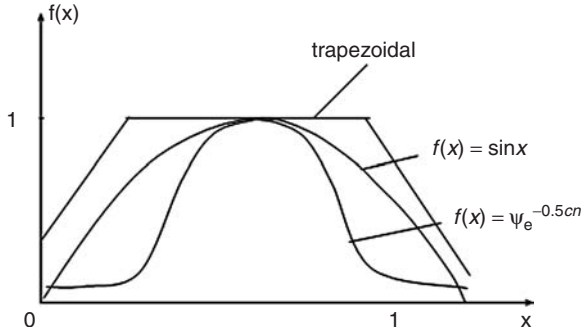

Figure 2.2 Shape of inter-slice shear force function.

justified by the elastic analysis. It is also difficult to define the suitable parameters for a general problem with soil nails, water table and external loads. This function is also not applicable for complicated cases, and a better inter-slice force function will be suggested in Section 2.9.

For the first four types of functions shown above, they are commonly adopted in the Morgenstern–Price and GLE methods, and both the moment and force equilibrium can be satisfied simultaneously. A completely arbitrary inter-slice force function is theoretically possible, but there is no simple way or theoretical background in defining this function except for the extremum principle introduced in Section 2.9, so the arbitrary inter-slice force function is seldom considered in practice.

Type 5: Corps of Engineers inter-slice force function. $f(x)$ is assumed to be constant and is equal to the slope angle defined by the two extreme ends of the failure surface.

Type 6: Lowe–Karafiath inter-slice force function. $f(x)$ is assumed to be the average of the slope angle of the ground profile and the failure surface at the section under consideration.

Type 7: $f(x)$ is defined as the tangent of the base slope angle at the section under consideration, and this assumption is used in the Load factor method in China.

For type 5 to type 7 inter-slice force functions, only force equilibrium is enforced in the formulation. The factors of safety from these methods are however usually very close to those by the 'rigorous' methods, and are usually better than the results by the Janbu simplified method. In fact, the Janbu method is given by the case of $\lambda = 0$ for the Corps of Engineers method, Lowe–Karafiath method and the Load factor method, and results from the Janbu analysis can also be taken as the first approximation in the Morgenstern–Price analysis.

Based on a Mohr circle transformation analysis, Chen and Morgenstern (1983) have established that $\lambda f(x)$ for the two ends of a slip surface which is

Table 2.5 Assumptions used in various methods of analysis (× means not satisfied and √ means satisfied)

Method	*Assumptions*	*Force equilibrium*		*Moment equilibrium*
		X	*Y*	
1 Swedish	$P = V = 0$	×	×	√
2 Bishop simplified	$V = 0$ or $\Phi = 0$	×	√	√
3 Janbu simplified	$V = 0$ or $\Phi = 0$	√	√	×
4 Lowe and Karafiath	$\Phi = (\alpha + \beta)/2$	√	√	×
5 Corps of Engineers	$\Phi = \beta$ or $\Phi_{i-1,i} = \frac{\alpha_{i-1} + \alpha_i}{2}$	√	√	×
6 Load transfer	$\Phi = \alpha$	√	√	×
7 Wedge	$\Phi = \phi$	√	√	×
8 Spencer	$\Phi =$ constant	√	√	√
9 Morgernstern–Price and GLE	$\Phi = \lambda f(x)$	√	√	√
10 Janbu rigorous	Line of thrust (Xp)	√	√	√
11 Leshchinsky	Magnitude and distribution of N	√	√	√

the inclination of the resultant inter-slice force should be equal to the ground slope angle. Other than this requirement, there is no simple way to establish $f(x)$ for a general problem. Since the requirement by Chen and Morgenstern (1983) applies only under an infinitesimal condition, it is seldom adopted in practice. Even though there is no simple way to define $f(x)$, Morgenstern (1992), among others, has however pointed out that, for normal problems, F from different methods of analyses are similar so that the assumptions on the internal force distributions are not major issues for practical use except for some particular cases. In views of the difficulty in prescribing a suitable $f(x)$ for a general problem, most engineers will choose $f(x) = 1.0$ which is satisfactory for most cases. Cheng *et al.* (2007d) have however established the upper and lower bounds of the factor of safety and the corresponding $f(x)$ based on the extremum principle which will be discussed in Section 2.9.

2.2.3 Reduction to various methods and discussion

The present unified formulation by Cheng and Zhu (2005) can reduce to most of the commonly used methods of analysis which is shown in Table 2.5. In Table 2.5, the angle of inclination of the inter-slice forces is prescribed for methods 2–9.

The classical Swedish method for undrained analysis (Fellenius analysis) considers only the global moment equilibrium and neglects all the internal forces between slices. For the Swedish method under drained analysis, the left and right inter-slice forces are assumed to be equal and opposite so that the base normal forces become known. The factor of safety can be obtained easily without the need of iteration analysis. The Swedish method is well known to be

conservative, and sometimes the results from it can be 20–30 per cent smaller than those from the 'rigorous' methods, hence the Swedish method is seldom adopted in practice. This method is however simple enough to be operated by hand or spreadsheet calculation, and there are no non-convergence problems as iteration is not required.

The Bishop method is one of the most popular slope stability analysis methods and is used worldwide. This method satisfies only the moment equilibrium given by eq. (2.13) but not the horizontal force equilibrium given by eq. (2.5), and it applies only for a circular failure surface. The centre of the circle is taken as the moment point in the moment equilibrium equation given by eq. (2.13). The Bishop method has been used for some non-circular failure surfaces, but Fredlund *et al.* (1992) have demonstrated that the factor of safety will be dependent on the choice of the moment point because there is a net unbalanced horizontal force in the system. The use of the Bishop method to the non-circular failure surface is generally not recommended because of the unbalanced horizontal force problem, and this can be important for problems with loads from earthquake or soil reinforcement. This method is simple for hand calculation and the convergence is fast. It is also virtually free from/convergence problems, and the results from it are very close to those by the 'rigorous' methods. If the circular failure surface is sufficient for the design and analysis, this method can be a very good solution for engineers. When applied to an undrained problem with $\phi = 0$, the Bishop method and the Swedish method will become identical.

For the Janbu simplified method (1956), force equilibrium is completely satisfied while moment equilibrium is not satisfied. This method is also popular worldwide as it is fast in computation with only few convergence problems. This method can be used for a non-circular failure surface which is commonly observed in sandy-type soil. Janbu (1973) later proposed a 'rigorous' formulation which is more tedious in computation. Based on the ratio of the factors of safety from the 'rigorous' and 'simplified' analyses, Janbu proposed a correction factor f_0 given by eq. (2.14) for the Janbu simplified method. When the factor of safety from the simplified method is multiplied with this correction factor, the result will be close to that from the 'rigorous' analysis.

$$\begin{aligned}
\text{For } c, \phi > 0, \qquad & f_0 = 1 + 0.5\left[\frac{D}{l} - 1.4\left(\frac{D}{l}\right)^2\right] \\
\text{For } c = 0, \qquad & f_0 = 1 + 0.3\left[\frac{D}{l} - 1.4\left(\frac{D}{l}\right)^2\right] \\
\text{For } \phi = 0, \qquad & f_0 = 1 + 0.6\left[\frac{D}{l} - 1.4\left(\frac{D}{l}\right)^2\right]
\end{aligned} \tag{2.14}$$

For the correction factor shown above, l is the length joining the left and right exit points while D is the maximum thickness of the failure zone with reference to this line. Since the correction factors by Janbu (1973) are based on limited

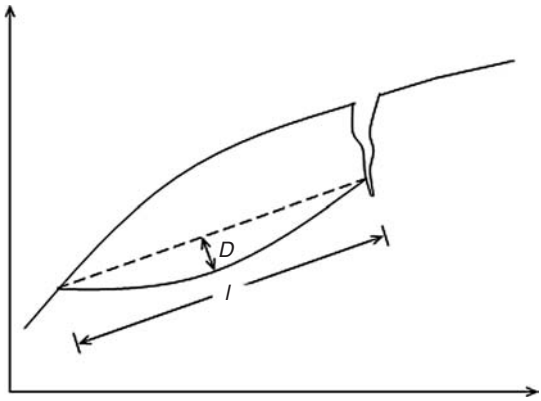

Figure 2.3 Definitions of D and l for the correction factor in the Janbu simplified method.

case studies, the uses of these factors to complicated non-homogeneous slopes are questioned by some engineers. Since the inter-slice shear force can sometimes generate a high factor of safety for some complicated cases which may occur in dam and hydropower projects, the use of the Janbu method is preferred over other methods in these kinds of projects in China.

The Lowe and Karafiath method and the Corps of Engineers method are based on the inter-slice force functions type 5 and type 6. These two methods satisfy force equilibrium but not moment equilibrium. In general, the Lowe and Karafiath method will give results close to that from the 'rigorous' method even though the moment equilibrium is not satisfied. For the Corps of Engineers method, it may lead to a high factor of safety in some cases, and some engineers actually adopt a lower inter-slice force angle to account for this problem (Duncan and Wright, 2005), and this practice is also adopted by some engineers in China. The load transfer and the wedge methods in Table 2.5 satisfy only the force equilibrium. These methods are used in China only and are seldom adopted in other countries.

The Morgenstern–Price method is usually based on the inter-slice force function types 1 to 4, though the use of the arbitrary function is possible and is occasionally used. If the type 1 inter-slice force function is used, this method will reduce to the Spencer method. The Morgenstern–Price method satisfies the force and the global moment equilibrium. Since the local moment equilibrium equation is not used in the formulation, the internal forces of an individual slice may not be acceptable. For example, the line of thrust (centroid of the inter-slice normal force) may fall outside the soil mass from the Morgenstern–Price analysis. The GLE method is basically similar to the Morgenstern–Price method, except that the line of thrust is determined and is closed at the last slice. The acceptability of the line of thrust for any intermediate slice may still be unacceptable from the GLE

analysis. In general, the results from these two methods of analysis are very close.

The Janbu rigorous method appears to be appealing in that the local moment equilibrium is used in the intermediate computation. The internal forces will hence be acceptable if the analysis can converge. As suggested by Janbu (1973), the line of thrust ratio is usually taken as one-third of the inter-slice height, which is basically compatible with the classical lateral earth pressure distribution. It should be noted that the equilibrium of the last slice is actually not used in the Janbu rigorous method, so the moment equilibrium from the Janbu rigorous method is not strictly rigorous. A limitation of this method is the relatively poor convergence in the analysis, particularly when the failure surface is highly irregular or there are external loads. This is due to the fact that the line of thrust ratio is pre-determined with no flexibility in the analysis. The constraints in the Janbu rigorous method are more than that in the other methods, hence convergence is usually poorer. If the method is slightly modified by assuming $h_t/h = \lambda f(x)$, where h_t = height of line of thrust above slice base and h = length of the vertical inter-slice, the convergence of this method will be improved. There is however difficulty in defining $f(x)$ for the line of thrust, and hence this approach is seldom considered. Cheng has developed another version of the Janbu rigorous method which is implemented in the program SLOPE 2000.

For the Janbu rigorous (1973) and Leshchinsky (1985) methods, Φ (or λ equivalently) is not known in advance. The relationship between the line of thrust Xp and angle Φ in the Janbu rigorous method can be derived in the following ways:

(a) Taking moment about middle of the slice base in the Janbu rigorous method, the moment equilibrium condition is given by:

$$W_i Xw_i + Vl_i Xs_i - HL_i Xh_i = P_{i,i+1} Xp_i - P_{i-1,i} Xp_{i-1} + \frac{1}{2}(P_{i,i+1} \tan \Phi_{i,i+1} + P_{i-1,i} \tan \Phi_{i-1,i}) B_i \quad (2.15)$$

From above, the inter-slice normal force is obtained as:

$$P_{i,i+1} = \frac{Al_i}{2Xp_i + B_i \tan \Phi_{i,i+1}} \quad (2.16)$$

where

$$Al_i = 2W_i Xw_i + 2VL_i Xs_i - 2VL_i Xh_i + 2P_{i-1,i} Xp_{i-1} - B_i P_{i-1,i} \tan \Phi_{i-1,i} \quad (2.17)$$

From eq. (2.9) the inter-slice normal force is also obtained as

$$P_{i,i+1} = \frac{A2_i}{-f_i \sin \alpha_i - f_i \cos \alpha_i \tan \Phi_{i,i+1} + K \cos \alpha_i + K \sin \alpha_i \tan \Phi_{i,i+1}} \quad (2.18)$$

where

$$A2_i = (J_i + G_i \times F)P_{i-1,i} + M_i + L_i + K_i F \tag{2.19}$$

From eqs (2.15) and (2.17), the relation between line of thrust Xp and angle Φ is given by:

$$\tan \Phi_{i,i+1} = -\frac{-2A2_i Xp_i - Al_i f_i \sin\alpha_i + Al_i F \cos\alpha_i}{-A2_i B_i - Al_i f_i \cos\alpha_i + Al_i F \sin\alpha_i} \tag{2.20}$$

(b) For the Leshchinsky method where the distribution of the base normal force N is assumed to be known, Φ can then be determined as:

$$\tan \Phi_{i,i+1} = -\frac{-N_i f_i \sin\alpha_i + N_i F \cos\alpha_i - P_{i-1,i} F \tan \Phi_{i-1,i} - c_i A_i \sin\alpha_i - W_i F - VL_i F}{-N_i f_i \cos\alpha_i + N_i F \sin\alpha_i + P_{i-1,i} F - c_i A_i \sin\alpha_i + VL_i F} \tag{2.21}$$

Once Φ is obtained from eq. (2.19) or (2.20), the calculation can then proceed as described previously.

2.2.4 Solution of the non-linear factor of safety equation

In eq. (2.11), the inter-slice normal force for slice i, $P_{i,i+1}$, is controlled by the inter-slice normal $P_{i-1,i}$. If we put the equation for inter-slice normal force $P_{1,2}$ (eq. 2.9) from slice 1 into the equation for inter-slice normal force $P_{2,3}$ for slice 2 (eq. 2.11), we will get a second order equation in factor of safety F as

$$P_{2,3} = \frac{(J_2 \times f_2 + G_2 \times F)P_{1,2} + L_2 + K_2 \times F + M_2}{H_2 + E_2 \times F} \tag{2.22}$$

The term $(J_2 \times f_2 + G_2 \times F)P_{1,2}$ is a second order function in F. The numerator on the right hand side of eq. (2.22) is hence a second order function in F. Similarly, if we put the equation $P_{2,3}$ into the equation for $P_{3,4}$, a third order equation in F will be achieved. If we continue this process to the last slice, we will arrive at a polynomial for F and the order of the polynomial is n for $P_{n,n+1}$ which is just 0! Sarma (1987) has also arrived at a similar conclusion for a simplified slope model. The importance of this polynomial under the present formulation is that there are n possible factors of safety for any prescribed Φ. Most of the solutions will be physically unacceptable and are either imaginary numbers or negative solutions. Physically acceptable factors of safety are given by the positive real solutions from this polynomial.

λ and F are the two unknowns in the above equations and they can be determined by several different methods. In most of the commercial programs, the factor of safety is obtained by the use of iteration with an initial trial factor of safety (usually 1.0) which is efficient and effective for

most cases. The use of the iteration method is actually equivalent to expressing the complicated factor of safety polynomial in a functional form as:

$$F = f(F) \tag{2.23}$$

Chen and Morgenstern (1983) and Zhu *et al.* (2001) have proposed the use of the Newton–Rhapson technique in the evaluation of the factor of safety F and λ. The gradient type methods are more complicated in the formulation but are fast in solution. Chen and Morgenstern (1983) suggested that the initial trial λ can be chosen as the tangent of the average base angle of the failure surface, and these two values can be determined by the use of the Newton–Rhapson method. Chen and Morgenstern (1983) have also provided the expressions for the derivatives of the moment and shear terms required for the Newton–Rhapson analysis. Zhu *et al.* (2001) admitted that the initial trials of F and λ can greatly affect the efficiency of the computation. In some cases, poor initial trials can even lead to divergence in analysis. Zhu *et al.* proposed a technique to estimate the initial trial value which appears to work fine for smooth failure surfaces. The authors' experience is that, for non-smooth or deep-seated failure surfaces, it is not easy to estimate a good initial trial value, and Zhu *et al.*'s proposal may not work for these cases.

As an alternative, Cheng and Zhu (2005) have proposed that the factor of safety based on the force equilibrium is determined directly from the polynomial as discussed above, and this can avoid the problems that may be encountered using the Newton–Rhapson method or iteration method. The present proposal can be effective under difficult problems while Chen's or Zhu's methods are more efficient for general smooth failure surfaces. The additional advantage of the present proposal is that it can be applied to many slope stability analysis methods if the unified formulation is adopted. To solve for the factor of safety, the following steps can be used:

1 From slice 1 to n, based on an assumed value of λ and $f(x)$ and hence Φ for each interface, the factors of safety can be determined from the polynomial by the Gauss–Newton method with a line search step selection. The internal forces P, V, N and S can be then be determined from eqs (2.5) to (2.11) without using any iteration analysis. The special feature of the present technique is that while determination of inter-slice forces is required for calculating the factor of safety in iterative analysis (for rigorous methods), the factor of safety is determined directly under the present formulation. Since the Bishop analysis does not satisfy horizontal force equilibrium, the present method cannot be applied to the Bishop analysis. This is not important as the Bishop method can be solved easily by the classical iterative algorithm.
2 For those rigorous methods, moment equilibrium has to be checked. Based on the internal forces as determined in step 1 for a specific physically acceptable factor of safety, the moment equilibrium equation (2.13) is then checked. If moment equilibrium is not satisfied with that

specific factor of safety based on the force equilibrium, repeat the step with the next factor of safety in checking the moment equilibrium.

3 If no acceptable factor of safety is found, try the next λ and repeat steps 1 and 2 above. In the actual implementation, the sign of the unbalanced moment from eq. (2.13) is monitored against λ and interpolation is used to accelerate the determination of λ which satisfies the moment equilibrium.

4 For the Janbu rigorous method or the Leshchinsky method, eqs (2.20) and (2.21) have to be used in the above procedures during each step of analysis.

It will be demonstrated in Chapter 3 that there are many cases where iteration analysis may fail to converge but the factors of safety actually exist. On the other hand, using the Gauss–Newton method and the polynomial from by Cheng and Zhu (2005) or the matrix form and the double QR method by Cheng (2003), it is possible to determine the factor of safety without iteration analysis. The root of the polynomial (factor of safety) close to the initial trial can be determined directly by the Gauss–Newton method. For the double QR method, the factor of safety and the internal forces are determined directly without the need of any initial trial at the expense of computer time in solving the matrix equation.

Based on the fact that the inter-slice forces at any section are the same for the slices to the left and to the right of that section, an overall equation can be assembled in a way similar to that in the stiffness method which will result in a matrix equation (Cheng, 2003). The factor of safety equation as given by eq. (2.22) can be cast into a matrix form instead of a polynomial (actually equivalent). The complete solution of all the real positive factors of safety from the matrix can be obtained by the double QR method by Cheng (2003), which is a useful numerical method to calculate all the roots associated with the Hessenberg matrix arising from eq. (2.22). It should be noted that imaginary numbers may satisfy the factor of safety polynomial, so the double QR method instead of the classical QR method is necessary to determine the real positive factors of safety. If a F value from the double QR analysis cannot satisfy the above requirement, the next F value will be computed. Processes 1 to 4 above will continue until all the possible F values are examined. If no factor of safety based on the force equilibrium can satisfy the moment equilibrium, the analysis is assumed to fail in convergence and only imaginary roots will be available.

The advantage of the present method is that the factor of safety and the internal forces with respect to force equilibrium are obtained directly without any iteration analysis. Cheng (2003) has also demonstrated that there can be at most n possible factors of safety (including negative value and imaginary number) from the double QR analysis for a failure mass with n slices. The actual factor of safety can be obtained from the force and moment balance at a particular λ value. The time required for the double QR computation is not excessively long as inter-slice normal and shear forces are not required to be determined in obtaining a factor of safety. In general, if the number of slices used for the analysis is less than 20, the solution time for the double QR method is only 50–100 per cent longer than the iteration method.

Since all the possible factors of safety are examined, this method is the ultimate method in the determination of the factor of safety. If other methods of analysis fail to determine the factor of safety, this method may still work which will be demonstrated in Chapter 3. On the other hand, if no physically acceptable solution is found from the double QR method, the problem under consideration has no solution by nature. More discussion about the use of the double QR method will be given in Section 2.9.

2.2.5 Examples on slope stability analysis

Figure 2.4 is a simple slope given by coordinates (4,0), (5,0), (10,5) and (12,5) while the water table is given by (4,0), (5,0), (10,4) and (12,4). The soil parameters are: unit weight = 19 kNm^{-3}, $c' = 5$ kPa and $\phi' = 36°$. To define a circular failure surface, the coordinates of the centre of rotation and the radius should be defined. Alternatively, a better method is to define the x-ordinates of the left and right exit ends and the radius of the circular arc. The latter approach is better as the left and right exit ends can usually be estimated easily from engineering judgement. In the present example, the x-ordinates of the left and right exit ends are defined as 5.0 and 12.0 m while the radius is defined as 12 m. The soil mass is divided into ten slices for analysis and the details are given below:

Slice	*Weight (kN)*	*Base angle (°)*	*Base length (m)*	*Base pore pressure (kPa)*
1	2.50	16.09	0.650	1.57
2	7.29	19.22	0.662	4.52
3	11.65	22.41	0.676	7.09
4	15.54	25.69	0.694	9.26
5	18.93	29.05	0.715	10.99
6	21.76	32.52	0.741	12.23
7	23.99	36.14	0.774	12.94
8	25.51	39.94	0.815	13.04
9	32.64	45.28	1.421	7.98
10	11.77	52.61	1.647	0.36

The results of analyses for the problem in Figure 2.4 are given in Table 2.6. For the Swedish method or the Ordinary method of slices where only the moment equilibrium is considered while the inter-slice shear force is neglected, the factor of safety from the global moment equilibrium takes the form of:

$$F_{\mathrm{m}} = \frac{\sum \left(c' l + (W \cos\alpha - ul) \tan\phi'\right)}{\sum W \sin\alpha} \tag{2.24}$$

A factor of safety 0.991 is obtained directly from the Swedish method for this example without any iteration. For the Bishop method, which assumes the inter-slice shear force V to be zero, the factor of safety by the global moment equilibrium will reduce to

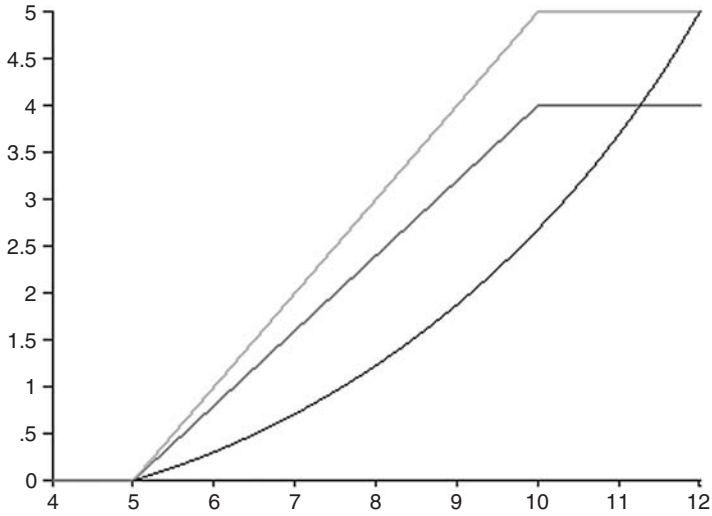

Figure 2.4 Numerical examples for a simple slope.

Table 2.6 Factors of safety for the failure surface shown in Figure 2.4

	Bishop	*Janbu simplified*	*Janbu rigorous*	*Swedish*	*Load factor*	*Sarma*	*Morgenstern–Price*
F	1.023	1.037	1.024	0.991	1.027	1.026	1.028

Note: The correction factor is applied to the Janbu simplified method. The results for the Morgenstern–Price method using $f(x) = 1.0$ and $f(x) = \sin(x)$ are the same. Tolerance in iteration analysis is 0.0005.

$$F_{\mathrm{m}} = \frac{\sum \left(c'b + (W - ul)\tan\phi'\right)\sec\alpha / m_\alpha}{\sum W \sin\alpha} \tag{2.25}$$

where $m_\alpha = \cos\alpha\left(1 + \tan\alpha \dfrac{\tan\phi'}{F}\right)$

Based on an initial factor of safety 1.0, the successive factors of safety during the Bishop iteration analysis are 1.0150, 1.0201, 1.0219, 1.0225 and 1.0226. For the Janbu simplified method, the factor of safety based on force equilibrium using the iteration analysis takes the form of:

$$F_{\mathrm{f}} = \frac{\sum [c'b + (W - ub)\tan\phi']/n_\alpha}{\sum W \tan\alpha} \quad \text{and} \quad n_\alpha = \cos\alpha \cdot m_\alpha \tag{2.26}$$

The successive factors of safety during the iteration analysis using the Janbu simplified method are 0.9980, 0.9974 and 0.9971. Based on a correction factor of 1.0402, the final factor of safety from the Janbu simplified analysis is 1.0372. If

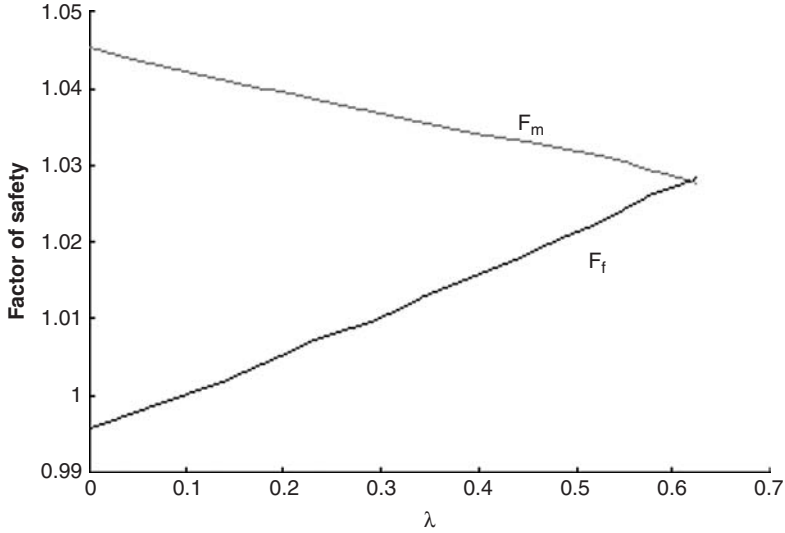

Figure 2.5 Variation of F_f and F_m with respect to λ for the example in Figure 2.4.

the double QR method is used for the Janbu simplified method, a value of 0.9971 is obtained directly from the first positive solution of the Hessenberg matrix without using any iteration analysis. For the Janbu rigorous method, the successive factors of safety based on iteration analysis are 0.9980, 0.9974, 0.9971, 1.0102, 1.0148, 1.0164, 1.0170, 1.0213, 1.0228, 1.0233 and 1.0235. For the Morgenstern–Price method, a factor of safety 1.0282 and the internal forces are obtained directly from the double QR method without any iteration analysis. The variation of F_f and F_m with respect to λ using the iteration analysis for this example is shown in Figure 2.5. It should be noted that F_f is usually more sensitive to λ than F_m in general, and the two lines may not meet for some cases which can be considered as no solution to the problem. There are cases where the lines are very close but actually do not intersect. If a tolerance large enough is defined, then the two lines can be considered as having an intersection and the solution converge. This type of 'false' convergence is experienced by many engineers in Hong Kong. These two lines may be affected by the choice of the moment point, and convergence can sometimes be achieved by adjusting the choice of the moment point. The results shown in Figure 2.5 assume the interslice shear forces to be zero in the first solution step, and this solution procedure appears to be adopted in many commercial programs. Cheng *et al.* (2008a) have however found that the results shown in Figure 2.5 may not be the true result for some special cases, and this will be further discussed in Chapter 3.

From Table 2.6, it is clear that the Swedish method is a very conservative method as first suggested by Whitman and Bailey (1967). Besides, the Janbu simplified method will also give a smaller factor of safety if the correction

factor is not used. After the application of the correction factor, Cheng found that the results from the Janbu simplified method are usually close to those 'rigorous' methods. In general, the factors of safety from different methods of analysis are usually close as pointed out by Morgenstern (1992).

2.3 Miscellaneous consideration on slope stability analysis

2.3.1 Acceptability of the failure surfaces and results of analysis

Based on an arbitrary inter-slice force function, the internal forces which satisfy both the force and moment equilibrium may not be kinematically acceptable. The acceptability conditions of the internal forces include:

1 Since the Mohr–Coulomb relation is not used along the vertical interfaces between different slices, it is possible though not common that the inter-slice shear forces and normal forces may violate the Mohr–Coulomb relation.
2 Except for the Janbu rigorous method and the extremum method as discussed in Section 2.8 under which the resultant of the inter-slice normal force must be acceptable, the line of thrust from other 'rigorous' methods which are based on overall moment equilibrium may lie outside the failure mass and is unacceptable.
3 The inter-slice normal forces should not be in tension. For the inter-slice normal forces near to the crest of the slope where the base inclination angles are usually high, if c' is high, it is highly likely that the inter-slice normal forces will be in tension to maintain the equilibrium. This situation can be eliminated by the use of a tension crack. Alternatively, the factor of safety with tensile inter-slice normal forces for the last few slices may be accepted, as the factor of safety is usually not sensitive to these tensile forces. On the other hand, tensile inter-slice normal forces near the slope toe are usually associated with special shape failure surfaces with kinks, steep upward slope at the slope toe or an unreasonably high/low factor of safety. The factors of safety associated with these special failure surfaces need special care in the assessment and should be rejected if the internal forces are unacceptable. Such failure surfaces should also be eliminated during the location of the critical failure surfaces.
4 The base normal forces may be negative near the toe and crest of the slope. For negative base normal forces near the crest of the slope, the situation is similar to the tensile inter-slice normal forces and may be tolerable. For negative base normal forces near the toe of the slope which is physically unacceptable, it is usually associated with deep-seated failure with a high upward base inclination. Since a very steep exit angle is not likely to occur, it is possible to limit the exit angle during the automatic location of the critical failure surface.

If the above criteria are strictly enforced to all slices of a failure surface, many slip surfaces will fail to converge. One of the reasons is the effect of the last slice when the base angle is large. Based on the force equilibrium, the tensile

inter-slice normal force will be created easily if c' is high. This result can propagate so that the results for the last few slices will be in conflict with the criteria above. If the last few slices are not strictly enforced, the factor of safety will be acceptable when compared with other methods of analysis. A suggested procedure is that if the number of slices is 20, only the first 15 slices are checked against the criteria above. The authors found that this approach is sufficiently good and is acceptable.

2.3.2 Tension crack

As the condition of limiting equilibrium develops with the factor of safety close to 1, a tension crack shown in Figure 2.3 may be formed near the top of the slope through which no shear strength can be developed. If the tension crack is filled with water, a horizontal hydrostatic force P_w will generate additional driving moment and driving force which will reduce the factor of safety. The depth of a tension crack z_c can be estimated as:

$$z_c = \frac{2c\sqrt{K_a}}{\gamma} \tag{2.27}$$

where K_a is the Rankine active pressure coefficient. The presence of tension crack will tend to reduce the factor of safety of a slope, but the precise location of a tension crack is difficult to be estimated for a general problem. It is suggested that if a tension crack is required to be considered, it should be specified at different locations and the critical results can then be determined. Sometimes, the critical failure surface with and without a tension crack can differ appreciably, and the location of the tension crack needs to be assessed carefully. In SLOPE 2000 by Cheng or some other commercial programs, the location of the tension crack can be varied automatically during the location of the critical failure surface.

2.3.3 Earthquake

Earthquake loadings are commonly modelled as vertical and horizontal loads applied at the centroid of the sliding mass, and the values are given by the earthquake acceleration factors k_v/k_h (vertical and horizontal) multiplied with the weight of the soil mass. This quasi-static simulation of earthquake loading is simple in implementation but should be sufficient for most design purposes, unless the strength of soil may be reduced by more than 15 per cent due to the earthquake action. Beyond that, a more rigorous dynamic analysis may be necessary which will be more complicated, and more detailed information about the earthquake acceleration as well as the soil constitutive behaviour is required. Usually, a single earthquake coefficient may be sufficient for the design, but a more refined earth dam earthquake code is specified in DL5073-2000 in China. The design earthquake coefficients will vary according to the height under consideration which will be different for different slices. Though this approach appears to be more reasonable, most of the design codes and existing commercial programs do

not adopt this approach. The program SLOPE 2000 by Cheng can however accept this special earthquake code.

2.3.4 Water

Increase in pore water pressure is one of the main factors for slope failure. Pore water pressure can be defined in several ways. The classical pore pressure ratio r_u is defined as $u/\gamma h$, and an average pore pressure for the whole failure mass is usually specified for the analysis. Several different types of stability design charts are also designed using an average pore pressure definition. The use of a constant averaged pore pressure coefficient is obviously a highly simplified approximation. With the advancement in computer hardware and software, the uses of these stability design charts are now mainly limited to the preliminary designs only. The pore pressure coefficient is also defined as a percentage of the vertical surcharge applied on the ground surface in some countries. This definition of the pore pressure coefficient is however not commonly used.

If pore pressure is controlled by the groundwater table, u is commonly taken as $\gamma_w h_w$, where h_w is the height of the water table above the base of the slice. This is the most commonly used method to define the pore pressure, which assumes that there is no seepage and the pore pressure is hydrostatic. Alternatively, a seepage analysis can be conducted and the pore pressure can be determined from the flow-net or the finite element analysis. This approach is more reasonable but is less commonly adopted in practice due to the extra effort to perform a seepage analysis. More importantly, it is not easy to construct a realistic and accurate hydrogeological model to perform the seepage analysis.

Pore pressure can also be generated from the presence of a perched water table. In a multi-layered soil system, a perched water table may exist together with the presence of a water table if there are great differences in the permeability of the soil. This situation is rather common for the slopes in Hong Kong. For example, slopes at mid-levels in Hong Kong Island are commonly composed of fill at the top which is underlain by colluvium and completely decomposed granite. Since the permeability of completely decomposed granite is 1 to 2 orders less than that for colluvium and fill, a perched water table can be easily established within the colluvium/fill zone during heavy rainfall while the standing water table may be within the completely decomposed granite zone. Considering Figure 2.6, a perched water table may be present in soil layer 1 with respect to the interface between soils 1 and 2 due to the permeability of soil 2 being ten times less than that of soil 1. For the slice base between A and B, it is subjected to the perched water table effect and pore pressure should be included in the calculation. For the slice base between B and C, no water pressure is required in the calculation, while the water pressure at the slice base between C and D is calculated using the groundwater table only.

For the problem shown in Figure 2.7, if EFG which is below the ground surface is defined as the groundwater table, the pore water pressure will be determined by EFG directly. If the groundwater table is above the ground

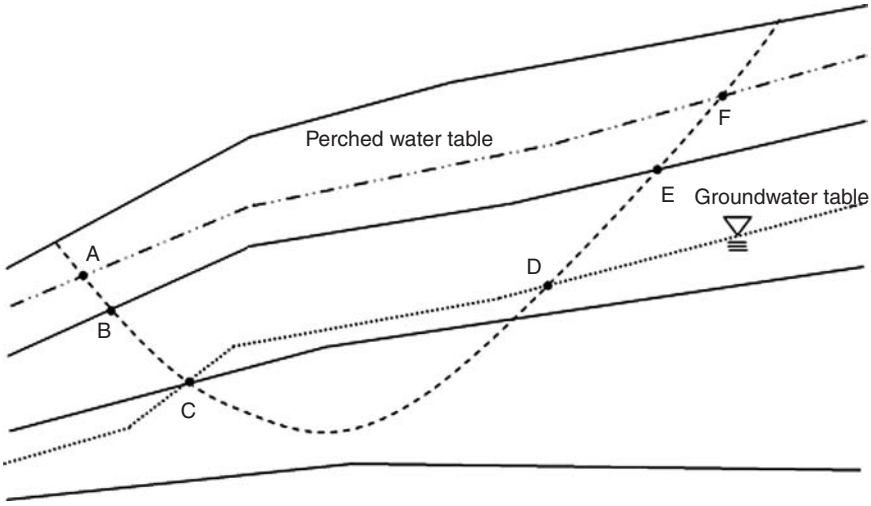

Figure 2.6 Perched water table in a slope.

surface and undrained analysis is adopted, ground surface CDB is impermeable and the water pressure arising from AB will become external load on surface CDB. For drained analysis, the water table given by AB should be used, but vertical and horizontal pressure corresponding to the hydrostatic pressure should be applied on surfaces CD and DB. Thus, a trapezoidal horizontal and vertical pressure will be applied to surfaces CD and DB while the water table AB will be used to determine the pore pressure.

For the treatment of the inter-slice forces, usually the total stresses instead of the effective stresses are used. This approach, though slightly less rigorous in the formulation, can greatly simplify the analysis and is adopted in virtually all the commercial programs. Greenwood (1987) and Morrison and Greenwood (1989) have reported that this error is particularly significant where the slices have high base angles with a high water table. King (1989) and Morrison and Greenwood (1989) have also proposed revisions to the classical effective stress limit equilibrium method. Duncan and Wright (2005) have in addition reported that some 'simplified' methods can be sensitive to the assumption of the total or effective inter-slice normal forces in the analysis.

2.3.5 Saturated density of soil

The unit weights of soil above and below the water table are not the same and may differ by 1–2 kNm^{-3}. For computer programs which cannot accept the input of saturated density, this can be modelled by the use of two different types of soil for a soil which is partly submerged. Alternatively, some engineers assume the two unit weights to be equal in view of the small differences between them.

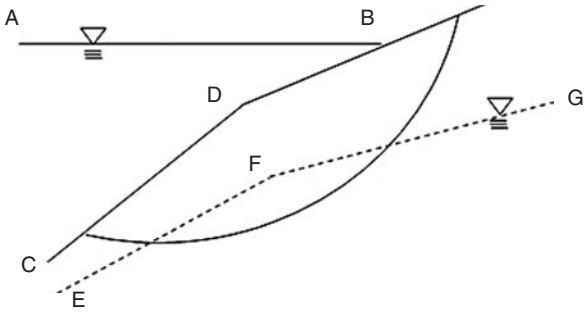

Figure 2.7 Modelling of ponded water.

2.3.6 Moment point

For simplified methods which satisfy only the force or moment equilibrium, the Janbu and the Bishop methods are the most popular methods adopted by engineers. There is a perception among some engineers that the factor of safety from the moment equilibrium is more stable and is more important than the force equilibrium in stability formulation (Abramson *et al.*, 2002). However, true moment equilibrium depends on the satisfaction of force equilibrium. Without force equilibrium, there is actually no moment equilibrium. Force equilibrium is, however, totally independent of the moment equilibrium. For methods which satisfy only the moment equilibrium, the factor of safety actually depends on the choice of the moment point. For the circular failure surface, it is natural to choose the centre of the circle as the moment point, and it is also well known that the Bishop method can yield a very good result even when the force equilibrium is not satisfied. Fredlund *et al.* (1992) have discussed the importance of the moment point on the factor of safety for the Bishop method, and the Bishop method cannot be applied to a general slip surface because the unbalanced horizontal force will create a different moment contribution to a different moment point. Baker (1980) has pointed out that for 'rigorous' methods, the factor of safety is independent of the choice of the moment point. Cheng *et al.* (2008a) have however found that the mathematical procedures to evaluate the factor of safety may be affected by the choice of the moment point. Actually, many commercial programs allow the user to choose the moment point for analysis. The double QR method by Cheng (2003) is completely not affected by the choice of the moment point in the analysis and is a very stable solution algorithm.

2.3.7 Use of soil nail/reinforcement

Soil nailing is a slope stabilization method that introduces a series of thin elements called nails to resist tension, bending and shear forces in the slope.

The reinforcing elements are usually made of round cross-section steel bars. Nails are installed sub-horizontally into the soil mass in a pre-bore hole, which is fully grouted. Occasionally, the initial portions of some nails are not grouted but this practice is not commonly adopted. Nails can also be driven into the slope, but this method of installation is uncommon in practice.

2.3.7.1 Advantages of soil nailing

Soil nailing presents the following advantages that have contributed to the widespread use of this technique:

- *Economy:* economical evaluation has led to the conclusion that soil nailing is a cost-effective technique as compared with a tieback wall. Cost of soil nailing may be 50 per cent of a tieback wall.
- *Rate of construction:* fast rates of construction can be achieved if adequate drilling equipment is employed. Shotcrete is also a rapid technique for placement of the facing.
- *Facing inclination:* there is virtually no limit to the inclination of the slope face.
- *Deformation behaviour:* observation of actual nailed structures demonstrated that horizontal deformation at the top of the wall ranges from 0.1 to 0.3 per cent of the wall height for well-designed walls (Clouterre, 1991; Elias and Juran, 1991).
- *Design flexibility:* soil anchors can be added to limit the deformation in the vicinity of existing structures or foundations.
- *Design reliability in saprolitic soils:* saprolitic soils frequently present relict weak surfaces which can be undetected during site investigation. Such a situation has happened in Hong Kong, and slope failures in such weak planes have also occurred. Soil nailing across these surfaces may lead to an increased factor of safety and increased reliability, as compared with other stabilization solutions.
- *Robustness:* deep-seated stability would be maintained.

The fundamental principle of soil nailing is the development of tensile force in the soil mass and renders the soil mass stable. Although only tensile force is considered in the analysis and design, soil nail function by a combination of tensile force, shear force and bending action is difficult to be analysed. The use of the finite element by Cheng has demonstrated that the bending and shear contribution to the factor of safety is generally not significant, and the current practice in soil nail design should be good enough for most cases. Nails are usually constructed at an angle of inclination from 10° to 20°. For an ordinary steel bar soil nail, a thickness of 2 mm is assumed as the corrosion zone so that the design bar diameter is totally 4 mm less than the actual diameter of the bar according to Hong Kong practice.The nail is usually protected by galvanization, paint, epoxy and cement grout. For the critical location, protection by expensive sleeving similar to that in rock

anchor may be adopted. Alternatively, fibre reinforced polymer (FRP) and carbon fibre reinforced polymer (CFRP) may be used for soil nails which are currently under consideration.

The practical limitations of soil nails include:

1 Lateral and vertical movement may be induced from excavation and the passive action of the soil nail is not as effective as the active action of the anchor.
2 Difficulty in installation under some groundwater conditions.
3 Suitability of the soil nail in loose fill is doubted by some engineers – the stress transfer between nail and soil is difficult to be established.
4 The collapse of the drill hole before the nail is installed can happen easily in some ground conditions.
5 For a very long nail hole, it is not easy to maintain the alignment of the drill hole.

There are several practices in the design of soil nails. One of the precautions in the adoption of soil nails is that the factor of safety of a slope without a soil nail must be greater than 1.0 if a soil nail is going to be used. This is due to the fact that the soil nail is a passive element, and the strength of the soil nail cannot be mobilized until the soil tends to deform. The effective nail load is usually taken as the minimum of:

(a) the bond strength between cement grout and soil;
(b) the tensile strength of the nail, which is limited to 55 per cent of the yield stress in Hong Kong, and 2 mm sacrificial thickness of the bar surface is allowed for corrosion protection;
(c) the bond stress between the grout and the nail.

In general, only factors (a) and (b) are the controlling factors in design. The bond strength between cement grout and soil is usually based on one of the following criteria:

(a) The effective overburden stress between grout and soil controls the unit bond stress on the soil nail, and is estimated from the formula ($\pi c'D + 2D\sigma_v'\tan\phi'$) for Hong Kong practice, while the Davis method allows an inclusion of the angle of inclination; D is the diameter of the grout hole. A safety factor of 2.0 is commonly applied to this bond strength in Hong Kong. During the calculation of the bond stress, only the portion behind the failure surface is taken into the calculation.
(b) Some laboratory tests suggest that the effective bond stress between nail and soil is relatively independent of the vertical overburden stress. This is based on the stress-redistribution after the nail hole is drilled and the surface of the drill hole should be stress free. The effective bond load will then be controlled by the dilation angle of the soil. Some of the laboratory tests in Hong Kong have shown that the effective overburden stress is not

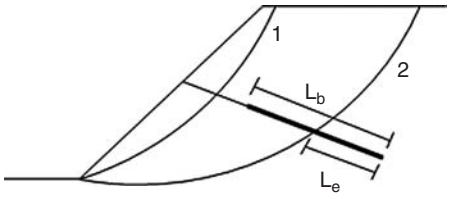

Figure 2.8 Definition of effective nail length in the bond load determination.

important for the bond strength. On the other hand, some field tests in Hong Kong have shown that the nail bond strength depends on the depth of embedment of the soil nail. It appears that the bond strength between cement grout and soil may be governed by the type of soil, method of installation and other factors, and the bond strength may be dependent on the overburden height in some cases, but this is not a universal behaviour.

(c) If the bond load is independent of the depth of embedment, the effective nail load will then be determined in a proportional approach shown in Figure 2.8.

For a soil nail of length L, bonded length L_b and total bond load T_{sw}, L_e for each soil nail and T_{mob} for each soil nail are determined from the formula below:

For slip 1: $T_{mob} = T_{sw}$

In this case, the slip passes in front of the bonded length and the full magnitude is mobilized to stabilize the slip.

For slip 2: $T_{mob} = T_{sw} \times (L_e/L_b)$

In this case the slip intersects the bonded length and only a proportion of the full magnitude provided by the nail length behind the slip is mobilized to stabilize the slip.

The effective nail load is usually applied as a point load on the failure surface in the analysis. Some engineers however model the soil nail load as a point load at the nail head or as a distributed load applied on the ground surface. In general, there is no major difference in the factors of safety from these minor variations in treating the soil nail forces.

The effectiveness of the soil nail can be illustrated by adding two rows of 5 m length soil nails inclined at an angle of 15° to the problem shown in Figure 2.4 which is shown in Figure 2.9. The x-ordinates of the nail heads are 7.0 and 9.0. The total bond load is 40 kN for each nail which is taken to be independent of the depth of embedment, while the effective nail loads are obtained as 27.1 and 24.9 kN considered by a simple proportion as given in Figure 2.8. The results of analysis shown in Table 2.7 have illustrated that: (1) the Swedish method is a conservative method in most cases; (2) the Janbu

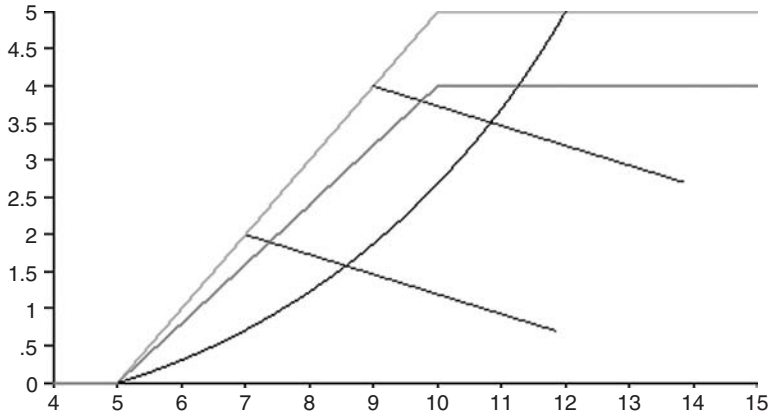

Figure 2.9 Two rows of soil nail are added to the problem in Figure 2.4.

Table 2.7 Factors of safety for the failure surface shown in Figure 2.4

	Bishop	*Janbu simplified*	*Janbu rigorous*	*Swedish*	*Load factor*	*Sarma*	*Morgenstern–Price*
F	1.807	1.882	Fail	1.489	1.841	1.851	1.810

rigorous method is more difficult to converge as compared with other methods. It is also noticed that when external load is present, there are greater differences between the results from different methods of analysis.

During the computation of the factor of safety, the factor of safety can be defined as

$$F = \frac{\text{shear strength}}{\text{mobilized shear} - \text{contribution from reinforcement}} \tag{2.28a}$$

or

$$F = \frac{\text{shear strength} + \text{contribution from reinforcement}}{\text{mobilized shear}} \tag{2.28b}$$

The results shown in Table 2.7 are based on eq. (2.28a) which is the more popular definition of the factor of safety with soil reinforcement. Some commercial software also offers an option for eq. (2.28b), and engineers must be clear about the definition of the factor of safety. In general, the factor of safety using eq. (2.28a) will be greater than that based on eq. (2.28b).

2.3.8 Failure to converge

Failure to converge in the solution of the factor of safety is sometimes found for 'rigorous' methods which satisfy both force and moment equilibrium. If

this situation is found, the initial trial factor of safety can be varied and convergence is sometimes achieved. Alternatively, the double QR method by Cheng (2003) can be used as this is the ultimate method in the solution of the factor of safety. If no physically acceptable answer can be determined from the double QR method, there is no result for the specific method of analysis. Under such conditions, the simplified methods can be used to estimate the factor of safety or the extremum principle in Sections 2.8 and 2.9 may be adopted to determine the factor of safety. The convergence problem of the 'rigorous' method will be studied in more detail in Section 2.9 and Chapter 3, and there are more case studies which are provided in the user guide of SLOPE 2000.

2.3.9 Location of the critical failure surface

The minimum factor of safety as well as the location of the critical failure surface are required for the proper design of a slope. For a homogeneous slope with a simple geometry and no external load, the log-spiral failure surface will be a good solution for the critical failure surface. In general, the critical failure surface for a sandy soil with a small c' value and high ϕ' will be close to the ground surface while the critical failure surface will be a deep-seated one for a soil with a high c' value and small ϕ'. With the presence of the external vertical load or soil nail, the critical failure surface will generally drive the critical failure surface deeper into the soil mass. For a simple slope with a heavy vertical surcharge on top of the slope (typical abutment problem), the critical failure surface will be approximately a two-wedge failure from the non-circular search. This failure mode is also specified by the German code for abutment design. For a simple slope without any external load or soil nail, the critical failure surface will usually pass through the toe. Based on the above characteristics of the critical failure surface, engineers can manually locate the critical failure surface with ease for a simple problem. The use of the factor of safety from the critical circular or log-spiral failure surface (Frohlich, 1953; Chen, 1972) which will be slightly higher than that from the non-circular failure surface is also adequate for simple problems.

For complicated problems, the above guidelines may not be applicable, and it will be tedious to carry out the manual trial and error in locating the critical failure surface. Automatic search for the critical circular failure surface is available in nearly all of the commercial slope stability programs. A few commercial programs also offer the automatic search for the non-circular critical failure surface with some limitations. Since the automatic determination of the effective nail load (controlled by the overburden stress) appears to be not available in most of the commercial programs, engineers often have to perform the search for the critical failure surface by manual trial and error and the effective nail load is separately determined for each trial failure surface. To save time, only limited failure surfaces will be considered in the routine design. The authors have found that reliance only on the manual trial and error in locating the critical failure surface may not be adequate, and the adoption of the modern optimization methods to overcome this problem will be discussed in Chapter 3.

2.3.10 3D analysis

All failure mechanisms are 3D in nature but 2D analysis is performed at present. The difficulties associated with true 3D analysis are: (1) sliding direction, (2) satisfaction of 3D force and moment equilibrium, (3) relating the factor of safety to the previous two factors and (4) a great amount of computational geometrical calculations is required. At present, there are still many practical limitations in the adoption of 3D analysis, and there are only a few 3D slope stability programs which is suitable for ordinary use. Simplified 3D analysis for a symmetric slope is available in SLOPE 2000 by Cheng, and true 3D analysis for a general slope is under development in SLOPE3D. 3D slope stability analysis will be discussed in detail in Chapter 5.

2.4 Limit analysis

The limit analysis adopts the concept of an idealized stress–strain relation, that is, the soil is assumed as a rigid, perfectly plastic material with an associated flow rule. Without carrying out the step-by-step elasto-plastic analysis, the limit analysis can provide solutions to many problems. Limit analysis is based on the bound theorems of classical plasticity theory (Drucker *et al*., 1951; Drucker and Prager, 1952). The general procedure of limit analysis is to assume a kinematically admissible failure mechanism for an upper bound solution or a statically admissible stress field for a lower bound solution, and the objective function will be optimized with respect to the control variables. Early efforts of limit analysis were mainly made on using the direct algebraic method or analytical method to obtain the solutions for slope stability problems with simple geometry and soil profile (Chen, 1975). Since closed form solutions for most practical problems are not available, later attention has been shifted to employing the slice techniques in traditional limit equilibrium to the upper bound limit analysis (Michalowski, 1995; Donald and Chen, 1997).

Limit analysis is based on two theorems: (a) the lower bound theorem, which states that any statically admissible stress field will provide a lower bound estimate of the true collapse load, and (b) the upper bound theorem, which states that when the power dissipated by any kinematically admissible velocity field is equated with the power dissipated by the external loads, then the external loads are upper bounds on the true collapse load (Drucker and Prager, 1952).

A statically admissible stress field is one that satisfies the equilibrium equations, stress boundary conditions, and yield criterion. A kinematically admissible velocity field is one that satisfies strain and velocity compatibility equations, velocity boundary conditions and the flow rule. When combined, the two theorems provide a rigorous bound on the true collapse load. Application of the lower bound theorem usually proceeds as stated in the following. (a) First, a statically admissible stress field is constructed. Often it will be a discontinuous field in the sense that we have a patchwork of regions of constant stress that together cover the whole soil mass. There will be one or more particular value of stress that is not fully specified by

the conditions of equilibrium. (b) These unknown stresses are then adjusted so that the load on the soil is maximized but the soil remains unyielded. The resulting load becomes the lower bound estimate for the actual collapse load.

Stress fields used in lower bound approaches are often constructed without a clear relation to the real stress fields. Thus, the lower bound solutions for practical geotechnical problems are often difficult to find. Collapse mechanisms used in the upper bound calculations, however, have a distinct physical interpretation associated with actual failure patterns and thus have been extensively used in practice.

2.4.1 Lower bound approach

The application of the conventional analytical limit analysis was usually limited to simple problems. Numerical methods therefore have been employed to compute the lower and upper bound solutions for the more complex problems. The first lower bound formulation based on the finite element method was proposed by Lysmer (1970) for plain strain problems. The approach used the concept of finite element discretization and linear programming. The soil mass is subdivided into simple three-node triangular elements where the nodal normal and shear stresses were taken as the unknown variables. The stresses were assumed to vary linearly within an element, while stress discontinuities were permitted to occur at the interface between adjacent triangles. The statically admissible stress field was defined by the constraints of the equilibrium equations, stress boundary conditions and the linearized yield criterion. Each non-linear yield criterion was approximated by a set of linear constraints on the stresses that lie inside the parent yield surface, thus ensuring that the solutions are a strict lower bound. This led to an expression for the collapse load which was maximized, subjected to a set of linear constraints on the stresses. The lower bound load could be solved by optimization, using the techniques of linear programming. Other investigations have worked on similar algorithms (Anderheggen and Knopfel, 1972; Bottero *et al.*, 1980). The major disadvantage of these formulations was the linearization of the yield criterion which generated a large system of linear equations, and required excessive computational times, especially if the traditional simplex or revised simplex algorithms were used (Sloan, 1988a). Therefore, the scope of the early investigations was mainly limited to small-scale problems.

Efficient analyses for solving numerical lower bounds by the finite element method and linear programming method have been developed recently (Bottero *et al.*, 1980; Sloan, 1988a,b). The key concept of these analyses was the introduction of an active set algorithm (Sloan, 1988b) to solve the linear programming problem where the constraint matrix was sparse. Sloan (1988b) has shown that the active set algorithm was ideally suited to the numerical lower bound formulation and could solve a large-scale linear programming problem efficiently. A second problem associated with the numerical lower bound solutions occurred when dealing with statically admissible conditions for an infinite-half space. Assdi and Sloan (1990) have

solved this problem by adopting the concept of infinite elements, and hence obtained rigorous lower bound solutions for general problems.

Lyamin and Sloan (1997) proposed a new lower bound formulation which used linear stress finite elements, incorporating non-linear yield conditions, and exploiting the underlying convexity of the corresponding optimization problem. They showed that the lower bound solution could be obtained efficiently by solving the system of non-linear equations that define the Kuhn–Tucker optimality conditions directly.

Recently, Zhang (1999) presented a lower bound limit analysis in conjunction with another numerical method – the rigid finite element method (RFEM) to assess the stability of slopes. The formulation presented satisfies both static and kinematical admissibility of a discretized soil mass without requiring any assumption. The non-linear programming method is employed to search for the critical slip surface.

2.4.2 Upper bound approach

Implementation of the upper bound theorem is generally carried out as follows. (a) First, a kinematically admissible velocity field is constructed. No separations or overlaps should occur anywhere in the soil mass. (b) Second, two rates are then calculated: the rate of internal energy dissipation along the slip surface and discontinuities that separate the various velocity regions, and the rate of work done by all the external forces, including gravity forces, surface tractions and pore water pressures. (c) Third, the above two rates are set to be equal. The resulting equation, called the energy–work balance equation, is solved for the applied load on the soil mass. This load would be equal to or greater than the true collapse load.

The first application of the upper bound limit analysis to the slope stability problem was by Drucker and Prager (1952) in finding the critical height of a slope. A failure plane was assumed, and analyses were performed for isotropic and homogeneous slopes with various angles. In the case of a vertical slope, it was found that the critical height obtained by the upper bound theorem was identical with that obtained by the limit equilibrium method. Similar studies have been done by Chen and Giger (1971) and Chen (1975). However, their attention was mainly limited to a rigid body sliding along a circular or log-spiral slip surface passing both through the toe and below the toe in cohesive materials. The stability of slopes was evaluated by the stability factor, which could be minimized using an analytical technique.

Karel (1977a,b) presented an energy method for soil stability analysis. The failure mechanisms used in the method included: (a) a rigid zone with a planar or a log-spiral transition layer; (b) a soft zone confined by plane or log-spiral surfaces; and (c) a composed failure mechanism consisting of rigid and soft zones. The internal dissipation of energy occurred along the transition layer for the rigid zone, and within the zone and along the transition layer for the soft zone. However, no numerical technique was proposed to determine the least upper bound of the factor of safety.

Izbicki (1981) presented an upper bound approach to slope stability analysis. A translational failure mechanism, which was confined by a circular slip surface in the form of rigid blocks similar to the traditional slice method, was used. The factor of safety was determined by an energy balance equation and the equilibrium conditions of the field of force associated with the assumed kinematically admissible failure mechanism. However, no numerical technique was provided to search for the least upper bound of the factor of safety in the approach.

Michalowski (1995) presented an upper bound (kinematical) approach of limit analysis in which the factor of safety for slopes derived is associated with a failure mechanism in the form of rigid blocks analogous to the vertical slices used in traditional limit equilibrium methods. A convenient way to include pore water pressure has also been presented and implemented in the analysis of both translational and rotational slope collapse. The strength of the soil between blocks was assumed explicitly that it was taken as zero or its maximum value set by the Mohr–Coulomb yield criterion.

Donald and Chen (1997) proposed another upper bound approach to evaluate the stability of slopes based on a multi-wedge failure mechanism. The sliding mass was divided into a small number of discrete blocks, with linear interfaces between the blocks and with either linear or curved bases to individual blocks. The factor of safety was iteratively calculated by equating the work done by external loads and body forces to the energy dissipated along the bases and interfaces of the blocks. Powerful optimization routines were used to search for the lowest factor of safety and the corresponding critical failure mechanism.

Other efforts have been made in solving the limit analysis problems by the finite element method, which represents an attempt to obtain the upper bound solution by numerical methods on a theoretically rigorous foundation of plasticity. Anderheggen and Knopfel (1972) appeared, having developed the first formulation based on the upper bound theorem, which used constant-strain triangular finite elements and linear programming for plate problems. Bottero *et al.* (1980) later presented the formulation for plain strain problems. In the formulation, the soil mass is discretized into three-node triangular elements whose nodal velocities were the unknown variables. Each element was associated with a specific number of unknown plastic multiplier rates. Velocity discontinuities were permitted along pre-specified interfaces of adjacent triangles. Plastic deformation could occur within the triangular element and at the velocity discontinuities. Kinematically admissible velocity fields were defined by the constraints of compatibility equations, flow rule of the yield criterion and velocity boundary conditions. The yield criterion was linearized using a polygonal approximation. Thus, the finite element formulation of the upper bound theorem led to a linear programming problem whose objective function was the minimization of the collapse load and was expressed in terms of the unknown velocities and plastic multipliers. The upper bound loads were obtained using the revised simplex algorithm. Sloan (1988b, 1989) adopted the same basic formulation as Bottero *et al.* (1980) but solved the linear programming problem using an active set algorithm. The major problem

encountered by Bottero *et al.* (1980) and Sloan (1988b, 1989) was caused by the incompressibility condition of the perfectly plastic deformation. The discretization using linear triangular elements must be arranged such that four triangles form a quadrilateral with the central nodes lying at its centroid. Yu *et al.* (1994) have shown that this constraint can be removed using higher order (quadratic) interpolation of the nodal velocities.

Another problem of the formulation used by Bottero *et al.* (1980) and Sloan (1988b, 1989) was that it could only handle a limited number of velocity discontinuities with pre-specified directions of shearing. Sloan and Kleeman (1995) have made significant progress in developing a more general numerical upper bound formulation in which the direction of shearing was solved automatically during the optimization solution. Yu *et al.* (1998) compare rigorous lower and upper bound solutions with conventional limit equilibrium results for the stability of simple earth slopes.

Many researchers (Mroz and Drescher, 1969; Collins, 1974; Chen, 1975; Michalowski, 1989; Drescher and Detournay, 1993; Donald and Chen, 1997; Yu *et al.*, 1998) pointed out that an upper bound limit analysis solution may be regarded as a special limit equilibrium solution but not vice versa. The equivalence of the two approaches plays a key role in the derivations of the limit load or factor of safety for materials following the non-associated flow rule.

Classically, algebraic expressions for the upper bound method are determined for the simple problems. Assuming a log-spiral failure mechanism for failure surface A shown in Figure 2.10, the work done by the weight of the soil is dissipated along the failure surface based on the upper bound approach by Chen (1975) using an associated flow rule, and the height of the slope can be expressed as

$$H = \frac{c'}{\gamma} f(\phi', \alpha, \beta, \theta_b, \theta_o) \tag{2.29}$$

where

$$f = \frac{\sin\beta\{\exp[2(\theta_b - \theta_o)\tan\varphi] - 1\}}{2\sin(\beta-\alpha)\tan\phi(f_1 - f_2 - f_3)} \{\sin(\theta_b + \alpha)\exp[(\theta_b - \theta_o)\tan\phi] - \sin(\theta_o + \alpha)\}$$

$$f_1 = \frac{1}{3(1+9\tan^2\phi)} \{(3\tan\phi\cos\theta_b + \sin\theta_b)\exp[3(\theta_b - \theta_o)\tan\phi] - (3\tan\phi\cos\theta_o + \sin\theta_o)\}$$

$$f_2(\theta_b, \theta_o) = \frac{1}{6}\frac{L}{r_o}\left(2\cos\theta_o - \frac{L}{r_o}\cos\alpha\right)\sin(\theta_o + \alpha)$$

$$f_3(\theta_b, \theta_o) = \frac{1}{6}\exp[(\theta_b - \theta_o)\tan\phi]\left[\sin(\theta_b - \theta_o) - \frac{L}{r_o}\sin(\theta_b + \alpha)\right] * \left\{\cos\theta_o - \frac{L}{r_o}\cos\alpha + \cos\theta_b\exp[(\theta_b - \theta_o)\tan\phi]\right\}$$

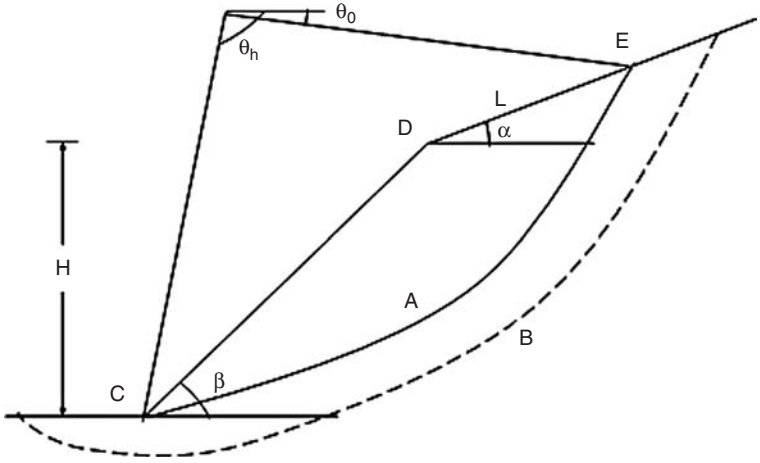

Figure 2.10 Critical log-spiral failure surface by limit analysis for a simple homogeneous slope.

The critical height of the slope is obtained by minimizing eq. (2.29) with respect to θ_0 and θ_h which has been obtained by Chen (1975). Chen has also found that failure surface A is the most critical log-spiral failure surface unless β is small. When β and ϕ' are small, a deep-seated failure shown by failure surface B in Figure 2.10 may be more critical. The basic solution as given by eq. (2.29) can however be modified slightly for this case. The critical result of $f(\phi',\alpha,\beta)$ as given by eq. (2.29) can be expressed as a dimensionless stability number N_s which is given by Chen (1975). In general, the stability numbers by Chen (1975) are very close to that by Taylor (1948).

Within the strict framework of limit analysis, 2D slice-based upper bound approaches have also been extended to solve 3D slope stability problems (Michalowski, 1989; Chen *et al.* 2001a,b). The common features for these approaches are that they all employ the column techniques in 3D limit equilibrium methods to construct the kinematically admissible velocity field, and have exactly the same theoretical background and numerical algorithm which involves a process of minimizing the factor of safety. More recently, a promising 2D and 3D upper bound limit analysis approach by means of linear finite elements and non-linear programming (Lyamin and Sloan, 2002b) has emerged. The approach obviates the need to linearize the yield surface as adopted in the 2D approach using linear programming (Sloan, 1989; Sloan and Kleeman, 1995). However, the approach nonetheless has stress involvement in performing the upper bound calculations.

2.5 Rigid element

The rigid element method (REM) originated from the rigid body-spring model (RBSM) proposed by Kawai (1977). More recently, Zhang and Qian (1993) used

the RBSM to evaluate the static and dynamic stability of slopes or dam foundations within the framework of stress-deformation analysis. Qian and Zhang (1995), and Zhang and Qian (1993) expanded the research field of REM to stability analysis. Zhang (1999) performed a lower bound limit analysis in conjunction with the rigid elements to assess the stability of slopes. Recently, Zhuo and Zhang (2000) conducted a systematical study on the theory, methodologies and algorithms of the REM, and demonstrated its application to a wide range of discontinuous mechanics problems with linear and non-linear material behaviour, beam and plate bending, as well as to the static and dynamic problems. It should be noted that there exist some different titles such as the RBSM, rigid finite element method and interface element method, and a uniform name REM is adopted here. The REM provides an effective approach to the numerical analysis of the stability of soils, rocks or discontinuous media. Further studies and applications of the REM are still being made, attracting the interest of many researchers.

The pre-processing and solution procedure in the REM is quite similar to that in the conventional FEM, except that the two main components in the REM are elements and interfaces while they are nodes and elements in the FEM.

In the REM, each element is assumed to be rigid. The medium under study is partitioned into a proper number of rigid elements mutually connected at the interfaces. Displacement of any point in a rigid element can be described as a function of the translation and rotation of the element centroid. The deformation energy of the system is stored only at the interfaces between rigid elements. The concept of contact 'overlap', though physically inadmissible because elements should not interpenetrate each other, may be accepted as a mathematical means to represent the deformability of the contact interfaces. In such a discrete model, though the relative displacements between adjacent elements show a discontinuous feature of deformation, the studied media can still be considered to be a continuum as a whole mass body.

In the REM, the element centroid displacements are the primary variables, while in the FEM the nodal displacements are selected. For the case of stress-deformation analysis, the forces on the element interfaces are calculated in the REM, different from the Gauss point stress tensor as calculated in the FEM. Thus, while using the Mohr–Coulomb failure (yield) condition, the normal and shear stresses on each interface can be directly incorporated into the failure function to have a check. This treatment in fact assumes that interfaces between the adjacent rigid elements may be the failure surfaces, and makes the calculation results quite sensitive to the mesh partition.

2.5.1 Displacements of the rigid elements

For the sake of convenience, a local reference coordinate system of *n–d–s* axes for the REM calculations is introduced. Consider the face in Figure 2.11: the *n*-axis is pointing along the outward normal of the face; the *d*-axis is the dip direction (the steepest descent on the face); the and the *s*-axis is the

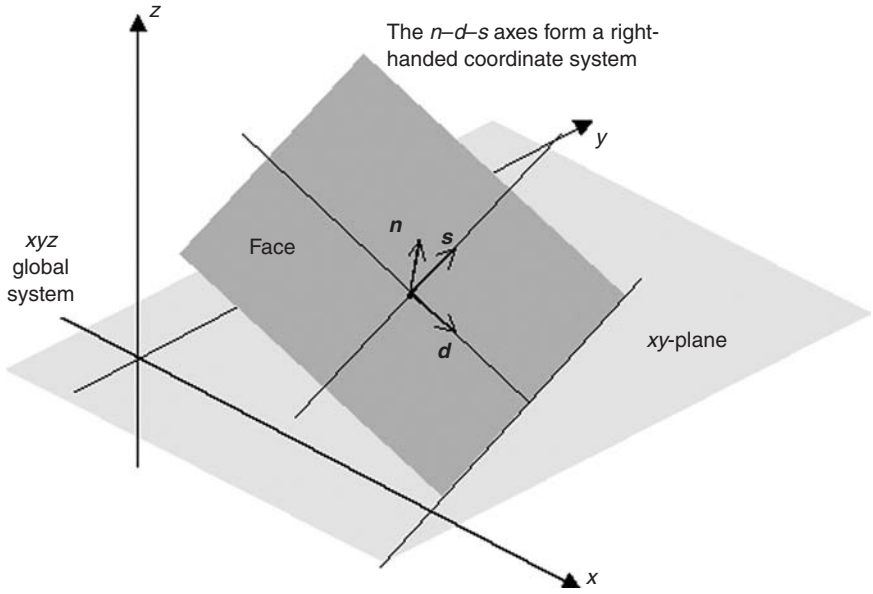

Figure 2.11 Local coordinate system defined by *n* (normal direction), *d* (dip direction) and *s* (strike direction).

strike direction (parallel to the projected intersection between the *xy*-plane and the face). The *n–d–s* axes form a right-handed coordinate system.

To illustrate the key features of rigid element analysis in a simple way, we restrict our attention on 2D computation in this chapter. In the 2D case, any point has two degrees of freedom, the *x* and *y* displacements denoted as u_x and u_y. Each rigid element is associated with a three-dimensional vector $\boldsymbol{u}_g$ of displacement variables at its centroid (similar to the discontinuous deformation analysis (DDA) by Shi, 1996, Cheng, 1998 and Cheng and Zhang, 2000, 2002), that is, the rigid element has both translational displacements u_{xg} and u_{yg}, and rotational displacement $u_{\theta g}$. The displacements at any point $P(x, y)$ of an interface in the global coordinate system can then be written as

$$\boldsymbol{u} = \boldsymbol{N}\boldsymbol{u}_g \tag{2.30}$$

$$\text{where} \qquad \boldsymbol{u} = [\,u_x \quad u_y\,]^{\mathrm{T}};\ \boldsymbol{u}_g = [\,u_{xg} \quad u_{yg} \quad u_{\theta g}\,]^{\mathrm{T}} \tag{2.31}$$

$$\boldsymbol{N} = \begin{bmatrix} 1 & 0 & y_g - y \\ 0 & 1 & x - x_g \end{bmatrix} \tag{2.32}$$

Superscript T denotes transpose; x_g and y_g are the abscissa and ordinate values of the centroid of the element, respectively; $\boldsymbol{N}$ is termed shape function.

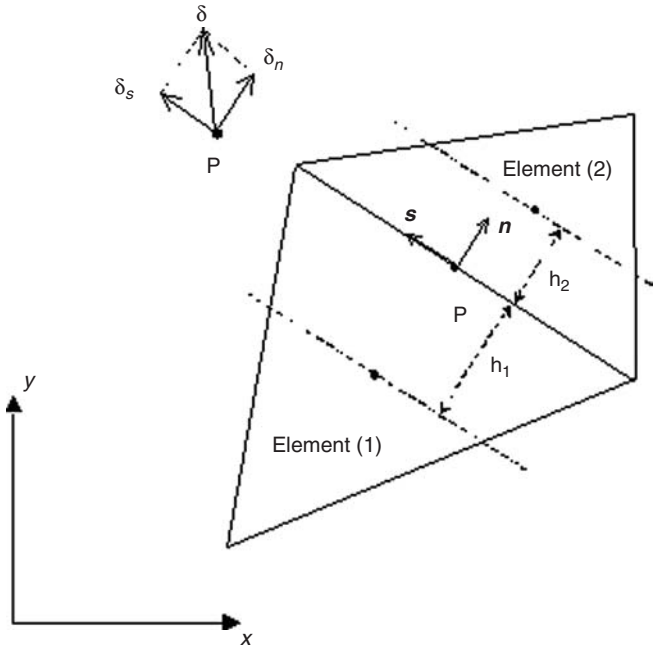

Figure 2.12 Two adjacent rigid elements.

As shown in Figure 2.12, the relative displacement $\boldsymbol{\delta}$ at a point P can be decomposed into two components in the n-axis and s-axis:

$$\boldsymbol{\delta} = [\,\delta_n \quad \delta_s\,]^{\mathrm{T}} \tag{2.33}$$

The relative displacement $\boldsymbol{\delta}$ can be further represented by

$$\boldsymbol{\delta} = -\boldsymbol{L}^{(1)}(\boldsymbol{N}^{(1)}\boldsymbol{u}_g^{(1)} - \boldsymbol{N}^{(2)}\boldsymbol{u}_g^{(2)}) \tag{2.34}$$

where the subscripts (1) and (2) denote elements (1) and (2), respectively; $\boldsymbol{L}^{(1)}$ is the matrix of direction cosines of the local n–s axes on the interface of Element (1) with respect to the global coordinate system and is expressed by

$$\boldsymbol{L}^{(1)} = \begin{bmatrix} \cos(\boldsymbol{n},\boldsymbol{x}) & \cos(\boldsymbol{n},\boldsymbol{y}) \\ \cos(\boldsymbol{s},\boldsymbol{x}) & \cos(\boldsymbol{s},\boldsymbol{y}) \end{bmatrix} \tag{2.35}$$

2.5.2 Contact stresses between rigid elements

From elasticity theory, the relation of the contact stress and displacement in the REM is expressed as

$$\boldsymbol{\sigma} = \boldsymbol{D}\boldsymbol{\delta} \tag{2.36}$$

$$\boldsymbol{\sigma} = [\sigma_n \quad \tau_s]^{\mathrm{T}} \tag{2.37}$$

$$\boldsymbol{D} = \begin{bmatrix} d_n & 0 \\ 0 & d_s \end{bmatrix} \tag{2.38}$$

$\boldsymbol{D}$ is termed the elasticity matrix, and for the plane strain problem it is given by

$$\begin{cases} d_n = \dfrac{E_1 E_2}{E_1 h_2 (1-\mu_2^2) + E_2 h_1 (1-\mu_1^2)} \\ d_s = \dfrac{E_1 E_2}{2E_1 h_2 (1+\mu_2) + 2E_2 h_1 (1+\mu_1)} \end{cases} \tag{2.39}$$

For the plane stress problem, it is given by

$$\begin{cases} d_n = \dfrac{E_1 E_2}{E_1 h_2 + E_2 h_1} \\ d_s = \dfrac{E_1 E_2}{2E_1 h_2 (1+\mu_2) + 2E_2 h_1 (1+\mu_1)} \end{cases} \tag{2.40}$$

where h_1 and h_2 are the distances from the centres of the two elements to the interface shown in Figure 2.12; E_1 and E_2 are the elastic moduli; and μ_1 and μ_2 are Poisson ratios of the materials to which elements (1) and (2) belong, respectively.

An interface is called a restriction interface while it is subjected to a certain displacement restriction, for example, a fixed interface or a symmetric interface. Such an interface also has contributions to the global stiffness matrix. For example, for a fixed interface

$$\text{Plane stress:} \quad d_n = \frac{E_1}{h_1(1-\mu_1^2)}; \quad d_s = \frac{E_1}{2h_1(1+\mu_1)} \tag{2.41}$$

$$\text{Plane strain:} \quad d_n = \frac{E_1}{h_1}; \quad d_s = \frac{E_1}{2h_1(1+\mu_1)} \tag{2.42}$$

$$\text{For a symmetric plane stress interface:} \quad d_n = \frac{E_1}{h_1(1-\mu_1^2)}; \quad d_s = 0 \tag{2.43}$$

$$\text{For a symmetric plane strain interface:} \quad d_n = \frac{E_1}{h_1}; \quad d_s = 0 \tag{2.44}$$

2.5.3 Principle of virtual work

The previous section describes how all the important quantities can be expressed in terms of the displacements of the element centroid. These relationships can be

used to derive the rigid element stiffness matrix. The principle of virtual work states that when a structure is in equilibrium the external work done by any virtual displacement is equal to the internal energy dissipation. For the REM, the deformation energy of the system is stored only at the interfaces between the rigid elements. The rigid element itself has no strain and thus there is no internal energy dissipation within the element. The virtual work done by the traction force at the interface can be viewed as an external work for the observed element. The total virtual external work done is the sum of the work done by the individual elements. The virtual work equation can be written as

$$\sum_e \left[\iiint_{\Omega_e} \delta \boldsymbol{u}^{\mathrm{T}} \boldsymbol{F} \mathrm{d}\Omega + \iint_{S_\sigma^e} \delta \boldsymbol{u}^{\mathrm{T}} \boldsymbol{X} \mathrm{d}S \right] + \sum_e \iint_{S_0^e} \delta \boldsymbol{u}_l^{\mathrm{T}} \boldsymbol{\sigma} \mathrm{d}S = 0 \tag{2.45}$$

where $\boldsymbol{F}$ and $\boldsymbol{X}$ are body forces and boundary loadings; u_l is the interface displacement represented in the local reference coordinate system; and S and Ω are the surface and volume of the structure body, respectively.

Using eqs (2.34) and (2.36) in eq. (2.45) gives:

$$\begin{aligned} &\sum_e \delta \boldsymbol{u}_g^{(1)^{\mathrm{T}}} \iint_{s_0^e} \boldsymbol{N}^{(1)^{\mathrm{T}}} \boldsymbol{L}^{(1)^{\mathrm{T}}} \boldsymbol{D} \boldsymbol{L}^{(1)} (\boldsymbol{N}^{(1)} \boldsymbol{u}_g^{(1)} - \boldsymbol{N}^{(2)} \boldsymbol{u}_g^{(2)}) \mathrm{d}S \\ &\quad = \sum_e \delta \boldsymbol{u}_g^{\mathrm{T}} \left[\iiint_{\Omega_e} \boldsymbol{N}^{\mathrm{T}} \boldsymbol{F} \mathrm{d}\Omega + \iint_{s_\sigma^e} \boldsymbol{N}^{\mathrm{T}} \boldsymbol{X} \mathrm{d}S \right] \end{aligned} \tag{2.46}$$

In REM formulations, we introduce a selection matrix $\boldsymbol{C}_e$ for each element which is defined by

$$\boldsymbol{u}_g = \boldsymbol{C}_e \boldsymbol{U} \tag{2.47}$$

and for element i, $\boldsymbol{C}_{ie}$ is given by

$$\boldsymbol{C}_{ie} = \begin{bmatrix} 0 & \dots & \overbrace{1}^{3i-2} & \overbrace{0}^{3i-1} & \overbrace{0}^{3i} & \dots & 0 \\ 0 & \dots & 0 & 1 & 0 & \dots & 0 \\ 0 & \dots & 0 & 0 & 1 & \dots & 0 \end{bmatrix} \tag{2.48}$$

where $\boldsymbol{U}$ is the global displacement matrix

$$\boldsymbol{U} = \left[\boldsymbol{u}_g^{(1)}, \boldsymbol{u}_g^{(2)}, \dots \right]^{\mathrm{T}} \tag{2.49}$$

Using the notations given by eqs (2.50) and (2.51), eq. (2.46) can be written as

$$\boldsymbol{C}_e{}^* = \left[\boldsymbol{C}_e^{(1)} \quad -\boldsymbol{C}_e^{(2)} \right]^{\mathrm{T}} \tag{2.50}$$

$$\boldsymbol{N}^* = \left[\boldsymbol{N}^{(1)} \quad \boldsymbol{N}^{(2)} \right] \tag{2.51}$$

$$\delta \boldsymbol{U}^{\mathrm{T}} \left[\sum_{e} \boldsymbol{C}_{e}^{(1)\mathrm{T}} \iint_{S_0^e} \boldsymbol{N}^{(1)^{\mathrm{T}}} \boldsymbol{L}^{(1)^{\mathrm{T}}} \boldsymbol{D} \boldsymbol{L}^{(1)} \boldsymbol{N}^{*} \, \mathrm{d}S \cdot \boldsymbol{C}_{e}^{*} \right] U$$

$$= \delta \boldsymbol{U}^{\mathrm{T}} \left[\sum_{e} \boldsymbol{C}_{e}^{\mathrm{T}} \left[\iiint_{\Omega_e} \boldsymbol{N}^{\mathrm{T}} \boldsymbol{F} \mathrm{d}\Omega + \iint_{s_\sigma^e} \boldsymbol{N}^{\mathrm{T}} \boldsymbol{X} \mathrm{d}S \right] \right] \tag{2.52}$$

2.5.4 Governing equations

Considering the arbitrary feature of a virtual displacement $\delta \boldsymbol{U}$ in eq. (2.52), the governing equation can be given in the form

$$\boldsymbol{K}\boldsymbol{U} = \boldsymbol{R} \tag{2.53}$$

$$\boldsymbol{K} = \sum \boldsymbol{C}_{e}^{*\mathrm{T}} \boldsymbol{k}_i \boldsymbol{C}_{e}^{*} \tag{2.54}$$

$$\boldsymbol{k}_i = \iint_{s_i} \boldsymbol{N}^{*\mathrm{T}} \boldsymbol{L}^{(1)^{\mathrm{T}}} \boldsymbol{D} \boldsymbol{L}^{(1)} \boldsymbol{N}^{*} \, \mathrm{d}s \tag{2.55}$$

$$\boldsymbol{R} = \sum_{e} \boldsymbol{C}_{e}^{\mathrm{T}} \boldsymbol{R}^{e} \tag{2.56}$$

$$\boldsymbol{R}^{e} = \iiint_{\Omega_e} \boldsymbol{N}^{\mathrm{T}} \boldsymbol{F} \mathrm{d}\Omega + \iint_{s_\sigma^e} \boldsymbol{N}^{\mathrm{T}} \boldsymbol{X} \mathrm{d}S \tag{2.57}$$

$\boldsymbol{K}$ and $\boldsymbol{R}$ are the global stiffness matrix and global force matrix, respectively; $\boldsymbol{k}_{\mathrm{i}}$ is the stiffness matrix of each interface; and $\boldsymbol{R}^{\mathrm{e}}$ is the force matrix at the centroid of the rigid element.

2.5.5 General procedure of the REM computation

The REM is a numerical procedure for solving engineering problems. Linear elastic behaviour is assumed here. The six steps of the REM analysis are summarized as follows:

1 Discretize the domain – this step involves subdividing the domain into elements and nodes. As one of the main components of the REM is the interface, it is necessary to set up the topological relations of nodes, elements and interfaces.
2 Select the element centroid displacements as primary variables – the shape function and elastic matrix need to be set up.
3 Calculate the global loading matrix – this will be done according to eqs (2.56) and (2.57).
4 Assemble the global stiffness matrix – this will be done according to eqs (2.54) and (2.55) after calculating the stiffness matrix for each interface.

5 Apply the boundary conditions – add supports and applied loads and displacements.
6 Solve the global equations – to obtain the displacement of each element centroid. The relative displacement and stress of each interface can then be obtained according to eqs (2.34) and (2.36), respectively.

2.5.6 Relation between the REM and the slice-based approach

This section demonstrates that the present formulation based on the REM can be easily reduced to the formulations of other upper bound limit analysis approaches proposed by Michalowski (1995) and Donald and Chen (1997), respectively, where slice techniques and translational failure mechanics are used.

We herein purposely divide the failing mass of the soil into rigid elements in the same way as the case of inclined slices (or 2D wedges) considered in the upper bound limit analysis approach by Donald and Chen (1997). As shown in Figure 2.13, the rigid elements below the assumed failure surface ABCDE are fixed with zero velocities and thus called base elements. The index k denotes the element number, ϕ_k is the internal friction angle on the base interface (the interface between element k and the base element below) and ϕ_k the internal friction angle at the left interface (the interface between elements k and $k-1$) of the kth element, respectively. α_k is the angle of inclination of the kth element base from the horizontal direction (anti-clockwise positive) and β_k is the inclination angle of the kth element's left interface from the vertical direction (anti-clockwise positive). Suppose the kth element has a velocity $\boldsymbol{V}_k$ (magnitude denoted as V_k, with v_{xk} and v_{yk} in x and y directions, respectively) in the global coordinate system. Note here that, due to the assumption of a translational collapse mechanism, the rotation velocity of the kth element equals zero.

As shown in Figure 2.13(b), the direction cosine matrix of the base interface of the kth element with respect to the base element can be written as

$$\boldsymbol{L}^{(1)} = \begin{bmatrix} -\sin\alpha_k & \cos\alpha_k \\ -\cos\alpha_k & -\sin\alpha_k \end{bmatrix} \tag{2.58}$$

The relative velocity of the base interface, $\boldsymbol{V}_k'$, can be expressed as

$$\boldsymbol{V}_k' = \begin{bmatrix} v_{nk} \\ v_{sk} \end{bmatrix} = \begin{bmatrix} -v_{xk}\sin\alpha_k + v_{yk}\cos\alpha_k \\ -v_{xk}\cos\alpha_k - v_{yk}\sin\alpha_k \end{bmatrix} \tag{2.59}$$

As shown in Figure 2.13(b), the element k has the tendency to move leftward with respect to the base element. According to the Mohr–Coulomb failure criterion (or yield criterion for perfect plasticity material) and the associated flow rule, the relationship between the normal velocity magnitude (Δv_n) and tangential velocity magnitude (Δv_s) jumps across the discontinuity and can be written as

$$\Delta v_n = -|\Delta v_s|\tan\phi' \tag{2.60}$$

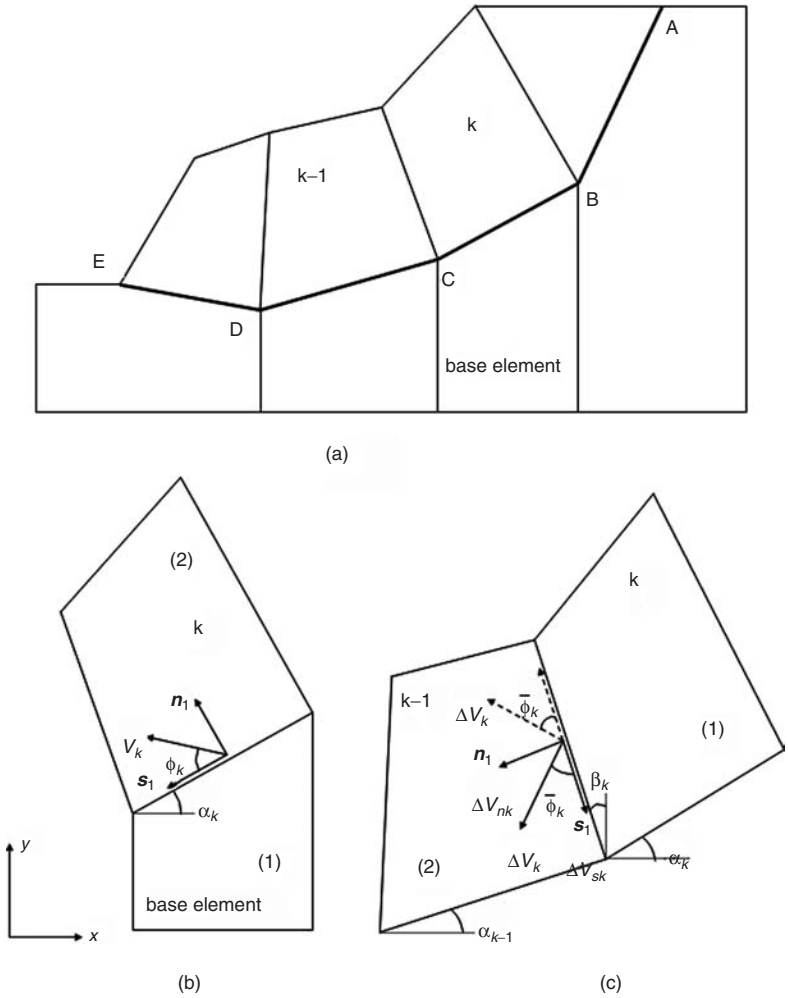

Figure 2.13 Failure mechanism similar to traditional slice techniques.

Using eq. (2.60), we have

$$\frac{v_{nk}}{v_{sk}} = \tan\phi_k \tag{2.61}$$

Thus, the following relationships can be obtained:

$$\begin{aligned} v_{xk} &= V_k \cos(\alpha_k - \phi_k) \\ v_{vk} &= V_k \sin(\alpha_k - \phi_k) \end{aligned} \tag{2.62}$$

Similarly, we can get

$$\begin{aligned} v_{x,k-1} &= V_{k-1}\cos(\alpha_{k-1}-\phi_{k-1}) \\ v_{y,k-1} &= V_{k-1}\sin(\alpha_{k-1}-\phi_{k-1}) \end{aligned} \tag{2.63}$$

From Figure 2.13(c), the direction cosine matrix of the left interface of the kth element with respect to the *(k – 1)*th element can be written as

$$L^{(1)} = \begin{bmatrix} -\cos\beta_k & -\sin\beta_k \\ \sin\beta_k & -\cos\beta_k \end{bmatrix} \tag{2.64}$$

Similarly, the relative velocity of the left interface of the kth element, ΔV_k, can be given in the form

$$\mathbf{\Delta V_k} = \begin{bmatrix} \Delta v_{nk} \\ \Delta v_{sk} \end{bmatrix} = \begin{bmatrix} \cos\beta_k(v_{xk}-v_{x,k-1}) & +\sin\beta_k(v_{yk}-v_{y,k-1}) \\ -\sin\beta_k(v_{xk}-v_{x,k-1}) & +\cos\beta_k(v_{yk}-v_{y,k-1}) \end{bmatrix} \tag{2.65}$$

From eq. (2.60), we can get

$$\frac{\Delta v_{nk}}{\Delta v_{sk}} = \pm\tan\overline{\phi}_k \tag{2.66}$$

where the case with a negative sign in the above equation coincides with the case where the *(k – 1)*th element has a tendency to move upward with respect to the kth element shown in Figure 2.13(c) with the dashed lines. It is noted that this case is identical to Case 1 defined in the method proposed by Donald and Chen (1997), and similarly the case with the positive mark in the above equation corresponds to Case 2 as discussed in Donald and Chen's method.

Putting eqs (2.62), (2.63) and (2.65) into eq. (2.66), we can get the following relationship:

$$V_k = V_{k-1}\frac{\cos[(\alpha_{k-1}-\phi_{k-1})-(\beta_k \mp \overline{\phi}_k)]}{\cos[(\alpha_k-\phi_k)-(\beta_k \mp \overline{\phi}_k)]} \tag{2.67}$$

With above eq. (2.67), and according to eq. (2.62), we can express v_{xk} and v_{yk} in terms of V_{k-1}

$$\begin{aligned} v_{xk} &= V_{k-1}\frac{\cos[(\alpha_{k-1}-\phi_{k-1})-(\beta_k \mp \overline{\phi}_k)]}{\cos[(\alpha_k-\phi_k)-(\beta_k \mp \overline{\phi}_k)]}\cos(\alpha_k-\phi_k) \\ v_{yk} &= V_{k-1}\frac{\cos[(\alpha_{k-1}-\phi_{k-1})-(\beta_k \mp \overline{\phi}_k)]}{\cos[(\alpha_k-\phi_k)-(\beta_k \mp \overline{\phi}_k)]}\sin(\alpha_k-\phi_k) \end{aligned} \tag{2.68}$$

Together with eq. (2.63), we put eq. (2.68) into (2.65) and then we have:

$$\Delta V_k = V_{k-1}\frac{\sin(\alpha_k-\phi_k-\alpha_{k-1}+\phi_{k-1})}{\cos[(\alpha_k-\phi_k)-(\beta_k \mp \overline{\phi}_k)]} \tag{2.69}$$

In the method proposed by Donald and Chen (1997), the velocities of 2D wedges can be determined by a hodograph:

$$V_r = V_l \frac{\sin(\theta_l - \theta_j)}{\sin(\theta_r - \theta_j)}$$
$$V_j = V_l \frac{\sin(\theta_r - \theta_l)}{\sin(\theta_r - \theta_j)} \tag{2.70}$$

Using the following definitions:

$$\theta_l = \pi + \alpha_l - \phi_{el}$$
$$\theta_r = \pi + \alpha_r - \phi_{er} \tag{2.71}$$

and

$$\theta_j = \frac{\pi}{2} - \delta + \phi_{ej} \quad \textit{for case } 1$$
$$\theta_j = \frac{3\pi}{2} - \delta - \phi_{ej} \quad \textit{for case } 2 \tag{2.72}$$

Variables V_l, V_r, V_j, α_l, ϕ_{el}, α_r, ϕ_{er} and ϕ_{ej} in Donald and Chen's approach are identical to those V_{k-1}, V_k, ΔV_k, α_{k-1}, α_k, ϕ_k and $\bar{\phi}_k$ defined in the present method, respectively. It should be noted that δ in their formulations equal to $-\beta_k$ in the present formulation, since the direction definition of δ (clockwise positive) is opposite to that of β_k used in the present method (anticlockwise positive).

Substituting V_{k-1}, V_k, ΔV_k, α_{k-1}, ϕ_{k-1}, α_k, ϕ_k, $\bar{\phi}_k$ and β_k into eq. (2.70), and keeping the consistency between corresponding cases in the two approaches, eq. (2.70) arrives at exactly the same form of eqs (2.67) and (2.69) in the proposed method.

In the method proposed by Michalowski (1995), vertical slices were employed. For vertical slices, β_k equals to zero, and eqs (2.67) and (2.69) can be reduced to the following two equations.

$$V_k = V_{k-1} \frac{\cos(\alpha_{k-1} - \phi_{k-1} - \bar{\phi}_k)}{\cos(\phi_k + \bar{\phi}_k - \alpha_k)} \tag{2.73}$$

$$\Delta V_k = V_k \frac{\sin(\phi_k - \phi_{k-1} - \alpha_k + \alpha_{k-1})}{\cos(\alpha_{k-1} - \phi_{k-1} - \bar{\phi}_k)} \tag{2.74}$$

It is noted that the above equations correspond to the case where the *(k – 1)*th element moves downward with respect to the *k*th element, that is, $\Delta V_{nk}/\Delta V_{sk} = \tan \bar{\phi}_k$. In such a case, the velocity relationships in the present method are identical to those under the translational failure mechanism in the method proposed by Michalowski (1995).

It has been proved above that the present formulations in the REM reduce to exactly the same formulations of the methods proposed by

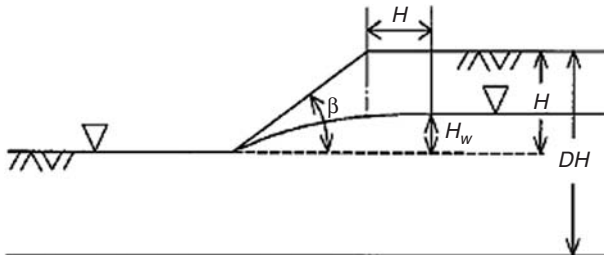

Figure 2.14 A simple homogeneous slope with pore water pressure.

Donald and Chen (1997) and Michalowski (1995) if the same slices with the same translational failure mechanism are used. In other words, the upper bound limit analyses using slices (or 2D wedges) may be viewed as a special and simple case of the formulation of the present method.

As shown in Figure 2.14, Kim *et al.* (1999) have studied the slope in nine cases with different depth factors D and slope inclinations β. In this study, we only take one case to investigate the feasibility of the present method, for example, consider the slope with depth factor $D = 2$, $H = 10$ m and $\beta = 45°$, and with soil properties $\gamma = 18$ kNm^{-3}, $c' = 20$ kNm^{-3} and $\phi' = 15°$. To assess the effects of pore water pressure, two locations of a water table with H_w = 4 and 6 m are considered in this study. Figure 2.15 shows three rigid finite element meshes (coarse, medium and fine meshes) used in the analysis, for the case of a water table $H_w = 6$ m. The relations between the number of rigid elements used in the mesh and calculated factor of safety, for the case of a water table $H_w = 4$ m and $H_w = 6$ m, are shown in Table 2.8.

2.6 Design figures and tables

For a simple homogeneous slope with geometry shown in Figure 2.17, the critical factor of safety can be determined from the use of a stability table instead of using a computer program. Stability tables and figures have been prepared by Taylor (friction circle), Morgenstern (Spencer method), Chen (limit analysis) and Cheng. In general, most of the results from these stability tables are closer. All the previous stability tables/figures are however designed for 2D problems. Cheng has prepared stability tables using both the 2D and 3D Bishop methods based on SLOPE 2000 which are given below (Tables 2.9 and 2.10).

For the 2D stability table by Cheng, the results are very close to those of Chen (1975) using a log-spiral failure surface. This also indicates that a circular failure surface is adequate to represent the critical failure surface

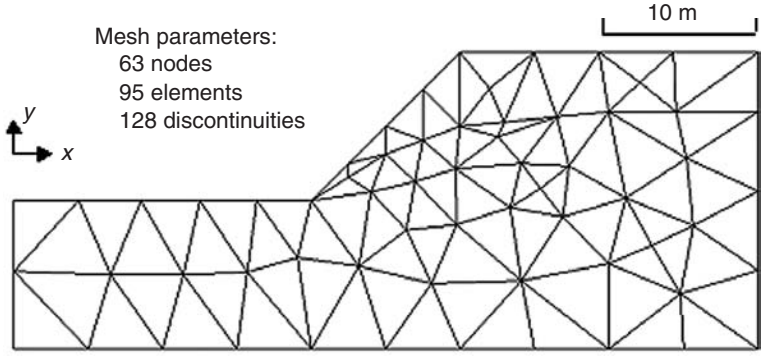

(a) Coarse mesh

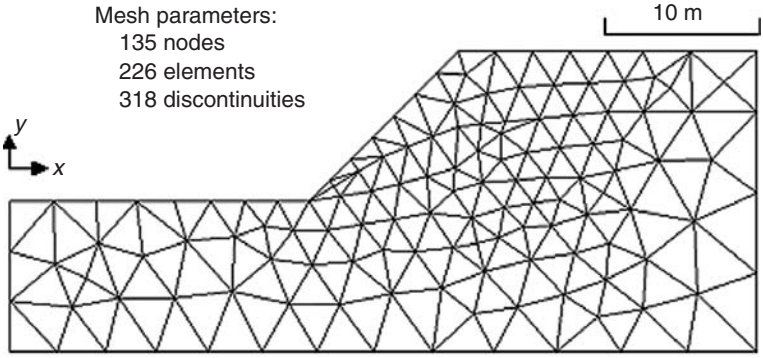

(b) Medium mesh

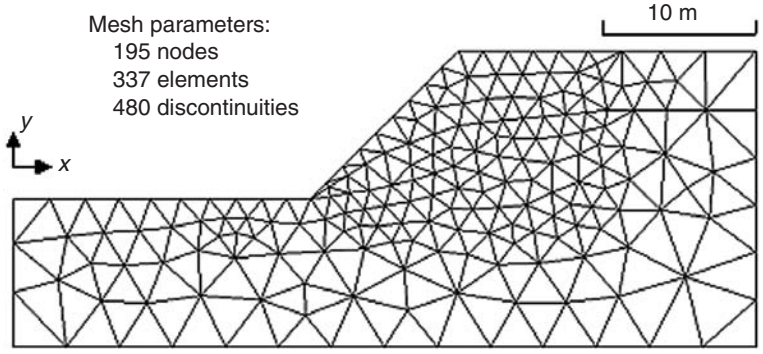

(c) Fine mesh

Figure 2.15 REM meshes – with H_w = 6 m: (a) coarse mesh, (b) medium mesh and (c) fine mesh.

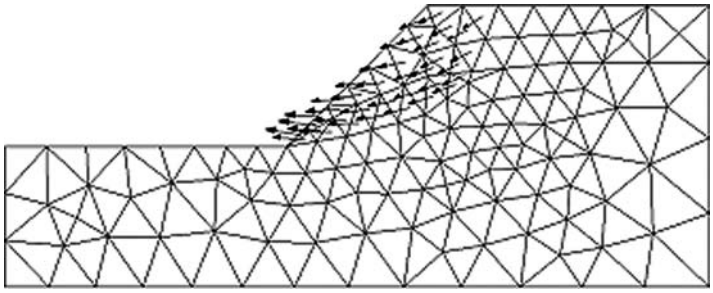

Figure 2.16 Velocity vectors (medium mesh).

Table 2.8 Comparisons of factors of safety for various conditions of a water table

H_w (m)	*Study by Kim et al. (1999)*			*Janbu chart (Janbu et al., 1956)*	*Present method (upper bound)*		
	Lower bound	*Bishop method (Bishop, 1955)*	*Upper bound*		*Coarse mesh*	*Medium mesh*	*Fine mesh*
4	1.036	1.101	1.166	1.030	1.403	1.276	1.202
6	0.971	1.036	1.068	0.973	1.284	1.162	1.096

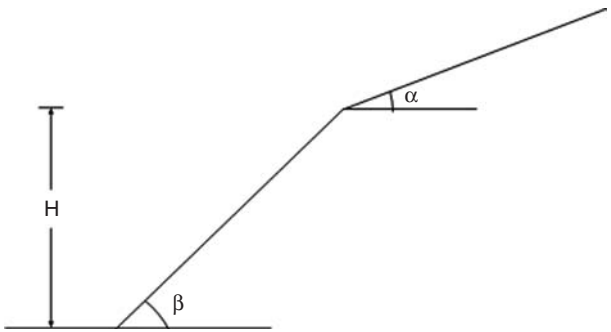

Figure 2.17 A simple slope for a stability chart by Cheng.

for a simple slope. When the slope angle and angle of shearing resistance are both small, the critical failure surface will be below the toe of the slope, which is equivalent to a deep-seated failure. Other than that, the critical failure surface will pass through the toe of the slope.

Table 2.9 Stability chart using 2D Bishop simplified analysis (* means below toe failure)

ϕ (°)	$\alpha\backslash\beta$ (°)	70	65	60	55	50	45	40	35	30	25	20	15
0	0	4.80	5.03	5.25	5.46	5.67	5.87	5.41*	5.43*	5.45*	5.43*	5.45*	5.46*
5	0	5.41	5.73	6.09	6.46	6.85	7.29	7.79	8.37	9.08*	9.97*	11.43*	14.38*
	5	5.30	5.63	5.96	6.32	6.70	7.11	7.59	8.14	8.77*	9.60*	10.96*	13.69*
10	0	6.05	6.52	7.09	7.71	8.40	9.21	10.22	11.54	13.45	16.62	23.14	45.57
	5	5.95	6.44	6.99	7.58	8.26	9.05	10.06	11.36	13.24	16.33	22.78	45.00
	10	5.84	6.33	6.86	7.41	8.07	8.83	9.78	11.11	12.84	15.79	21.90	42.86
15	0	6.94	7.58	8.37	9.36	10.50	11.94	13.90	16.79	21.69	32.14	69.23	—
	5	6.77	7.50	8.30	9.25	10.36	11.80	13.74	16.59	21.48	31.86	68.97	
	10	6.67	7.38	8.18	9.09	10.20	11.61	13.51	16.33	21.13	31.36	68.18	
	15	6.53	7.22	8.01	8.89	9.96	11.25	13.14	15.85	20.45	30.25	68.18	
20	0	7.97	9.01	10.14	11.61	13.51	16.07	20.00	26.67	41.38	94.74	—	
	5	8.04	8.91	10.04	11.50	13.38	15.93	19.82	26.55	41.10	94.74		
	10	7.69	8.82	9.92	11.35	13.22	15.76	19.61	26.28	40.72	93.75		
	15	7.60	8.66	9.75	11.16	12.97	15.49	19.25	25.79	40.18	92.78		
	20	7.59	8.44	9.55	10.91	12.66	15.06	18.71	25.00	38.54	88.24		
25	0	9.42	11.01	12.57	14.80	18.04	22.93	31.47	50.28	120.00	—		
	5	9.28	10.91	12.46	14.69	17.91	22.78	31.03	50.00	120.00			
	10	9.50	10.84	12.33	14.57	17.73	22.56	31.03	49.72	119.21			
	15	9.00	10.60	12.16	14.35	17.51	22.28	30.72	49.32	118.42			
	20	8.97	10.51	12.00	14.12	17.22	21.95	30.25	48.65	116.88			
	25	8.81	10.17	11.73	13.74	16.74	21.25	29.27	46.75	111.80			
30	0	11.89	13.79	16.07	19.65	25.53	35.64	58.63	144.00	—			
	5	11.54	13.74	16.00	19.52	25.35	35.64	58.44	144.00				
	10	11.43	13.75	15.83	19.35	25.17	35.43	58.25	144.00				
	15	11.04	13.53	15.65	19.19	25.00	35.16	57.32	142.86				
	20	10.71	13.31	15.49	18.95	24.66	34.75	57.32	142.29				
	25	10.81	12.93	15.23	18.60	24.19	34.16	56.60	140.63				
	30	10.43	12.11	14.86	18.09	23.44	32.97	54.22	134.33				
35	0	14.83	18.00	21.25	27.48	39.30	65.93	166.67	—				
	5	14.94	17.82	21.18	27.40	39.30	65.69	166.67					
	10	14.25	17.65	21.08	27.27	39.13	65.45	165.90					
	15	14.04	17.54	20.93	27.03	38.79	65.45	165.14					
	20	13.85	17.65	20.69	26.87	38.63	64.98	165.14					
	25	13.19	16.32	20.55	26.55	38.30	64.29	165.14					
	30	12.82	15.76	20.18	26.01	37.50	63.16	163.64					
	35	12.54	15.67	19.35	25.14	36.14	61.02	155.17					
40	0	20.07	24.03	30.10	42.35	72.29	185.57	—					
	5	19.13	23.68	29.41	42.06	72.00	185.57						
	10	19.82	23.72	29.27	42.35	71.43	185.57						
	15	18.95	23.53	30.28	41.86	71.43	183.67						
	20	17.61	23.38	29.32	41.47	71.43	183.67						
	25	16.93	23.23	28.85	41.10	70.87	183.67						
	30	16.36	22.70	28.57	40.72	70.04	181.82						
	35	16.04	21.05	28.13	40.00	68.97	180.00						
	40	15.72	20.00	27.69	38.46	65.93	171.43						

Table 2.10 Stability chart using 3D Bishop simplified analysis by Cheng (* means below toe failures)

ϕ (°)	$\alpha\backslash\beta$ (°)	70	65	60	55	50	45	40	35	30	25	20	15
0	0	6.16	6.43*	6.55*	6.67*	6.79*	6.92*	6.27*	6.25*	6.25*	6.25*	6.21*	6.15*
5	0	6.81	7.20	7.66	8.11*	8.57*	9.04*	9.52*	10.11*	10.84*	12.00*	13.74*	17.48*
	5	6.72	7.09	7.53	7.96*	8.41*	8.82*	9.23*	9.73*	10.47*	11.46*	13.14*	16.45*
10	0	7.74	8.20	8.96	9.78	10.71	11.69	12.86	14.52	16.82	20.69	29.03	58.06
	5	7.77	8.09	8.82	9.68	10.53	11.52	12.68	14.17	16.44	20.36	28.48	56.25
	10	7.63	7.99	8.70	9.50	10.29	11.26	12.33	13.74	15.93	19.57	27.27	53.25
15	0	9.23	9.78	10.65	11.92	13.33	15.25	17.65	21.43	27.69	41.10	90.00	—
	5	9.23	9.68	10.53	11.76	13.24	15.06	17.48	21.18	27.27	40.72	90.00	
	10	9.08	9.57	10.40	11.61	12.99	14.75	17.14	20.69	26.87	40.18	86.54	
	15	8.96	9.40	10.23	11.39	12.77	14.40	16.82	20.22	26.09	38.30	87.38	
20	0	11.39	11.84	13.28	15.13	17.22	20.45	25.35	33.96	52.94	124.14	—	
	5	11.46	11.84	12.90	15.03	17.14	20.22	25.35	33.96	52.94	122.45		
	10	11.39	11.69	12.77	14.52	16.98	20.00	25.00	33.33	51.72	121.62		
	15	11.07	11.54	12.59	14.42	16.67	19.78	24.66	32.73	51.43	118.42		
	20	10.17	11.39	12.41	13.95	16.32	19.19	23.97	31.86	49.18	112.50		
25	0	14.46	14.81	16.81	19.62	23.68	29.03	40.00	64.29	155.17	—		
	5	14.63	14.88	16.67	20.00	23.62	29.03	40.00	64.29	155.17			
	10	13.93	14.75	17.82	19.21	22.78	28.57	39.30	63.38	153.85			
	15	14.62	14.81	15.93	18.71	22.50	28.21	38.30	63.38	152.54			
	20	12.68	14.52	15.79	18.09	21.95	27.69	38.22	61.64	151.26			
	25	12.00	14.40	15.57	17.65	21.18	26.87	37.11	59.02	142.86			
30	0	18.56	18.95	21.95	28.13	33.33	45.23	75.00	187.50	—			
	5	18.37	18.91	21.63	28.13	33.33	45.23	75.00	183.67				
	10	18.56	18.93	21.18	28.13	32.85	45.00	73.77	183.67				
	15	17.79	18.87	20.93	25.64	32.61	44.33	72.00	183.67				
	20	16.29	18.95	20.69	24.39	32.73	44.12	72.58	183.67				
	25	15.25	18.65	20.22	24.00	31.03	43.27	72.00	176.47				
	30	14.63	17.14	20.16	23.38	29.51	41.67	69.23	168.22				
35	0	23.38	25.00	30.00	40.00	50.56	82.57	209.30	—				
	5	24.03	25.00	30.03	38.22	51.43	82.57	209.30					
	10	23.50	24.49	29.80	38.30	51.28	81.82	206.90					
	15	23.47	24.26	28.57	38.30	51.58	82.57	206.90					
	20	21.69	24.39	28.13	35.86	50.56	82.57	206.90					
	25	20.00	24.32	27.69	34.62	48.91	80.36	209.30					
	30	19.15	24.23	26.87	33.33	48.65	78.95	204.55					
	35	20.11	21.69	26.09	32.14	45.00	76.92	195.65					
40	0	29.95	34.09	45.23	60.40	90.91	236.84	—					
	5	30.00	33.64	43.90	58.06	90.00	236.84						
	10	30.15	33.33	43.90	60.00	90.00	233.77						
	15	30.86	32.73	41.47	59.21	90.00	233.77						
	20	30.82	32.26	40.91	59.41	90.00	230.77						
	25	28.13	32.14	39.13	59.02	88.24	230.77						
	30	26.47	32.49	38.30	54.55	85.71	227.85						
	35	25.55	33.09	37.50	51.43	86.54	227.85						
	40	22.73	28.57	36.79	48.65	84.11	214.29						

2.7 Method based on the variational principle or extremum principle

The most critical limitation of the LEM is the requirement on the inter-slice force function which is specified by the user before the analysis. To overcome this limitation, the lower bound method can be adopted. Based on the lower bound theorem, any statically admissible stress field not exceeding the yield will be a lower bound of the ultimate state. Pan (1980) has stated that the slope stability problem is actually a dual optimization problem, which is actually equivalent to the upper and lower bound but appears to be not well known outside China. On the one hand, the soil mass should redistribute the internal forces to resist the failure, which will result in a maximum factor of safety for any given slip surface. This is called the maximum extremum principle which is actually a lower bound method as demonstrated by Chen (1988). On the other hand, the slip surface with the minimum factor of safety is the most possible failure surface, which is called the minimum extremum principle. The minimum extremum principle is actually equivalent to the upper bound method which will be covered in Chapter 3. The maximum extremum principle is not new in engineering, and the ultimate limit state of a reinforced concrete beam is actually the maximum extremum state where the stresses in the compressive zone of the concrete beam redistribute until a failure mechanism is formed. The ultimate limit state design of a reinforced concrete beam under moment is equivalent to the maximum extremum principle. Pan's extremum principle (1980) can provide a practical guideline for the slope stability analysis, and it is very similar to the calculus of the variation method by Baker and Garber (1978), Baker (1980) and Revilla and Castillo (1977). This dual extremum principle is proved by Chen (1998) based on the lower and upper bound analysis, and is further elaborated with applications to rock slope problems by Chen *et al.* (2001a,b).

Pan (1980) has only stated a general extremum principle without providing an actual formulation suitable for numerical analysis. Baker's (1980) variational approach which is equivalent to the extremum principle is not suitable for application in complicated non-homogeneous problems or problems with soil reinforcement. Cheng *et al.* (2007c) have provided a discretized numerical formulation based on the extremum principle, and an improved global optimization scheme based on the particle swarm optimization algorithm (PSO) and harmony search (HS) by Cheng *et al.* (2007e,f) considered suitable for the extremum optimization analysis.

There are two possible approaches to implement the lower bound method or the maximum extremum principle: single factor of safety and different local factors of safety. The single factor of safety approach is covered in Section 2.9 while the varying local factor of safety approach is covered in this section. The actual failure of a slope is usually a progressive phenomenon. If the shear strength of a certain slice has been fully mobilized, the unbalanced forces will

distribute to the adjacent slices until a failure mechanism is formed. This process is called the progressive failure of slope. This may not be significant for work hardening materials, but can be very important for work softening materials. This phenomenon is well known, but is difficult to be considered by the classical LEM. Chugh (1986) presented a procedure for determining a variable factor of safety along the failure surface within the framework of the LEM. Chugh pre-defined a characteristic shape for the variation of the local factor of safety along a failure surface, and this idea actually follows the idea of the variable inter-slice shear force function in the Morgenstern–Price method (1965). The suitability of this variable factor of safety distribution function is however questionable, and there is no simple way to define this function for a general problem, as the local factor of safety should be mainly controlled by the local soil properties, topography and shape of failure surface.

Lam *et al.* (1987) proposed a limit equilibrium method for the study of the progressive failure in a slope under a long-term condition. His main idea involved the recognition of the local failure and the operation of the post-peak strength. This concept is one of the progressive failure phenomena which applies when the deformation is very large and there is a major reduction in the shear strength of soil, but this approach cannot be applied to the general progressive failure phenomenon.

Baker and Garber (1978), Baker (1980) and Revilla and Castillo (1977) have applied the calculus of variation to the determination of the factor of safety of a slope. Baker (1980) has also prepared design figures for simple slopes based on the variational principle. Although this principle requires very few assumptions with no convergence problems during the solution, it is difficult to be adopted when the geometry or the ground/loading conditions are complicated. Furthermore, for problems where the global minimum is not governed by the condition of the gradient of the objective function being zero (e.g. see Cheng, 2003), the global minimum will not be determined by the calculus of variation. The variational formulation by Baker (1980) was criticized by De Jong (1980, 1981) who argued that the stationary value may have an indefinite character rather than a minimum. Consequently, he concluded that the variational formulation is, in principle, meaningless, despite its apparent advantages. This conclusion was supported by Castilo and Luceno (1980, 1982) which was based on a series of counter-examples. Baker (2003) later incorporated some additional physical restrictions into the basic limiting equilibrium framework, and has verified that those restrictions guarantee that the slope stability problem has a well-defined solution (minimum). These restrictions are implied, without being explicitly stated, in all practical applications of this methodology, and under usual circumstances they do not change the solution of the problem (they are non-active constraints).

In the maximum extremum principle, the values and locations of the inter-slice forces are viewed as the control variables, and the group of

inter-slice forces satisfying static equilibrium will be optimized to determine the maximum factor of safety for a prescribed failure surface. Consider the slope shown in Figure 2.1; the soil mass between the potential slip surface and the ground surface is divided into n vertical slices, numbering from 1 to n and from left to right. The local factor of safety for slice i is defined as the ratio of the available shear strength along a slice base on the driving shear stress along the slice as:

$$F_s^i = \frac{N_i \tan \phi_i + c_i}{S_i} \tag{2.75}$$

where F_s^i is the local factor of safety for slice i, ϕ_i is the effective friction angle of the slice base, c_i equals $c_i' l_i$ and l_i is the base length of slice i. The total/global factor of safety is defined as the ratio of the available shear strength along the slip surface to the driving shear stress along the whole slip surface, and it is given by eq. (2.76) as:

$$F_s = \frac{\sum_{i=1}^{n} (N_i \tan \phi_i + c_i)}{\sum_{i=1}^{n} S_i} \tag{2.76}$$

If the magnitude and locations of the internal forces are taken as the control variables and F_s defined by eq. (2.76) is optimized, the internal forces and the local/global factors of safety can be evaluated without defining a $f(x)$. This idea was recently developed by Cheng *et al.* (2007c), which takes two forms: Ailc and Aglc. In Ailc, the local factor of safety can take any arbitrary value greater than 0. In Aglc, the minimum factor of safety on each slice is maintained to be 1.0 by distributing the residual force/moment to adjacent slices. In doing so, the residual strength approach by Lam *et al.* (1987) can be adopted easily. In formulating the optimization process, the upper and lower bounds of the control variables have to be controlled within acceptable limits, otherwise unreasonable results can appear from the optimization process.

Consider the problems shown in 2.9; the use of the present extremum principle gives a factor of safety of 1.876 and 1.86 for Ailc and Aglc analyses. The line of thrust for this problem is determined from the optimization analysis and is shown in Figure 2.18, while the local factor of safety along the failure surface is shown in Figure 2.19. It is noticed that the local factor of safety for the Ailc formulation has a higher fluctuation than the Aglc formulation, which is true for other examples as well.

Sarma and Tan (2006) have assumed that the factor of safety along the interfaces between slices is unity at all the interfaces. The limit analysis by Chen (1975) and Chen *et al.* (2001a,b) also implicitly assumes this factor of safety to be unity. Chen *et al.* (2001a,b) have found that this factor of safety is not unity by using the rigid element method. The authors view that there is no strong theoretical background behind this assumption, and this assumption will be checked against the present formulation as well as the Spencer method.

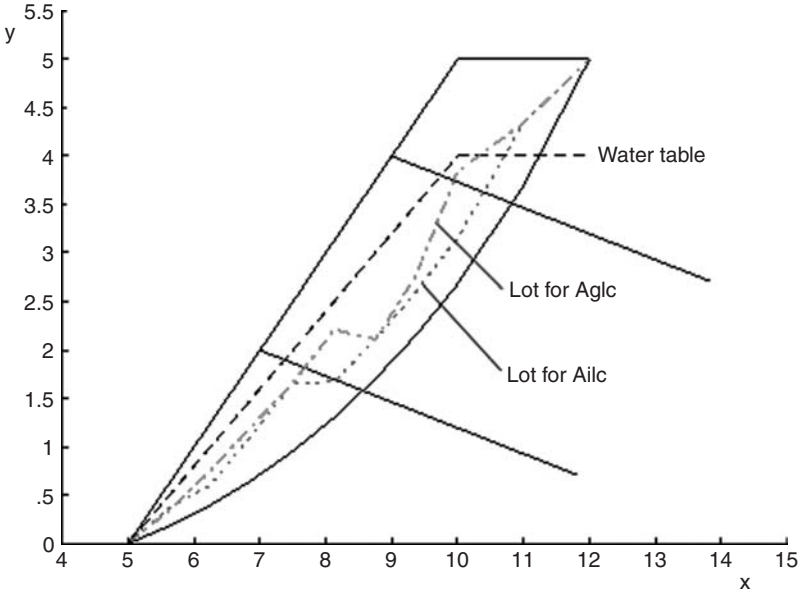

Figure 2.18 Line of thrust (LOT) computed from extremum principle for the problem in Figure 2.9.

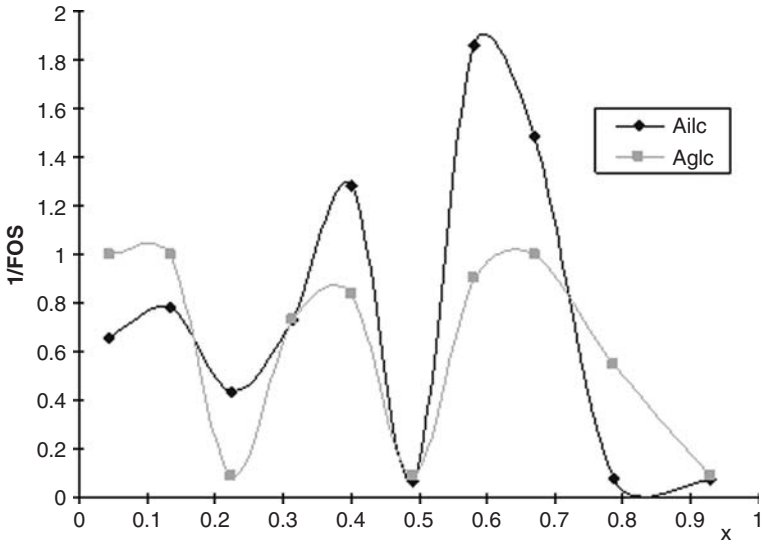

Figure 2.19 Local factor of safety along the failure surface for the problem in Figure 2.9.

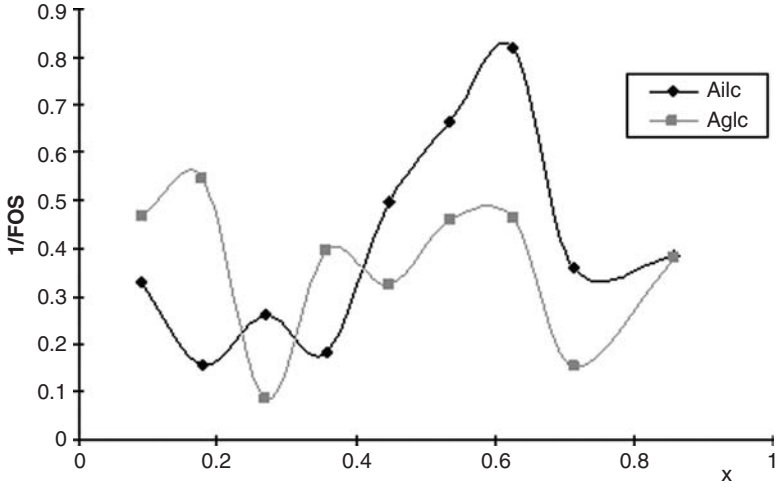

Figure 2.20 Local factor of safety along the interfaces for the problem in Figure 2.9.

The local factor of safety along the interface between two adjoining slices is defined as $\zeta_i = \dfrac{F_i \cos\beta_i \tan\phi_{vi} + C_{vi}}{F_i \sin\beta_i}$, where ϕ_{vi} is the average friction angle along the ith inter-slice and C_{vi} is the average cohesion along the ith inter-slice. It is however found that this interface factor of safety is much greater than unity as shown in Figure 2.20, which is greatly different from the assumption by Sarma and Tan (2006). If the Spencer method is used for this problem, the local factor of safety is also not equal to 1.0, and the assumption in limit analysis and the formulation by Sarma and Tan may not be applicable. In this respect, the present approach has the advantage of requiring less assumptions in the basic formulation. To avoid the violation of the Mohr–Coulomb relation along the interface, this relation can be added as a constraint in the optimization analysis which is available in SLOPE 2000.

2.8 Upper and lower bounds to the factor of safety and $f(x)$ by the lower bound method

The previous extremum principle assumes the factor of safety to be different among different slices. The extremum principle can also be formulated assuming a single factor of safety by utilizing the Morgenstern–Price method which is based on the force and moment equilibrium with an assumption of $f(x)$. Then the bounds to the actual factor of safety will be given by the upper

and lower bounds of the factor of safety arising from all combinations of $f(x)$. If a pattern search is used where 10 combinations are assigned for each $f(x)$, a problem with 11 slices will require 10^{10} combinations with tremendous computation and has hence never been tried in the past. This approach appears to be impossible until the modern artificial intelligence-based optimization methods are developed, which will be discussed in Chapter 3.

To determine the bounds of the factor of safety and $f(x)$, the slope shown in Figure 2.18 can be considered. For a failure surface with n slices, there are $n-1$ interfaces and hence $n-1$ control variables representing $f(x_i)$. $f(x)$ will lie within the range 0–1.0, while the mobilization factor l and the objective function FOS based on the Morgenstern–Price method will be determined for each set of $f(x_i)$. The maximum and minimum factors of safety of a prescribed failure surface satisfying force and moment equilibrium will then be given by the various possible $f(x_i)$ which requires the use of modern global optimization methods with the requirement given by eq. (2.77),

$$\text{Maximize (or minimize) FOS subject to } 0 \le f(x_i) \le 1.0 \text{ for all } i \quad (2.77)$$

In carrying out the optimization analysis as given by eq. (2.77), the constraints from the Mohr–Coulomb relation along the interfaces between slices as given by eq. (2.78) should be considered.

$$V \le P\tan\phi' + c'L, \quad (2.78)$$

where L is the vertical length of the interface between slices. The constraint by eq. (2.78) can have a major impact on λ but not the FOS, and this will be illustrated by the numerical examples in the following section. Since other than $f(x)$ the Morgenstern–Price method is totally governed by the force and moment equilibrium, the maximum and minimum factors of safety from varying $f(x)$ will provide the upper and lower bounds to the factor of safety of the slope which is not possible with the classical approach.

Cheng (2003) and Cheng and Yip (2007) have applied the simulated annealing method complying with eqs (2.77) and (2.78) to evaluate the bounds to the factor of safety and have coded the method into a general purpose commercially available program, SLOPE 2000. Consider the cases shown in Figures 2.4 and 2.9; the bounds to the factor of safety are given as 1.032/1.022 (Figure 2.4) and 1.837/1.826 (Figure 2.9) if eq. (2.78) is enforced. It is noticed that while for normal problems with no soil nail or external loads, the upper and lower bounds to the factor of safety are usually close so that $f(x)$ has a negligible effect on the analysis; the results for Figure 2.9 is extreme in that there is significant difference between the upper and lower bounds of the factors of safety. Based on lots of trial tests, the authors have found that this situation is rare but is not uncommon. The $f(x)$ associated with the maximum and minimum

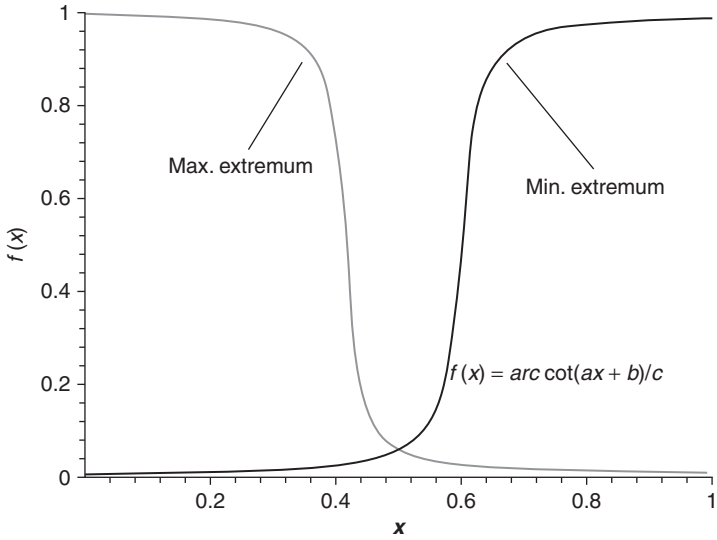

Figure 2.21 Simplified $f(x)$ for the maximum and minimum extrema determination.

extrema can be approximated by the relations shown in Figure 2.21, where $f(x)$ is plotted from the toe of slope to the crest of slope along the increasing x direction. It should be noted that this figure applies only to a simple slope passing through the toe of slope, and the slope has a level instead of inclined back. For a general slope with external load and soil nails, the use of a simple inter-slice force function is difficult, and the use of the numerical method available in SLOPE 2000 is recommended. A worked example in evaluating $f(x)$ by the lower bound method is given in the Appendix of this book.

The previous studies on convergence by Baker (1980) or by Cheng *et al.* (2008a) are mainly concerned with the numerical results instead of investigating the fundamental importance of $f(x)$. For a problem with a set of consistent and acceptable internal forces, the FOS must exist as it can be determined explicitly if the internal forces are known. Failure to converge will not occur if the double QR method is used, though the use of the iteration method may fail to converge due to the limitation of the mathematical method. If no FOS can be determined from the double QR method, this is equivalent to a consistent set of internal forces under the specified $f(x)$ not existing. If a problem fails to converge for a particular $f(x)$, a FOS can usually be found by tuning $f(x)$. Physically, it means that $f(x)$ cannot be arbitrarily assigned to a slope. If $f(x)$ is not associated with a consistent set

of internal forces, then that $f(x)$ is not acceptable. That means that $f(x)$ cannot be randomly specified or else there will be no consistent internal forces (and hence FOS) associated with the $f(x)$. The present approach provides a systematic way to determine $f(x)$ for an arbitrary problem, and convergence is virtually eliminated in the analysis. The basic trend of $f(x)$ shown in Figure 2.21 for the two extrema established by Cheng *et al.* (2007d) is good enough for practical purposes.

For the two extrema from the present analysis, the authors view that the maximum extremum should be taken as the factor of safety of the prescribed failure surface. As discussed, the internal forces within the soil mass should re-distribute until the maximum resisting capacity of the soil mass is fully mobilized, which is the lower bound approach. The present definition also possesses an advantage in that it is independent of the definition of $f(x)$. It is well known that there are cases where $f(x)$ may have a noticeable influence on the factor of safety. There is no clear guideline on the acceptance of the FOS due to the use of different $f(x)$. The use of the maximum extremum can also avoid this dilemma which has been neglected in the past. Using the lower bound approach, $f(x)$ is not an arbitrary function and can be uniquely determined, so the question on $f(x)$ can be viewed as settled as far as the lower bound theorem is concerned.

2.9 Finite element method

In the classical limit equilibrium and limit analysis methods, the progressive failure phenomenon cannot be estimated except for the method by Pan. Some researchers propose to use the finite element method to overcome some of the basic limitations in the traditional methods of analysis. At present, there are two major applications of the finite element in slope stability analysis.

The first approach is to perform an elastic (or elasto-plastic) stress analysis by applying the body force (weight) due to soil to the slope system. Once the stresses are determined, the local factors of safety can be determined easily from the stresses and the Mohr–Coulomb criterion. The global factor of safety can also be defined in a similar way by determining the ultimate shear force and the actual driving force along the failure surface. Pham and Fredlund (2003) have adopted the dynamic programming method to perform this optimization search, and they suggested that this approach can overcome the limitations of the classical limit equilibrium method. The authors however view that the elastic stress analysis is not a realistic picture of the slope at the ultimate limit state. In view of these limitations, the authors do not think that this approach is really better than the classical approach. It is also interesting to note that both the factor of safety and the location of the critical failure surface from such analysis are usually close to that by the limit equilibrium method. To adopt the elasto-plastic finite element slope stability analysis, one

precaution should be noted. If the deformation is too large so that the finite element mesh is greatly modified, the geometric non-linear effect may induce a major effect on the results. The authors have come across a case where the geometric non-linear effect has induced more than a 10 per cent change in the factor of safety. An illustration of this approach will be given in Chapter 4.

The second finite element slope stability approach is the strength reduction method (SRM). In the SRM, the gravity load vector for a material with unit weight γ_s is determined from eq. (2.79) as:

$$\{f\} = \gamma_s \int [N]^{\mathrm{T}} \mathrm{dv} \tag{2.79}$$

where $\{f\}$ is the equivalent body force vector and $[N]$ is the shape factor matrix. The constitutive model adopted in the non-linear element is usually the Mohr–Coulomb criterion, but other constitutive models are also possible, though seldom adopted in practice. The material parameters c' and ϕ' are reduced according to

$$c_{\mathrm{f}} = c'/F; \quad \phi_{\mathrm{f}} = \tan^{-1}\{\tan(\phi'/F)\} \tag{2.80}$$

The factor of safety F keeps on changing until the ultimate state of the system is attained, and the corresponding factor of safety will be the factor of safety of the slope. The termination criterion is usually based on one of the following:

1 the non-linear equation solver cannot achieve convergence after a pre-set maximum number of iteration;
2 there is a sudden increase in the rate of change of displacement in the system;
3 a failure mechanism has developed.

The location of the critical failure surface is usually determined from the contour of the maximum shear strain or the maximum shear strain rate.

The main advantages of the SRM are as follows: (i) the critical failure surface is found automatically from the localized shear strain arising from the application of gravity loads and the reduction of shear strength; (ii) it requires no assumption on the inter-slice shear force distribution; (iii) it is applicable to many complex conditions and can give information such as stresses, movements and pore pressures which are not possible with the LEM. Griffiths and Lane (1999) pointed out that the widespread use of the SRM should be seriously considered by geotechnical practitioners as a powerful alternative to the traditional limit equilibrium methods. One of the important criticisms of the SRM is the relative poor performance of the finite element method in capturing the localized shear band formation. Although the determination of the factor of safety is relatively easy and consistent, many engineers find that it is not easy to determine the critical failure surfaces in some cases as the yield zone is spread over a

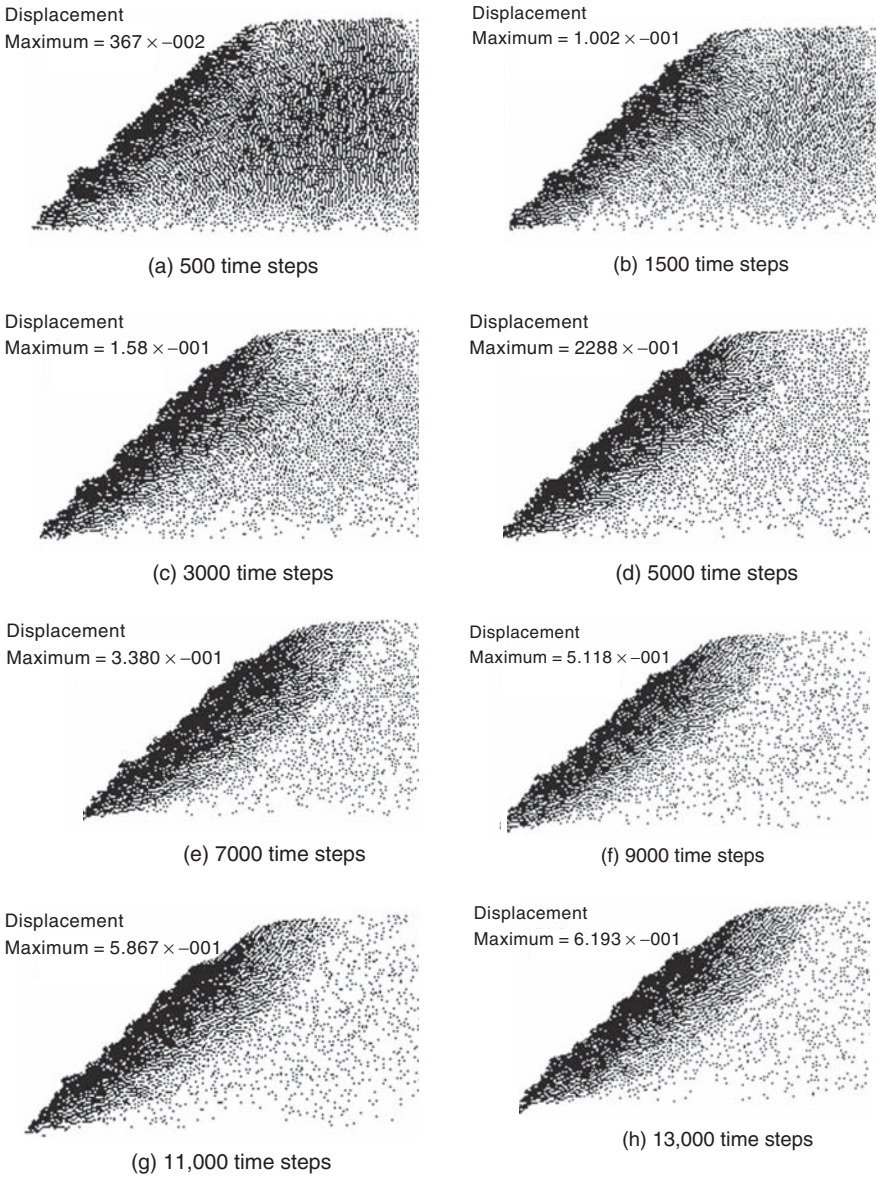

Figure 2.22 Displacement of the slope at different time steps when a 4 m water level is imposed.

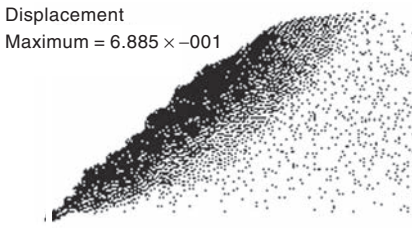

(i) 15,000 time steps

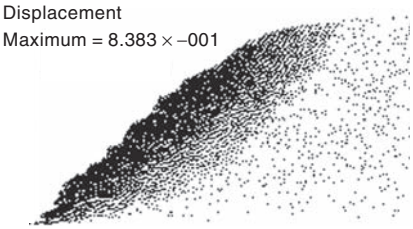

(j) 19,000 time steps

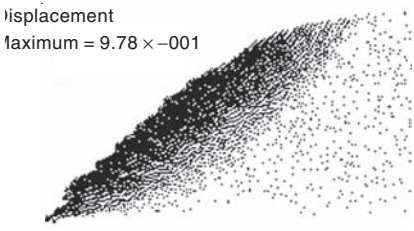

(k) 23,000 time steps

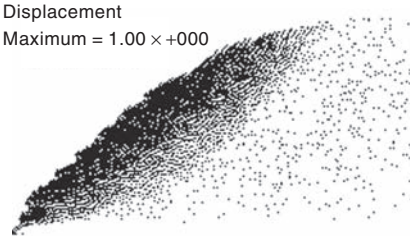

(l) 27,000 time steps

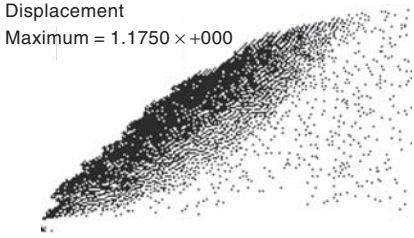

(m) 31,000 time steps

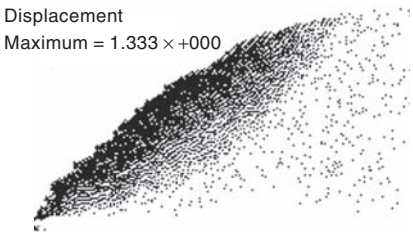

(n) 35,000 time steps

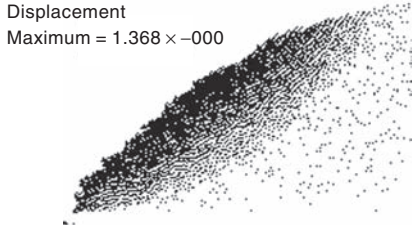

(o) 39,000 time steps

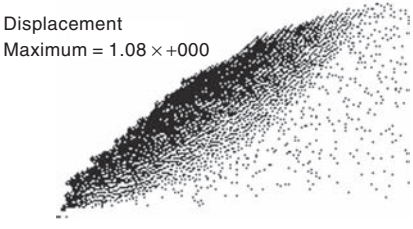

(p) 43,000 time steps

Figure 2.22 (*Continued*).

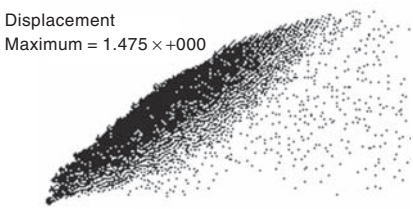

(q) 47,000 time steps

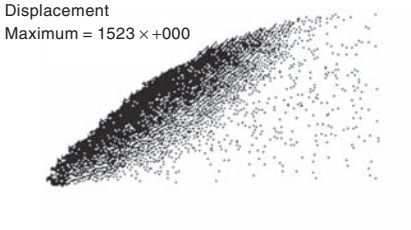

(r) 51,000 time steps

Figure 2.22 (*Continued*)

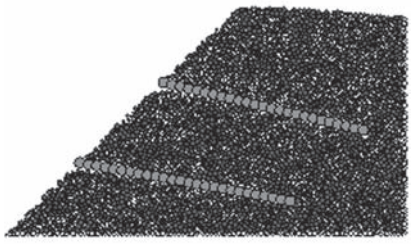

(a) 2 soil nails inclined at 10° installed

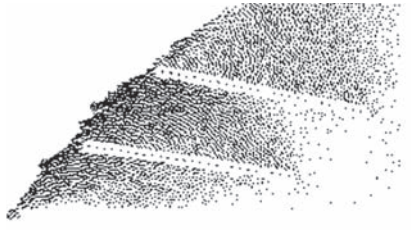

(b) Displacement field after 4 m water is imposed

Figure 2.23 Effect of soil nail installation. (a) Two soil nails inclined at 10° installed and (b) displacement field after 4 m water is imposed.

wide domain instead of localizing within a soft band. Other limitations of the SRM include the choice of an appropriate constitutive model and parameters, boundary conditions and the definition of the failure condition/failure surface, and the detailed comparison between the SRM and LEM will be given in Chapter 4.

2.10 Distinct element method

The finite element method which is based on continuity theory is not applicable after the failure has initialized. To assess the complete failure mechanism, the distinct element method can provide a qualitative assessment. Two distinct element approaches have been used by Cheng. A slope can be formed by an assembly of particles or triangular rigid blocks. To avoid the use of an excessive number of particles or rigid blocks which requires extensive computation time for analysis, a limited number in the

range of 10,000—100,000 is used by Cheng. Initially, the initial stress state of the system is generated from known soil mechanism principle. The vertical stress is practically equal to the overburden stress while the horizontal stress is evaluated by an assumed at-rest pressure coefficient. Once the initial state is established, the change of the water table/pore pressure or the application of external load will be applied to the system. The complete displacement history of the system from initial movement to a complete collapse can be qualitatively assessed. While the use of the distinct element method is difficult to provide a factor of safety for design, the collapse mechanism can be assessed which is not possible with all the classical methods as discussed.

The distinct element approach by Cheng (1998) can reproduce the results obtained by the classical analytical/numerical method. When the applied load is large enough, failure starts to initiate, which can be captured easily by the distinct element method but not the classical method. The limitations of the distinct element method in slope stability analysis include:

1 A very long computation time is required.
2 The contact material parameters for the contact cannot be assessed easily.
3 The classical soil parameters cannot be introduced directly in the particle form distinct element analysis.
4 Sensitivity of the method to the various parameters and modelling method.

As an illustration, a 5 m 45° slope is modelled with the distinct element method by imposing the initial condition in the first step (Figure 2.22). The vertical stress is basically equal to the overburden stress while an at-rest pressure coefficient 0.5 is employed in the present example. The unit weight of the particle is 17 kNm^{-3} while the friction factor is 0.5. Due to raining, a 4 m water table is established which is equivalent to a body force of -9.81 kNm^{-3} applied to the particle system. The slope finally collapses which is shown in Figure 2.22r. The results of the intermediate analysis shown in Figure 2.22 are actually interesting. When the number of time steps is small, no distinct failure zone can be observed. Starting from 3000 time steps, a failure zone is observed from the displacement vector plot, and this failure zone stops to expand at a time step of about 13,000. The failure domain is relatively stable over the remaining analysis and keeps moving until the slope finally collapses at a time step of 51,000. It should be noted that the failure mass moves above the stable zone which is basically constant after a time step of 13,000. The power of the distinct element is that while the ultimate limit state can be estimated from the limit equilibrium and finite element method, the final collapse mechanism or the flow of the failure mass can be estimated from the distinct element which is not possible with the classical methods. The results shown in Figure 2.22

are however qualitative and precise results for design are difficult to be determined from the distinct element method at present.

To stabilize the slope, two soil nails are added to the system shown in Figure 2.23a. The soil nails are modelled by a collection of particles connected together, and 4 m water is then applied to the system. The final displacement field is shown in Figure 2.23b, which indicates that the soil nails have effectively inhibited the collapse of the slope.

3 Location of critical failure surface, convergence and other problems

The various methods for the analysis of two-dimensional slope stability problems have been discussed in Chapter 2. There are other issues in slope stability analysis which have not been well addressed in the past, and some of these important issues will be addressed here.

3.1 Difficulties in locating the critical failure surface

According to the upper bound theory, any prescribed failure surface will be an upper bound to the true solution. For the critical failure surface which corresponds to the global minimum, some of the difficulties and interesting phenomena in locating the critical failure surface will be discussed. Consider a one-dimensional function $y = f(x)$ defined over a solution domain AB shown in Figure 3.1. The local minima where the gradients of the function are equal to 0 ($f'(x) = 0$) are given by points C and D, while the global minimum is defined by point E. If the y-ordinate of B is lower than the y-ordinate of E, point B will then be the global minimum, but the gradient of the function is not equal to 0 at B. Cheng (2003) has demonstrated that this situation can happen for a slope stability problem using an example from the ACADS (1989) study. For the multi-variable optimization analysis required by the slope stability problem, the factor of safety objective function is highly complicated, and the problem will be a complicated N-P hard type, which has attracted the attention of many researchers.

Another special feature about the critical failure surface for a simple slope is shown in Figure 3.2. There are only minor changes in the factors of safety if the trial failure surfaces fall within the shaded region as shown in Figure 3.2. In this respect, there is no strong need to determine the precise location of the critical failure surface if the geometry and ground conditions for a slope are simple. For complicated slopes or slopes with a soft band which will be illustrated in this chapter, it is however possible that a minor change in the location of the failure surface can induce a major change in the factor of safety. Under this case, the robustness of the optimization algorithm will be important for the success in locating the critical solution.

Failure surfaces can be divided into the circular and the non-circular failure surfaces. A circular failure surface is actually a sub-set of the non-circular

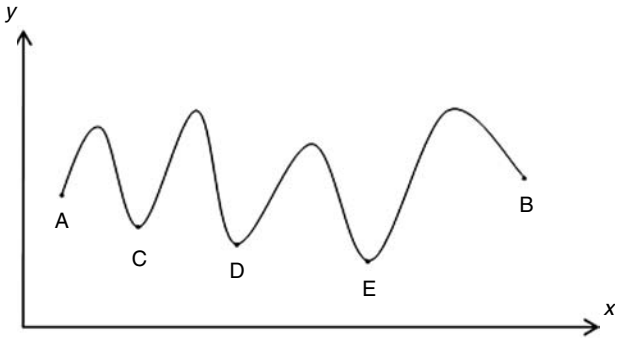

Figure 3.1 A simple one-dimensional function illustrating the local minima and the global minimum.

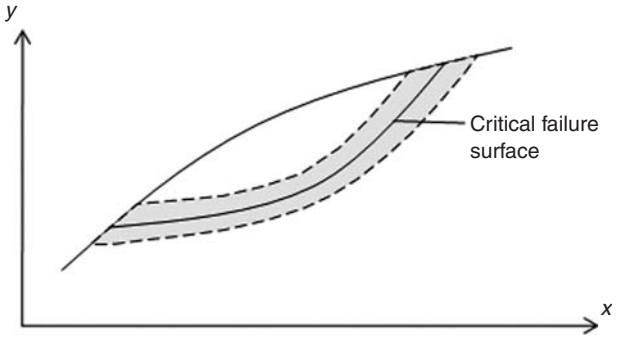

Figure 3.2 Region where factors of safety are nearly stationary around the critical failure surface.

failure surface, but it is useful because: (1) some stability formulations apply to the circular failure surface only and (2) the critical circular failure surface is a good approximation to the critical solution for some simple problems and is simple to be evaluated. For the circular failure surface, the location of the critical failure surface is usually determined by the method of grids shown in Figure 3.3. There are three control variables in this case: x and y ordinates of the centre of rotation and the radius of the failure surface. Each grid point is used as the centre of rotation while different radii are considered for the circular failure surface, and the minimum factor of safety from different radii is assigned to this grid point. Different factors of safety are hence assigned to different grid points, and the trend of the global minimum can be assessed by drawing the factor of safety contours from the factors of safety associated with the grid points. This method is robust and is simple to operate, but the accuracy will depend on the spacing between the grid points. The specified

grid must also be large enough to embrace all the possible local minima and the global minimum to obtain a clear picture about the distribution of the factor of safety. The grid method is simple to implement and is available in most of the commercial slope stability programs.

For the general non-circular failure surface, the number of control variables which is controlled by the number of points for the failure surface is usually much greater than three. To locate the critical failure surface, the geometric method similar to that for the circular failure surface will be very inefficient in application and requires a lot of effort in defining the solution domain for each control variable (though adopted by some commercial programs). Special features of the objective function of the safety factor F for this case include:

1 The objective function of the safety factor F is usually non-smooth, non-convex and discontinuous over the solution domain. Discontinuity of the objective function can be generated by: generation of an unacceptable failure surface; 'failure to converge' of the objective function; presence of obstructions in the form of a sheet pile, retaining wall, large boulders, a tension crack or others. Gradient-type optimization methods are applicable only to the continuous function and will break down if there are discontinuities in the objective function.
2 Chen and Shao (1988) have demonstrated that multiple minima similar to that shown in Figure 3.3 will exist in general. Duncan and Wright (2005) have also shown the existence of multiple local minima even for a simple homogeneous slope which is also illustrated by Cheng *et al.* (2007e). The local minimum close to the initial trial will be obtained by

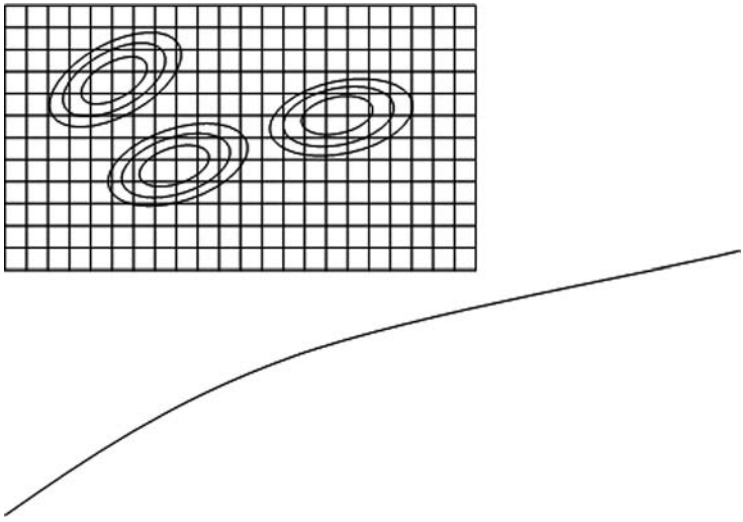

Figure 3.3 Grid method and presence of multiple local minima.

the classical gradient-type optimization methods. If an initial trial close to the global minimum is used, the global minimum can usually be found by classical methods, but a good initial trial is difficult to be established for a general multi-variable problem. The success of a global optimization algorithm to escape from the local minima for an initial solution far from the global minimum is crucial in the slope analysis problem.

3 A good optimization algorithm should be effective and efficient over different topography, soil parameters and loadings. The analysis should also be insensitive to the optimization parameters as well.

Various classical optimization methods for the non-circular failure surface have been proposed and used in the past. Baker and Garber (1978) have proposed the use of the variational principle, but this method is complicated even for a simple slope and is not adopted for practical problems. Moreover, if the gradient of the global minimum is not zero, the variational principle will miss the critical solution. Chen and Shao (1988) and Nguyen (1985) have suggested the use of the simplex method for this problem which is actually suitable only for linear problems. The simplex method has been adopted by the program EMU, developed by Chen, and it works fairly well for simple problems. The authors have however come across many complicated cases in China where manual interaction is required with the simplex method before a good solution can be found. The simplex method also fails to work automatically for cases where the local minimum and global minimum differ by a very small value but differ significantly in the location. Celestino and Duncan (1981) have adopted the alternating variable method while Arai and Tagyo (1985) and Yamagami and Jiang (1997) have adopted the conjugate-gradient method and dynamic programming, respectively. These classical methods are applicable mainly to continuous functions, but they are limited by the presence of the local minimum, as the local minimum close to the initial trial will be obtained in the analysis. There is also a possibility that the global minimum within the solution domain is not given by the condition that the gradient of the objective function $\nabla f = 0$, and a good example has been illustrated by Cheng (2003). The presence of the other local minima or the global minimum will not be obtained by the classical methods unless a good initial trial is adopted, but a good initial trial is difficult to be established for a general problem.

In view of the limitations of the classical optimization methods, the current approach to locate the critical failure surface is the adoption of the heuristic global optimization methods. The term heuristic is used for algorithms which find solutions among all the possible ones, but they do not guarantee that the best will be found; therefore, they may be considered as approximate and not accurate algorithms. These algorithms usually find a solution close to the best one, and they find it fastly and easily. Another important feature is that the requirement of human judgement or interaction should be minimized or even eliminated if possible, and the authors have come across some hydropower projects in China where there are several weak zones (strong local minima) for which nearly all existing methods fail to work well.

Greco (1996) and Malawi *et al.* (2001) have adopted the Monte Carlo technique for locating the critical slip surface with success for some cases, but there is no precision control on the accuracy of the global minimum. Zolfaghari *et al.* (2005) adopted the genetic algorithm while Bolton *et al.* (2003) used the leap-frog optimization technique to evaluate the minimum factor of safety. All of the above methods are based on the use of static bounds to the control variables, which means that the solution domain for each control variable is fixed and is pre-determined by engineering experience. Cheng (2003) has developed a procedure which transforms the various constraints and the requirement of a kinematically acceptable failure mechanism to the evaluation of upper and lower bounds of the control variables, and the simulated annealing algorithm is used to determine the critical slip surface. The control variables are defined with dynamic domains which are changing during the solution, and the bounds are controlled by the requirement of a kinematically acceptable failure mechanism. Through such an approach, there is no need to define the pre-determined static solution domain to each control variable based on engineering experience, and a precision control during the search for the critical solution will be possible.

There are two major aspects in the location of the critical failure surface which will be discussed in the following sections, and they are the generation of the trial failure surface and the global optimization algorithms for the search for the critical failure surface.

3.2 Generation of the trial failure surface

For the classical gradient-type optimization method, once an initial trial is defined the refinement of the critical failure surface will be given by the gradient of the objective function (which can be obtained by a simple finite difference operation). On the other hand, for the heuristic global optimization methods, trial failure surfaces are required to be generated which are controlled by the bounds for each control variable. Different methods in generating the failure surfaces have been proposed by Greco (1996), Malkwai *et al.* (2001), Cheng (2003), Cheng *et al.* (2007b,e,f), Bolton *et al.* (2003), Li *et al.* (2005) and Zolfaghari *et al.* (2005). In general, these methods are very similar in the basic operations. The coordinates of the points defining the failure surface are taken as the control variables, and lower and upper bounds are assigned to each control variable. Consider the failure defined by ABCDEF shown in Figure 3.4. If each control variable is defined over static lower and upper bounds, point D, which is unlikely to be acceptable for a normal problem, can be generated by the random number generator. Since segment CD will be a kink which hinders the development of the failure, D is highly unlikely to be acceptable except for some special cases which will be discussed later.

To generate a convex surface by the method proposed by Cheng (2003), consider a typical failure surface ACDEFB shown in Figure 3.5. The x-ordinates of the two exit ends A and B are taken as the control variables of the objective function and the upper and lower bounds of these two variables

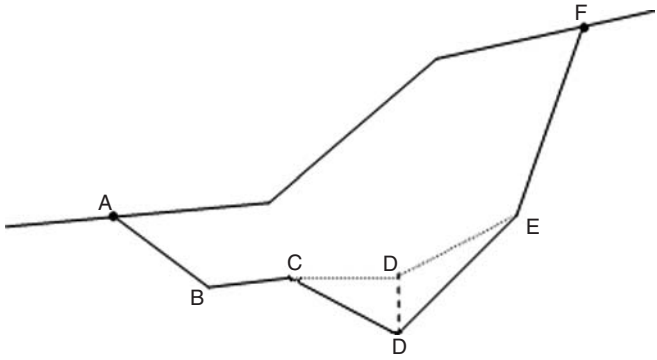

Figure 3.4 A failure surface with a kink or non-convex portion.

Source: Reproduced with permission of Taylor & Francis.

are specified by the engineer (bounds for the first two control variables are fixed). The static bounds for the first two control variables can be defined easily for the present problem with engineering experience. Once the two exit ends A and B of the failure surface are defined, the requirements on the kinematically acceptable mechanism can be implemented as:

1 The *x*-ordinates of the interior points C, D, E and F of the failure surface can be obtained by the uniform division of the horizontal distance between A and B which is Xright–Xleft. The *x*-ordinates of C, D, E and F are hence not control variables. Alternatively, the division can be made to follow the slope profile and the *x*-ordinates of the interior points are also not control variables.
2 Points A and B are connected and C1 is determined as a point located vertically above C. The *y*-ordinate of C1 is the lower value of either: (1) the *y*-ordinate of the ground profile as determined by the *x*-ordinate of C; (2) the *y*-ordinate of the point lying along the line joining points A and B and determined by the *x*-ordinate of C. C1 is the upper bound to the *y*-ordinate of the first inter-slice. The lower bound of the *y*-ordinate of C (third control variable) is set by Cheng (2003) as C1–AB/4. In fact, such a lower bound can allow for a deep-seated failure surface and is adequate for all the cases that Cheng has encountered. The lower bound of the *y*-ordinate of C can be set to C1–AB/5 (instead of C1–AB/4 which is a conservative estimation of the lower bound) in most situations without affecting the solution. The *y*-ordinate of point C is a control variable of the objective function and it is confined within the upper and lower bounds as determined in Step 2.
3 Once a *y*-ordinate of C is chosen in the simulated annealing analysis, it connects A and C and extrapolates the line to G which is defined by the *x*-ordinate of point D. The lower bound of the *y*-ordinate of point D will be point G to maintain a concave failure shape. The upper bound of D

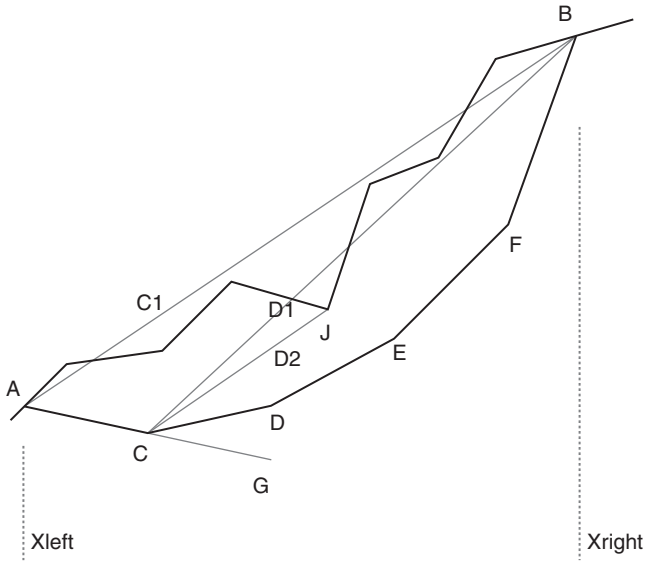

Figure 3.5 Generation of dynamic bounds for the non-circular surface.

Source: Reproduced with permission of Taylor & Francis.

which is D1 is determined in the same way as for point C1. If part of the ground profile lies below the line joining B and C and affects the determination of D1 (e.g. point J in Figure 3.5), it connects C and J instead of B and C and determines the upper bound as D2 instead of D1.

4 Perform Step 3 for the remaining points until all upper and lower bounds of the control variables are defined.

5 To allow for a non-concave failure surface which is unlikely to occur in reality, an option where the lower bound of point E will be set to a lower value as determined in Step 3 or the *y*-ordinate of point D is allowed. The *y*-ordinate of point E cannot be lower than that of D or else there will be a kink in the failure surface which prevents failure to occur. The lower bound to the *y*-ordinate is sometimes totally eliminated which is required for problems with a soft band. A non-convex failure surface can hence be generated from the present proposal by removing the lower bound requirement as required in the present method.

In Figure 3.5, the control variables are the *x*-ordinates of A and B the *y*-ordinates of points C, D, E and F. A control variable vector $\boldsymbol{X}$ is used to store these control variables and the order of the control variables must be in (X_A, X_B, Y_C, Y_D, Y_E, Y_F). For the location of the global minimum of the objective function, engineers need to define only the upper and lower bounds of the first two control variables. An initial trial will be determined in a way similar to the

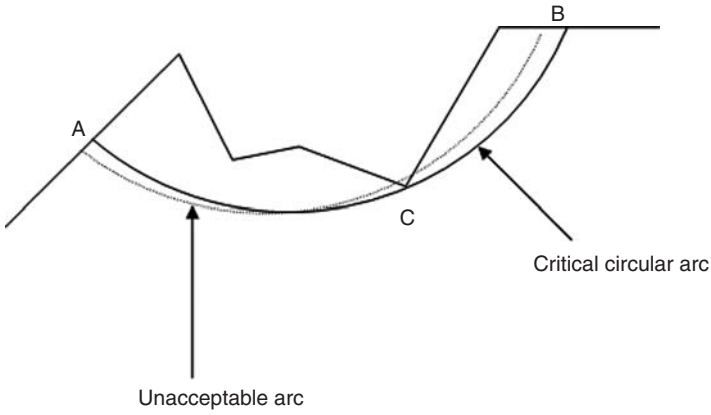

Figure 3.6 Dynamic bounds to the acceptable circular surface.

Source: Reproduced with permission of Taylor & Francis.

approaches shown above. The upper and lower bounds of the other control variables will then be calculated according to Steps 2 and 3. If the number of slices is n, then the number of control variables will be $n + 1$. If rock is encountered in the problem, the lower bound determination shown above has to be modified slightly. In Steps 2 and 3, the lower bound will either be the y-ordinate of point G or the y-ordinate of the rock profile as determined by the x-ordinate of D.

For the circular failure surface, there are only three control variables which are the x and y coordinates of the centre of rotation and the radius of the failure surface. Cheng (2003) however adopts the x-ordinates of the two exit ends and the radius of the failure surface as the three control variables in analysis as it is easier to define the upper and lower bounds for the two exit ends (see Figure 3.6). This approach is also used by many commercial programs. The control variable vector $\boldsymbol{X}$ will be (X_A, X_B, r). For the lower and upper bounds of the radius, the lower bound is set to half of the length of line AB which is the minimum possible radius. The upper bound of the radius is set to 50× AB (any value which is not too small will be acceptable). An unacceptable failure surface will not be generated in the analysis and the constraints will control the lower and upper bounds of the radius when the two exit ends are defined. The constraints include:

1 The failure surface cannot cut the ground profile at more than two points within the two exit ends. As seen in Figure 3.6, point C will control the upper bound of the radius.
2 The failure surface cannot cut into the rock stratum which will control the lower bound of the radius.
3 The y-ordinate of the centre of rotation is higher than the y-ordinate of the right exit end. For this case, the last slice cannot be defined. This constraint will also control the lower bound of the radius.

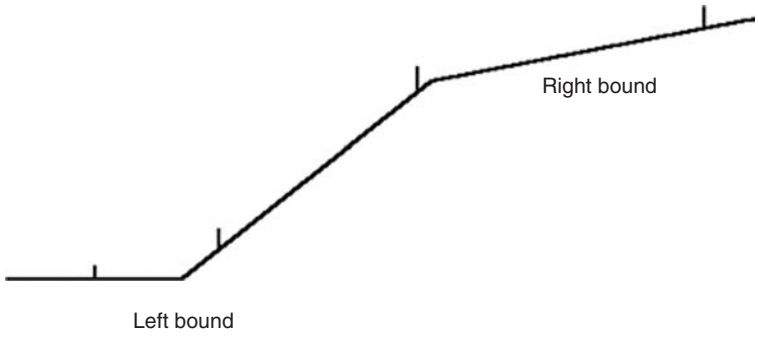

Figure 3.7 Domains for the left and right ends decided by engineers to define a search for the global minimum.

In the present method, the first two variables which are the x-ordinates for the left and right ends are varied within the user defined lower and upper bounds which are constant during the analysis. Besides these two variables, the bounds for the remaining variables (y-ordinates of the failure surface) are computed sequentially according to the guidelines shown above for circular and non-circular failure surfaces. The bounds from the present method are dynamic and are different from the classical simulated annealing methods or other global optimization methods where the bounds remain unchanged during the analysis. The generation of trial failure surfaces and the search direction will then proceed in accordance with the normal simulated annealing procedure and the global minimum can be located easily with a very high accuracy under the present proposal. The minimization process in the present formulation will depend on the lower and upper bounds of the left and right exit ends shown in Figure 3.7, which can be decided easily with experience and engineering principle. For inexperienced engineers, a wide range can be defined for the lower and upper bounds and the number of trials required for analysis will only increase slightly with the increase in the left and right ranges, which is another major advantage of the approach by Cheng (2003). For example, Cheng found that when the ranges for the left and right exit ends are increased by two times, the number of trials required will remain unchanged in many cases and may increase by less than 15 per cent in some rare cases.

In the present algorithm, the x-ordinates are not considered as the control variables to reduce the number of control variables. This is usually satisfactory as Cheng (2003) found that the y-ordinates are more important than the x-ordinates in the factor of safety. Cheng *et al.* (2008b) have also proposed that the x-ordinates can be adopted as the control variables. This approach will approximately double the number of control variables, and is considered to be useful only for those problems controlled by a soft band where the factor of safety is highly sensitive to the x-ordinates as well.

3.3 Global optimization methods

Global optimization problems are typically difficult to be solved, and in the context of combinatorial problems, they are often N-P hard type. The difficulties in performing the global optimization analysis and the requirement for a robust optimization algorithm have been discussed in Section 3.1. With the development of computer software and hardware, many artificial intelligence-based algorithms based on natural selection and the mechanisms of population genetics have been developed. These algorithms are commonly applied in pattern recognition, electronic, production/ control engineering or signal processing systems. These new heuristic optimization algorithms have been successfully applied to many different disciplines for both continuous and discrete optimization problems, but there are only limited uses of these methods in slope stability problems.

Since most of the heuristic algorithms which are artificial intelligence-based methods are relatively new and are not familiar to the geotechnical practitioners, a brief review on several simple but effective methods (with various improvements by Cheng *et al.*) will be given in this section. Readers can try the performance of all these optimization methods by using the demo SLOPE 2000 which is given in the Appendix. These modern optimization methods can be easily adapted to other types of geotechnical problems which are under consideration by Cheng.

3.3.1 Simulated annealing algorithm (SA)

The simulated annealing algorithm (Kirkpatrick, 1983) is a combinatorial optimization technique based on the simulation of a very slow cooling process of heated metal called annealing. The concept of this algorithm is similar to heating a solid to a high temperature, and cooling the molten material slowly in a controlled manner until it crystallizes, which is the minimum energy level of the system. The solution starts with a high temperature t_0, and a sequence of trial vectors are generated until the inner thermal equilibrium is reached. Once the thermal equilibrium is reached at a particular temperature, the temperature is reduced by using the coefficient λ and a new sequence of moves will start. This process is continued until a sufficiently low temperature t_e is reached, at which point no further improvement in the objective function can be achieved.

The flowchart of the SA is shown in Figure 3.8, where t_0, t_e and λ are the initial temperature, the stopping temperature and the cooling temperature coefficient, respectively. Usually, the higher the value of t_0, the lower will be the value of t_e and hence the smaller will be the value of λ; more trials will be required in the optimization analysis. The parameter N identifies the number of iterations for a given temperature to reach its inner thermal equilibrium, and the array $ft(neps)$ restores the objective function values obtained at the consecutive neps inner thermal equilibriums and to terminate the optimization algorithm. $\mathbf{V}_g$ and f_g are the best solution found so far and its associated objective function value. *Nit* is the number of iterations for the current temperature. r_s is a random number in the range [0,1], after N iterations

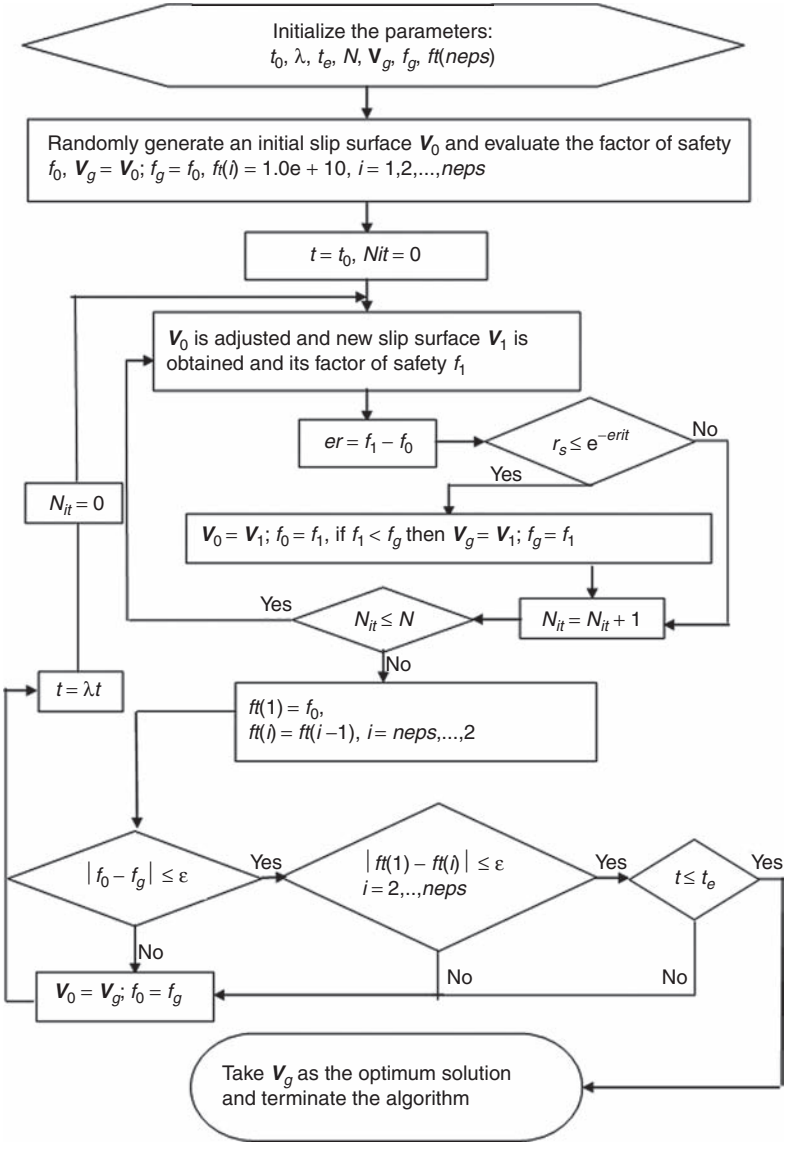

Figure 3.8 Flowchart for the simulated annealing algorithm.

are performed. If the termination criterion is not satisfied, $\mathbf{V}_g$ and f_g are given to $\mathbf{V}_0$ and f_0, and the procedure by Cheng (2003) is different from the classical SA in that the best solution found so far is used instead of the randomly adjusted solution to generate the next solution.

3.3.2 Genetic algorithm (GA)

The genetic algorithm is developed by Holland (1975) and has received great attention in various disciplines. It is an optimization approach based on the concepts of genetics and natural reproduction and the evolution of living creatures, in which an optimum solution evolves through a series of generations. Each generation consists of a number of possible solutions (individuals) to the problem, defined by an encoding. The fitness of an individual within the generation is evaluated, and it influences the reproduction of the next generation. The algorithm starts with an initial population of M individuals. An individual is composed of real coordinates associated with the variables of the objective function. The current generation is called parent generation, by which offspring generations are created using operators such as crossover and mutation. Other M individuals are re-chosen from the parent and offspring generations according to their fitness value. The flowchart for the genetic algorithm is given in Figure 3.9, where ρ_c and ρ_m are the probabilities of crossover and mutation in the algorithm. Usually, the value of ρ_c varies from 0.8 to 0.9 while ρ_m falls in the range of 0.001–0.1. N_1 represents the number of iterations in the first stage, while N_2 represents the time interval by which the termination criterion is defined. If the best individual with the fitness value f_g remains unchanged after N_2 iterations, the algorithm will stop. *Niter* is the variable restoring the total iterations performed by the algorithm. j_1 and j_2 are used to perform the non-uniform mutation operations. The crossover operator is given by eq. (3.1).

$$\begin{cases} v_{oj+1,l} = v_{fi,l} \times r_c + (1.0 - r_c) \times v_{mi,l} \\ v_{oj+2,l} = v_{mi,l} \times r_c + (1.0 - r_c) \times v_{fi,l} \\ l = 1, 2, \ldots, n+1 \end{cases} \tag{3.1}$$

where $v_{oj+1,l}$ and $v_{oj+2,l}$ mean the lth element of the vector $\mathbf{V}_{oj+1}$ and $\mathbf{V}_{oj+2}$, respectively, given by eq. (3.2). Similarly, $v_{mi,l}$ and $v_{fi,l}$ represent the lth element of the mother parent and father parent vectors $\mathbf{V}_{mi}$ and $\mathbf{V}_{fi}$, respectively, and $n + 1$ is the number of control variables in this study.

$$\begin{cases} v_{oj+1,l} = v_{oj+1,l} - \left(v_{oj+1,l} - v_{l\min}\right) \times \left(1.0 - \frac{j_1}{j_2}\right)^2 \times r_m & r_{nd} \le 0.5 \\ v_{oj+1,l} = v_{oj+1,l} + \left(v_{l\max} - v_{oj+1,l}\right) \times \left(1.0 - \frac{j_1}{j_2}\right)^2 \times r_m & r_{nd} > 0.5 \end{cases} \tag{3.2}$$

where r_m and r_{nd} are random numbers in the range 0–1. $v_{l\min}$ and $v_{l\max}$ are the lower and upper bounds to the lth variable in ($\mathbf{V} = x_1, x_{n+1}, \sigma_2, \ldots, \sigma_n$). ε is the tolerance for termination of the search.

3.3.3 Particle swarm optimization algorithm (PSO)

The PSO is an algorithm developed by Kennedy and Eberhart (1995). This method has received wide applications in continuous and discrete optimization problems, and an improved version for slope stability analysis

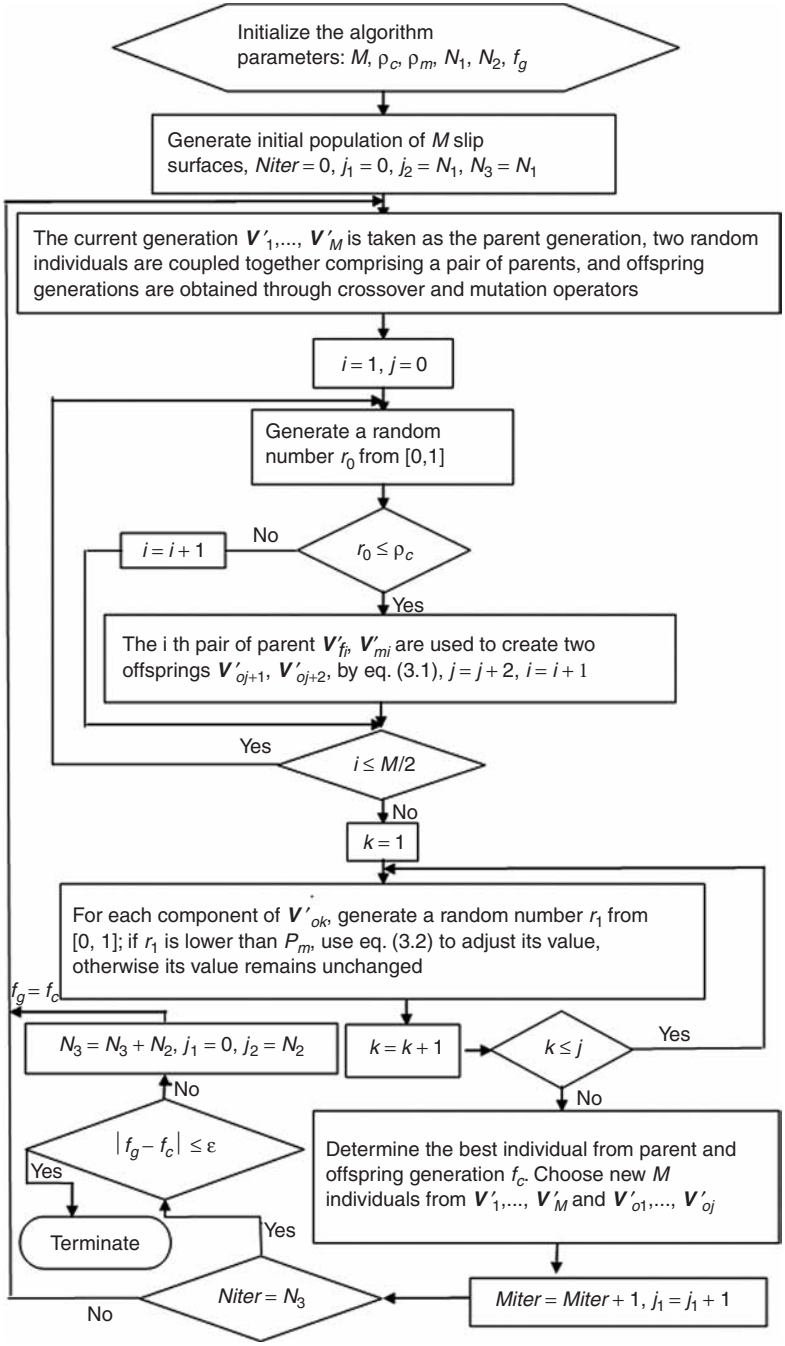

Figure 3.9 Flowchart for the genetic algorithm.

has been developed by Cheng *et al.* (2007e). Yin (2004) has proposed a hybrid version of the PSO for the optimal polygonal approximation of digital curves, while Salman *et al.* (2002) and Ourique *et al.* (2002) have adopted the PSO for the task assignment problem and dynamical analysis in chemical processes, respectively. The PSO is based on the simulation of simplified social models, such as bird flocking, fish schooling and the swarming theory. It is related to evolutionary computation procedures, and has strong ties with the genetic algorithms. This method is developed on a very simple theoretical framework, and it can be implemented easily with only primitive mathematical operators. Besides, it is computationally inexpensive in terms of both the computer memory requirements and the speed of the computation.

In the PSO, a group of particles (generally double the number of the control variables, M) referred to as the candidates or the potential solutions [as $\boldsymbol{V}$ described above] are flown in the problem search space to determine their optimum positions. This optimum position is usually characterized by the optimum of a fitness function (e.g. factor of safety for the present problem). Each 'particle' is represented by a vector in the multi-dimensional space to characterize its position ($\mathbf{V}^k_i$), and another vector to characterize its velocity ($\mathbf{W}^k_i$) at the current time step k. The algorithm assumes that particle i is able to carry out simple space and time computations to respond to the quality environment factors. That is, a group of birds can determine the average direction and speed of flight during the search for food, based on the amount of the food found in certain regions of the space. The results obtained at the current time step k can be used to update the positions of the next time step. It is also assumed that the group of particles is able to respond to the environmental changes. In other words, after finding a good source of food in a certain region of the space, the group of particles will take this new piece of information into consideration to formulate the 'flight plan'. Therefore, the best results obtained throughout the current time step are considered to generate the new set of positions of the whole group.

To optimize the fitness function, the velocity $\mathbf{W}^k{}_i$ and hence the position $\boldsymbol{V}^k{}_i$ of each particle are adjusted in each time step. The updated velocity $\mathbf{W}^{k+1}{}_i$ is a function of the three major components:

1 the old velocity of the same particle ($\mathbf{W}^k{}_i$);
2 difference of the ith particle's best position found so far (called $\boldsymbol{P}_i$) and the current position of the ith particle $\boldsymbol{V}^k{}_i$;
3 difference of the best position of any particle within the context of the topological neighbourhood of the ith particle found so far (called $\boldsymbol{P}_g$; its objective function value called f_g) and current position of the ith particle $\boldsymbol{V}^k{}_i$.

Each of the components 2 and 3 mentioned above are stochastically weighted and added to component 1 to update the velocity of each particle, with enough oscillations that should empower each particle to search for a better pattern within the problem space. In brief, each particle employs eq. (3.3) to update its position.

$$\begin{aligned}
&\boldsymbol{W}_i^{k+1} = \omega \boldsymbol{W}_i^k + c_1 r_1 \left(\boldsymbol{P}_i - \boldsymbol{V}_i^k \right) + c_2 r_2 \left(\boldsymbol{P}_g - \boldsymbol{V}_i^k \right) \\
&\boldsymbol{V}_i^{k+1} = \boldsymbol{V}_i'^k + \boldsymbol{W}_i^{k+1} \\
&i = 1, 2, ..., 2n
\end{aligned} \tag{3.3}$$

where c_1 and c_2 are responsible for introducing the stochastic weighting to components 2 and 3, respectively. These parameters are commonly chosen as 2 which will also be used in this study. r_1 and r_2 are two random numbers in the range [0,1], and ω is the inertia weight coefficient. A larger value for ω will enable the algorithm to explore the search space, while a smaller value of ω will lead the algorithm to exploit the refinement of the results. Chatterjee and Siarry (2006) have introduced a nonlinear inertia weight variation for dynamic adaptation in the PSO. The flowchart for the PSO in searching for the critical slip surface is shown in Figure 3.10.

The termination criterion for the PSO is not stated explicitly by Kennedy and Eberhart (1995) (same for other modern global optimization methods). Usually a fixed number of trials are carried out with the minimum value from all the trials taken as the global minimum, and this is the limitation of the original PSO or other global optimization algorithms. Based on the termination proposal by Cheng *et al.* (2007e), if $\boldsymbol{P}_g$ remains unchanged after N_2 iterations are performed, the algorithm will terminate as given by eq. (3.4):

$$\left| f_{sf} - f_g \right| \leq \varepsilon \tag{3.4}$$

where $\boldsymbol{V}_{sf}$, f_{sf} mean the best solution found so far and its related objective function value. ε is the tolerance of termination. All global optimization methods require some parameters which are difficult to be established for general problems. Based on extensive internal tests, it is found that the PSO is not sensitive to the optimization parameters in most problems, which is an important consideration for recommending this method to be used for slope stability analysis.

3.3.4 Simple harmony search algorithm (SHM)

Geem *et al.* (2001) and Lee and Geem (2005) developed a harmony search meta-heuristic algorithm that was conceptualized using the musical process of searching for a perfect state of harmony. Musical performances seek to find pleasing harmony (a perfect state) as determined by an aesthetic standard, just as the optimization process seeks to find a global solution determined by an objective function. The harmony in music is analogous to the optimization solution vector, and the musician's improvisations are analogous to local and global search schemes in the optimization process. The SHM uses a stochastic random search that is based on the harmony memory considering rate *HR* and the pitch-adjusting rate *PR*, and it is a population-based search method. A harmony memory HM of size *M* is used to generate a new harmony, which is probably better than the optimum in the current harmony memory. The

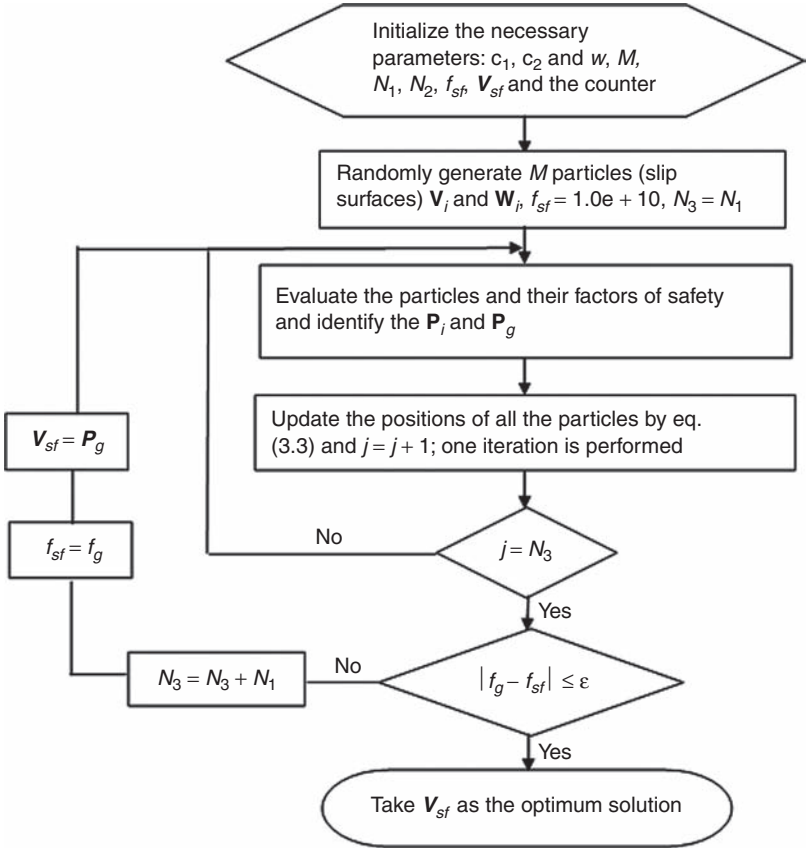

Figure 3.10 Flowchart for the particle swarm optimization method.

harmony memory consists of M harmonies (slip surfaces), and M harmonies are usually generated randomly. Consider HM = $\{hm_1, hm_2, \ldots, hm_M\}$

$$hm_i = (v_{i1}, v_{i2}, \ldots, v_{im}) \tag{3.5}$$

where each element of hm_i corresponds to that in vector $\boldsymbol{V}$ described above. Consider the following function optimization problem, where $M = 6$, $m = 3$. Suppose $HR = 0.9$ and $PR = 0.1$.

$$\begin{cases} \min \quad f(x_1, x_2, x_3) = (x_1 - 1)^2 + x_2^2 + (x_3 - 2.0)^2 \\ s.t. \quad 0 \le x_1 \le 2 \quad 1 \le x_2 \le 3 \quad 0 \le x_3 \le 2 \end{cases} \tag{3.6}$$

Six randomly generated harmonies comprise the HM shown in Table 3.1. The new harmony can be obtained by the harmony search algorithm with the following procedures. A random number in the range [0, 1] is generated, for

Table 3.1 The structure of the HM

HM	*Control variables*			*Objective function*
	x_1	x_2	x_3	
hm_1	1.0	1.5	0.5	4.50
hm_2	1.5	2.0	1.8	4.29
hm_3	0.5	1.5	1.0	3.50
hm_4	1.8	2.5	0.9	8.10
hm_5	0.9	2.2	1.2	5.49
hm_6	1.1	1.9	1.5	3.87

example, 0.6(<*HR*), and one of the values from {1.0, 1.5, 0.5, 1.8, 0.9, 1.1} should be chosen as the value of x_1 in the new harmony. Take 1.0 as the value of x_1; then another random number of 0.95(>*HR*) is obtained. A random value in the range [1, 3] for x_2 is generated (say 1.2), and similarly 0.5 is chosen from the HM as the value of x_3, thus a coarse new harmony $hm'_n = (1.0,1.2,0.5)$ is generated. The improved new harmony is obtained by adjusting the coarse new harmony according to the parameter *PR*. Suppose three random values in the range [0, 1] (say 0.7, 0.05, 0.8) are generated. Since the former value 0.7 is greater than *PR*, the value of hm'_n remains unchanged. The second value 0.05 is lower than *PR*, so the value of 1.2 should be adjusted (say 1.10). The above procedures proceed until the final new harmony $hm_n = (1.0,1.10,0.5)$ is obtained. The objective function of the new harmony is determined as 3.46. The objective function value of 3.46 is better than that of the worst harmony hm_4, thereby hm_4 is excluded from the current HM, while hm_n is included in the HM. Up to this stage, one iteration step has finished. The algorithm will continue until the termination criterion is achieved.

The iterative steps of the harmony search algorithm in the optimization of eq. (3.6) as given in Figure 3.11 are as follows:

Step 1: Initialize the algorithm parameters *HR*, *PR*, *M* and randomly generate *M* harmonies (slip surfaces) and evaluate the harmonies.

Step 2: Generate a new harmony (shown in Figure 3.11) and evaluate it.

Step 3: Update the HM. If the new harmony is better than the worst harmony in the HM, the worst harmony is replaced with the new harmony. Take the *i*th value of the coarse harmony, for reference. Its lower bound and upper bounds are named as $v_{i\min}$ and $v_{i\max}$, respectively. A random number r_0 in the range [0, 1] is generated. If $r_0 > 0.5$, then v'_{ni} is adjusted to v_{ni} using eq. (3.7); otherwise, eq. (3.8) is used to calculate the new value of v_{ni}.

$$v_{ni} = v'_{ni} + \left(v_{i\max} - v'_{ni}\right) \times rand \quad r_0 > 0.5 \tag{3.7}$$

$$v_{ni} = v'_{ni} - \left(v'_{ni} - v_{i\min}\right) \times rand \quad r_0 \leq 0.5 \tag{3.8}$$

where *rand* means a random number in the range [0, 1].

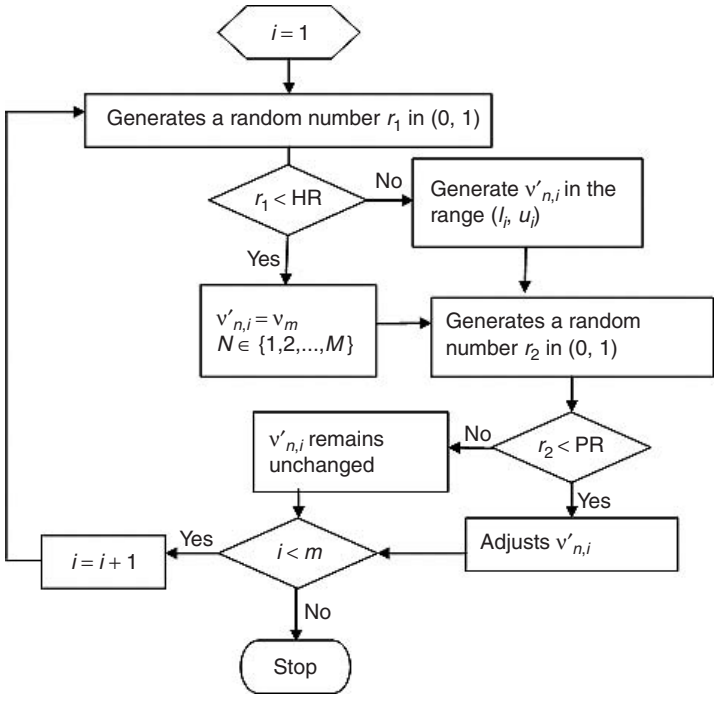

Figure 3.11 Flowchart for generating a new harmony.

Step 4: Repeat Steps 2 and 3 until the termination criterion is achieved.

In the original harmony search by Geem *et al.* (2001) and Lee and Geem (2005), an explicit termination criterion is not given. Cheng *et al.* (2007b,f) have proposed a termination criterion for the optimization process. Suppose $M \times N_1$ iterations are first performed, and the best solution found so far is called $\boldsymbol{V}_{sf}$, with the objective function value equal to f_{sf}. Another $M \times N_2$ iteration is then performed, and the best harmony in the current HM is called $\boldsymbol{V}_g$, with the objective function value equal to f_g. The optimization process can terminate if eq. (3.9) is satisfied.

$$|f_{sf} - f_g| \leq \varepsilon \tag{3.9}$$

3.3.5 Modified harmony search algorithm (MHM)

Based on many trials by Cheng, it is found that the SHM works fast and gives good solutions for simple problems with less than 25 control variables. For more complicated problems with a large number of control variables, the original harmony search algorithm becomes inefficient and can be trapped by the local minima easily. Cheng *et al.* (2007f) have developed improved

harmony search algorithms (MHM) to overcome the limitations of the SHM, which differs from the SHM in the following two aspects.

1 Instead of using a uniform probability in the original harmony search method, the better the objective function value of one harmony, the more probable will it be chosen for the generation of a new harmony. A parameter δ ($0 < \delta \leq 1$) is introduced and all the harmonies in HM are sorted by ascending order, and a probability is assigned to each of them. For instance, $pr(i)$ means the probability to choose the ith harmony which is given as

$$pr(i) = \delta \times (1 - \delta)^{i-1} \tag{3.10}$$

for $i = 1,2,...,M$. From eq. (3.10), it can be seen that the larger the value of δ, the more probable will be the first harmony being chosen. An array $ST(i), i = 0,1,2,...,M$ as given by eq. (3.11) should be used to implement the above procedures for choosing the harmony.

$$ST(i) = \sum_{j=1}^{i} pr(j) \tag{3.11}$$

where $ST(i)$ represents the accumulating probability for the ith harmony. $ST(0)$ equals 0.0 for the sake of implementation. A random number r_c is generated from the range $[0, ST(M)]$, and the kth harmony in HM is to be chosen if the following criterion is satisfied.

$$ST(k-1) < r_c \leq ST(k), \quad k = 1, 2, ..., M \tag{3.12}$$

2 Instead of one new harmony, a certain number of new harmonies (Nhm) are generated during each iteration step in the modified harmony search algorithm. The utilization of the HM is intuitively more exhaustive by generating several new harmonies than by generating one new harmony during one iteration. To retain the structure of the HM unchanged, the M harmonies with lower objective functions (for the minimization optimization problem) from $M + Nhm$ harmonies are included in the HM again, and the harmonies of the higher objective function values are rejected.

The HM shown in Table 3.1 is now reordered increasingly, and the new structure is illustrated in Table 3.2. Suppose $\delta = 0.5$ and $Nhm = 2$; the arrays pr and ST obtained are listed in columns 6 and 7, respectively, in Table 3.2. A random number in the range [0, 1] is generated, say 0.6(<HR). One of the values from {1.0, 1.5, 0.5, 1.8, 0.9, 1.1} should be chosen as the value of x_1 in the new harmony. Given the value of r_c is equal to 0.4 for example, by using criterion (18), 0.5 is chosen to be the value of x_1. Another random number of 0.95(>HR) is obtained, and a random value in the range [1, 3], 1.2, is generated. Similarly, a random number of 0.6 and $r_c = 0.80$ are also obtained. The value of x_3 is chosen from

Table 3.2 The reordered structure of HM

HM	*Control variables*			*Objective function*	*pr()*	*ST()*
	x1	*x2*	*x3*			
hm_1	0.5	1.5	1.0	3.50	0.5	0.5
hm_2	1.1	1.9	1.5	3.87	0.25	0.75
hm_3	1.5	2.0	1.8	4.29	0.125	0.875
hm_4	1.0	1.5	0.5	4.50	0.0625	0.9375
hm_5	0.9	2.2	1.2	5.49	0.03125	0.9687
hm_6	1.8	2.5	0.9	8.10	0.01562	0.9843

Table 3.3 Structure of HM after first iteration in the MHM

HM	*Control variables*			*Objective function*	*pr()*	*ST()*
	x1	*x2*	*x3*			
hm_1	0.5	1.10	1.8	1.50	0.5	0.5
hm_2	0.9	1.5	1.3	2.75	0.25	0.75
hm_3	0.5	1.5	1.0	3.50	0.125	0.875
hm_4	1.1	1.9	1.5	3.87	0.0625	0.9375
hm_5	1.5	2.0	1.8	4.29	0.03125	0.9687
hm_6	1.0	1.5	0.5	4.50	0.01562	0.9843

the HM as 1.8, thus a coarse new harmony $hm'_n = (0.5,1.2,1.8)$ is generated. The fine new harmony is obtained by adjusting the coarse new harmony according to the parameter *PR*. Suppose two random values in the range [0, 1], say 0.7, 0.05, 0.8, are generated randomly. Since the former is greater than the *PR*, the value of x_1 in hm'_n remains unchanged. The latter value is lower than the *PR*, so the value of 1.2 should be adjusted. Suppose 1.10 is the new value of x_2; the improved new harmony $hm'_n = (0.5,1.10,1.8)$ is obtained. Similarly, the second new harmony $hm'_n = (0.9,1.5,1.3)$ is also obtained. The objective functions of the two new harmonies are calculated as 1.5 and 2.75, respectively. So the six harmonies with lower objective functions hm_1, hm_2, hm_3, hm_6, hm'_n, hm''_n are introduced into the HM as illustrated in Table 3.3 and one iteration is finished. The algorithm continues until the termination criterion is satisfied.

Based on extensive numerical tests by Cheng *et al*. (2007b), it is found that the modified harmony search algorithms shown in Figure 3.12 are more effective in overcoming the local minima as compared with the original harmony search method for complicated problems. It is also more efficient than the original HM when the number of control variables is large, but is less efficient when there are only a few control variables.

3.3.6 Tabu search algorithm

The Tabu search (Glover, 1989, 1990) is not exactly an optimization algorithm, but a collection of guidelines to develop optimization algorithms. The

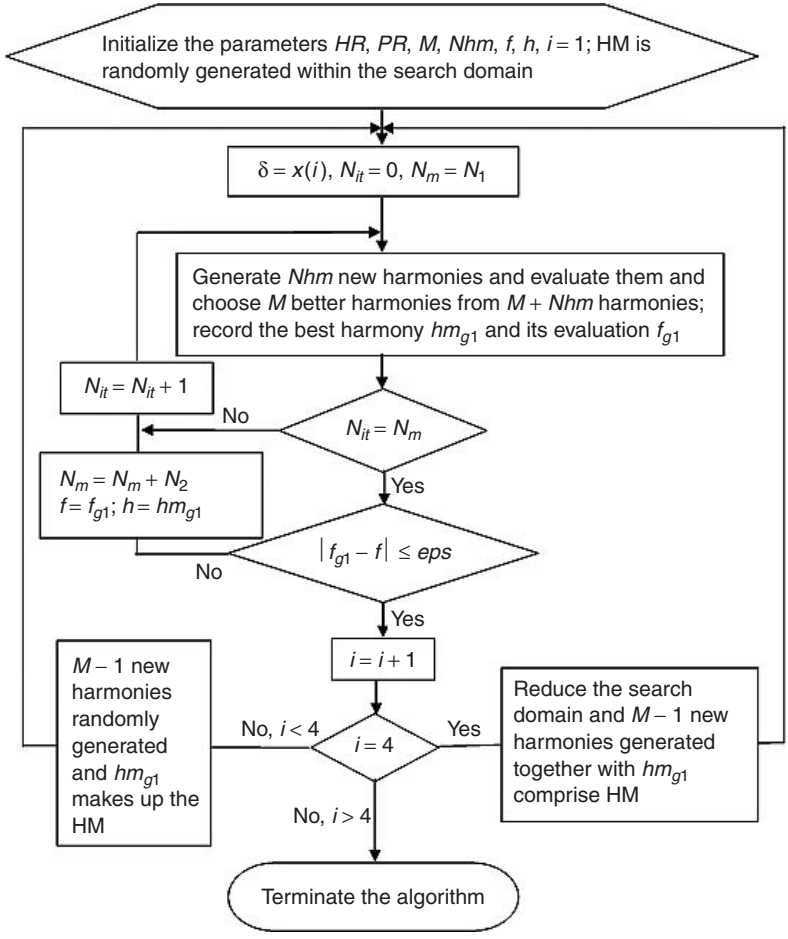

Figure 3.12 Flowchart for the modified harmony search algorithm.

basic idea of the Tabu search is to explore the trial solutions for the problem, moving from a point to another point in its neighbourhood with solutions which have little difference from the point under consideration. Reverse moves and cycles are avoided by the use of a 'tabu list', where the moves previously done are memorized. To implement the Tabu search, the first step is the discretization of the problem space. Each dimension is divided into d elements, and altogether d^m hyper-cubes are obtained. If a solution is tabu, it means that the super-cube in which the solution locates is also tabu. It is very difficult to directly generate a solution within the super-cubes which are not tabu, and a trial procedure is proposed by Cheng *et al.* (2007b). The procedure by which the new harmonies are obtained in the harmony search algorithm is used to obtain the trial solutions. If the super-cube of the new trial

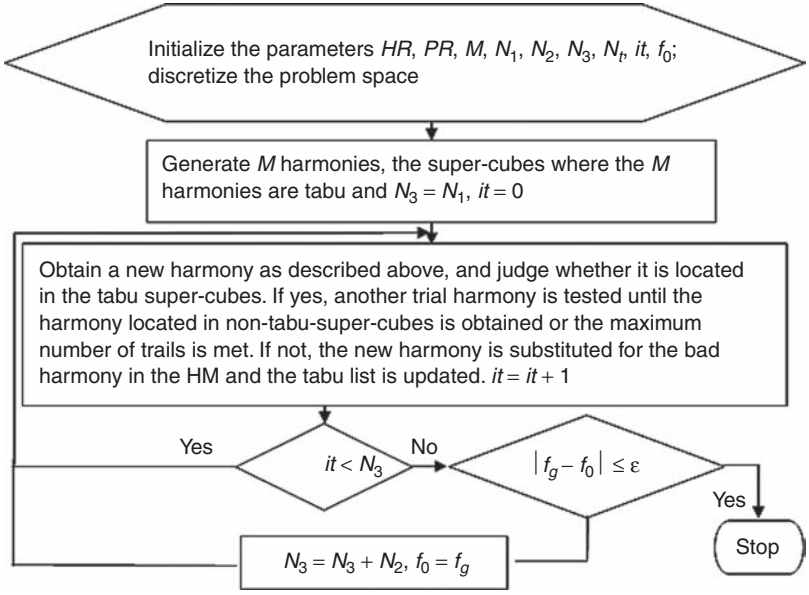

Figure 3.13 Flowchart for the Tabu search.

solution is tabu, another trial solution will be tested until a trial solution which does not belong to the tabu super-cubes is found. The flowchart for the Tabu search algorithm is shown in Figure 3.13.

In Figure 3.13 f_g is the objective function value of the best harmony in the HM, and the parameters of N_1, N_2, N_3 are used to terminate the algorithm. ε is the tolerance for the termination of the search.

3.3.7 Ant-colony algorithm

The ant-colony algorithm is a meta-heuristic method using natural metaphors to solve the complex combinatorial optimization problems, which is originated by Dorigo (1992). It is inspired by the natural optimization mechanism conducted by real ants. Basically, a problem under the study is transformed into a weighted graph. The ant-colony algorithm iteratively distributes a set of artificial ants onto the graph to construct tours corresponding to the potential optimal solutions. The optimization mechanism of the ant-colony algorithm is based on two important features: (1) the probabilistic state transition rule that is applied when an ant is choosing the next vertex to visit and (2) the pheromone updating rule that dynamically changes the preference degree for the edges that have been travelled through.

The continuous optimization problem should be first transformed into a weighted graph. In the case of locating the critical slip surface, each

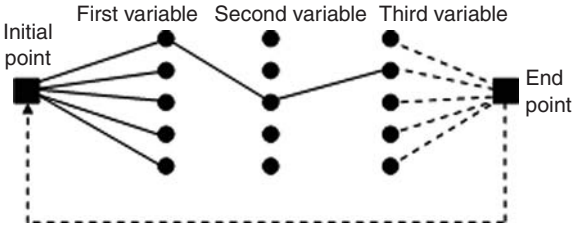

Figure 3.14 The weighted graph transformed for the continuous optimization problem.

dimension is equally divided into d subdivisions and m dimensions (5 and 3, respectively, in Figure 3.14) in the optimization problem. The solid circles located in adjacent columns are connected between each other.

An ant is first located at the initial point. Based on the probabilistic transition rule, one solid circle in the 'first variable' column is chosen and thus the value of the first variable is determined, and the procedures proceed to other variables. When an ant finishes determining the value of the end variable, it will go back to the initial point through the end point for the next iteration. Figure 3.15 shows the flowchart for the ant-colony algorithm. In Figure 3.15, N_a means the total number of ants. The probabilistic transition rule and pheromone updating rule are described briefly as follows:

1 *Probabilistic transition rule:*

$$\rho_{ij} = \frac{\tau_{ij}^k}{\sum_{i=1}^{d} \tau_{ij}^k}, \quad j = 1, 2..., m \tag{3.13}$$

where τ^k_{ij} represents the pheromone deposited on the ith solid circle of the jth variable within the kth iteration step, and ρ_{ij} means the probability of the ith solid circle of the jth variable to be chosen.

2 *Pheromone updating rules:*

$$\tau_{ij}^{k+1} = (1.0 - \mu) \times \tau_{ij}^k + \Delta\tau_{ij} \tag{3.14}$$

where $\mu \in [0,1]$ is a parameter which simulates the evaporation rate of the pheromone intensity. $\Delta\tau_{ij}$ is obtained using eq. (3.15)

$$\Delta\tau_{ij} = \begin{cases} \sum_{l=1}^{N_a} Q/fs_l & \text{condition1} \\ 0 & \text{condition2} \end{cases} \tag{3.15}$$

where fs_l represents the objective function value of the solution found by the lth ant; condition1 means that the lth ant has chosen the ith solid circle of the

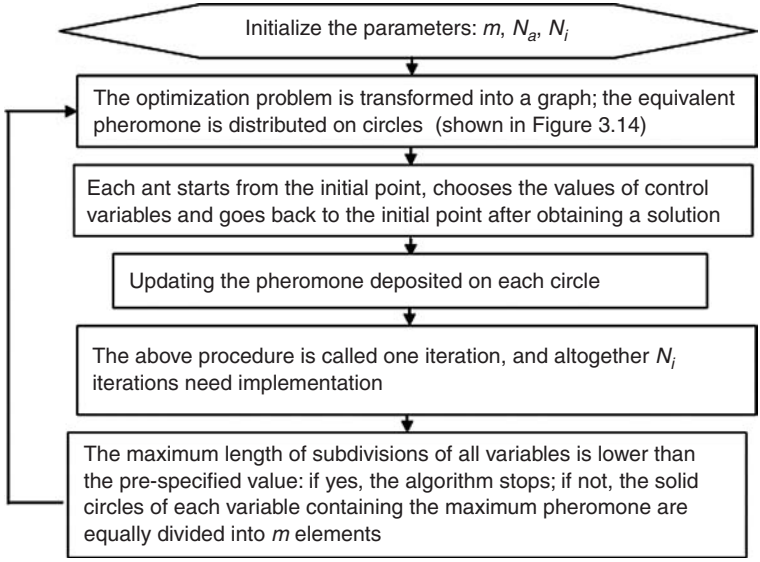

Figure 3.15 Flowchart for the ant-colony algorithm.

*j*th variable. Correspondingly, condition2 means that no ant has chosen the *i*th solid circle of the *j*th variable within the *k*th iteration step.

3.4 Verification of the global minimization algorithm

The majority of the modern global optimization schemes have not been used in slope stability analysis in the past. The SA, SHM, MHM, PSO, Tabu and ant-colony methods were first used by Cheng (2003), Cheng *et al.* (2007b,e,f) and Cheng (2007) with various modifications to suit the slope stability problems. For the first demonstration of the applicability of these modern optimization methods, eight test problems are used to illustrate the effectiveness of Cheng's (2003) proposal on the modified SA algorithm, and problems 4 and 8 are shown in Figures 3.16 and 3.17. Problems 1–3 are similar to problem 4 except for the external load. For problems 1–4 which are shown in Figure 3.16, in total there are two types of soils with a water table. In problem 1, there is no external load while the horizontal load is applied in problem 2. Vertical load is applied in problem 3 while both vertical load and horizontal loads are applied in problem 4. Problems 5–7 are also similar to problem 8 except for the external load. For problems 5–8 which are shown in Figure 3.17, in total there are three types of soils, a water table and a perched water table. In problem 5, there is no external load while the horizontal load is applied in problem 6. Vertical load is applied in problem 7 while both vertical and horizontal loads are applied in problem 8. The cohesive strengths of

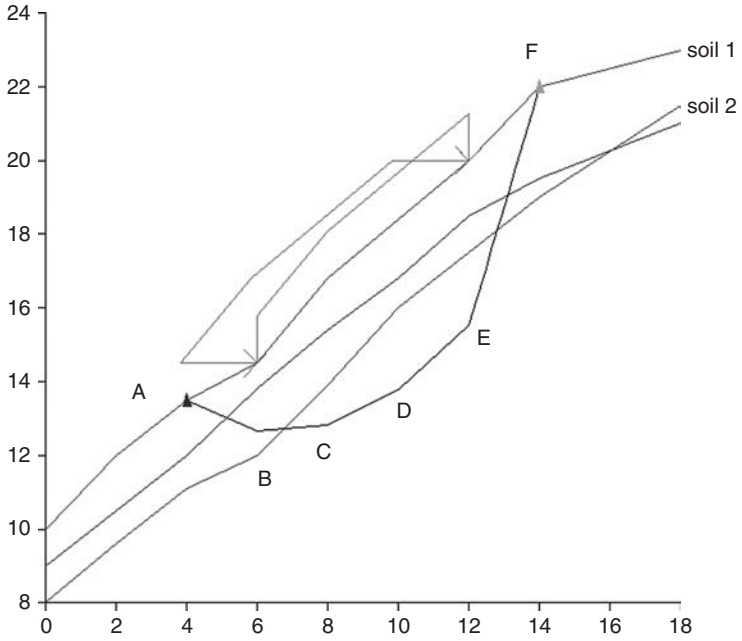

Figure 3.16 Problem 4 with horizontal and vertical load (critical failure surface is shown by ABCDEF).

Source: Reproduced with permission of Taylor & Francis.

soils for problems 1–4 are 5 and 2 kPa, respectively, for soil 1 and soil 2 while the corresponding cohesive strengths for problems 5–8 are 5, 2 and 5 kPa. The friction angles of soils for problems 1–4 are 35° and 32°, respectively, for soil 1 and soil 2 while the corresponding friction angles for problems 5–8 are 32°, 30° and 35°. The unit weight of soil is kept constant at 19 kNm^{-3} in all these cases. It is not easy to minimize the factor of safety for these problems by a manual trial and error approach as the precise location of the failure surface will greatly influence the factor of safety. The minimum reference factors of safety are determined by an inefficient but robust pattern search approach. To limit the amount of computer time used, the number of slices is limited to 5 in these studies and the slices are divided evenly.

The critical solution from the present study is shown in Figures 3.16 and 3.17 by ABCDEF. The x-ordinates of the left exit end A (4.0 for problems 1–4 and 5.0 for problems 5–8) and right exit end F (14.0 for all problems) of the failure surfaces are fixed so that only the y-ordinates of B, C, D, E are variables (x-ordinates of B, C, D, E are obtained by even division). There are hence four control variables in the present study. Based on the critical result BCDE obtained from the minimization analysis (round up to two decimal

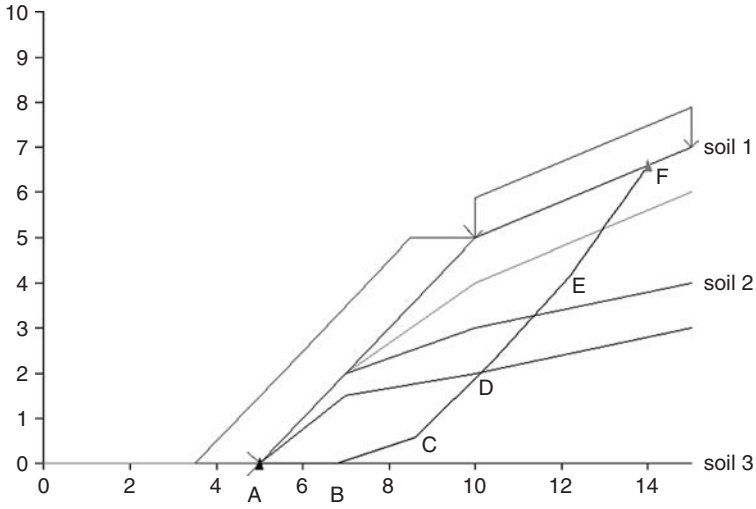

Figure 3.17 Problem 8 with horizontal and vertical load (critical failure surface is shown by ABCDEF).

Source: Reproduced with permission of Taylor & Francis.

places), a grid is set up 0.5 m directly above and below B, C, D, E as obtained by the simulated annealing analysis. The spacings between the upper and lower bounds are hence 1.0 m for all the four control variables. The grid spacing for each control variable is 0.01 m so that each control variable can take 101 possible locations. The present grid spacing is fine enough for pattern search minimization and all the possible combinations of failure surfaces are tried, which are 101 × 101 × 101 × 101 or 10,406,041 combinations.

The factors of safety shown in Table 3.4 have clearly illustrated that the combined use of the failure surface generation and the simulated annealing method is able to minimize the factors of safety with high precision, and the results are similar to those obtained by a pattern search based on 10,406,041 trials. The location of the critical failure surface obtained from the simulated annealing analysis for problem 4 shown in Table 3.5 is very close to that obtained by the pattern search and similar results are also obtained for all the other problems. The results in Tables 3.4 and 3.5 have clearly illustrated the capability of the proposed modified SA algorithm in minimizing the factors of safety, so that the burden of engineers can be relieved by the adoption of modern global optimization techniques. Besides the simulated annealing method, the other global optimization techniques as modified by Cheng's methods (2007b) can also be worked with satisfaction for all these eight problems.

To illustrate the advantages of the present dynamic bound technique as compared with the classical static bounds to the control variables, the same problems are considered with static bounds analysis. The static bounds are

Table 3.4 Comparison between minimization search and pattern search for eight test problems using the simulated annealing method (tolerance in minimization search = 0.0001)

Case	*Trials required in SA*	*FS from SA*	*FS from pattern search*
1	10081	0.7279	0.7279
2	10585	0.8872	0.8872
3	9577	0.7684	0.7685
4	10585	0.9243	0.9243
5	12097	0.7727	0.7726
6	13105	1.1072	1.1072
7	11593	0.7494	0.7492
8	12601	1.0327	1.0327

FS = factor of safety, SA = simulated annealing analysis.
Source: Reproduced with permission of Taylor & Francis.

Table 3.5 Coordinates of the failure surface with minimum factor of safety from SA and from pattern search for Figure 3.4 (values with * are fixed and are not control variables)

Point	*x-ordinate*	*y-ordinate from SA*	*y-ordinate from pattern search*
A	4	13.5*	13.5*
B	6	12.677	12.67
C	8	12.831	12.82
D	10	13.784	13.78
E	12	15.539	15.54
F	14	22.0*	22.0*

Source: Reproduced with permission of Taylor & Francis.

defined as 0.5 m above and below the critical failure surface BCDE and the results are shown in Table 3.6 (the same minimum values are obtained from the two analyses). It is clear that the present proposal can greatly reduce the time of computation as compared with the classical simulated annealing technique which is highly beneficial for real problems. This advantage is particularly important when the number of control variables is great.

3.5 Presence of a Dirac function

If there is a very thin soft band where the soil parameters are particularly low, the critical failure surface will be controlled by this soft band. This type of problem poses a great difficulty as normal random number generation (uniform probability) is used within the solution domain, and this feature is difficult to be captured automatically. The thickness of the soft band can be so small that it can be considered as a Dirac function within the solution domain. Such failures have been reported in Hong Kong, and the slope failure at Fei Tsui Road is one of the famous examples in Hong Kong where failure is controlled by a thin band of soil.

Table 3.6 Comparisons between the number of trials required for dynamic bounds and static bounds in simulated annealing minimization

Case	*Trials in DB*	*Trials from SB*
1	10,081	19,823
2	10,585	21,023
3	9577	17,234
4	10,585	22,131
5	12,097	23,968
6	13,105	25,369
7	11,593	23,652
8	12,601	25,104

SB = static bounds, DB = dynamic bounds.
Source: Reproduced with permission of Taylor & Francis.

For a thin soft band, the probability of the control variables falling within this region will be small with the use of the classical random number. From principles of engineering, the probability of the control variables falling within this soft-band region should however be greater than that falling within other regions. For this difficult case, Cheng (2007) proposes to increase the probability of the search within the soft band. Since the location of the soft-band region is not uniform within the solution domain, it is difficult to construct a random function with increased probability within the soft-band region at different locations. This problem can be solved by a simple transformation proposed by Cheng, as shown in Figure 3.18, where a classical random function is used in simulated annealing analysis. In Figure 3.18, the actual domain for a control variable x_i ($N + 1 > i > 2$ in present method) is represented by a segment AB with a soft band CD in between AB. For control variables x_j where $i \neq j$, the location of the soft band CD and the solution bound AB for control variable x_i will be different from that for control variable x_j. For segment AB, several virtual domains with a width of CD for each domain are added adjacent to CD as shown in Figure 3.18. The transformed domain AB′ is used as the control domain of variable x_i. Every point generated within the virtual domain D1–D2, D2–D3, D3–D4 is mapped to the corresponding point in segment CD1. This technique is effectively equivalent to giving more chances to those control variables within the soft band. The weighting to the variables within the soft-band zone can be controlled easily by the simple transformation as suggested in Figure 3.18. To Cheng's knowledge, the search for the critical failure surface with a 1 mm thick soft band has never been minimized successfully, but this has been solved effectively by the proposed domain transformation by Cheng (2007). The transformation technique is coded into SLOPE 2000 and has been used to overcome several very difficult hydropower projects in China where there are several layers of highly irregular soft bands. For that project, several commercial programs have been used to locate the critical failure surface without satisfaction.

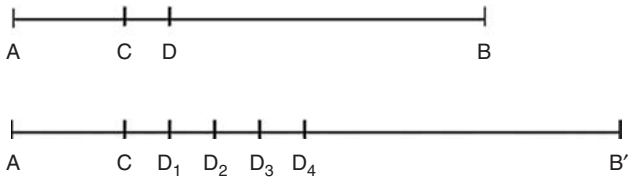

Figure 3.18 Transformation of domain to create a special random number with weighting.

Table 3.7 Minimum factor of safety for example 1 (Spencer method)

Optimization methods	*Minimum factors of safety*	*NOFs*	
		Total	*Critical*
Simple genetic algorithm by Zolfaghari *et al.* (2005)	1.75	Unknown	
SA	1.7267	103,532	102,590
GA	1.7297	49,476	49,476
PSO	1.7282	61,600	60,682
SHM	1.7264	107,181	98,607
MHM	1.7279	28,827	28,827
Tabu	1.7415	58,388	988
Ant-colony	1.7647	83,500	16,488

NOFs = number of trials.

3.6 Numerical studies of the efficiency and effectiveness of various optimization algorithms

The greater the number of control variables, the more difficult will be the global optimization analysis. For the heuristic global optimization methods which have been discussed in the previous section, all of them are effective for simple cases with a small number of control variables. The practical differences between these methods are the effectiveness and efficiency under some special conditions with a large number of control variables. Consider example 1 shown in Figure 3.19. It is a simple slope taken from the study by Zolfaghari *et al.* (2005). The soil parameters are: unit weight 19.0 kNm^{-3}, cohesion 15.0 kPa, and effective friction angle 20°. Zolfaghari *et al.* used a simple genetic algorithm and the Spencer method and obtained a minimum factor of safety of 1.75 for the non-circular failure surface.

For this simple slope example, the results of analyses are shown in Table 3.7 and Figure 3.19. All of the methods under consideration are effective in the optimization analysis. The SA and the SHM give the lowest factors of

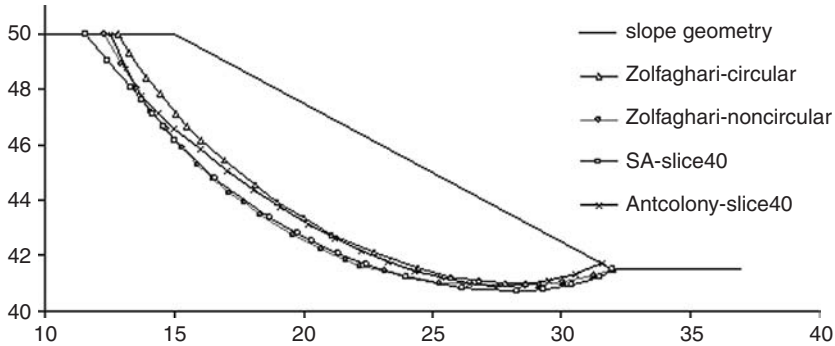

Figure 3.19 Example 1: Critical failure surface for a simple slope example 1 (failure surfaces by SA, MHM, SHM, PSO, GA are virtually the same; failure surfaces by Tabu and Zolfaghari are virtually the same).

safety, which are only slightly smaller than those by the other methods, but the NOFs are up to about 100,000, which is much greater than those for the other methods. The MHM finds a minimum of 1.7279 which is slightly larger than those by the SA and SHM, but only 28,827 trials are required which is much more efficient in the analysis. The PSO and GA give slightly larger factors of safety which are 1.7297 and 1.7282, but the number of evaluations are modest when compared with those required by the SA and SHM.

Example 2 is taken from the work by Bolton *et al.* (2003). There is a weak soil layer sandwiched between two strong layers. Unlike the previous example, the minimum factor of safety will be very sensitive to the precise location of the critical failure surface. The soil parameters for soil layers 1, 2 and 3, respectively, are friction angles 20°, 10° and 20°; cohesive strength 28.73, 0.0 and 28.73 kPa; and unit weight is 18.84 kNm^{-3} for all three soil layers. The results of analysis are shown in Table 3.8.

For this problem, all the methods are basically satisfactory except for the Tabu search and the ant-colony methods. The performance of the Tabu search and the ant-colony method are poor for this example, which indicates that these two methods are trapped by the presence of the local minima in the analysis. Overall, the PSO is the most effective method for this problem, while the MHM ranks the second with the least trials. The critical failure surfaces from the different methods of optimization are shown in Figure 3.20.

Example 3 is a case considered by Zolfaghari *et al.* (2005), where there is a natural slope with four soil layers, shown in Figure 3.21. Zolfaghari *et al.* have adopted the GA and the Spencer method for this example. The geotechnical parameters for this example are shown in Table 3.9. Four loading cases are considered by Zolfaghari *et al.*: no water pressure and no earthquake loadings (case 1); water pressure and no earthquake loading (case 2); earthquake loading (coefficient = 0.1) and no water pressure (case 3); and

Table 3.8 Results for example 2 (Spencer method)

Optimization methods		*Minimum factors of safety*	*NOFs*	
			Total	*Critical*
Leap-frog (Bolton *et al.*, 2003)		1.305	Unknown	
SA	20 slices	1.2411	51,770	51,745
	30 slices	1.2689	77,096	75,314
	40 slices	1.3238	190,664	190,648
GA	20 slices	1.2819	28,808	28,808
	30 slices	1.2749	39,088	39,088
	40 slices	1.2855	115,266	115,202
PSO	20 slices	1.2659	42,000	33,012
	30 slices	1.2662	64,800	55,810
	40 slices	1.2600	94,400	94,400
SHM	20 slices	1.3414	29,942	29,760
	30 slices	1.2784	118,505	97,055
	40 slices	1.2521	123,581	106,210
MHM	20 slices	1.2813	34,668	34,648
	30 slices	1.2720	26,891	26,891
	40 slices	1.2670	38,827	38,817
Tabu	20 slices	1.5381	30,548	1148
	30 slices	1.5354	44,168	768
	40 slices	1.5341	58,188	788
Ant-colony	20 slices	1.4897	43,500	4721
	30 slices	1.5665	63,500	7726
	40 slices	1.5815	83,500	1501

water pressure and earthquake loading (case 4). The numbers of slices are 40, 41, 44 and 45 for case 1 to case 4. The critical failure surfaces are given in Figures 3.22–3.25 and Table 3.10. For this example, the Tabu search and the ant-colony methods are not good while all the other methods are basically satisfactory. The PSO, the GA and the MHM are the most effective and efficient methods for this example.

The minimization of the factor of safety for a general slope stability problem is a difficult N-P hard-type problem because of the special features of the objective functions which have been discussed before. Since there are many limitations in using the classical optimization methods in the slope stability problem, the current trend is the adoption of the modern global optimization methods in this type of problem. All these six types of heuristic algorithms can function well for normal problems which are demonstrated in examples 1 and 2 and some other internal studies by Cheng. For simple problems where the number of control variables is less than 25, it appears that the SHM and MHM are the most efficient optimization methods. The SHM, the Tabu search and the ant-colony method can perform well in many other applications, but they have been demonstrated to be less satisfactory for slope stability problems. Since the ant-colony method aims at continuous optimization problems, it is not surprising that it is less satisfactory for

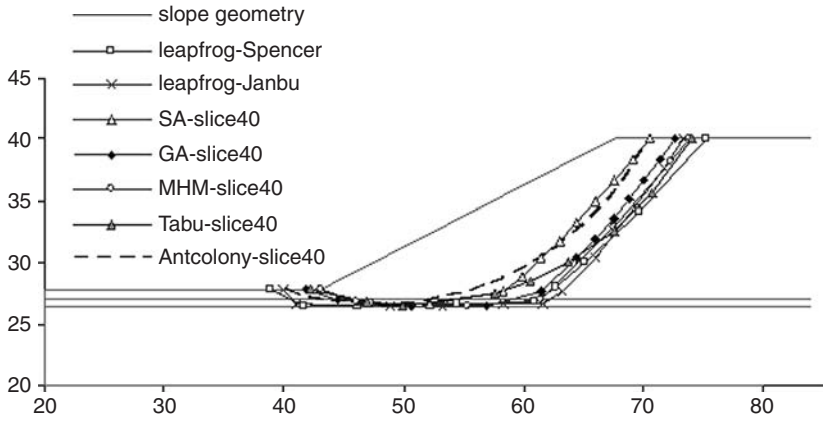

Figure 3.20 Critical slip surfaces for example 2 (failure surfaces by GA, PSO and SHM are virtually the same).

Table 3.9 Geotechnical parameters of example 3

Layers	γ *(kNm*$^{-3}$*)*	*c′ (kPa)*	$\phi'(^{o})$
1	19.0	15.0	20.0
2	19.0	17.0	21.0
3	19.0	5.0	10.0
4	19.0	35.0	28.0

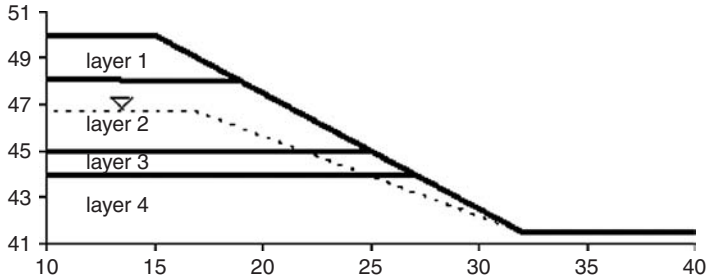

Figure 3.21 Geotechnical features of example 3.

slope stability problems where the discontinuity of the objective function is generated by divergence of the factor of safety. Similarly, when there are great differences in the soil properties between different soils, the SHM will be less

Table 3.10 Example 6 with four loading cases for example 3 (Spencer method)

Optimization methods		*Minimum factors of safety*	*NOFs*	
			Total	*Critical*
Case 1 GA by Zolfaghari *et al.* (2005)		1.48	Unknown	
Case 2 GA by Zolfaghari *et al.* (2005)		1.36	Unknown	
Case 3 GA by Zolfaghari *et al.* (2005)		1.37	Unknown	
Case 4 GA by Zolfaghari *et al.* (2005)		0.98	Unknown	
SA	Case 1	1.3961	135,560	135,069
	Case 2	1.2837	106,742	106,662
	Case 3	1.1334	108,542	106,669
	Case 4	1.0081	111,386	109,667
GA	Case 1	1.3733	63,562	63,496
	Case 2	1.2324	77,178	77,114
	Case 3	1.0675	98,332	98,332
	Case 4	0.9631	84,272	84,272
PSO	Case 1	1.3372	62,800	33,116
	Case 2	1.2100	83,400	83,400
	Case 3	1.0474	69,600	69,600
	Case 4	0.9451	68,600	24,440
SHM	Case 1	1.3729	172,464	149,173
	Case 2	1.2326	126,445	100,529
	Case 3	1.0733	99,831	98,070
	Case 4	0.9570	212,160	186,632
MHM	Case 1	1.3501	32,510	32,500
	Case 2	1.2247	40,697	40,687
	Case 3	1.0578	40,476	40,440
	Case 4	0.9411	33,236	33,236
Tabu	Case 1	1.4802	58,588	1188
	Case 2	1.3426	59,790	990
	Case 3	1.1858	63,796	796
	Case 4	1.0848	65,398	998
Ant-colony	Case 1	1.5749	100,200	13,400
	Case 2	1.4488	102,600	1801
	Case 3	1.3028	109,800	5689
	Case 4	1.1372	112,200	18,436

satisfactory due to the use of uniform probability to individual harmony. The present study has illustrated the special feature of slope stability analysis during the optimization analysis, which is not found in other applications as production, system control or other similar disciplines.

On the other hand, for large-scale optimization problems or problems similar to example 3 with the presence of a thin layer of soft band which will create difficulties in the optimization analysis, the effectiveness and the efficiency of the different heuristic optimization methods vary significantly between different problems. The Tabu search and the ant-colony methods have been

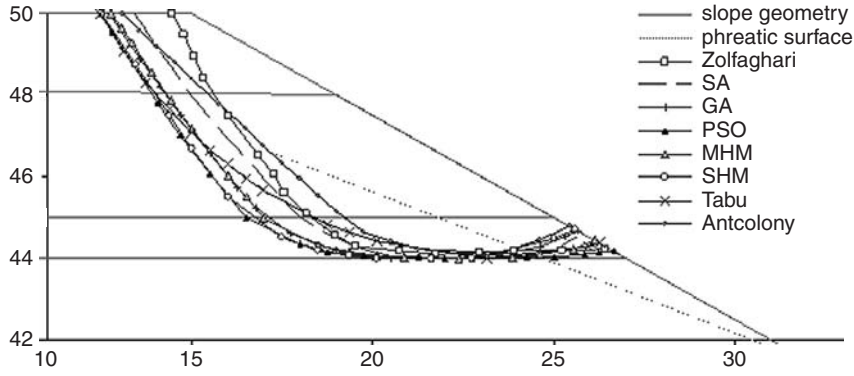

Figure 3.22 Critical slip surfaces for case 1 of example 3.

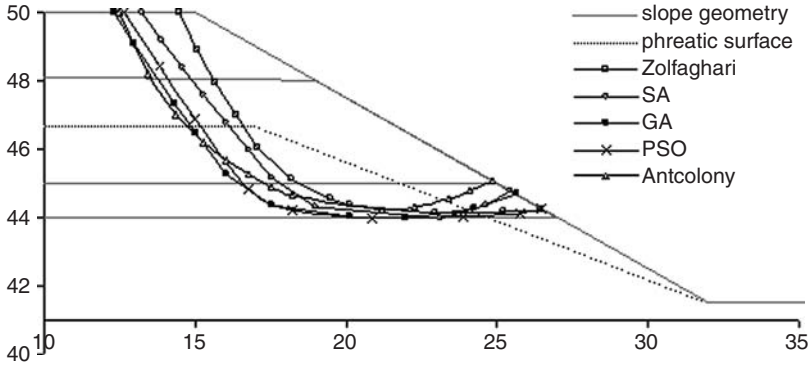

Figure 3.23 Critical slip surfaces for case 2 of example 3 (failure surfaces by GA, MHM, SHM and Tabu are virtually the same).

demonstrated to give poor results in some of the problems, while the PSO method appears to be the most stable and efficient and is recommended for use in such cases. The presence of a thin soft band is difficult for analysis, as a random number with equal opportunity in every solution domain is used in the generation of the trial failure surface. In the present study, the domain transformation method has not been used. If the domain transformation technique as suggested by Cheng (2007) is adopted, all six methods can work effectively and efficiently for problems with soft bands, with the MHM and PSO being the best solution algorithms in terms of efficiency.

For Figure 3.26 where the water table is above the ground surface at the left-hand side of the slope, the SHM and the MHM cannot locate the global minimum using the Spencer method even when the optimization parameters are varied, unless the initial trial failure surface is close to the critical solution.

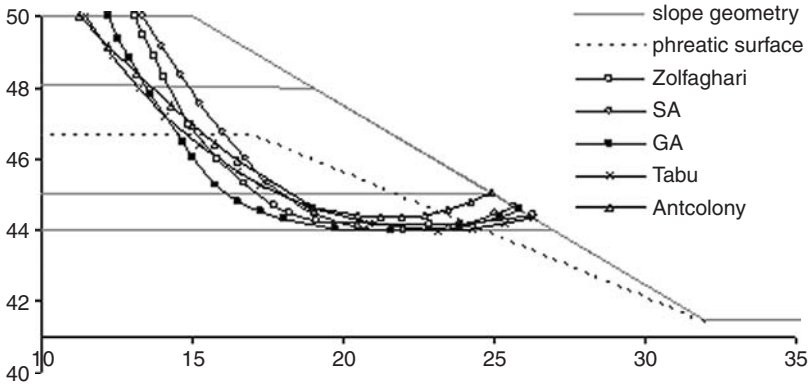

Figure 3.24 Critical slip surfaces for case 3 of example 3 (failure surfaces by GA, PSO, MHM and SHM are virtually the same).

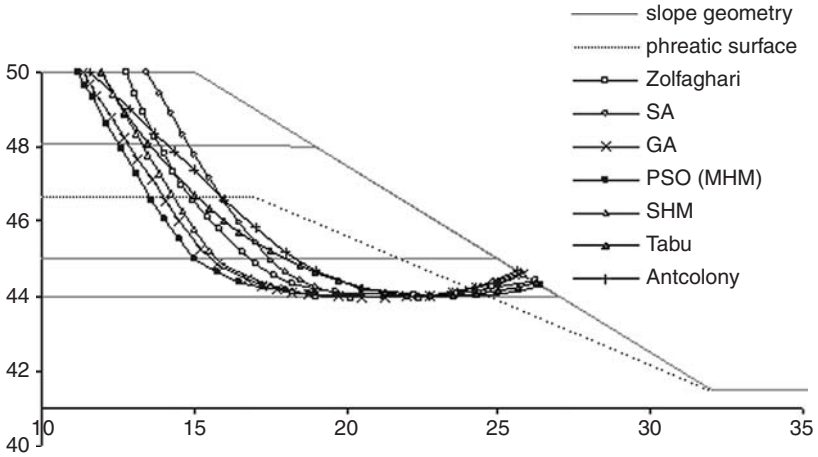

Figure 3.25 The critical slip surfaces for case 4 of example 3.

Cheng has noted that many of the trial failure surfaces (20 per cent) fail to converge in the optimization analysis, which is equivalent to the presence of discontinuity in the objective function. The SHM and the MHM are trapped by the local minima under such cases if the initial trial is not close to the critical solution and there are major discontinuities in the objective function. The GA, the Tabu search and the ant-colony methods all suffer from this limitation. On the other hand, the PSO and the SA can locate the critical solution effectively.

Another interesting case is a steep slope in Beijing, where there is a thin layer of soft material, a tension crack, two soil nails, an external surcharge and water pressure at the tension crack (Figure 3.27). Only the SA method can work

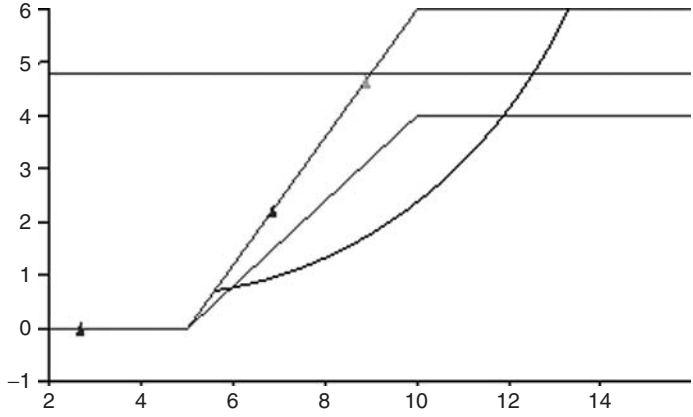

Figure 3.26 Slope with pond water.

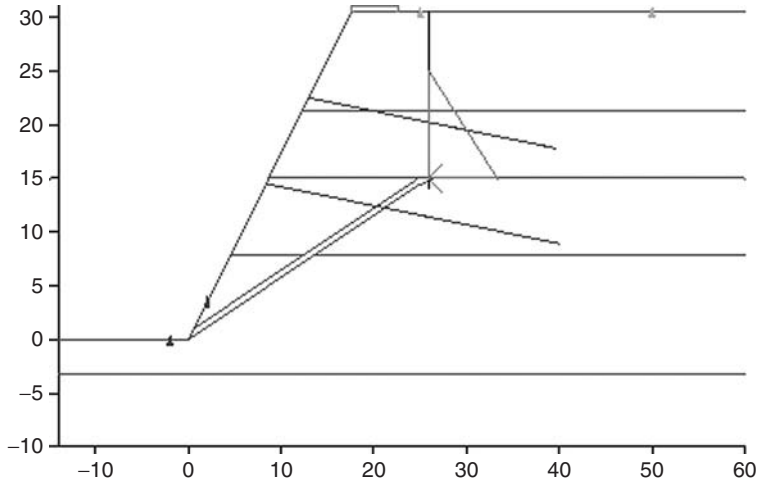

Figure 3.27 Steep slope with tension crack and soil nail.

properly with the Spencer method for this case, while all the methods fail to work properly unless a good initial trial is used. For this problem, Cheng *et al.* (2007b) noticed that all the initial 400–500 trials failed to converge with the Spencer method. Such a major discontinuity in the objective function creates a great difficulty in determining the directions of search for all the global optimization methods, and no solution is obtained from all the optimization methods (complete breakdown) except for the SA. This case is particularly interesting because the optimization methods (except for the SA) lose the direction of search and fail to find even one converged result before termination, unless the optimization parameters and the initial trial are specially tuned. This

Table 3.11 The effects of parameters on SA analysis for examples 1 and 3 ($F_{\lambda} = 0.14$, $F_{t_0} = 0.47$, $F_N = 3.86$, $F_{0.05} = 7.7$, $F_{0.01} = 21.2$)

	1 – 0.5 *2 – 0.8*	*1 – 10.0* *2 – 20.0*	*1 – 100* *2 – 300*	*Ex. 1*	*Ex. 3*	*NOFs*	
						Ex. 1	*Ex. 3*
1	1	1	1	1.7256	1.3232	176,562	140,522
2	2	2	2	1.7241	1.2990	915,902	956,523
3	1	2	2	1.7235	1.2514	339,602	408,482
4	2	1	1	1.7264	1.2745	423,522	349,422
5	2	1	2	1.7258	1.2846	852,602	986,534
6	1	2	1	1.7239	1.3193	183,422	135,262
7	2	2	1	1.7262	1.3213	463,782	360,242
8	1	1	2	1.7268	1.2582	492,122	252,302

special example has also illustrated the difficulty in locating the critical failure surface for some special problems, where convergence is a critical issue. The SA is less sensitive to the discontinuity of the objective function because it is based on the Markov chain with a double looping search technique.

3.7 Sensitivity of the global optimization parameters on the performance of the global optimization method

In all of the heuristic global optimization methods, there is no simple rule to determine the parameters used in the analysis. In general, these parameters are established by experience and numerical tests. It is surprising to find that the sensitivity of different global optimization methods with respect to different parameters is seldom considered in the past, and the sensitivity of the parameters in slope stability analysis has not been reported. The authors consider this issue to be important for geotechnical engineering problems as there are different topographies, sub-soil conditions, ground water conditions, soil parameters, soil nails and external loads controlling the problem. It appears that many researchers have not appreciated the importance of the parameters used for the global optimization. The sensitivity of each parameter can be obtained through the nine numerical tests by the statistical orthogonal tests given in Tables 3.11–3.17 for examples 1 and 3. If the F value (Factorial Analysis of Variance after Fisher; Fisher and Yates, 1963) of one parameter is larger than the critical value $F_{0.05}$ and is smaller than $F_{0.01}$, it implies that the calculated result is sensitive to this parameter; otherwise if the F value is smaller than $F_{0.05}$, the result is insensitive to this parameter. If the F value is larger than $F_{0.01}$, the result is hyper-sensitive to this parameter.

For the simple problem given by example 1, every method can be worked with satisfaction for different optimization parameters. For example 3 which is a difficult problem with a soft band (similar to a Dirac function), the Tabu search and the ant-colony methods are poor in performance (the domain transformation technique is not used) while all the other optimization methods are basically

Table 3.12 The effects of parameters on GA analysis for examples 1 and 3 (F_{ρ_c} = 0.18, F_{ρ_m} = 0.38, $F_{0.05}$ = 161.4, $F_{0.01}$ = 4052)

	ρ_c	ρ_m	*Results*		*NOFs*	
	1 – 0.85 *2 – 0.95*	*1 – 0.001* *2 – 0.1*	*Ex. 1*	*Ex. 3*	*Ex. 1*	*Ex. 3*
1	1	1	1.7273	1.2849	80,384	94,418
2	1	2	1.7266	1.2794	52,544	40,626
3	2	1	1.7272	1.2767	89,806	104,116
4	2	2	1.7266	1.2998	58,612	45,224

Table 3.13 The effects of parameters on PSO analysis for examples 1 and 3 (F_{c_1} = 0.60, F_{c_2} = 0.37, F_{ω} = 0.52, $F_{0.05}$ = 7.7, $F_{0.01}$ = 21.2)

	c_1	c_2	ω	*Results*		*NOFs*	
	1 – 1.0 *2 – 3.0*	*1 – 1.0* *2 – 3.0*	*1 – 0.3* *2 – 0.8*	*Ex. 1*	*Ex. 3*	*Ex. 1*	*Ex. 3*
1	1	1	1	1.7287	1.4430	59,200	45,200
2	2	2	2	1.7401	1.2671	59,200	45,200
3	1	2	2	1.7353	1.2692	59,200	94,800
4	2	1	1	1.7226	1.2368	108,400	231,800
5	2	1	2	1.7309	1.2545	59,800	46,400
6	1	2	1	1.7269	1.2405	75,600	57,600
7	2	2	1	1.7376	1.2747	59,200	45,200
8	1	1	2	1.7266	1.2479	59,200	58,200

Table 3.14 The effects of parameters on SHM analysis for examples 1 and 3 (F_{HR} = 1.91, F_{PR} = 1.13, $F_{0.05}$ = 161.4, $F_{0.01}$ = 4052)

	HR	*PR*	*Results*		*NOFs*	
	1 – 0.80 *2 – 0.95*	*1 – 0.05* *2 – 0.10*	*Ex. 1*	*Ex. 3*	*Ex. 1*	*Ex. 3*
1	1	1	1.7330	1.2947	57,717	180,221
2	1	2	1.7438	1.3748	57,763	81,194
3	2	1	1.7231	1.2799	107,191	68,529
4	2	2	1.7259	1.2824	57,931	118,340

acceptable with the F value less than $F_{0.05}$. The efficiency of different methods for this case is however strongly related to the choice of the parameters, unless the transformation technique by Cheng (2007) is adopted, which is equivalent to the use of a random number with more weighting in the soft-band region.

Every global optimization method can be tuned to work well if suitable optimization parameters or an initial trial are adopted. Since the suitable optimization

Table 3.15 The effects of parameters on MHM analysis for examples 1 and 3 (F_{HR} = 0.97, F_{PR} = 0.07, F_{Nhm} = 0.10, F_{δ} = 0.26, $F_{0.05}$ = 10.1, $F_{0.01}$ = 34.1)

	HR	*PR*	*Nhm*	*δ*	*Results*		*NOFs*	
	1 – 0.80 *2 – 0.95*	*1 – 0.05* *2 – 0.10*	*1 – 0.1* *2 – 0.3*	*1 – 0.3* *2 – 0.8*	*Ex. 1*	*Ex. 3*	*Ex. 1*	*Ex. 3*
1	1	1	1	1	1.7348	1.2838	7654	13,547
2	1	1	1	2	1.7323	1.3523	13,654	9545
3	1	2	2	1	1.7295	1.3102	31,446	34,436
4	1	2	2	2	1.7347	1.3025	31,446	45,235
5	2	1	2	1	1.7270	1.2976	17,159	27,053
6	2	1	2	2	1.7271	1.2874	16,986	26,591
7	2	2	1	1	1.7273	1.2989	9640	15,219
8	2	2	1	2	1.7271	1.2878	19,621	13,128

Table 3.16 The effects of parameters on Tabu analysis for examples 1 and 3 (F_d = 0.63, F_{N_t} = 0.17, F_{HR} = 0.49, F_{PR} = 1.43, $F_{0.05}$ = 10.1, $F_{0.01}$ = 34.1)

	d	N_t	*HR*	*PR*	*Results*		*NOFs*	
	1 – 2 *2 – 5*	*1 – 30* *2 – 50*	*1 – 0.80* *2 – 0.95*	*1 – 0.05* *2 – 0.10*	*Ex. 1*	*Ex. 3*	*Ex. 1*	*Ex. 3*
1	1	1	1	1	1.7411	1.5714	58,388	44,168
2	1	1	1	2	1.7413	1.5391	58,188	44,168
3	1	2	2	1	1.7424	1.5661	58,188	44,168
4	1	2	2	2	1.7413	1.5661	58,188	44,168
5	2	1	2	1	1.7429	1.5661	58,588	44,168
6	2	1	2	2	1.7415	1.5427	58,188	44,168
7	2	2	1	1	1.7415	1.5470	58,188	44,368
8	2	2	1	2	1.7354	1.5561	59,188	44,168

Table 3.17 The effects of parameters on ant-colony analysis for examples 1 and 3 (F_{μ} = 11.8, F_Q = 0.002, F_d = 39.7, $F_{0.05}$ = 7.7, $F_{0.01}$ = 21.2)

	μ	*Q*	*d*	*Results*		*NOFs*	
	1 – 0.3 *2 – 0.8*	*1 – 10.0* *2 – 50.0*	*1 – 10* *2 – 20*	*Ex. 1*	*Ex. 3*	*Ex. 1*	*Ex. 3*
1	1	1	1	1.7447	1.5332	83,500	76,200
2	2	2	2	1.7404	1.9239	66,800	50,800
3	1	2	2	1.7636	1.8787	66,800	50,800
4	2	1	1	1.7717	1.7420	83,500	76,200
5	2	1	2	1.7377	1.9239	66,800	50,800
6	1	2	1	1.7538	1.5049	83,500	76,200
7	2	2	1	1.7569	1.7420	83,500	76,200
8	1	1	2	1.7591	1.8435	66,800	50,800

parameters or the initial trial is difficult to be established for a general problem, the performance of a good optimization method should be relatively insensitive to these factors. Based on the numerical examples and the two special cases shown in Figures 3.26 and 3.27 and some other internal studies by the authors, the general comments on the different heuristic artificial intelligence-based global optimization methods are:

1 For normal and simple problems, practically every method can work well. The harmony method and the genetic algorithm are the most efficient methods when the number of control variables is less than 20. The Tabu search and the ant-colony method are sometimes extremely efficient in the optimization process, but the efficiency of these two methods fluctuate significantly between different problems and are not recommended.
2 For normal and simple problems where the number of control variables exceeds 20, the MHM and the PSO are the recommended solutions as they are more efficient in the solution, and the solution time will not vary significantly between different problems.
3 For more complicated problems or when the number of control variables is great, the effectiveness and efficiency of the PSO is nearly the best in all of the examples.
4 A thin soft band creates great difficulty in the global optimization analysis and the PSO will be the best method in this case. However, using the domain transformation strategy by Cheng (2007), all the global optimization methods can work well for this case.
5 For problems where an appreciable amount of trial failure surfaces will fail to converge, the simulated annealing method and the PSO are the recommended solutions.

In view of the differences in the performance between different global optimization algorithms, a more satisfactory solution is the combined use of two different algorithms. For example, the PSO or the MHM can be adopted for normal problems, while the SA can be adopted when the 'failure to convergence' counter is high. Further improvement can be achieved by using the optimized results from a particular optimization method as a good initial trial, and a second optimization method adopts the optimized result from the first optimization algorithm for the second stage of optimization with a reduced solution domain for each control variable.

3.8 Convexity of critical failure surface

From Cheng's extensive trials, it can be concluded that most of the critical failure surfaces are convex in shape. The generation of the convex failure surfaces as given in Section 3.2 is adequate for most cases. There are, however, some cases where the ground conditions may generate non-convex critical failure surfaces, which have been discussed by Janbu (1973), and this is further investigated in this section. The slope with a middle soft band is shown in Figure 3.28.

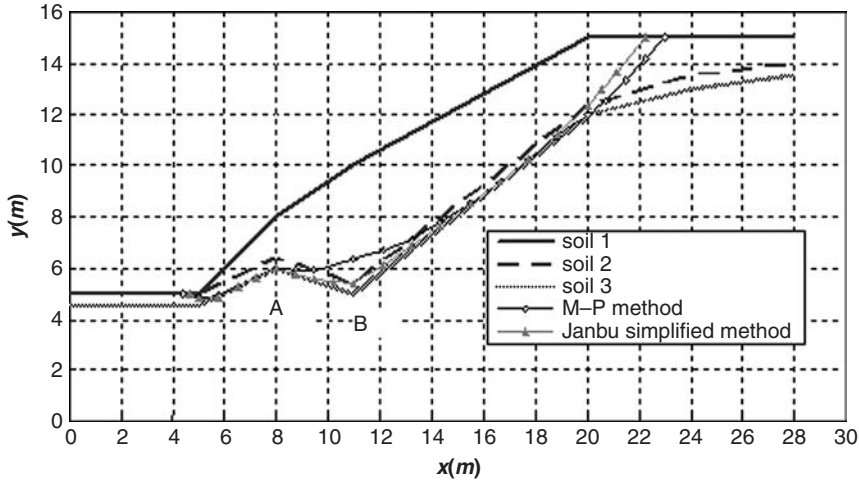

Figure 3.28 Critical failure surfaces for a slope with a soft band by the Janbu simplified method and the Morgenstern–Price method.

The soil properties for the three soils are: c' = 4 kPa, ϕ' = 33°; c' = 0 kPa, ϕ' = 25°; and c' = 10 kPa, ϕ' = 36°, measured from top to bottom. This slope is analysed using the Janbu simplified method and the Morgenstern–Price method, and the critical failure surfaces from the analyses are shown in Figure 3.28. The two critical failure surfaces are controlled by the soft band and are similar in location except for section AB. Using the Janbu simplified method, which satisfies only force equilibrium, the critical failure surface (FOS = 0.985 without correction factor) basically follows the profile of the soft band even though the kink AB should hinder the failure of the slope. On the other hand, if the Morgenstern–Price method is used, the kink AB becomes important in the moment equilibrium and no kink is found for the critical failure surface unless the friction angle of soil 2 is lowered to 20° (a mild kink only). This result illustrates that different stability formulations may require different generations of the slip surface algorithm. These kinds of non-convex critical failure surfaces are not commonly encountered but should be allowed in the generation of trial failure surfaces if necessary. The slip surface generation scheme outlined in Section 3.2 can achieve this requirement easily by simply eliminating the requirement on the lower bound of each control variable. This option is also available in SLOPE 2000 which can be chosen if required.

3.9 Lateral earth pressure determination

Slope stability analysis methods based on the limit equilibrium approach are upper bound methods. In the Janbu simplified approach, the basic assumptions are:

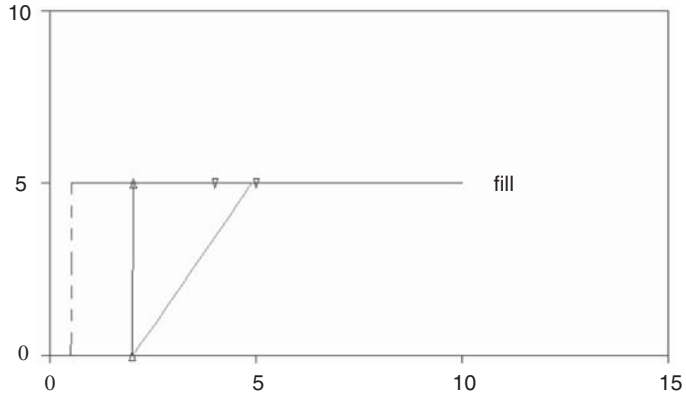

Figure 3.29 Critical failure surface from Janbu simplified without f_0 based on non-circular search, completely equal to Rankine solution.

1 upper bound limit equilibrium approach;
2 Mohr–Coulomb relation; and
3 force equilibrium.

In the classical earth pressure problems, the Coulomb earth pressure theory is also based on the upper bound approach with consideration of force equilibrium but not moment equilibrium. The assumption used in the Coulomb theory is actually the same as that in the Janbu simplified method, so the two problems should actually be equivalent problems. Consider a 5 m height slope with a level back. The soil parameters are $c' = 0$, $\phi' = 30°$ and unit weight = 20 kNm^{-3}. The horizontal lateral pressure 16.665 kNm^{-1} is found by a trial and error approach when the minimum factor of safety is equal to 1.0. It should be noted that since force equilibrium is used in the Janbu simplified method, the use of point load, uniformly distributed load or triangular load will be completely equivalent in the present analysis. The correction factor f_0 should not be used in this case because only force equilibrium is considered in the Coulomb mechanism while f_0 will correct the inter-slice shear force and moment equilibrium for the Janbu simplified analysis.

The minimum factor of safety as found is 1.0001 and the critical failure surface shown in Figure 3.29 is completely equivalent to the classical Rankine solution. The total load on this slope is 16.665 × 5 = 83.325 kN. The active pressure coefficient can be back calculated as

$$83.325 = 0.5\, K_a \times 20 \times 5^2 \qquad \Rightarrow \qquad K_a = 0.3333 = (1 - \sin\phi)/(1 + \sin\phi)$$

This result is exactly the same as the Rankine solution or the Coulomb solution. The critical failure surface from the non-circular search is also found

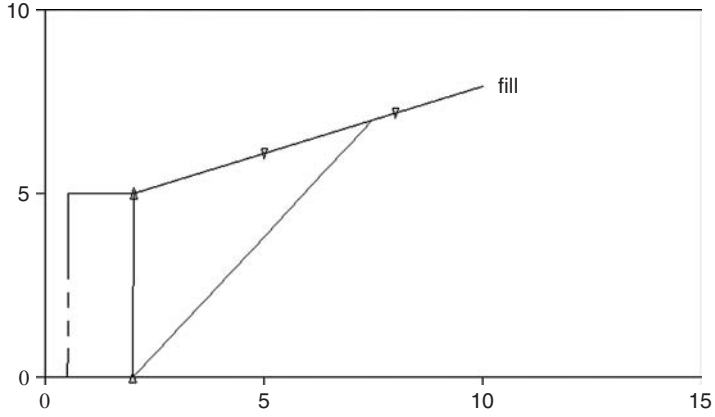

Figure 3.30 Critical failure surface from Janbu simplified without f_0 based on non-circular search, completely equal to Rankine solution.

to be a plane surface inclined at an angle of 60° with the horizontal direction, which is equivalent to 45° + ϕ/2 from the Rankine solution. The next example is the same as the previous one with a 20° slope behind the 5 m high slope. The total load on this slope for a minimum factor of safety of 1.0 is 110.25 kN. The active pressure coefficient can be calculated as

$$110.25 = 0.5\ K_a \times 20 \times 5^2 \qquad \Rightarrow \qquad K_a = 0.441$$

This result is exactly the same as the Coulomb solution for a slope with a 20° back which is shown in Figure 3.30. The failure surface is also found to incline at an angle of 52°. The angle of inclination for this case can be found from Design Manual 7 (see 7.2–65) which is given by

$$\tan\theta = \tan\phi + (1 + \tan^2\phi - \tan\beta/\sin\phi/\cos\phi)^{0.5}$$

If we put in $\beta = 20°$, θ is obtained as 52°, and this is exactly the same as that obtained from the non-circular search as discussed before (see also the user guide of SLOPE 2000 for the detailed results).

The point of application of the active pressure can be determined from the moment balance of the failure mass and is found to be at one-third the height of the retaining wall. The present technique can be extended for a retaining wall with a non-homogeneous backfill, and the point of application of the active pressure can be determined by the moment equilibrium between the base normal and shear forces, the weight of soil and the total active pressure from slope stability analysis.

3.10 Convergence

The factor of safety function is a highly nonlinear equation (Sarma, 1987). Presently, most of the slope analysis programs are based on the iteration method which requires an initial trial in the analyses (commonly 1.0). Cheng *et al*. (2008a) have noticed that while the iteration method has been used for a long time, it has never been proved to be effective under all the cases. Many engineers have experienced the problem of convergence with the M–P method or similar methods in determining the factor of safety, in particular when there are soil nails or external loads in the problems. In all the slope stability programs, if convergence is not achieved during evaluation of the factor of safety, an arbitrary large factor of safety is usually assigned to the trial failure surface. If the phenomenon of 'failure to converge' is not a true phenomenon, the use of a large factor of safety (discontinuity of the safety factor function) can greatly affect the search for the critical failure surface, in particular when the gradient-type method is used for the optimization analysis. This problem will be serious if convergence is important, and this will be demonstrated in a later section by some cases from Hong Kong.

In the search for the critical failure surface by the manual trial and error approach, most engineers tackle the problem of 'failure to converge' by modifying the shape and location of the prescribed failure surface until a converged result is achieved. The minimum factor of safety will then correspond to the minimum value from the limited trial failure surfaces which can converge by iteration analysis. It is also interesting to note that it has never been proved that a failure surface which fails to converge by iteration analysis is not a critical failure surface!

Failure to converge for the 'rigorous' method is experienced by many geotechnical engineers as the iteration method is used in most of the commercial programs. Cheng (2003) has formulated the slope stability problem in a matrix approach where the factor of safety and internal forces can be determined directly from a complex double QR matrix method without the need of an initial factor of safety. Cheng has proved that there are N factors of safety associated with the nonlinear factor of safety equation for a problem with N slices. In the double QR method, all the N factors of safety can be determined directly from the tedious matrix equation *without* using any iteration, and the factors of safety can be classified into three groups:

1 imaginary number;
2 negative number; and
3 positive number.

If all the factors of safety are either imaginary or negative, the problem under consideration has no physically acceptable answer by nature. Otherwise, the positive number (usually 1–2 positive numbers left) will be examined for the physical acceptability of the corresponding internal forces and a factor of safety will then be obtained. Under this new formulation, the fundamental nature of the problem is *fully* determined. If no physically

acceptable answer is obtained from the double QR method (all results are imaginary or negative numbers), the problem under consideration has no answer by nature, and the problem can be classified as 'failure to converge' under the assumption of the specific method of analysis. If a physically acceptable answer exists for a specific problem, it will be determined by this double QR method. The authors have found that many problems which fail to converge with the classical iteration method actually possess meaningful answers by the double QR method. That means that the phenomenon of 'failure to converge' may come from the use of the iteration analysis and may be a false phenomenon in some cases. Cheng *et al.* (2008a) have found that many failure surfaces which fail to converge are normal in shape and should not be neglected in ordinary analysis and design. This situation is usually not critical for the slope with simple geometry and no soil nail/external load, but convergence for the 'rigorous' method will be a more critical issue when soil nails/external loads are present in a problem. Since the use of the soil nail is now very common in many countries, the problem of convergence which is faced by many geotechnical engineers should not be overlooked.

To evaluate the importance of the convergence on the analysis, specific problems and parametric studies using commercial programs will be considered. Figure 3.31 shows a simple slope with no water or soil nail, and the soil parameters are $c' = 5$ kPa, $\phi' = 36°$ and unit weight = 20 kNm^{-3}. The prescribed circular failure surface fails to converge with the iteration method (even when the correct factor of safety is used as the initial solution), but a factor of safety equal to 1.129 for M–P analysis is found by using the double QR method. The corresponding result for Sarma analysis is 1.126 which is also similar to that by M–P analysis. This simple problem has illustrated that a failure surface which fails to converge by the iteration method may actually possess physically acceptable answers. Since many Hong Kong engineers have encountered convergence problems with a soil-nailed slope, the second problem shown in Figure 3.32 is considered, where the soil nail loads are 30, 40 and 50 kN from left to right. The soil parameters for the top soil are $c' = 3$ kPa, $\phi' = 33°$ and unit weight = 18 kNm^{-3} while the soil parameters for the second layer of soil are $c' = 5$ kPa, $\phi' = 35°$ and unit weight = 19 kNm^{-3}. The nail loads are applied at the nail head as well as on the slip surface for comparisons in this study. The results of analyses based on the iteration method by three commercial programs and the double QR method by Cheng (2003) are shown in Table 3.18.

For those in Table 3.18, the double QR method gives physically acceptable answers (or converged answers) for all the cases while the iteration method fails to work for some of the M–P analyses. It is clear from Table 3.18 that the M–P method using the iteration method suffers from the 'failure to converge' problem, but answers actually exist for some of these problems. When only soil nail 3 is applied to the slope, it is noticed from Table 3.18 that one of the commercial programs can converge while the other commercial program fails to converge. It appears that convergence also depends on the specific procedures in the iteration analysis or the use of moment point in the individual program. Cheng *et al.* (2008a) have also found that the use of over-shooting in iteration analysis may generally

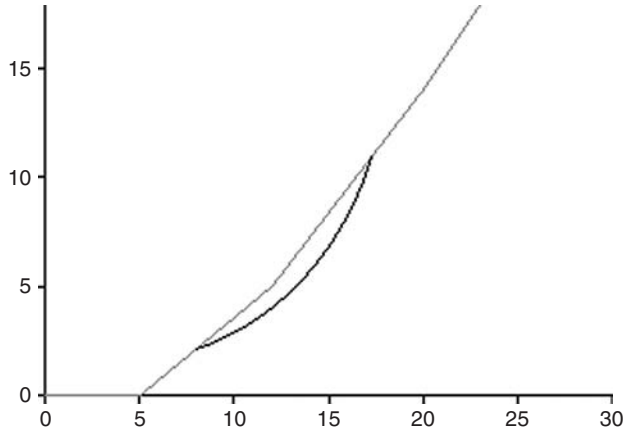

Figure 3.31 A simple slope fails to converge with iteration.

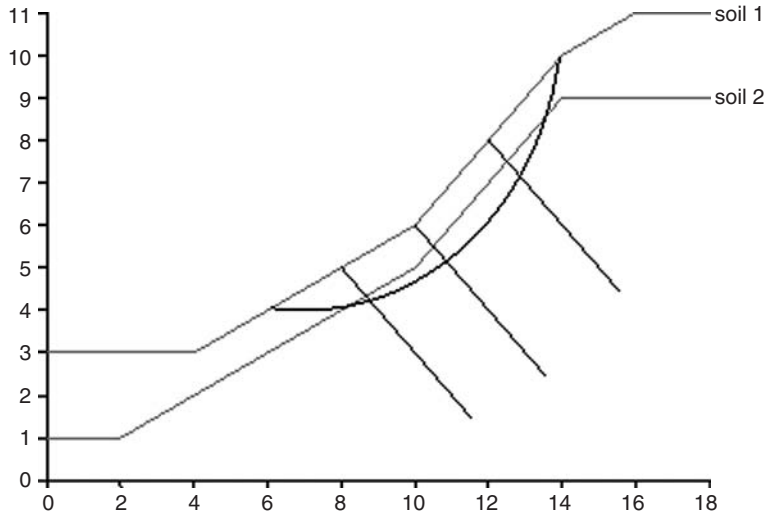

Figure 3.32 A slope with three soil nails.

improve the computation speed but is slightly poorer in convergence (from internal study). For the slope with no soil nail shown in Figure 3.31, Cheng *et al.* (2008a) have tried different moment points but convergence is still not achieved with the iteration method. The authors have also found that some problems may converge by the iteration method if a suitable moment point is chosen for analysis, but great effort will be required to try this moment. For an arbitrary problem, the region suitable for use as the moment point has to be established by a trial and error

Table 3.18 Performance of iteration analysis with three commercial programs based on iteration analysis for the problem in Figure 3.35 (c means converged by iteration analysis; fail means failure to converge by iteration analysis)

	Soil nail 1 – 30 kN	*Soil nail 2 – 40 kN*	*Soil nail 3 – 30 kN*	*No nail*
Load applied at nail head				
Spencer	c/c/c	c/c/c	c/c/c	c/c/c
Load applied at slip surface				
Spencer	Fail/fail/c	Fail/fail/fail	c/fail/c	c/c/c

	Soil nail 1 + 2	*Soil nail 1 + 3*	*Soil nail 2 + 3*	*Soil nail 1 + 2 + 3*
Load applied at nail head				
Spencer	c/c/c	Fail/fail/fail	c/c/c	c/c/c
Load applied at slip surface				
Spencer	Fail/fail/fail	c/c/c	Fail/fail/fail	Fail/fail/fail

approach, and there is no simple way to pre-determine this region in general. The convergence problem is critical for the M–P method but is rare for the Janbu simplified method. Cheng *et al.* (2008a) have however constructed a deep-seated non-circular failure surface shown in Figure 3.33 where $c' = 5$ kPa, $\phi' = 36°$ and unit weight = 20 kNm^{-3}. The Janbu analysis fails to converge with an initial factor of safety equal to 1.0, but convergence is possible with an initial trial of 2.0. The double QR method can work satisfactorily for this problem as no initial factor of safety is required and the factor of safety is obtained directly. For this problem, the iteration method can work by changing the initial factor of safety, but this technique seldom works for those 'rigorous' methods. In general, convergence is important mainly for 'rigorous' methods, but is rare for those 'simplified' methods. Up to present, Cheng *et al.* cannot construct a problem where the Bishop method fails to converge but possesses a physically acceptable answer, and it appears that the Bishop method is virtually free from convergence problems. In fact, if the failure surface is circular in shape, Cheng *et al.* are not able to construct any case for Bishop or Janbu analysis where the iteration method fails to work, but a physically acceptable answer can be determined from the double QR method.

Cheng *et al.* (2008a) have come across an interesting case in Hong Kong which is shown in Figure 3.34. For this slope with a retaining wall, the Morgenstern–Price method is adopted in the analysis. Engineers have experienced great difficulties in drawing suitable failure surfaces which can converge in the analysis, and a minimum factor of safety of 1.73 is determined from several trials which can converge. When the iteration analysis is used by the authors using an automatic location of the critical failure surface, no solution can be found for the first 20,162 trials during the simulated annealing analysis, which has demonstrated that this problem is difficult to

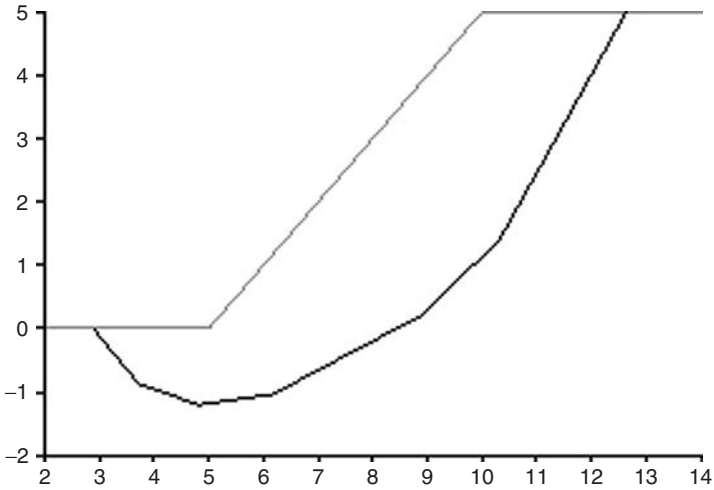

Figure 3.33 Failure to converge with the Janbu simplified method when initial factor of safety = 1.0.

converge by the iteration analysis. When Cheng *et al*. re-considered this problem using the double QR method, 'failure to converge' was greatly reduced and a minimum factor of safety of 1.387 was found, which is much lower than that found by the engineers. The critical failure surface shown in Figure 3.34 is re-considered by the iteration analysis using some commercial programs, but convergence cannot be achieved even if the correct answer is used as the initial factor of safety. This case has clearly illustrated the importance of the convergence for some difficult problems.

3.10.1 Parametric study on convergence

To investigate the phenomenon of convergence, a systematic parametric study using the Morgenstern–Price method is carried out for the simple slope shown in Figure 3.35 with only soil 1 and water. Nearly 20 test cases with different c' and ϕ' are used in the parametric tests, and the soil parameters are shown in Table 3.19. For the 20 test cases, three conditions are considered: no soil nail, three soil nails with each nail load equal to 30 kN and three soil nails with each nail load equal to 300 kN (maximum nail load in Hong Kong is 400 kN). A search for the critical circular failure surface is considered in generating trial failure surfaces by using a commercial program. The x-ordinates of the left exit end of the failure surface is controlled within $x = 0$ m to $x = 3.0$ m, while the x-ordinate of the right exit is controlled within $x = 3.1$ m to $x = 16$ m. Several thousands of failure surfaces are generated during the optimization search for each test case, and the percentage of 'failure to

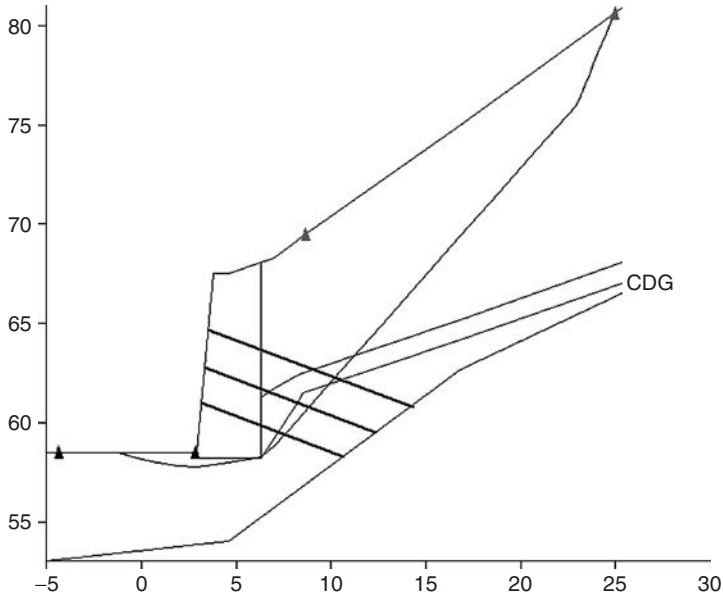

Figure 3.34 A problem in Hong Kong which is very difficult to converge with the iteration method.

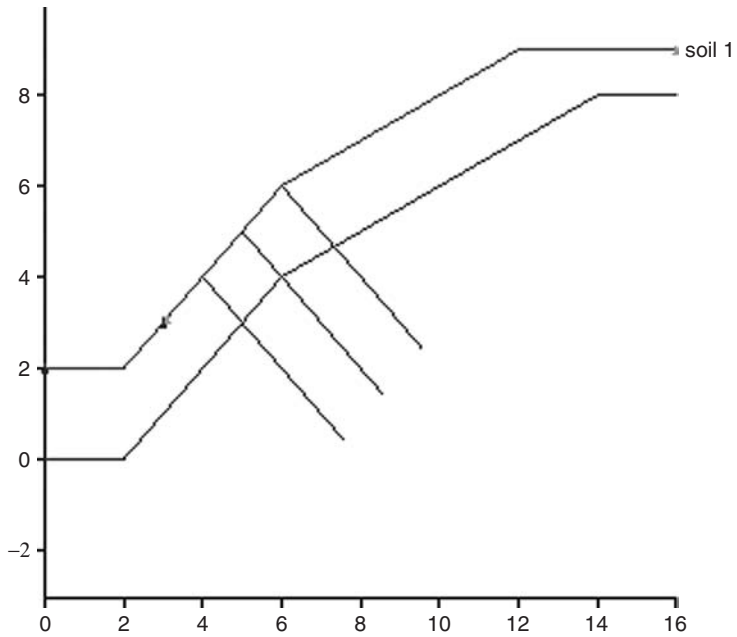

Figure 3.35 A slope for parametric study.

Table 3.19 Soil properties for Figure 3.35

Case	*c′ (kPa)*	*ϕ′ (°)*	*Case*	*c′ (kPa)*	*ϕ′ (°)*	*Case*	*c′ (kPa)*	*ϕ′ (°)*	*Case*	*c′ (kPa)*	*ϕ′ (°)*
1	0	10	6	0	20	11	0	30	16	0	40
2	5	10	7	5	20	12	5	30	17	5	40
3	10	10	8	10	20	13	10	30	18	10	40
4	15	10	9	15	20	14	15	30	19	15	40
5	20	10	10	20	20	15	20	30	20	20	40

Source: Reproduced with permission of Taylor & Francis.

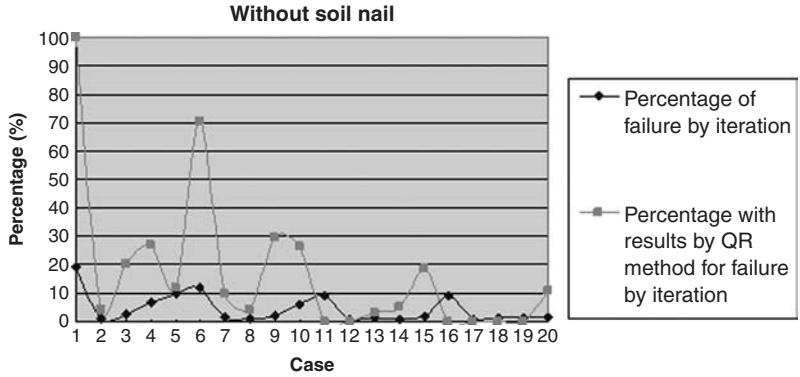

Figure 3.36 Percentage failure type 1 for no soil nail.

converge' is determined. Those cases which fail to converge with the iteration method are analysed by the double QR method individually, and many of these cases actually possess physically acceptable answers. The results of these analyses are shown in Figures 3.36–3.41.

There are two types of 'failure to converge' in the commercial program adopted for the comparison which are worth discussion. For type 1, the converged result is not obtained with respect to the tolerance of iteration analysis. For type 2, the 'converged' results are very small with unreasonable internal forces. The authors have also independently obtained very small 'converged' factors of safety based on iteration analysis and the internal forces are all extremely large. If the factor of safety during the iteration analysis becomes very small, the difference between two successive trials can be less than the tolerance and a 'false' convergence is achieved. If the tolerance is further reduced towards 0, the factor of safety will also further reduce and tends to 0 while the internal forces will tend to infinity. When the double QR method is used, the small factor of safety is actually not the root of the factor of safety matrix, so the use of the double QR method will not experience such 'false' convergence as in the iteration analysis.

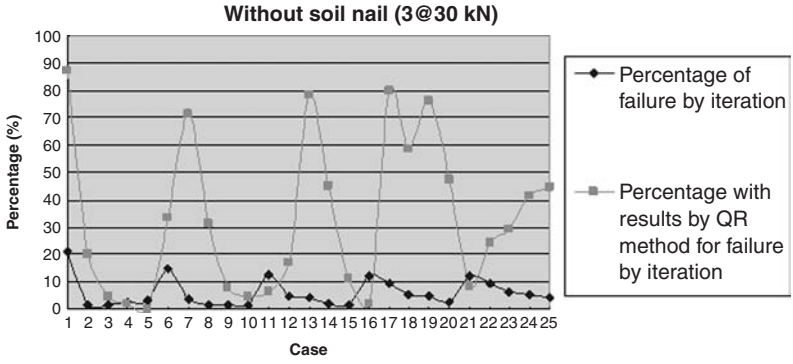

Figure 3.37 Percentage of failure type 1 for 30 kN soil nail loads.

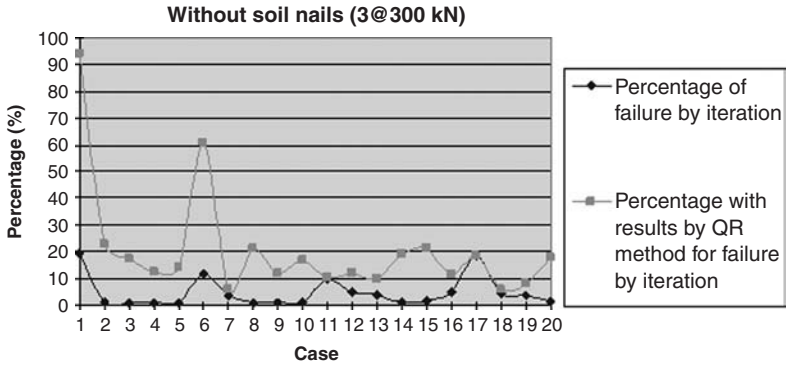

Figure 3.38 Percentage of failure type 1 for 300 kN soil nail loads.

As shown in Figures 3.36–3.38, the use of the iteration method by a commercial program experiences 'failure to converge' with an interesting wave pattern for both type 1 and type 2 'failure to converge'. It is noticed that when ϕ' is 0 or very small, the use of the iteration method will experience more failure to converge while the double QR method is effective in determining meaningful answers for most of the cases. When the friction angle is high, the iteration method appears to perform well. Besides that, the use of great soil nail forces will create great difficulties in convergence, which is also shown in Figures 3.38 and 3.41. The double QR method can however provide meaningful answers to many of the problems with great soil nail forces. The results shown in Figures 3.38 and 3.41 are particularly important to Hong Kong, as large diameter soil nails with a maximum load of 400 kN for each bar are sometimes used there. Many Hong Kong engineers have also experienced the

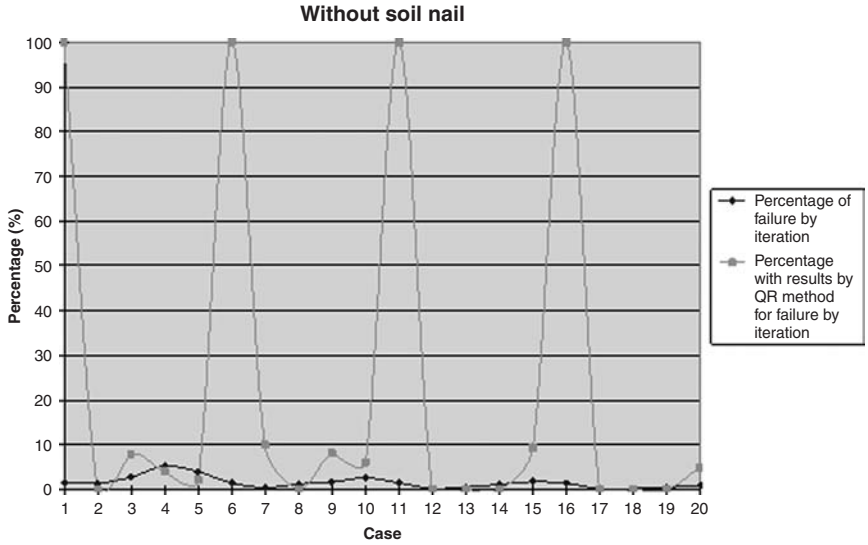

Figure 3.39 Percentage failure type 2 for no soil nail.

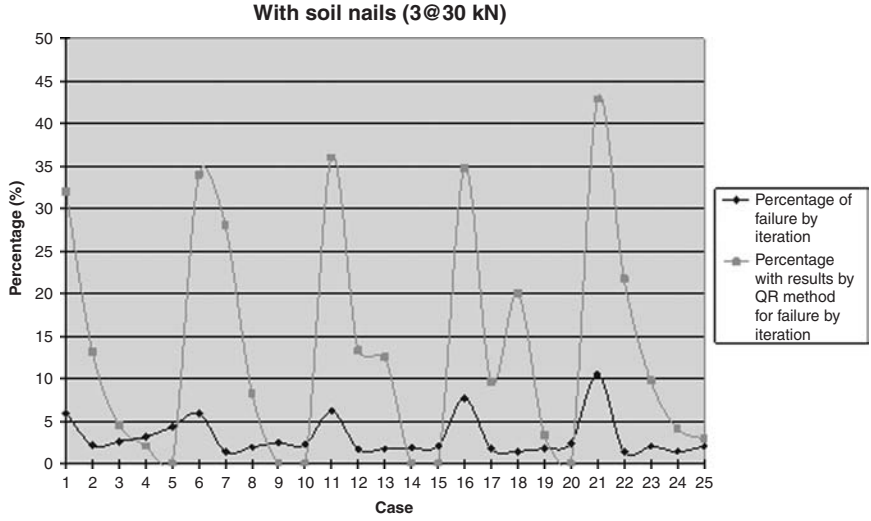

Figure 3.40 Percentage of failure type 2 for 30 kN soil nail loads.

problem of convergence with the presence of soil nails, and the problem in Figure 3.34 is a good illustration of the importance of the convergence in slope stability analysis.

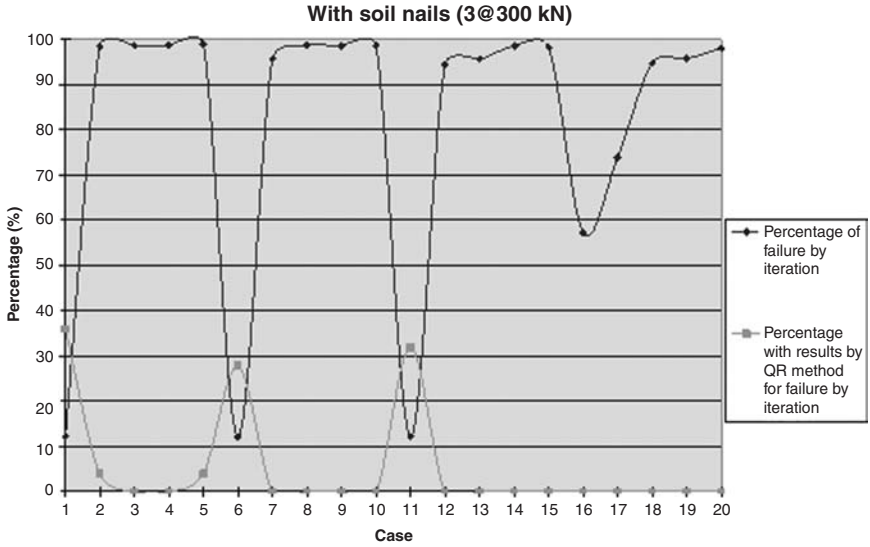

Figure 3.41 Percentage of failure type 2 for 300 kN soil nail loads.

3.10.2 Combined impact of optimization and double QR analysis

The previous section has illustrated the importance of the convergence on slope stability analysis. In this section, some cases from Hong Kong which are analysed by experienced engineers are re-considered by the authors. For the 13 cases shown below, all of them are analysed by engineers using the classical approach: manual location of the critical non-circular failure surface with 10–20 trials, while those failure surfaces which fail to converge will be neglected in the analysis. Cheng *et al.* (2008a) have used the double QR method in reducing convergence in the Morgenstern–Price analyses, and the critical failure surfaces are located by the use of the simulated annealing method (Cheng 2003). The results of analyses and the comparisons are shown in Table 3.20.

In Table 3.20, the differences between the results by the engineers and those by Cheng *et al.* (2008a) are due to the optimization search and the convergence problems, but the individual contribution from these two factors cannot be separated clearly. Out of these 13 cases, the percentage differences are smallest for cases 7, 8 and 11, where the slope angles are not high and only a small amount of soil nails is required. The convergence problem is also less critical for these cases during the optimization search. The critical failure surfaces for cases 2 and 5 are the deep-seated type which lie below the retaining wall, and convergence is difficult for these deep-seated failure surfaces by

Table 3.20 Impact of convergence and optimization analysis for 13 cases with Morgenstern–Price analysis

Case	*FS by engineer*	*FS by double QR*	*% difference*	*Remark*
1	1.404	1.196	17.4	3 soil, no soil nail
2	1.458	1.152	26.6	4 soil, retaining wall, surcharge
3	1.5	1.18	27.1	2 soil, 12 soil nails
4	1.43	1.09	31.2	4 soil, 8 soil nails, surcharge
5	1.73	1.388	24.6	2 soil, retaining wall, 3 soil nails
6	1.406	1.253	12.2	3 soil, 7 soil nails
7	1.406	1.324	6.2	2 soil, 3 soil nails
8	1.4	1.293	8.3	3 soil, 4 soil nails
9	1.41	1.05	34.3	3 soil, 6 soil nails, steep slope
10	1.5	1.279	17.3	3 soil, 5 soil nails
11	1.408	1.328	6	2 soil, 3 soil nails
12	1.51	1.027	47	4 soil, 9 soil nails, steep slope
13	1.25	1.059	18	2 soil, 3 soil nails

iteration analysis with some commercial programs. The slopes are steep for cases 3, 4, 9 and 12, and convergence with iteration analysis is difficult for these cases. It is noticed that, for steep slopes, deep-seated failure mechanisms or slopes stabilized with many soil nails, greater differences are found between the engineers' results and the refined results by the authors. For these cases, convergence is usually a problem, and only limited trials can be achieved by the manual trial and error approach.

3.10.3 Reasons for failure to converge

To investigate the reason behind 'failure to converge' even when the correct answer is used as the initial solution, the equilibrium equations shown below should be considered.

For the slice shown in Figure 3.42, the total base normal force P and the inter-slice normal forces are given by:

$$N = [W - (V_R - V_L) - \frac{1}{F}(c'l \sin\alpha - ul \tan\phi' \sin\alpha)]/m_\alpha \tag{3.16}$$

$$P_R - P_L = N \sin\alpha - [c'l + (N - ul)\tan\phi']\cos\alpha/F \tag{3.17}$$

where $m_\alpha = \cos\alpha(1 + \tan\alpha \frac{\tan\phi'}{F})$

In solving the equilibrium equations to determine the factor of safety F, the inter-slice shear force V_R and V_L are usually assumed to be 0 in eq. (3.16) in the first step during the classical iteration method or the Newton–Rhapson method by Chen *et al.* (1983) or Zhu *et al.* (2001, 2005). When the correct factor of safety is used as the initial trial in eq. (3.16), N and hence F will not

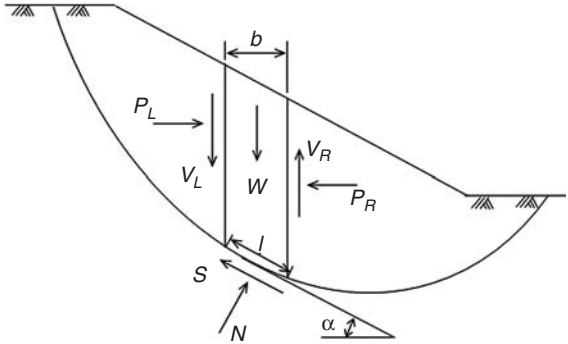

Figure 3.42 Forces acting on a slice.

be correct even when F is correct in the right-hand side of eq. (3.16), as V_R and V_L are assumed to be 0 which is clearly not correct. The inter-slice normal force from eq. (3.17) will then be incorrect, which leads to the inter-slice shear force which is computed based on $V = \lambda f(x)P$ to be incorrect. Eq. (3.17) which is one step behind eq. (3.16) will not be correct as F is not correctly obtained from the left-hand side of eq. (3.16) in the first step. This iteration approach based on $V = 0$ in the first step is used classically and is possibly the solution algorithm adopted in the commercial programs. Referring to Figure 3.42 which is example 1 shown in Figure 3.31, the initial F_m based on the iteration analysis is close to the correct solution 1.553 when λ is 0 (factor of safety is not sensitive to the inter-slice shear force when λ is small). However, F_f is sensitive to the inter-slice shear force V when it is assumed to be 0 in the first step. When λ increases, V is no longer zero but will deviate more and more from the correct value, and the effect on F_f becomes worse when an incorrect V is used in the iteration process. The results shown in Figure 3.43 will however be completely different when 10 per cent of the correct inter-slice shear force is specified in the first step of iteration analysis. As long as a constant ratio of 10 per cent (or more) is specified for all the slices, F_f will be much closer to F_m initially by iteration analysis, and convergence can be achieved easily with λ = 0.71 and F = 1.553. While many problems are not sensitive to the inter-slice shear force so that the iteration method can work well, example 1 is very sensitive to the inter-slice shear force so that the iteration analysis leads to a wrong solution path during the nonlinear equation solution, even when the correct F is used for the right-hand side of eq. (3.16) in the first step.

In Figure 3.43, the centroid of the soil mass is taken as the moment point for the analysis. If the moment point is varied, the results can be different and sometimes some problems may get converged using a different moment point. This practice is sometimes adopted by engineers to overcome the convergence problem, and many commercial programs allow the use of different moment

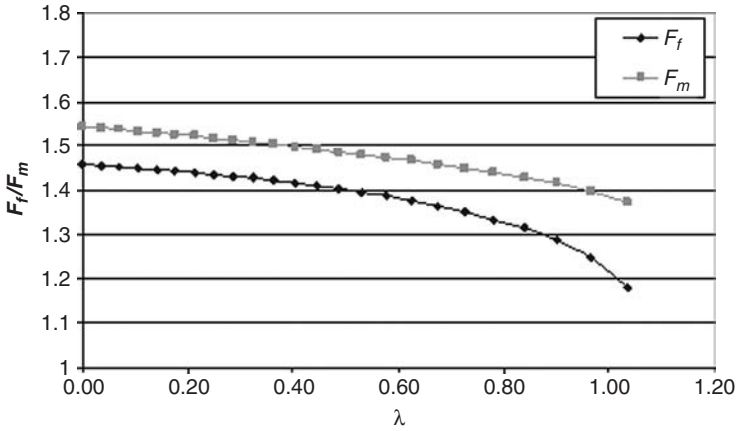

Figure 3.43 F_f and F_m from iteration analysis based on an initial factor of safety 1.553 for example 1.

points in the evaluation of the factors of safety. There is however no systematic and automatic way to change the moment point for general cases, so the moment point will be kept constant during the optimization search in commercial programs.

Cheng *et al.* (2008a) have also tried to adopt the approach by Baker (1980) where the iteration method does not require $V = 0$ in the first step. It is found that convergence is improved by removing this requirement, but there are still cases where 'failure to converge' exists while the double QR method can find physically acceptable solutions. It can be concluded that the inter-slice shear force is the main cause for the 'failure to converge' in the classical iteration method. To overcome the convergence problem, the extremum principle outlined in Section 2.9 can be used. This approach will give the factor of safety practically for every failure surface.

3.11 Importance of the methods of analysis

In general, different methods will give a similar factor of safety, and the differences between the 'rigorous' and the 'simplified' methods are small. Cheng has however come across many cases where there are noticeable differences in the factor of safety which is worth discussing. Consider the problem in Figure 3.44 which is a project in China. For the prescribed failure surface, the factors of safety for the simplified methods are 2.358 (f_0 = 1.068), 2.159, 2.796 and 3.563 for the Janbu simplified, Corps of Engineers, Lowe–Karafiath and load factor methods. The factors of safety for the rigorous methods are 3.06, 3.38, 3.857, 3.361 and 3.827 for the Sarma, M–P ($f(x) = 1.0$

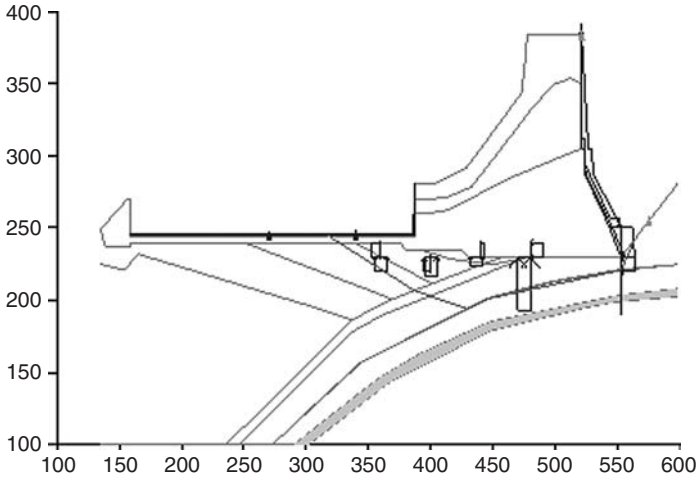

Figure 3.44 A complicated problem where there is a wide scatter in the factor of safety.

and sin(x)) and GLE methods ($f(x)$ = 1.0 and sin(x)). Since there is a wide scatter in the results which means that the effect of the inter-slice shear force is critical in the analysis, there is a great difficulty in the interpretation of the results. The result by the Janbu simplified method was finally accepted by the engineers for the sake of safety. As a good practice, the factors of safety for complicated projects using different limit equilibrium methods should be determined and assessed before the final interpretation.

4 Discussions on limit equilibrium and finite element methods for slope stability analysis

The limit equilibrium method (LEM) and the strength reduction method (SRM) based on the finite element/finite difference method are currently the most popular methods among engineers. The limit analysis (including the rigid element) and distinct element method, by contrast, remain unpopular with engineers, and comparisons between the two methods will not be demonstrated in this chapter. Some of the engineers responsible for the design of dams in China even have doubts as to the activation of the energy balance along the vertical interfaces in limit analysis that is shown to be not valid in Figure 2.20 (see page 71).

4.1 Comparisons of the SRM and LEM

The LEM, which is based on the force and moment equilibrium, is a popular method among engineers. Besides the LEM (introduced previously in Chapter 2), the use of the finite difference/finite element methods has also attracted engineers in recent times (introduced in Section 2.9). This approach is currently adopted in several well-known commercial geotechnical finite element programs. The SRM by finite element analysis was used for slope stability analysis as early as 1975 by Zienkiewicz *et al.* Later, the SRM was applied by Naylor (1982), Donald and Giam (1988), Matsui and San (1992), Ugai and Leshchinsky (1995), Song (1997), Dawson *et al.* (1999), Griffiths and Lane (1999), Zheng *et al.* (2005) and others. In the SRM, the domain under consideration is discretized and the equivalent body forces are applied to the system. The yield criterion adopted is usually the Mohr–Coulomb criterion, but the use of other yield criteria is also possible. Different researchers and commercial programs have adopted different definitions to assess the factor of safety (FOS). The most popular definitions for the FOS include the following: (1) a sudden change in the displacement of the system; (2) failure to converge after a pre-determined number of iterations have been performed; (3) a continuous yield zone is formed.

Many researchers have compared the results between the SRM and LEM and found that generally both the methods will give similar FOS. Most studies are, however, limited to homogeneous soil slopes where the geometry of the problem is relatively regular with no special features (e.g. the presence of

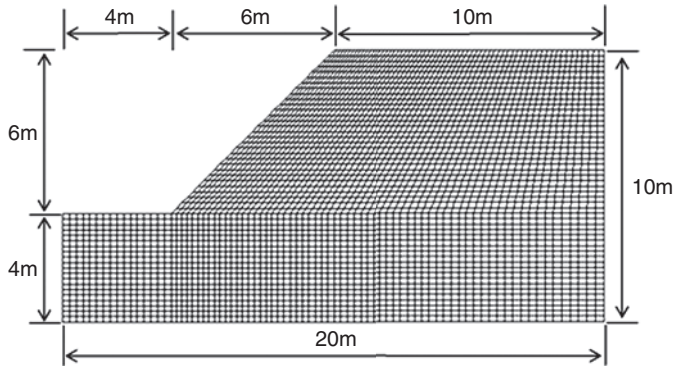

Figure 4.1 Discretization of a simple slope model.

a thin layer of soft material or special geometry). Furthermore, there are only limited studies that compare the critical failure surfaces from the LEM and SRM as the FOS appears to be the primary quantity of interest. In this chapter, these two methods are compared under different conditions and both the FOS and the locations of the critical failure surfaces are considered in the comparisons. In this chapter, both a non-associated flow rule (SRM1 and dilation angle = 0) and an associated flow rule (SRM2 and dilation angle = friction angle) are applied in the SRM analyses. To define the critical failure surface from the SRM, both the maximum shear strain and the maximum shear strain increment definition can be used. Cheng *et al.* (2007e) have found that these two definitions will give similar results in most cases and the maximum shear strain increment is chosen for the present study.

In this chapter, the LEM is considered using the Morgenstern–Price method with $f(x) = 1.0$ (equivalent to the Spencer method). It is also found that the differences of the FOS and the critical failure surfaces from $f(x) = 1.0$ and $f(x) = \sin(x)$ are small for the present study. In performing the SRM analysis, many soil parameters and boundary conditions are required to be defined that are absent in the corresponding LEM analysis. The importance of the various parameters and the applicability of the SRM in several special cases are considered in the following sections.

4.2 Stability analysis for a simple and homogeneous soil slope using the LEM and SRM

To investigate the differences between the LEM and SRM, a homogeneous soil slope with a slope height equal to 6 m and slope angle equal to 45° (Figure 4.1) is considered in this section. For the three cases in which the friction angle is 0°, because the critical slip surface is a deep-seated surface with a large horizontal extent, the models are larger than the one shown in

Table 4.1 Factors of safety (FOS) by the LEM and SRM

Case	*c′ (kPa)*	*φ′ (°)*	*FOS (LEM)*	*FOS (SRM1, non-associated)*	*FOS (SRM2, associated)*	*FOS difference with LEM (SRM1, %)*	*FOS difference with LEM (SRM2, %)*	*FOS difference between SRM1 and SRM2*
1	2	5	0.25	0.25	0.26	0	4.0	4.0
2	2	15	0.50	0.51	0.52	2.0	4.0	2.0
3	2	25	0.74	0.77	0.78	4.0	5.4	1.3
4	2	35	1.01	1.07	1.07	5.9	5.9	0
5	2	45	1.35	1.42	1.44	5.2	6.7	1.4
6	5	5	0.41	0.43	0.43	4.9	4.9	0
7	5	15	0.70	0.73	0.73	4.3	4.3	0
8	5	25	0.98	1.03	1.03	5.1	5.1	0
9	5	35	1.28	1.34	1.35	4.7	5.5	0.7
10	5	45	1.65	1.68	1.74	1.8	5.5	3.6
11	10	5	0.65	0.69	0.69	6.2	6.2	0
12	10	15	0.98	1.04	1.04	6.1	6.1	0
13	10	25	1.30	1.36	1.37	4.6	5.4	0.7
14	10	35	1.63	1.69	1.71	3.7	4.9	1.2
15	10	45	2.04	2.05	2.15	0.5	5.4	4.9
16	20	5	1.06	1.20	1.20	13.2	13.2	0
17	20	15	1.48	1.59	1.59	7.4	7.4	0
18	20	25	1.85	1.95	1.96	5.4	5.9	0.5
19	20	35	2.24	2.28	2.35	1.8	4.9	3.1
20	20	45	2.69	2.67	2.83	0.7	5.2	6.0
21	5	0	0.20	—	0.23	—	15.0	—
22	10	0	0.40	—	0.45	—	12.5	—
23	20	0	0.80	—	0.91	—	13.8	—

Figure 4.1 and have a width of 40 m and a height of 16 m. In the parametric study, different shear strength properties are used and the LEM, SRM1 and SRM2 analyses are carried out. The cohesive strength c' of the soil varies from 2 kPa, 5 kPa, 10 kPa to 20 kPa, whereas the friction angle varies from 5°, 15°, 25°, 35° to 45°. The density, elastic modulus and Poisson ratio of the soil are kept at 20 kN/m^3, 14 MPa and 0.3, respectively, in all the analyses. As shown in Figure 4.1, the size of the domain for the SRM analyses is 20 m in width and 10 m in height and there are 3520 zones and 7302 grid points in the mesh for analysis. Based on limited mesh refinement studies, it was found that the discretization shown in Figure 4.1 is sufficiently good, so that the results of analyses are practically insensitive to a further reduction in the element size. For the LEM, the Spencer method that satisfies both the moment and force equilibrium is adopted and the critical failure surface is evaluated by the modified simulated annealing technique proposed by Cheng (2003). The tolerance for locating the critical failure surface by the simulated annealing method is 0.0001, which is sufficiently accurate for the present study.

From Table 4.1 and Figures 4.2 and 4.3, it is found that the FOS and critical failure surfaces determined by the SRM and LEM are very similar

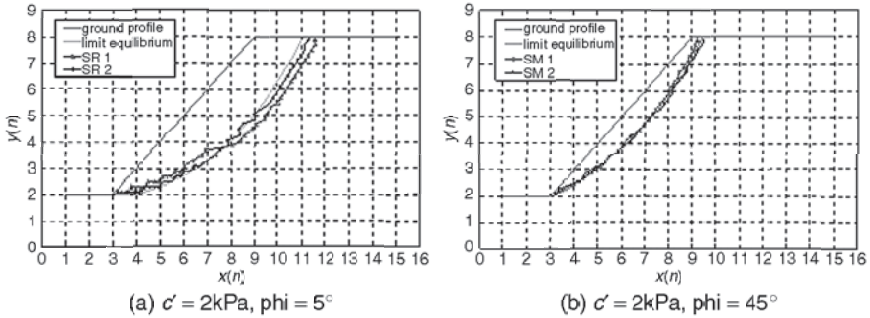

Figure 4.2 Slip surface comparison with increasing friction angle (c' = 2kPa).

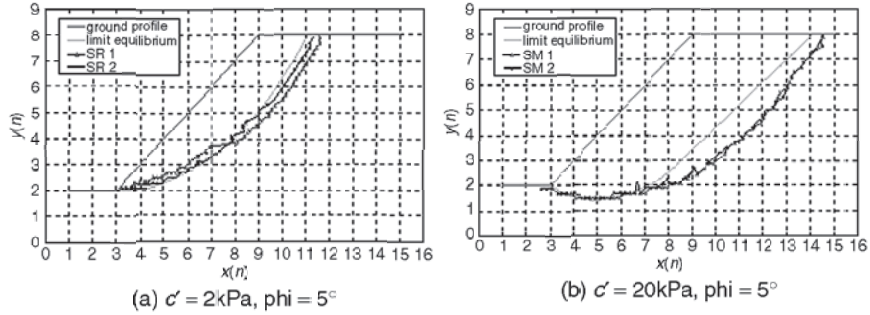

Figure 4.3 Slip surface comparison with increasing cohesion (phi = 5°).

under different combinations of soil parameters for most cases, except when $\phi' = 0$. When the friction angle is greater than 0, most of the FOS by the SRM differ by less than 7.4 per cent with respect to the LEM results, except for case 16 (c' = 20 kPa, $\phi' = 5°$) where the difference is up to 13.2 per cent. When the friction angle is very small or zero, there are relatively major differences between the SRM and LEM for both the FOS and the critical slip surface (Table 4.1 and Figure 4.4). The differences in the FOS between the LEM and SRM reported by Saeterbo Glamen *et al.* (2004) are greater than those found in the present study. Cheng *et al.* (2007a) suspect that this is due to the manual location of the critical failure surfaces by Saeterbo Glamen *et al.*, as opposed to the global optimization method used here. Based on Table 4.1 and Figures 4.2 and 4.3, some conclusions can be made as follows:

1 Most of the FOS obtained from the SRM are slightly larger than those obtained from the LEM with only few exceptions.
2 The FOS from an associated flow rule (SRM2) are slightly greater than those from a non-associated flow (SRM1), and this difference increases with an increasing friction angle. These results are reasonable and are

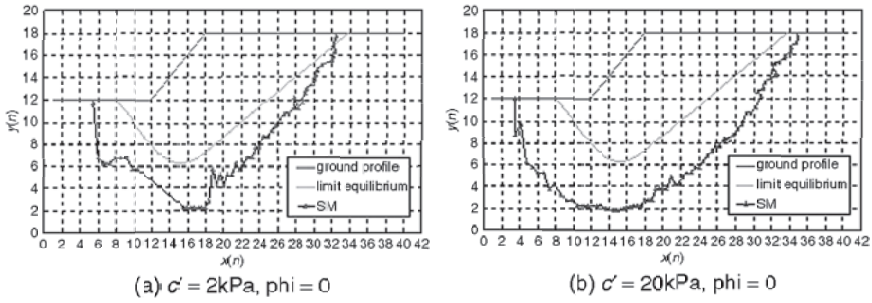

Figure 4.4 Slip surface comparison with increasing cohesion (phi = 0).

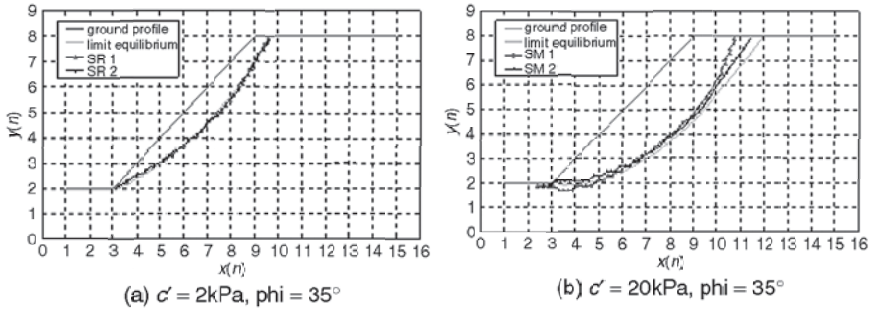

Figure 4.5 Slip surface comparison with increasing cohesion (phi = 35°).

expected. The differences between the two sets of results are, however, small because the problem has a low level of 'kinematic constraint'.

3 When the cohesive strength of the soil is small, the differences in FOS between the LEM and SRM (SRM1 and SRM2) are greatest for higher friction angles. When the cohesion of the soil is large, the differences in FOS are greatest for lower friction angles. This result is somewhat different from that of Dawson *et al.* (2000), who concluded that the differences are greatest for higher friction angles when the results between the SRM and limit analysis are compared.

4 The failure surfaces from the LEM, SRM1 and SRM2 are similar in most cases. In particular, the critical failure surfaces obtained by the SRM2 appear to be closer to those from the LEM than those obtained from the SRM1. The critical failure surfaces from the SRM1, SRM2 and LEM are practically the same when the cohesive strength is small (it is difficult to differentiate clearly in Figures 4.2a, 4.2b, 4.3a and 4.5a), but noticeable differences in the critical failure surfaces are found when the cohesive strength is high (Figures 4.3b, 4.4a, 4.4b and 4.5b).

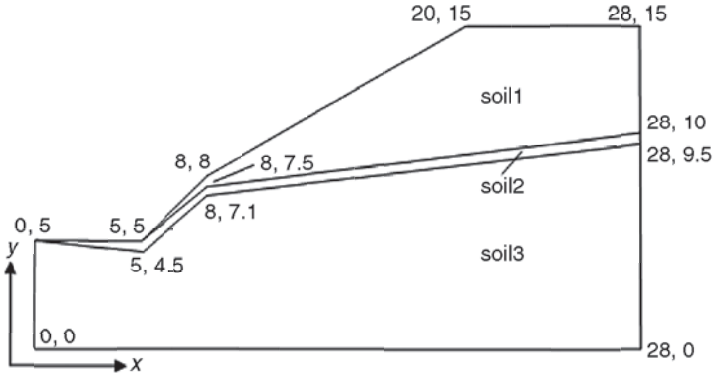

Figure 4.6 A slope with a thin soft band.

5 The right end of the failure surface moves closer to the crest of the slope as the friction angle of the soil is increased (which is a well-known result). This behaviour is more obvious for those failure surfaces obtained from the SRM1. For example, for the five cases where the cohesion of the soil is 2 kPa (Figure 4.2), when the friction angles are 5°, 15° and 25°, the right end-point of the failure surface derived from the SRM1 is located to the right of the right end-point of the critical failure surface obtained from the LEM. When the friction angle is 35°, the right end-point of the failure surface obtained by the SRM1 and LEM is nearly at the same location. When the friction angle is 45°, the distance of the right end-point derived from the SRM1 is located to the left of the right end-point derived from the LEM.

6 For SRM analyses, when the friction angle of soil is small, the differences between the slip surfaces for the SRM1 and SRM2 are greatest for a smaller cohesion (Figure 4.3). When the friction angle is large, the differences between the slip surface for the SRM1 and SRM2 are greatest for a higher cohesion (Figure 4.5).

7 It can also be deduced from Figures 4.2 to 4.5 that the potential failure volume of the slope becomes smaller with the increasing friction angle but increases with increasing cohesion. This is also a well-known behaviour, as when the cohesive strength is high, the critical failure surface will be deeper.

Although there are some minor differences in the results between the SRM and LEM in this example, the results from these two methods are generally in good agreement, which suggests that the use of either the LEM or SRM is satisfactory in general. Cheng *et al.* (2007a) have, however, constructed an interesting case where the limitations of the SRM are demonstrated.

Table 4.2 Soil properties for Figure 4.6

Soil name	*Cohesion (kPa)*	*Friction angle (degree)*	*Density (kN/m^3)*	*Elastic modulus (MPa)*	*Poisson ratio*
Soil1	20	35	19	14	0.3
Soil2	0	25	19	14	0.3
Soil3	10	35	19	14	0.3

4.3 Stability analysis of a slope with a soft band

A special problem with a soft band has been constructed by Cheng *et al.* (2007a) as it appears that similar problems have not been considered previously. The geometry of the slope is shown in Figure 4.6 and the soil properties are shown in Table 4.2. It is noted that c' is zero and ϕ' is small for soil layer 2 that has a thickness of just 0.5 m. The critical failure surface is obviously controlled by this soft band, and slope failures in similar conditions have actually occurred in Hong Kong.

To consider the size effect (boundary effect) in the SRM, three different numerical models are developed to perform the SRM using Mohr–Coulomb analysis, and the widths of the domains are 28 m, 20 m and 12 m, respectively (Figure 4.7). In these three SRM models, various mesh sizes were tried until the results were insensitive to the number of elements used for the analysis. For example, when the domain size is 28 m, the FOS was found to be 1.37 (Table 4.3) with 12,000 elements, 1.61 with 6000 elements and 1.77 with 3000 elements using SRM1 analysis and the program Phase.

Because the FOS for this special problem have great differences from those found using the LEM, Cheng *et al.* (2007a) have tried several well-known commercial programs and obtained very surprising results. The locations of the critical failure surfaces from the SRM for solution domain widths of 12 m, 20 m and 28 m are virtually the same. The local failures from the SRM, shown in Figure 4.8b, range from $x = 5$ m to $x = 8$ m, and the failure surfaces are virtually the same for the three different solution domains. A majority part of the critical failure surface lies within layer 2, which has a low shear strength, and is far from the right boundary. It is surprising to find that different programs produce drastically different results (Table 4.3A) for the FOS, even though the locations of the critical failure surface from these programs are very similar. For the cases shown in Figure 4.1, and other cases in a latter part of this study, the results are practically insensitive to the domain size, whereas the cases shown in Figure 4.6 are very sensitive to the size of domain for the programs Flac3D (SRM1 and SRM2) and Phase (SRM2). Results from the Plaxis program appear not to be sensitive to the domain size but are quite sensitive to the dilation angle (which is different from the previous example). The SRM1 results from the program Phase are also not sensitive to the domain size for SRM1, but results from SRM2 behave differently. The FOS from Flac3D appear to be overestimated when the soil parameters for the soft band are low, but the results from this program are not sensitive to the dilation angle that is similar to all the other

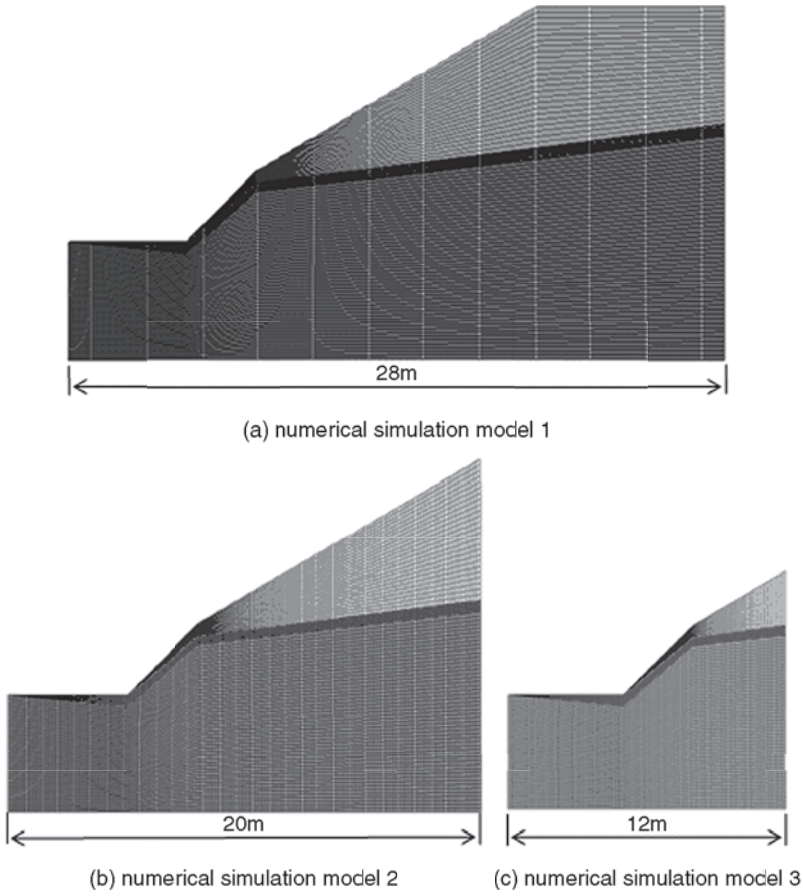

Figure 4.7 Mesh plot of the three numerical models with a soft band.

Table 4.3A FOS by SRM from different programs when c' for soft band is 0. The values in each cell are based on SRM1 and SRM2, respectively (min. FOS = 0.927 from Morgenstern–Price analysis)

Program/FOS	*12 m domain*	*20 m domain*	*28 m domain*
Flac3D	1.03/1.03	1.30/1.28	1.64/1.61
Phase	0.77/0.85	0.84/1.06	0.87/1.37
Plaxis	0.82/0.94	0.85/0.97	0.86/0.97
Flac2D	No solution	No solution	No solution

examples in the present study. For the SRM1, the results from Phase and Plaxis appear to be more reasonable as the results are not sensitive to the domain sizes, whereas for the SRM2, Cheng *et al.* (2007a) take the view that the results from

Table 4.3B FOS by SRM from different programs when $\phi' = 0$ and $c' = 10$ kPa for soft band. The values in each cell are based on SRM1 and SRM2, respectively (min. FOS = 1.03 from the Morgenstern–Price analysis)

Program/FOS	*28 m domain*
Flac3D	1.06/1.06
Phase	0.99/1.0
Plaxis	1.0/1.03
Flac2D	No solution

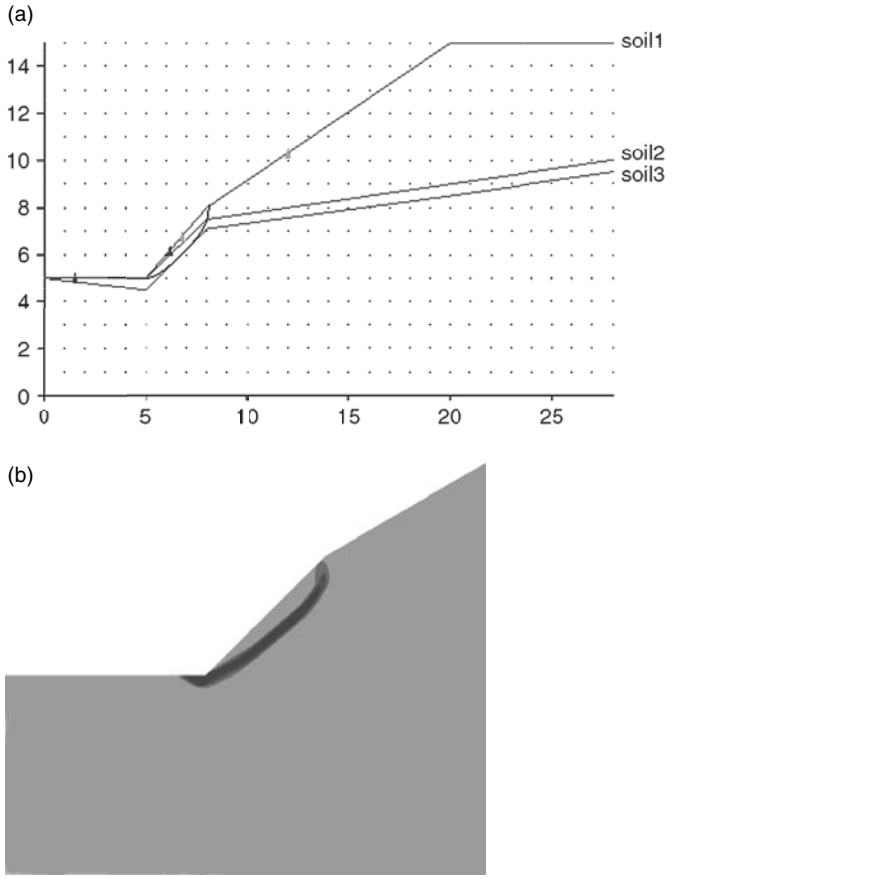

Figure 4.8 Locations of critical failure surfaces from the LEM and SRM for the frictional soft band problem. (a) Critical solution from LEM when soft band is frictional material (FOS = 0.927). (b) Critical solution from SRM for 12m width domain.

Plaxis may be better. It is also surprising to find that Flac2D cannot give any result for this problem, even after many different trials, but the program worked properly for all the other examples in this chapter.

Table 4.4 FOS with non-associated flow rule for 12 m domain

Element number	*Tolerance (stress analysis)*	*Maximum number of iterations*	*FOS*
1500	0.001	100	0.8
2000	0.001	100	No result
2000	0.003	100	No result
2000	0.004	100	No result
2000	0.005	100	No result
2000	0.008	100	0.81
2000	0.01	100	0.82
2000	0.001	500	0.74
2000	0.003	500	0.77
2000	0.004	500	0.77
2000	0.005	500	0.79
3000	0.001	100	No result
3000	0.003	100	0.79
3000	0.004	100	0.8
3000	0.005	100	0.8
3000	0.01	100	0.84
3000	0.001	500	0.77

Table 4.5 FOS with associated flow rule for 12 m domain

Element number	*Tolerance (stress analysis)*	*Maximum number of iterations*	*FOS*
1000	0.001	100	1.03
1200	0.001	100	1
1500	0.001	100	No result
1500	0.003	100	No result
1500	0.004	100	1
1500	0.005	100	1.39
1500	0.01	100	2.09
1500	0.001	500	0.86
1500	0.003	500	0.98
3000	0.001	100	No result
3000	0.003	100	No result
3000	0.004	100	No result
3000	0.005	100	No result
3000	0.01	100	No result
3000	0.001	500	0.85
3000	0.003	500	0.89
3000	0.004	500	0.9
3000	0.005	500	1.5
3000	0.01	500	2.09

There is another interesting and important issue when the SRM is adopted for the present problems. For the problem with a 12 m domain, Phase cannot provide a result with the default settings and the default settings are varied (including the tolerance and number of iterations allowed) until convergence is achieved. The results of analysis for a 12 m domain with Phase are shown in Tables 4.4 and 4.5.

It is observed that the number of elements used for the analysis has a very significant effect on the FOS, which is not observed for the cases in Table 4.1. The tolerance used in the nonlinear equation solution also has a major impact on the results for this case. This is less obvious for other cases considered in this chapter.

Besides the special results shown above, the FOS from the 28 m domain analysis appear to be large for Flac3D and Phase when the strength parameters for the soil layer 2 are low. In fact, it is not easy to define an appropriate FOS from the SRM analysis for this problem. If the cohesive strength of the top soil is reduced to zero, the FOS can be estimated as 0.57 from the relation $\tan\phi/\tan\theta$, where q is the slope angle. It can be seen that, for the LEM, the cohesive strength 20 kPa for soil 1 helps to bring the FOS to 0.927 and a high FOS for this problem is not reasonable. Without the results from the LEM for comparison, it may be unconservative to adopt the values of 1.64 (1.61) from the SRM based on Flac3D.

When the soil properties of the soft band are changed to $c' = 10$ kPa and $\phi' = 0$, the results of analyses are shown in Table 4.3B. It is found that the critical failure will extend to a much greater distance so that a 28 m wide domain is necessary. The FOS from the different programs are virtually the same, which is drastically different from the results in Table 4.3A (the same meshes were used for Tables 4.3A and 4.3B).

If the soil properties of soils 2 and 3 are interchanged so that the third layer of soil is the weak soil, the FOS from the SRM2 are 1.33 (with all programs) for all three different domain sizes. The corresponding FOS from the LEM is 1.29 from the Spencer analysis. The locations of the critical failure surface from the SRM and LEM for this case are also very close, except for the initial portion shown in Figures 4.9a and 4.9b. It appears that the presence of a soft band with frictional material, instead of major differences in the soil parameters, is the actual cause for the difficulties in the SRM analysis. Great care is required in the implementation of a robust nonlinear equation solver for the SRM.

The problems shown in Table 4.3A may reflect the limitations of commercial programs rather than the limitations of the SRM, but they illustrate that it is not easy to compute a reliable FOS for this type of problem using the SRM. The results are highly sensitive to different nonlinear solution algorithms that are not clearly explained in the commercial programs. Great care, effort and time are required to achieve a reasonable result from the SRM for this special problem and comparisons with the LEM are necessary. It is not easy to define a proper FOS from the SRM alone for the present problem, as the results are highly sensitive to the size of domain and the flow rule. In this respect, the LEM appears to be a better approach for this type of problem.

4.4 Local minimum in the LEM

For the LEM, it is well known that many local minima may exist besides the global minimum. This makes it difficult to locate the critical failure surface by classical optimization methods. Comparisons of the LEM and SRM with respect to local minima have not been considered in the past, but this actually

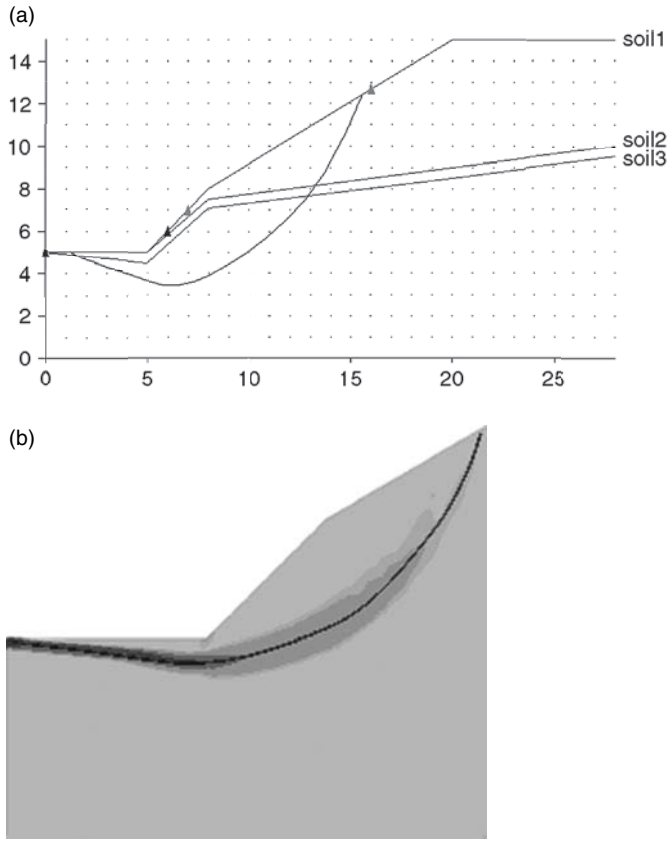

Figure 4.9 Critical solutions from the LEM and SRM when the bottom soil layer is weak. (a) Critical failure surface from LEM when the bottom soil layer is weak (FOS = 1.29). (b) Critical failure surface from SRM2 and 12 m domain (FOS = 1.33).

is a very important issue that is illustrated by the following examples. In the SRM, there is no local minimum as the formation of the shear band will attract strain localization in the solution process. To investigate this issue, an 11 m height slope shown in Figure 4.10 is considered. The slope angle for the lower part of the slope is 45°, whereas the slope angle for the upper part of the slope is 26.7°. The cohesion and friction angle of the soil are 10 kPa and 30°, respectively, and the density of the soil is 20 kN/m^3.

The failure mechanism by the SRM is shown in Figure 4.11 and the FOS is 1.47 for both non-associated flow and associated flow. The right end-point of the failure surface is located to the right of the crest of the slope. The results derived from the LEM are presented in Figure 4.12 (number of slices is 50). The global minimum FOS is 1.383 but a local minimum FOS of 1.3848 is

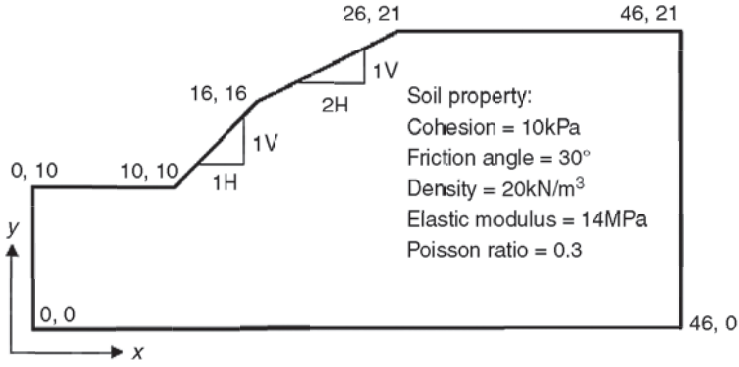

Figure 4.10 Slope geometry and soil property.

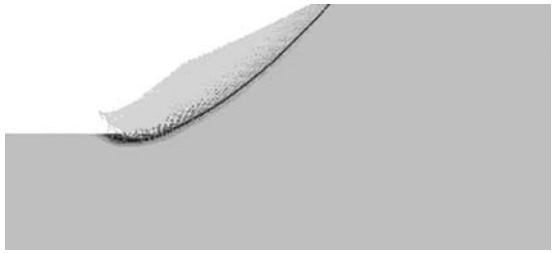

Figure 4.11 Result derived by SRM.

also found. The location of the failure surface for the local minimum 1.3848 is very close to that from the SRM, and the failure surface for the global minimum from the LEM is not the critical failure surface from the SRM. Because the FOS for the two critical failure surfaces from the LEM are so close, that both failure surfaces are probable failure surfaces should be considered in slope stabilization. For the SRM, there is only one unique failure surface from the analysis and another possible failure mechanism cannot be easily determined. Thus, the SRM analysis may yield a local failure surface of less importance while a more severe global failure surface remains undetected, as illustrated in the next example. This is clearly a major drawback of the SRM as compared with the LEM.

Cheng *et al.* (2007a) have also constructed another interesting case that is worth discussion. Figure 4.13 shows a relatively simple slope with a total height of 55 m in a uniform soil. The soil parameters are $c' = 5$ kPa and $\phi' = 30°$ while the unit weight is 20 kN/m^3. The global minimum and local minima are determined in accordance with the procedures of Cheng (2003) and different boundaries for the left and right exit ends are specified in the study. Using the LEM, the global minimum FOS is obtained as 1.33 (Figure 4.13a)

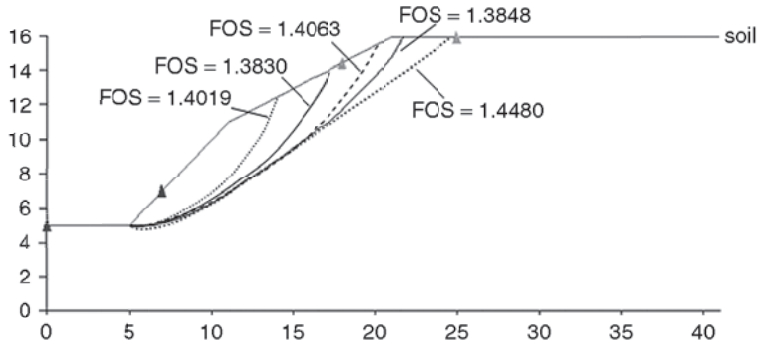

Figure 4.12 Global and local minima by LEM.

but several local minima are found with factors of safety in the range 1.38 to 1.42 shown in Figure 4.13a. From the SRM, only the FOS 1.327 shown in Figure 4.13b is found that is similar to the global minimum shown in Figure 4.13a. If slope stabilization is only carried out for this failure surface, the possible failure surfaces given by the local minimum in Figure 4.13a will not be considered. Baker and Leshchinsky (2001) have proposed the concept of the 'safety map', which enables the global minimum and local minima from the LEM to be visualized easily, but the construction of such a map using the SRM is tedious. In this respect, the LEM is a better tool for slope stability analysis. It is possible that the use of the SRM may miss the location of the next critical failure surface (with a very small difference in the FOS but a major difference in the location of the critical failure surface) so that the slope stabilization measures may not be adequate. This interesting case has illustrated a major limitation of the SRM for the design of slope stabilization works. It is true that the use of the safety map by the SRM can also overcome the limitation of the local minimum, but the evaluation of all the local minima using the LEM and the modern optimization method requires only 10 min for the complete analysis, which is much faster than using the safety map. The assessment of the local minima and the global minimum can also give a picture similar to that by the safety map. In the authors' view, there is not a strong need to use the safety map concept.

4.5 Discussion and conclusion

In the present study, a number of interesting features of the SRM were highlighted that are important for a proper analysis of a slope. Although most research has concentrated on the FOS between the LEM and SRM, the present works have compared the locations of the critical failure surfaces from these two methods. In a simple and homogeneous soil slope, the differences in the FOS and locations of the critical failure surfaces from the

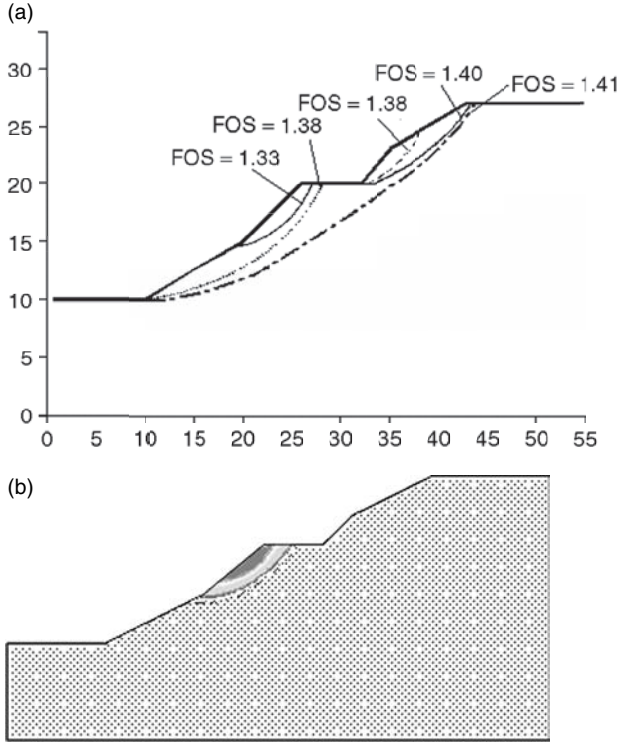

Figure 4.13 (a) Global and local minimum factors of safety are very close for a slope. (b) FOS = 1.327 from SRM.

SRM and LEM are small and both methods are satisfactory for engineering use. It is found that when the cohesion of the soil is small, the difference in the FOS from the two methods is greatest for higher friction angles. When the cohesion of the soil is large, the difference in the FOS is greatest for lower friction angles. With regard to the flow rule, the FOS and locations of the critical failure surface are not greatly affected by the choice of the dilation angle (which is important for the adoption of the SRM in slope stability analysis). When an associated flow rule is assumed, the critical slip surfaces from the SRM2 appear to be closer to those from the LEM than those from the SRM1. The use of the SRM requires Young's modulus, Poissons' ratio and the flow rule being defined. The importance of the flow rule has been discussed in the previous section. Cheng *et al.* (2007a) have also tried different combinations of Young's modulus and Poissons' ratio and found these two parameters to be insensitive to the results of analysis.

For the SRM, the effects of the dilation angle, the tolerance for nonlinear equation analysis, the soil moduli and the domain size (boundary effects) are

usually small but still noticeable. In most cases, these factors cause differences of just a few per cent and are not critical for engineering use of the SRM. Because the use of different LEM methods will also give differences in the FOS of several per cent, the LEM and SRM can be viewed as similar in performance for normal cases.

Drastically different results are determined from different computer programs for the problem with a soft band. For this special case, the FOS is very sensitive to the size of the elements, the tolerance of the analysis and the number of iterations allowed. It is strongly suggested that the LEM be used to check the results from the SRM. This is because the SRM is highly sensitive to the nonlinear solution algorithms and flow rule for this special type of problem. The SRM has to be used with great care for problems with a soft band of this nature.

The two examples with local minima for the LEM illustrate another limitation of the SRM in engineering use. With the SRM, there is strain localization during the solution and the formation of local minima is unlikely. In the LEM, the presence of local minima is a common phenomenon, and this is a major difference between the two methods. Thus, it is suggested that the LEM should be preformed in conjunction with the SRM as a routine check.

Through the present study, two major limitations of the SRM have been established: (1) it is sensitive to nonlinear solution algorithms/flow rule for some special cases and (2) it is unable to determine other failure surfaces that may be only slightly less critical than the SRM solution but still require treatment for good engineering practice. If the SRM is used for routine analysis and design of slope stabilization measures, these two major limitations have to be overcome and it is suggested that the LEM should be carried out as a cross-reference. If there are great differences between the results from the SRM and LEM, great care and engineering judgement should be exercised in assessing a proper solution. There is one practical problem in applying the SRM to a slope with a soft band. When the soft band is very thin, the number of elements required to achieve a good solution is extremely large, so that very significant computer memory and time are required. Cheng (2003) has tried a slope with a 1 mm soft band and has effectively obtained the global minimum FOS by the simulated annealing method. If the SRM is used for a problem with a 1 mm thick soft band, it is extremely difficult to define a mesh with a good aspect ratio unless the number of elements is huge. For the SRM with a 500 mm thick soft band, about 1 hr of CPU time for a small problem (several thousand elements) and several hours for a large problem (more than 10,000 elements) were required for the Phase program, whereas the program Flac3D required 1–3 days (for small to large meshes). If a problem with a 1 mm thick soft band is to be modelled with the SRM, the computer time and memory required will be huge and the method is not applicable for this special case. The LEM is perhaps better than the SRM for these cases.

For the SRM, there are further limitations that are worth observing. Shukha and Baker (2003) have found that there are minor but noticeable

differences in the factors of safety from Flac using square elements and distorted elements. The use of distorted elements is however unavoidable in many cases. Furthermore, when both the soil parameters c' and ϕ' are very small, it is well known that there are numerical problems with the SRM. The failure surface in this case will be deep and wide and a large domain is required for analysis. It has been found that the solution time is extremely long and a well-defined critical failure surface is not well established from the SRM. For the LEM, there is no major difficulty in estimating a FOS and the critical failure surface under these circumstances.

The advantage of the SRM is the automatic location of the critical failure surface without the need for a trial and error search. With the use of modern global optimization techniques, the location of critical failure surfaces by a simulated annealing method, a genetic algorithm or other methods as discussed in Chapter 3 is now possible and a trial and error search with the LEM is no longer required. Although the LEM suffers from the limitation of an interslice shear force assumption, the SRM requires a flow rule and suffers from being sensitive to the nonlinear solution algorithm/flow rule for some special cases.

Griffith and Lane (1999) have suggested that a non-associated flow rule should be adopted for slope stability analysis. As the effect of flow rule on the SRM is not negligible in some cases, such as those involving a soft band, the flow rule is indeed an issue for a proper slope stability analysis. It can be concluded that both the LEM and SRM have their own merits and limitations, and the use of the SRM is not really superior to the use of the LEM in routine analysis and design. Both methods should be viewed as providing an estimation of the FOS and the probable failure mechanism, but engineers should also appreciate the limitations of each method when assessing the results of their analyses.

Although 2D SRM is available in several commercial programs, there are still various difficulties with 3D SRM and the authors have tested two commercial softwares. For simple and normal problems, there is no major problem with the 3D SRM, and the results are also close to the 3D LEM. There are, however, various difficulties with the 3D SRM for complicated non-homogeneous problems with contrasting soil parameters. More importantly, many strange results may appear when soil nails are present, and there is a lack of good termination criteria for the FOS determination in this case. The authors have also found that the reliance on the default setting for 3D SRM programs may not be adequate for many cases, and there is a lack of a clear and robust method for the FOS determination when a soil nail is present. The authors are still working on this issue in various aspects, and, in general, the authors' view is that the 3D SRM is far from being mature for ordinary engineering use.

5 Three-dimensional slope stability analysis

5.1 Limitations of the classical limit equilibrium methods – sliding direction and transverse load

All slope failures are three-dimensional (3D) in nature, but two-dimensional (2D) modelling is usually adopted as this will greatly simplify the analysis. At present, there are many drawbacks in most of the existing 3D slope stability methods that include the following:

1 Direction of slide is not considered in most of the existing slope stability formulations so that the problems under consideration must be symmetrical in geometry and loading.
2 Location of the critical non-spherical 3D failure surface under general conditions is a difficult N-P hard-type global optimization problem that has not been solved effectively and efficiently.
3 Existing methods of analyses are numerically unstable under transverse horizontal forces.

Because of the above-mentioned limitations, 3D analysis based on limit equilibrium is still seldom adopted in practice. Cavounidis (1987) has demonstrated that the factor of safety (FOS) for a normal slope under 3D analysis is greater than that under 2D analysis, and this can be important for some cases.

Baligh and Azzouz (1975) and Azzouz and Baligh (1983) presented a method that extended the concepts of the 2D circular arc shear failure method to 3D slope stability problems. The method was just appropriate for a slope in cohesive soil. The results obtained by the method showed that the 3D effects could lead to a 4–40 per cent increase in the FOS. Hovland (1977) proposed a general 3D method for cohesion-frictional soils. The method was an extension of the 2D ordinary method of slices (Fellenius, 1927). The inter-column forces and pore-water pressure were not considered in this formulation. Two special cases have been analysed: (a) a cone-shaped slip surface on a vertical slope and (b) a wedge-shaped slip surface. It was shown that the 3D factors of safety were generally higher than the 2D ones, and the

ratio of FOS in 3D to that in 2D was quite sensitive to the magnitudes of cohesion and friction angles and to the shape of the slip surface in 3D.

Chen and Chameau (1982) extended the Spencer 2D method to 3D. The sliding mass was assumed to be symmetrical and divided into several vertical columns. The inter-column forces had the same inclination throughout the mass, and the shear forces were parallel to the base of the column. It was shown that: (a) The configuration of a sliding mass in 3D had significant effects on the FOS when the length of the sliding mass was small. (b) For gentle slopes, the dimensional effects were significant for soils with high cohesion and low friction angles. (c) In certain circumstances, the 3D FOS for cohesionless soils may be slightly less than the 2D one.

Hungr (1987) directly extended Bishop's simplified 2D method of slices to analyse the slope stability in 3D. The method was derived based on the two key assumptions: (a) the vertical forces of each column were neglected; (b) both the lateral and the longitudinal horizontal force equilibrium conditions were neglected. Hungr *et al.* (1989) presented a comparison of the 3D Bishop and Janbu simplified methods with other published limit equilibrium solutions. It was concluded that Bishop's simplified method might be conservative for some slopes with non-rotational and asymmetric slip surfaces. The method appeared reasonably accurate in the important class of problems involving composite surfaces with weak basal planes.

Zhang (1988) proposed a simple and practical method of 3D stability analysis for concave slopes in plane view using equilibrium concepts. The sliding mass was symmetrical and divided into many vertical columns. The slip surface was approximately considered as the surface of an elliptic revolution. To render the problem statically determinate, the forces acting on the sides and ends of each column, which were perpendicular to the potential direction of movement of the sliding mass, were neglected in the equilibrium conditions. The investigations using the method showed that: (a) The stability of concave slopes in a plane view increased with the decreases in their relative curvature. (b) The effect of a plane curvature on the stability of concave slopes in the plane view increased with the increase in the lateral pressure coefficient. However, the lateral pressure coefficient had only a small effect on the stability of the straight plane.

By using the method of columns, Lam and Fredlund (1993) extended the 2D general limit equilibrium formulation (Fredlund and Krahn, 1977) to analyse a 3D slope stability problem. The inter-column force functions of an arbitrary shape to simulate various directions for the inter-column resultant forces were proposed. All the inter-column shear forces acting on the various faces of the column were assumed to be related to their respective normal forces by the inter-column force functions. A geostatistical procedure (i.e. the Kriging technique) was used to model the geometry of a slope, the stratigraphy, the potential slip surface and the pore-water pressure conditions. It was found that the 3D factors of safety determined by the method (Lam and Fredlund,

1993) were relatively insensitive to the form of the inter-column force functions used in the method. Lam and Fredlund (1993), however, have not given a clear and systematic way for solving a general 3D problem.

Chang (2002) developed a 3D method of analysis of slope stability based on the sliding mechanism observed in the 1988 failure of the Kettleman Hills Landfill slope and the associated model studies. Using a limit equilibrium concept, the method assumed the sliding mass as a block system in which the contacts between blocks were inclined. The lines of intersection of the block contacts were assumed to be parallel, which enabled the sliding kinematics. In consideration of the differential straining between blocks, the shear stresses on the slip surface and the block contacts were evaluated based on the degree of shear strength mobilization on those contacts. The overall FOS was calculated based on the force equilibrium of the individual block and the entire block system as well. Due to the assumed inter-block boundary pattern, the method was not fully applicable for dense sands or overly consolidated materials under drained conditions.

In addition, 3D stability formulations based on the limit equilibrium method and variational calculus have been proposed by Leshchinsky *et al.* (1985), Ugai (1985) and Leshchinsky and Baker (1986). The functionals are the force and/or moment equations where the FOS can be minimized while satisfying several other conditions. The shape of a slip surface can be determined analytically. In such approaches, the minimum FOS and the associated failure surface can be obtained at the same time. These methods were however limited to homogeneous and symmetrical problems only. In the follow-up studies, Leshchinsky and Huang (1992) developed a generalized approach that is appropriate for symmetrical slope stability problems only. The analytical solutions approach based on the variational analysis is difficult to obtain for practical problems with complicated geometric forms and loading conditions. Cheng is currently working in this direction of using the modern optimization method to replace the tedious variational principle.

Most of the existing 3D methods rely on an assumption of a plane of symmetry in the analysis which are summarized in Table 5.1. For complicated ground conditions, this assumption is no longer valid, and the failure mass will fail along a direction with *least resistance* so that the sliding direction will also control the FOS of a slope. Stark and Eid (1998) have also demonstrated that the FOS of a 3D slope is controlled by the direction of slide and a symmetric failure may not be suitable for a general slope. Yamagami and Jiang (1996, 1997) and Jiang and Yamagami (1999) have developed the first method for asymmetric problems where the classical stability equations (without direction of slide/direction of slide is zero) are used while the direction of slide is considered by a minimization of the FOS with respect to rotation of axes. Yamagami and Jiang's formulation can be very time consuming even for a single failure surface as the formation of columns and the determination of geometry information with respect to

rotation of axes is the most time-consuming computation in the stability analysis. Huang and Tsai (2000) have proposed the first method for the 3D asymmetrical Bishop method where the sliding direction enters directly into the determination of the safety factor. The generalized 3D slope stability method by Huang *et al.* (2002) is practically equivalent to the Janbu rigorous method with some simplifications on the transverse shear forces. Because it is difficult to satisfy completely the line of thrust constraints in the Janbu rigorous method, which is well known in 2D analysis, the generalized 3D method by Huang *et al.* (2002) will also face converge problems so that this method is less useful to practical problems.

At the verge of failure, the soil mass can be considered as a rigid body. The direction of slide can take three possibilities:

1 soil columns are moving in the same direction with a unique sliding direction – adopted by Cheng and Yip (2007) and many other researchers in the present formulation;
2 soil columns are moving towards each other – this violates the assumption of a rigid failure mass and is not considered;
3 soil columns are moving away from each other – adopted by Huang and Tsai (2000) and Huang *et al.* (2002).

Because the sliding directions of soil columns are not unique in Huang and Tsai's (2000) and Huang *et al.*'s (2002) formulations and some columns are moving apart, the summation process in determining the FOS may not be applicable as some of the columns are separating from the others. Cheng and Yip (2007) have demonstrated in a later section that, under transverse load, the requirement of different sliding directions for different soil columns may lead to failure to converge. For soil columns moving away from each other, the distinct element method is the recommended method of analysis and a simple illustration is given in Section 2.11. Because the parameters required for the distinct element analysis are different from the classical soil strength parameters, it is not easy to adopt the results from the distinct element analysis directly, and the results should be considered as the qualitative analysis of the slope stability problem.

The assumption of a unique sliding direction may be an acceptable formulation for the analysis of the ultimate limit state, and the present formulation is based on this assumption. It is not a bad assumption to assume that all soil columns slide in one unique direction at the verge of failure. After failure has initiated, the soil columns may separate from each other and sliding directions can be different among different columns.

5.2 New formulation for 3D slope stability analysis – Bishop, Janbu simplified and Morgenstern–Price by Cheng

For 3D analysis, the potential failure mass of a slope is divided into a number of columns. At the ultimate equilibrium condition, the internal and external

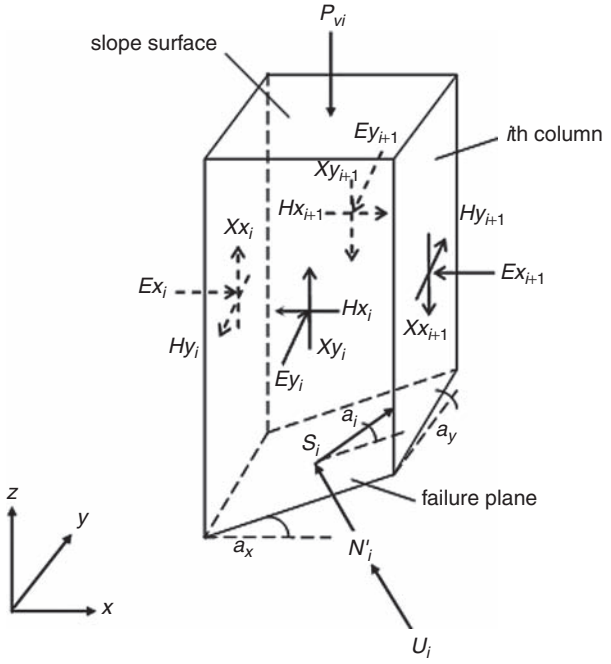

Where:
a_i = space sliding angle for sliding direction with respect to the direction of slide projected to the x–y plane (see also a' in Figure 5.2 and eq. 5.3);
a_x, a_y = base inclination along x and y directions measured at centre of each column (shown at the edge of column for clarity);
Ex_i, Ey_i = inter-column normal forces in x and y directions, respectively;
Hx_i, Hy_i = lateral inter-column shear forces in x and y directions, respectively;
N_i, U_i = effective normal force and base pore water force, respectively;
P_{vi}, S_i = vertical external force and base mobilized shear force, respectively;
Xx_i, Xy_i = vertical inter-column shear force in plane perpendicular to x and y directions.

Figure 5.1 External and internal forces acting on a typical soil column.

forces acting on each soil column are shown in Figure 5.1. The weight of soil and vertical load are assumed to act at the centre of each column for simplicity. This assumption is not exactly true but is good enough if the width of each column is small enough, and the resulting equations will be highly simplified and should be sufficiently good for practical purposes. The assumptions required in the present 3D formulation are the following:

1 The Mohr–Coulomb failure criterion is valid.
2 For the Morgenstern–Price method, the FOS is determined based on the sliding angle where factors of safety with respect to force and moment are equal.
3 The sliding angle is the same for all soil columns (Figure 5.2).

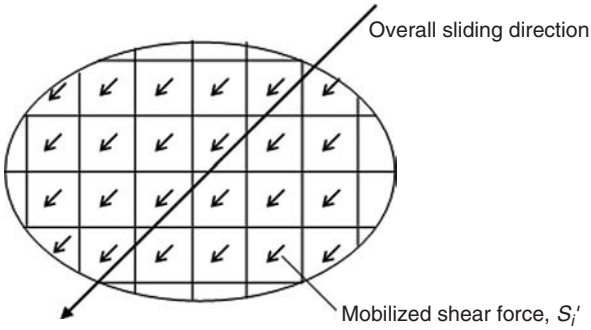

Figure 5.2 Unique sliding direction for all columns (on plan view).

By Mohr–Coulomb criteria, the global FOS, F, is defined as

$$F = \frac{S_{fi}}{S_i} = \frac{C_i + N_i' \times \tan\phi_i}{S_i} \tag{5.1}$$

where F is the FOS, S_{fi} is the ultimate resultant shear force available at the base of column i, N_i' is the effective base normal force and C_i is $c'A_i$ and A_i is the base area of the column. The base shear force S and base normal force N with respect to x, y and z directions for column i are expressed as the components of forces by Huang and Tsai (2000) and Huang *et al.* (2002):

$$\begin{aligned} &S_{xi} = f_1 \times S_i;\ S_{yi} = f_2 \times S_i;\ \text{and}\ S_{zi} = f_3 \times S_i \\ &N_{xi} = g_1 \times N_i;\ N_{yi} = g_2 \times N_i;\ \text{and}\ N_{zi} = g_3 \times N_i \end{aligned} \tag{5.2}$$

in which $\{f_1 \times f_2 \times f_3\}$ and $\{g_1 \times g_2 \times g_3\}$ are unit vectors for S_i and N_i (see Figure 5.1). The projected shear angle a' (individual sliding direction) is the same for all the columns in the x–y plane in the present formulation, and by using this angle, the space shear angle a_i (see Figure 5.3) can be found for each column and is given by Huang and Tsai (2000) as eq. (5.3):

$$a_i = \tan^{-1}\left\{\frac{\sin\theta_i}{\left[\cos\theta_i + \left(\frac{\cos a_{yi}}{\tan a' \times \cos a_{xi}}\right)\right]}\right\} \tag{5.3}$$

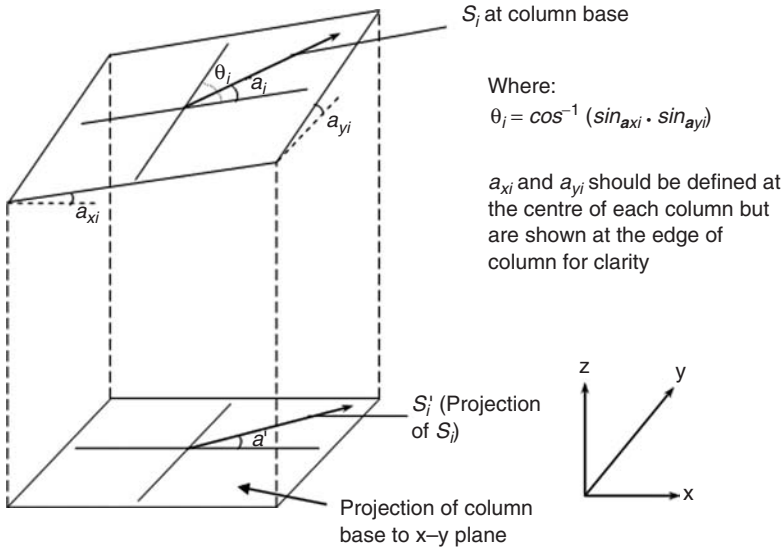

Figure 5.3 Relationship between projected and space shear angle for the base of column *i*.

$$n_i = \left\{ \frac{\pm \tan a_{xi}}{J}, \frac{\pm \tan a_{yi}}{J}, \frac{1}{J} \right\} = \{g_1, g_2, g_3\}$$ [–ve adopted by Huang and Tsai (2000) and +ve adopted by Cheng and Yip (2007)]

$$s_i = \left\{ \frac{\sin(\theta_i - a_i) \times \cos a_{xi}}{\sin \theta_i}, \frac{\sin a_i \times \cos a_{yi}}{\sin \theta_i}, \frac{\sin(\theta_i - a_i) \times \sin a_{xi} + \sin a_i \times \sin a_{yi}}{\sin \theta_i} \right\} = \{f_1, f_2, f_3\}$$

in which $J = \sqrt{\tan^2 a_{xi} + \tan^2 a_{yi} + 1}$

An arbitrary inter-column shear force function $f(x, y)$ is assumed in the present analysis, and the relationships between the inter-column shear and normal forces in the x and y direction are given as follows:

$$Xx_i = Ex_i \times f(x, y) \times \lambda_x; \; Xy_i = Ey_i \times f(x, y) \times \lambda_y \tag{5.4}$$

$$Hx_i = Ey_i \times f(x, y) \times \lambda_{xy}; \; Hy_i = Ex_i \times f(x, y) \times \lambda_{yx}, \tag{5.5}$$

where λ_x and λ_y = inter-column shear force X mobilization factors in x and y directions, respectively; λ_{xy} and λ_{yx} = inter-column shear force H mobilization factors in xy and yx planes, respectively.

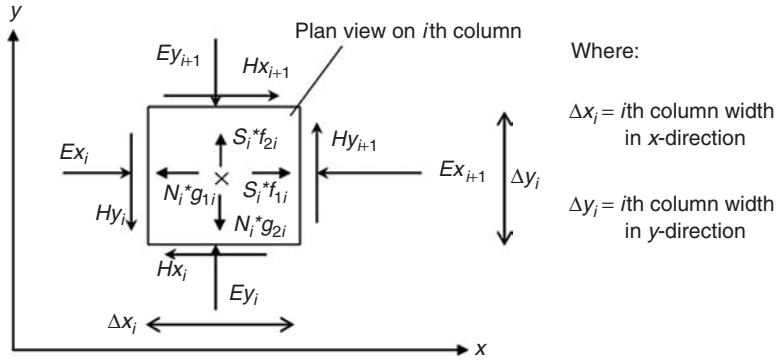

Figure 5.4 Force equilibrium in *x*–*y* plane.

Taking moment about the *z* axis at the centre of the *i*th column, the relations between lateral inter-column shear forces can be expressed as follows:

$$\Delta y_i \times (Hx_{i+1} + Hx_i) = \Delta x_i \times (Hy_{i+1} + Hy_i) \tag{5.6}$$

from (5.6),

$$Hx_{i+1} = \frac{\Delta x_i}{\Delta y_i} \times (Hy_{i+1} + Hy_i) - Hx_i \tag{5.7}$$

from (5.6),

$$Hy_{i+1} = \frac{\Delta y_i}{\Delta x_i} \times (Hx_{i+1} + Hx_i) - Hy_i, \tag{5.8}$$

where Δx_i and Δy_i are the widths of the column defined in Figure 5.4. Hx_i and Hy_i for the exterior columns should be zero in most cases or equal to the applied horizontal forces if defined. By using the property of the complementary shear (or moment equilibrium in the *xy*-plane), Hy_{i+1} or Hx_{i+1} can then be determined from eqs. (5.5) and (5.7) or (5.8) accordingly, so only λ_{xy} or λ_{yx} is required to be determined but not both. The important concept of complementary shear force which is similar to the complementary shear stress ($\tau_{xy} = \tau_{yx}$) in elasticity has not been used in any 3D slope stability analysis method in the past but is crucial in the present formulation. It should be noted that Huang *et al.* (2002) have actually assumed Hy_i to be 0 for an asymmetric problem to render the problem determinate, which is valid for symmetric failure only. Although the concept of complementary shear is applicable only in an infinitesimal sense, if the size of column is not great, this assumption will greatly simplify the equations. More importantly, Cheng and Yip (2007) have demonstrated that the effect of λ_{xy} or λ_{yx} is small in a later section of this chapter and the error in this assumption is actually not important.

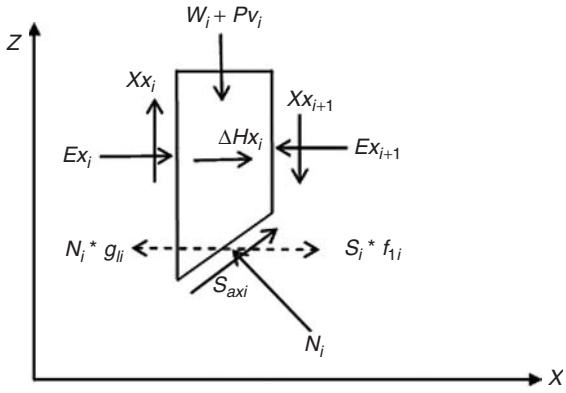

Figure 5.5 Horizontal force equilibrium in x direction for a typical column (ΔHx_i = Net lateral inter-column shear force).

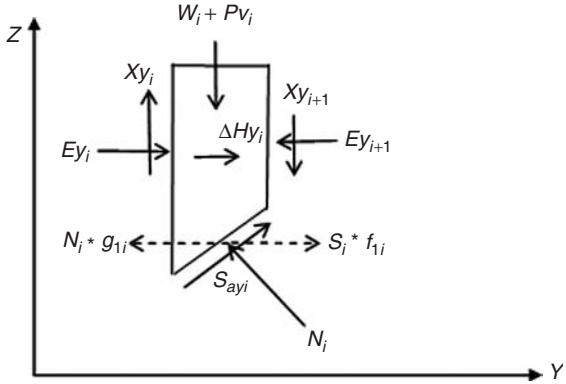

Figure 5.6 Horizontal force equilibrium in y direction for a typical column (ΔHy_i = Net lateral inter-column shear force).

Force equilibrium in X, Y and Z directions

Considering the vertical and horizontal forces, equilibrium for the ith column (Figures 5.5 and 5.6) in z, x and y directions gives the following:

$$\sum F_z = 0 \rightarrow N_i \times g_{3i} + S_i \times f_{3i} - (W_i + P_{vi}) = (Xx_{i+1} - Xx_i) + (Xy_{i+1} - Xy_i) \quad (5.9)$$

$$\sum F_x = 0 \rightarrow S_i \times f_{1i} - N_i \times g_{1i} + P_{hxi} - Hx_i + Hx_{i+1} = Ex_{i+1} - Ex_i \quad (5.10)$$

$$\sum F_y = 0 \rightarrow S_i \times f_{2i} - N_i \times g_{2i} + P_{hyi} - Hy_i + Hy_{i+1} = Ey_{i+1} - Ey_i \quad (5.11)$$

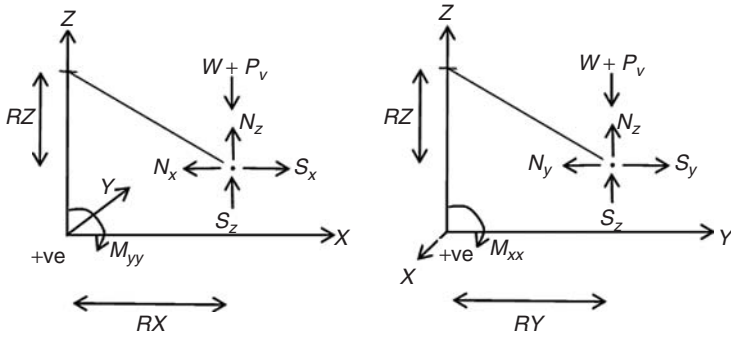

Figure 5.7 Moment equilibrium in x and y directions *(earthquake loads and net external moments are not shown for clarity)*.

Solving eqs. (5.1), (5.4) and (5.9), the base normal and shear forces can be expressed as follows:

$$N_i = A_i + B_i \times S_i; \quad S_i = \frac{C_i + (A_i - U_i) \times \tan\phi_i}{F\left(1 - \dfrac{B_i \times \tan\phi_i}{F}\right)},$$

$$A_i = \frac{W_i + P_{vi} + \Delta Ex_i \times \lambda_x + \Delta Ey_i \times \lambda_y}{g_{3i}}; \quad B_i = -\frac{f_{3i}}{g_{3i}}; \; U_i = u_i A_i \tag{5.12}$$

(u_i = average pore pressure at the ith column)

Overall force and moment equilibrium in X and Y directions
Considering the overall force equilibrium in the x direction:

$$-\sum Hx_i + \sum N_i \times g_{1i} - \sum S_i \times f_{1i} = 0. \tag{5.13}$$

Let $F_x = F$ in eq. (5.1); using eq. (5.12) and rearranging eq. (5.13), the directional safety factor F_x can be determined as follows:

$$F_x = \frac{\Sigma[(N_i - U_i) \times (\tan\phi_i + C_i)] \times f_{1i}}{\Sigma N_i \times g_{1i} - \Sigma Hx_i}, \quad 0 < F_x < \infty. \tag{5.14}$$

From the overall moment equilibrium in the x direction (Figure 5.7):

$$\sum (W_i + P_{vi} - N_i \times g_{3i} - S_i \times f_{3i}) \times RX + \sum (N_i \times g_{1i} - S_i \times f_{1i}) \times RZ = 0 \tag{5.15}$$

RX, RY and RZ are the lever arms to the moment point. Similarly, considering the overall force equilibrium in the y direction:

$$-\sum Hy_i + \sum N_i \times g_{2i} - \sum S_i \times f_{2i} = 0. \tag{5.16}$$

Let $F_y = F$ in eq. (5.1); using eq. (5.12) and rearranging eq. (5.16), the directional safety factor (F_y) can be determined as follows:

$$F_y = \frac{\Sigma[(N_i - U_i) \times (\tan\phi_i + C_i)] \times f_{2i}}{\Sigma N_i \times g_{2i} - \Sigma Hy_i}, \quad 0 < F_y < \infty. \tag{5.17}$$

Overall moment equilibrium in the y direction (Figure 5.7):

$$\sum (W_i + P_{vi} - N_i \times g_{3i} - S_i \times f_{3i}) \times RY + \sum (N_i \times g_{2i} - S_i \times f_{2i}) \times RZ = 0. \tag{5.18}$$

Based on a trial sliding angle, λ_x is kept on changing with a specified interval in eq. (5.14), until the calculated F_x satisfies the overall moment equilibrium eq. (5.15) in the x direction. A similar procedure is applied to λ_y until the calculated F_y also satisfies the overall moment equilibrium eq. (5.18) in the y direction. If F_x is not equal to F_y, the sliding angle will be varied until $F_x = F_y$ and then force as well as moment equilibrium will be achieved. Because all the equilibrium equations have been used in the formulation, there is no equation to determine λ_{xy} unless additional assumptions are specified. In the present formulation, Cheng and Yip (2007) suggest that λ_{xy} can be specified by the user or can be determined from the minimization of the FOS with respect to λ_{xy}. The problem associated with λ_{xy} and the importance of this parameter will be further discussed in Section 5.2.7.

5.2.1 Reduction to the 3D Bishop and Janbu simplified methods

The 3D asymmetric Morgenstern–Price method takes a relative long time for a solution and the convergence is less satisfactory as compared with the simplified method. The initial solutions from the 3D Janbu or Bishop analysis can be adopted to accelerate the Morgenstern–Price solution, and many engineers may still prefer to use the simplified method for routine design. The proposed Morgenstern–Price formulation will be simplified by considering only force or moment equilibrium equations and neglecting all the inter-column vertical and horizontal shear forces. Consider *overall moment equilibrium* in the x direction and about an axis passing through (x_o, y_o, z_o) (centre of rotation of the spherical failure surface) and parallel to the y axis. Letting $F_{my} = F$ in eq. (5.1) and rearranging eq. (5.15) gives the following:

$$F_{my} = \frac{\sum \{[K_{yi} \times [f_{1i} RZ_i + f_{3i} RX_i]\}}{\sum (W_i + P_{vi}) \times RX_i + \sum N_i \times (g_{1i} \times RZ_i - g_{3i} \times RX_i)}. \tag{5.19}$$

The corresponding F_{mx} is obtained from eq. (5.18) as

$$F_{mx} = \frac{\sum \{K_{xi} \times [f_{2i} RZ_i + f_{3i} RY_i]\}}{\sum (W_i + P_{vi}) \times RY_i + \sum N_i \times (g_{2i} \times RZ_i - g_{3i} \times RY_i)} \tag{5.20}$$

in which

$$K_{yi} = \frac{\left\{ C_i + \left[\frac{(W_i + P_{vi})}{g_{3i}} - U_i \right] \tan \phi_i \right\}}{1 + \frac{f_{3i} \times \tan \phi_i}{g_{3i} \times F_{my}}};$$

$$K_{xi} = \frac{\left\{ C_i + \left[\frac{(W_i + P_{vi})}{g_{3i}} - U_i \right] \tan \phi_i \right\}}{1 + \frac{f_{3i} \times \tan \phi_i}{g_{3i} \times F_{mx}}}.$$

Considering *overall moment equilibrium* about an axis passing through (x_o, y_o, z_o) and parallel to the z axis gives the following:

$$\sum (-N_i \times g_{1i} + S_i \times f_{1i}) \times RY + \sum (N_i \times g_{2i} - S_i \times f_{2i}) \times RX = 0. \quad (5.21)$$

Letting $F_{mz} = F$ in eq. (5.1) and rearranging eq. (5.21) gives,

$$F_{mz} = \frac{\sum [K_{zi} \times (f_{2i} \times RX_i - f_{3i} \times RY_i)]}{\sum N(g_{2i} \times RX_i - g_{1i} \times RY_i)};$$

$$K_{zi} = \frac{\left\{ C_i + \left[\frac{(W_i + P_{vi})}{g_{3i}} - U_i \right] \tan \phi_i \right\}}{1 + \frac{f_{3i} \times \tan \phi_i}{g_{3i} \times F_{mz}}}. \quad (5.22)$$

For the 3D asymmetric Bishop method, at the moment equilibrium point the directional factors of safety, F_{mx}, F_{my} and F_{mz}, are equal to each other. Under this condition, the global FOS F_m based on moment can be determined as follows:

$$F_m = F_{mx} = F_{my} = F_{mz} \quad (5.23)$$

The sliding direction can be found by changing the *projected shear direction* at a *specified angular interval*, until F_{mx}, F_{my} and F_{mz} are equal to each other. In reality, there is no way to ensure complete 3D moment equilibrium in the Bishop method as eq. (5.21) is redundant and is not used in the present method or the method by Huang and Tsai (2000) and Huang *et al.* (2002) as eqs. (5.19) and (5.20) are already sufficient for the solution of the FOS. The left-hand side of eq. (5.21) can hence be viewed as an *unbalanced moment term*. For a completely symmetric slope, this term is exactly zero and the 3D moment equilibrium is automatically achieved. In general, this term is usually small if the asymmetrical loading or sliding direction is not great. Cheng and Yip (2007) hence adopt eqs. (5.19) and (5.20) in the formulation which is equivalent to assigning $F_{mx} = F_{my}$. This is a limitation of the present 3D asymmetric Bishop simplified method as well as all the other existing 3D

Bishop methods for the general asymmetric problem as eq. (5.21) is a redundant equation.

By neglecting the inter-column shear forces for the Janbu analysis, eqs. (5.14) and (5.17) simplify to

$$F_{sx} = \frac{\sum A_{xi}\left(f_{1i} + \dfrac{f_{3i} \times g_{1i}}{g_{3i}}\right)}{\sum \dfrac{g_{1i}}{g_{3i}} \times (W_i + P_{vi})};\ A_{xi} = \frac{\left\{C_i + \left[\dfrac{(W_i + P_{vi})}{g_{3i}} - U_i\right] \tan \phi_i\right\}}{1 + \dfrac{f_{3i} \times \tan \phi_i}{g_{3i} \times F_{sx}}} \tag{5.24}$$

$$F_{sy} = \frac{\sum A_{yi}\left(f_{2i} + \dfrac{f_{3i} \times g_{2i}}{g_{3i}}\right)}{\sum \dfrac{g_{2i}}{g_{3i}} \times (W_i + P_{vi})};\ A_{yi} = \frac{\left\{C_i + \left[\dfrac{(W_i + P_{vi})}{g_{3i}} - U_i\right] \tan \phi_i\right\}}{1 + \dfrac{f_{3i} \times \tan \phi_i}{g_{3i} \times F_{sy}}} \tag{5.25}$$

For the 3D asymmetric Janbu method, at the force equilibrium point the directional factors of safety, F_{sx} and F_{sy}, are equal to each other. Under this condition, the global FOS F_f based on force can be determined as

$$F_f = F_{sx} = F_{sy}. \tag{5.26}$$

Because the FOS is also used in vertical force equilibrium, 3D force equilibrium is completely achieved in the 3D Janbu simplified method.

5.2.2 Numerical implementation of the Bishop, Janbu and Morgenstern–Price methods

To determine the FOS, the domain under consideration is divided into a regular grid. An initial value for the projected shear angle a' is chosen for analysis and a_i is then computed by eq. (5.3). In the program SLOPE3D developed by Cheng, an initial value of 2° is chosen for a' and an increment of a' is chosen to be 1° in the analysis. Once a_i is defined, the unit vectors n_i and s_i as given in Figure 5.1 can then be determined. Equations (5.19) and (5.20) are used to compute F_{my} and F_{mx} for the Bishop method until convergence is achieved. For the Janbu method, eqs. (5.24) and (5.25) are used to compute F_{sx} and F_{sy} until convergence is achieved. If $F_{my} \neq F_{mx}$ or $F_{sx} \neq F_{sy}$, a' will increase by 1° for the next loop. From the difference between two consecutive directional safety factors, the bound between a' can then be determined. Suppose a' is bounded between 10° and 11°; the directional safety factors will be computed again for a' based on 10.5°. The a' will then be bounded within the 0.5° range and a simple interpolation will be used to compute a refined value for a'. This formulation is relatively simple to operate and is good enough for analysis.

There are four major parameters to be determined for the 3D Morgenstern–Price analysis: F, sliding angle, λ_x and λ_y, whereas λ_{xy} will be prescribed by the engineer or determined from a minimization of the FOS.

To accelerate the Morgenstern–Price solution, 3D Janbu simplified analysis or Bishop analysis is performed in the first stage. The sliding angle and the inter-column normal forces Ex_i and Ey_i from the simplified analysis will be taken as a trial initial solution for the calculation of the inter-column shear forces Xx_i and Xy_i in the first step. To solve for the FOS, Cheng and Yip (2007) have tried two methods that are as follows:

1 *Simple triple looping technique*: To solve for a', λ_x and λ_y, a triple looping technique can be adopted. That means that a', λ_x and λ_y will be varied sequentially until all the previous equations are satisfied. This formulation is simple to be programmed but convergence is extremely slow even for a modern CPU.
2 *Double looping Brent method*: Cheng and Yip (2007) have found that the non-linear equations solver by Brent (1973) can perform well for the 3D Janbu and Bishop method. If the directional safety factors from simplified methods are used as the initial values in the Brent method, convergence with the Brent method will be good. Using the Brent method, one level of looping is removed and is replaced by a solution of a system of nonlinear equations $F_{sx} - F_{sy} = 0$ and $F_{mx} - F_{my} = 0$. Unlike the simplified 3D method of analysis, if arbitrary values of the directional safety factors (other than those from the simplified 3D analysis) are used as the initial values in the Brent method, failure to convergence can happen easily. Such behaviour is possibly induced by the effect of inter-column shear forces on the analysis that is neglected in the corresponding simplified 3D stability analysis.

5.2.3 Numerical examples and verification

Based on the present formulation and the formulation by Huang and Tsai (2000), Cheng *et al.* (2005) and Cheng and Yip (2007) have developed the program SLOPE3D and several examples are used for the study of the proposed formulations. In this chapter, function $f(x, y)$ is taken to be 1.0 for the Morgenstern–Price analysis and the method is hence actually Spencer analysis. Cheng and Yip (2007) have tried $f(x, y)$ for limited cases and the results from the use of $f(x) = 1.0$ and $f(x, y) = \sin(x, y)$ are virtually the same which is similar to the corresponding 2D analysis. It is expected that, for a highly irregular failure surface, the results may be sensitive to the choice of $f(x, y)$. The first example is a laterally symmetric slope (Figure 5.8) considered by Baligh and Azzouz (1975) with an assumed spherical sliding surface, and the results of analysis are shown in Table 5.2. For Example 1, SLOPE3D gives a sliding angle exactly equal to 0 and the results are also very close to those by other researchers except the one by Hungr (1987). Cheng and Yip (2007) view that the result by Hungr (1987), 1.422, is actually not correct as he obtained this result based on eq. (5.27):

$$F = \frac{\sum (W_i \tan \phi_i + C_i A_i \cos \gamma_z)/m_\alpha}{\sum W_i \sin \alpha_y} \tag{5.27}$$

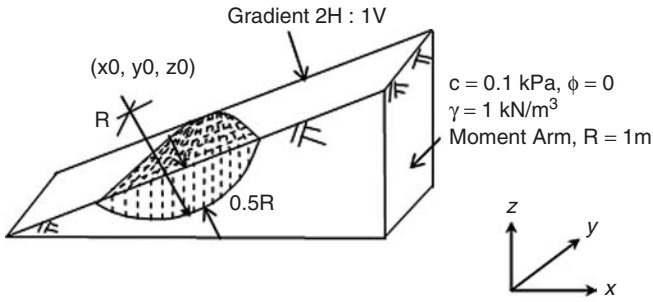

Figure 5.8 Slope geometry for Example 1.

Table 5.1 Summary of some 3D limit equilibrium methods

Method	*Related 2D method*	*Assumptions*	*Equilibrium*
Hovland (1977)	Ordinary method of slice	No inter-column force	Overall moment equilibrium
Chen and Chameau (1982)	Spencer method	Constant inclination	Overall moment equilibrium Overall force equilibrium
Hungr (1987)	Bishop simplified method	Vertical equilibrium	Overall moment equilibrium Vertical force equilibrium
Lam and Fredlund (1993)	General limit equilibrium	Inter-column force function	Overall moment equilibrium Overall force equilibrium
Huang and Tsai (2000)	Bishop simplified method	Consider direction of slide	Overall moment equilibrium Vertical force equilibrium
Cheng and Yip (2007)	Bishop and Janbu simplified, Morgenstern–Price	Consider direction of slide	Overall force equilibrium, and overall moment equilibrium for Morgenstern–Price

Equation (5.27) is not correct because moment equilibrium is considered about the centre of rotation of the spherical failure surface. Moment is a vector and should be defined about an axis instead of a point so that the moment contribution from each section cannot be added directly as in eq. (5.27). To correct eq. (5.27), the moment equilibrium should be considered

about an axis passing through the centre of rotation and the smaller radius at each section should be adopted and is given by the following:

$$F = \frac{\sum (W_i \tan \phi_i + C_i A_i \cos \gamma_z) r_i / m_\alpha}{\sum W_i r_i \sin \alpha_y}, \tag{5.28}$$

where $r_i = \sqrt{R^2 - y^2}$ and R is the radius of the spherical failure mass. In eq. (5.28), the radius at each section, r_i, is smaller than the global radius of rotation R and cannot be cancelled out because r_i is changing at different sections. Cheng and Yip (2007) have tried eq. (5.27) and have obtained the value 1.42 (same as Hungr), whereas an answer of 1.39 is obtained by eq. (5.28) for Example 1.

Table 5.2 Comparison of F_s for Example 1

Method	*Baligh and Azzouz (1975)*	*Hungr et al. (1989)*	*Lam and Fredlund (1993)*	*Huang and Tsai (2000)*	*SLOPE3D (Huang's approach)*	*SLOPE3D (Cheng's approach)*
Bishop simplified	1.402	1.422 (1.39)	1.386 (1200c)	1.399 (5300c)	1.390 (8720c)	1.390 (8720c)
Janbu simplified	—	—	—	—	1.612 (8720c)	1.612 (8720c)

Note: Number of columns in the analyses. For Hungr's result, the factor of safety after correction is 1.39.

Example 2 (Huang and Tsai, 2000) is a vertical cut slope (Figure 5.9) with an assumed spherical sliding surface. The failure mass is symmetrical about an axis inclined at 45° to the x axis, and this result is predicted with both Huang and Tsai's formulation and the present formulation. The results by the present formulations agree well with the results by Huang and Tsai, which have demonstrated that the new formulation gives results close to those from Huang and Tsai's formulation.

Example 3 is a vertical cut slope (Figure 5.10) in which a wedge-like failure is considered in the analysis. The FOS for this rigid block failure is determined explicitly from the simple rigid block failure as 0.726. Similar results are determined by the present 3D Janbu and Morgenstern–Price analyses (Table 5.3). This has demonstrated that if the correct failure mode is adopted, the present formulation can give reasonable results for 3D analysis. For 3D Bishop analysis, the FOS based on the moment point (x_0, y_0, z_0) is not correct as the present failure mode is a sliding failure while the Bishop method does not fulfil horizontal force equilibrium. The value of 0.62 from the Bishop method should not be adopted because the Bishop method does not satisfy horizontal force equilibrium while the wedge actually fails by sliding. If any moment point is chosen for the Bishop analysis, the FOS will be different and this is a

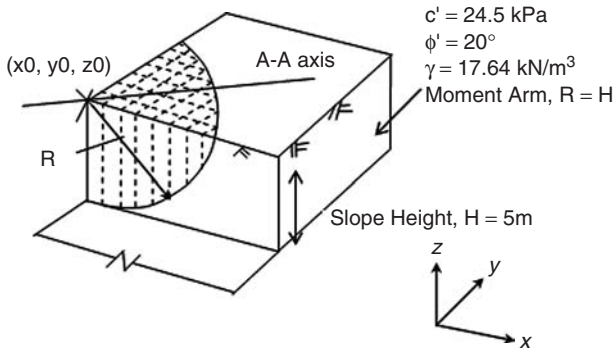

Figure 5.9 Slope geometry for Example 2.

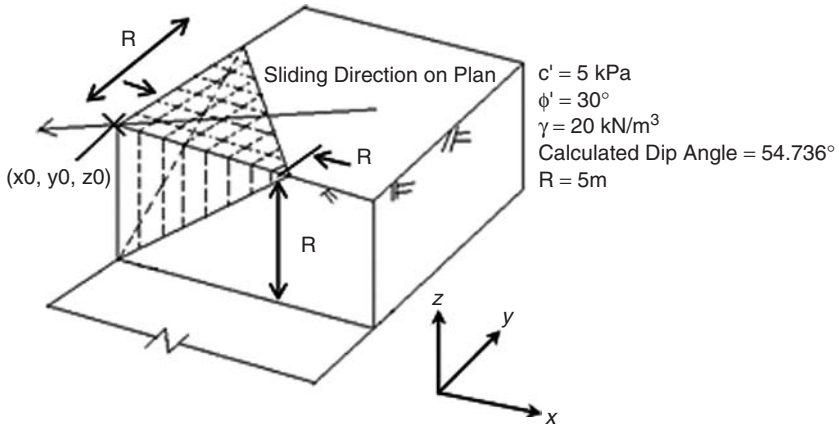

Figure 5.10 Slope geometry for Example 3.

well-known problem for the Bishop method. For the determination of the 3D FOS, the failure mechanism should be considered in the selection of a suitable method of analysis. Example 4 is an asymmetric rigid block failure with a size 2 m × 4 m, shown in Figure 5.11. The FOS and the sliding with respect to the x axis can be determined explicitly as 0.2795 and 63.4°, respectively, which are also determined exactly from SLOPE3D with the 3D Janbu and Morgenstern–Price analyses. The factors of safety for Examples 3 and 4 are correctly predicted by the present formulation that is a support to the present formulation.

For the FOS of a simple slope where $c' = 0$, F_s is given as $\tan\phi'/\tan\theta$, where θ is the slope angle. The critical failure surface is a planar surface parallel to the ground surface. From a spherical/elliptical optimization search, the minimum factors of safety for a simple slope from the present formulations are

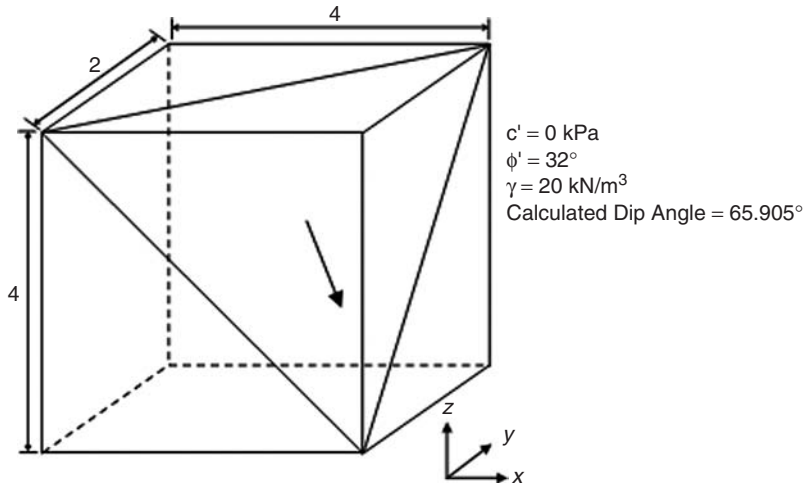

Figure 5.11 Slope geometry for Example 4 (F = 0.2795, sliding direction = 63.4° with respect to the x axis).

equal to $\tan\phi/\tan\theta$ for the Bishop, Janbu and Morgenstern–Price analyses, and the results comply well with the requirement of basic soil mechanics.

The results in Examples 1 to 4 show that the present theory gives sliding directions similar to those computed by Huang and Tsai's (2000) method. Cheng and Yip (2007) have also tried many other examples, and the differences between the FOS and sliding direction from Huang and Tsai's (2000) formulation and the present formulation are small in general, if there is no transverse load.

5.2.4 Comparison between Huang and Tsai's method and the present methods for transverse earthquake load

In Huang and Tsai's (2000) method, the mobilized shear force, S_i, has two components at the bottom plane of each column, namely S_{xzi} and S_{yzi}. Besides the global safety factor F_s, two additional safety factors are further defined as F_{sx} and F_{sy} for the mobilized shear force in the x and y direction, respectively. The individual sliding direction a_i can be obtained by using the *calculated and converged* values of F_{sx} and F_{sy} based on different methods (such as the Bishop method). By using the value of F_{sx}, F_{sy} and a_i, the corresponding F_s can be determined in each iteration. The final solution can then be obtained if the tolerance of the analysis is achieved. However, by using this method, before the final solution of F_s is achieved, *three convergent criteria* are required to be satisfied. They are the criteria for F_{sx}, F_{sy} and a_i, respectively. As a_i is mainly determined by F_{sx} and F_{sy}, a correct solution cannot be obtained for F_s unless

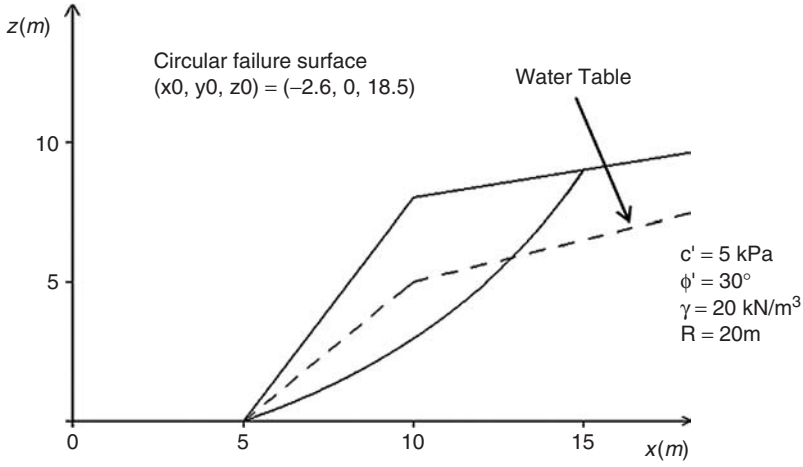

Figure 5.12 Slope geometry for Example 5.

the computational process can converge for F_{sx} and F_{sy}, respectively. Furthermore, a_i appears in the solution of F_s as well as the solution of F_{sx} and F_{sy} in each iteration; therefore, if a_i is determined incorrectly, F_{sx} and F_{sy} will be incorrectly determined that gives a wrong F_s value. Huang and Tsai's (2000) formulation may hence face difficulty in convergence for more complicated problems.

By using the present method, only *two convergent criteria* are required to be satisfied. They are the criteria for F_{sx} and F_{sy}, respectively. The a_i is unique in the present formulation and is determined by a simple looping process instead of the three convergent criteria so that the propagation of errors as that in Huang and Tsai's (2000) method will be eliminated. F_s is determined directly by the values of the directional safety factor F_{sx} or F_{sy} at the equilibrium point. To illustrate the important difference between the two methods, Example 5 (Figure 5.12), where transverse earthquake load Qy is applied normal to the section as shown, is considered and the results of analysis are shown in Table 5.4. Huang and Tsai's method fails to converge in analysis. In examining the intermediate results, Cheng and Yip (2007) find that even though F_{sx} and F_{sy} can converge in the first and second iteration, the converged values appear to be unreasonable. It is because, in Huang and Tsai's method, an initial constant value is assigned for all a_i values. As the computation process starts, F_{sy} is determined incorrectly based on these initial a_i values that are the same among different columns in the first step. This leads to the value of F_s being determined wrongly in the consequent iteration that is shown in Table 5.5. Also, based on the value of F_{sy}, new set of a_i values is calculated with F_{sx}. Thus, both F_{sx} and F_{sy} are determined incorrectly in the subsequent iteration because both F_{sx} and F_{sy} are directly determined by the a_i

Table 5.3 Comparison of F_s for Examples 2, 3 and 4

Method	*Example 2*			*Example 3*		
	Huang and Tsai (2000)	*SLOPE3D (Huang's approach)*	*SLOPE3D (Cheng's approach)*	*Analytical*	*SLOPE3D (Huang's approach)*	*SLOPE3D (Cheng's approach)*
Bishop simplified	1.766	1.781 (45°)[a]	1.801 (45°)[b]	0.726	0.620 (45°)[a]	0.620 (45°)[b]
Janbu simplified	—	2.820 (45°)[a]	2.782 (45°)[b]		0.722 (45°)[a]	0.722 (45°)[b]
Morgenstern–Price	—	—	1.803 (45°)[b]		—	0.724 (45°)[b]

Notes: For Examples 2 and 3, 2039 columns are used by Huang and Tsai. For Examples 2, 3 and 4, 10,000, 23,871 and 2500 columns, respectively, have been used by Cheng.

a The average overall sliding direction in degrees.
b The unique overall sliding direction [or the equilibrium point] in degrees.

values. In the present study, a_i has been assigned from 0.05 to the 0.5 radian (2.9° to 28.6°) in an increment of 0.05 using Huang and Tsai's method but convergence is still not achieved.

On the other hand, the present formulation can converge without problem that is demonstrated in Figures 5.13 and 5.14. Although the F_{sy} is unreasonable when the sliding angle is small, once the sliding angle is reasonable, F_{sy} will also be reasonable. Cheng and Yip (2007) suspect that the non-unique sliding direction in Huang and Tsai's formulation is the main cause for the failure to converge, as this method gives larger sliding angles for those soil columns near the edge of the failure mass from the figures by Huang and Tsai (2000). Figures 5.13 and 5.14 have also demonstrated that the FOS can be very sensitive to the sliding angle, and the use of varying sliding angles between different soil columns may not be a good assumption. When a transverse load is present, the sliding angles at the edge of the failure soil mass are greatly increased and loss of contact will generate internal tensile forces between soil columns and unreasonable F_{sy} so that convergence cannot be achieved.

5.2.5 Relation with the classical 3D analysis methods

Most of the existing 3D slope stability methods have not considered sliding direction explicitly in their formulation and transverse direction is not considered. Jiang and Yamagami (1999) and Yamagami and Jiang (1996, 1997) have proposed to rotate the axes while the classical 3D methods (without consideration of sliding direction) are used until the minimum FOS is obtained. The FOS and sliding direction as determined from this axes rotation procedure are reasonable but tedious work is required for this formulation and it is not

Table 5.4 Comparison between the present method and Huang and Tsai's method with a transverse earthquake

Earthquake Load[a] *(%)*		*Bishop simplified method Safety Factor, F_s Sliding Direction (°)*				*Janbu simplified method Safety Factor, F_s Sliding Direction (°)*			
Qx	*Qy*	*Huang and Tsai (2000)*	*The present method (F_s)*	*Huang and Tsai (2000)*	*The present method (°)*	*Huang and Tsai (2000)*	*The present method (F_s)*	*Huang and Tsai (2000)*	*The present method (°)*
50	50	Fail	0.3366	Fail	29.925	Fail	0.3064	Fail	31.84
30	30	Fail[b]	0.4787	Fail	22.004	Fail[b]	0.4524	Fail	23.789
30	20	Fail	0.4888	Fail	15.147	Fail	0.463	Fail	16.476
30	10	Fail	0.4953	Fail	7.73	Fail	0.4699	Fail	8.444
30	1	Fail	0.4975	Fail	0.636	Fail	0.4723	Fail	0.732

Notes
a *Qx* and *Qy* are the earthquake load (in per cent of soil weight) in the *x* direction and normal to the section shown in Figure 5.11.
b See Table 5.4 for details on failure to converge.

Table 5.5 Factors of safety during analysis based on Huang and Tsai's method

Iteration No.	*Bishop simplified method*[a] *Converged Safety Factor*			*Janbu simplified method*[a] *Converged Safety Factor*		
	F_{sx}	F_{sy}	F_s	F_{sx}	F_{sy}	F_s
1	0.498	0.583×10^{-3}	-0.149×10^{-4}	0.472	0.592×10^{-3}	-0.151×10^{-4}
2	0.211×10^{-2}	0.276×10^{-4}	-0.165×10^{-6}	0.226×10^{-2}	0.419×10^{-4}	0.581×10^{-5}
3	Fail	Fail	Fail	Fail	Fail	Fail

Note
a Thirty per cent earthquake load is set in both the *x* and *y* directions.

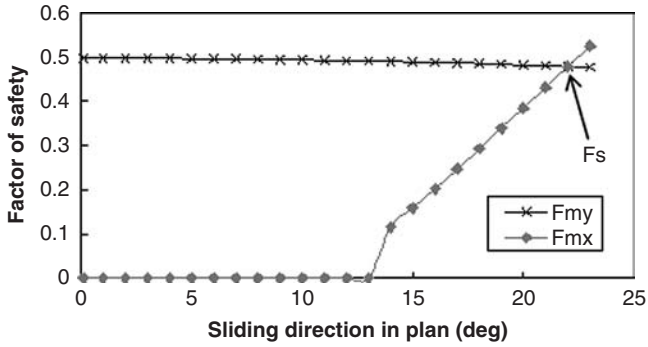

Figure 5.13 Convergent criteria based on the present method – by using the Bishop simplified method (30 per cent earthquake load in both the x and y directions).

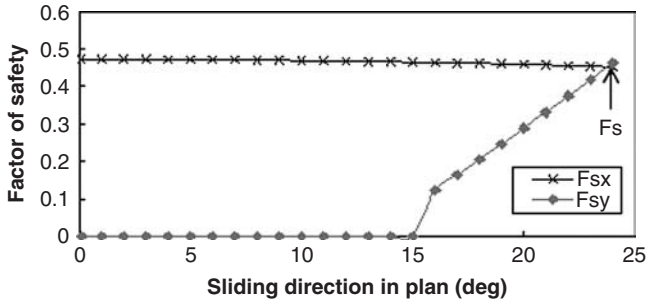

Figure 5.14 Convergent criteria based on the present method – by using the Janbu simplified method (30 per cent earthquake load in both the x and y directions).

commonly adopted. Cheng and Yip (2007) have tried the Bishop and Janbu methods for Examples 2 and 3 and the results are shown in Figure 5.15. The curves shown in Figure 5.15 are symmetric about a sliding direction of 45° and the minimum factors of safety are equal to that shown in Table 5.2 using the present formulation where the sliding direction is considered. If a high accuracy for the sliding direction is required, Jiang and Yamagami's formulation can be very time consuming, which is experienced by Cheng and Yip (2007) for the cases shown in Figure 5.15. For the cases shown in Figure 5.15, the computer time required for Jiang and Yamagami's formulation by the rotation of axes is approximately three times that for the present formulation if the accuracy of the sliding direction is controlled within 1°. The present formulation is actually equivalent to Jiang and Yamagami's formulation but re-formulations of mesh and geometry computations with rotation of axes are not required.

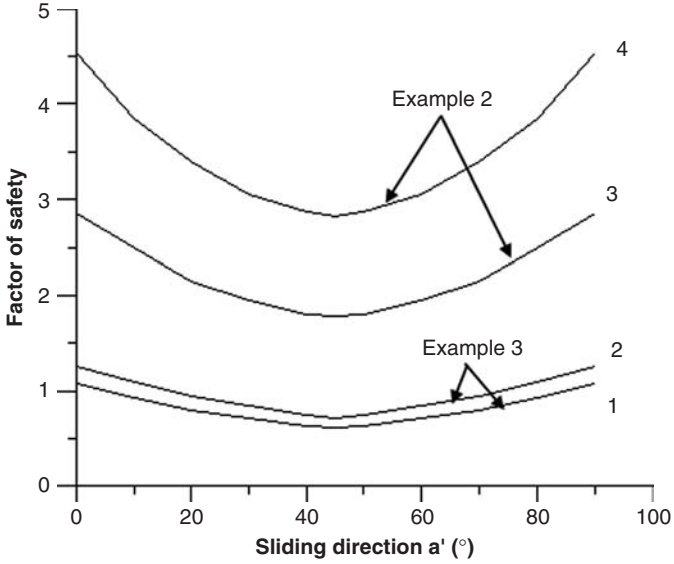

Figure 5.15 Factor of safety against sliding direction using classical 3D analysis methods (Curves 1 and 2 are Bishop and Janbu analyses for Example 3, whereas Curves 3 and 4 are Bishop and Janbu analyses for Example 2).

5.2.6 Problem of cross-section force/moment equilibrium for the Morgenstern–Price method

The three-dimensional asymmetric Morgenstern–Price formulation is highly statically indeterminate, which indicates that cross-sectional force or moment equilibrium cannot be enforced simultaneously in the analysis. In fact, it is one of the major theoretical difficulties in 3D limit equilibrium analysis as the number of redundant equations is much more than the corresponding 2D analysis. In the 2D Morgenstern–Price method, the inter-slice normal (and shear) force of the last slice can be determined from the last interface (from second last slice). The equation of horizontal force equilibrium becomes redundant for the last slice. However, horizontal force equilibrium can still be maintained for all slices as overall horizontal force equilibrium is enforced. In the calculation of the inter-slice normal force, the calculation progresses from slice to slice, automatically ensuring that horizontal force equilibrium is satisfied even for the last slice. However, this condition cannot be enforced automatically for 3D analysis as the safety factor equations are based on the overall force equilibrium as given by eqs. (5.13) and (5.15) instead of section horizontal force equilibrium. That means that horizontal force equilibrium cannot be automatically enforced in *each cross-section*. Also, there is no way to enforce *cross-section moment equilibrium* in the analysis, as the overall moment equilibrium instead

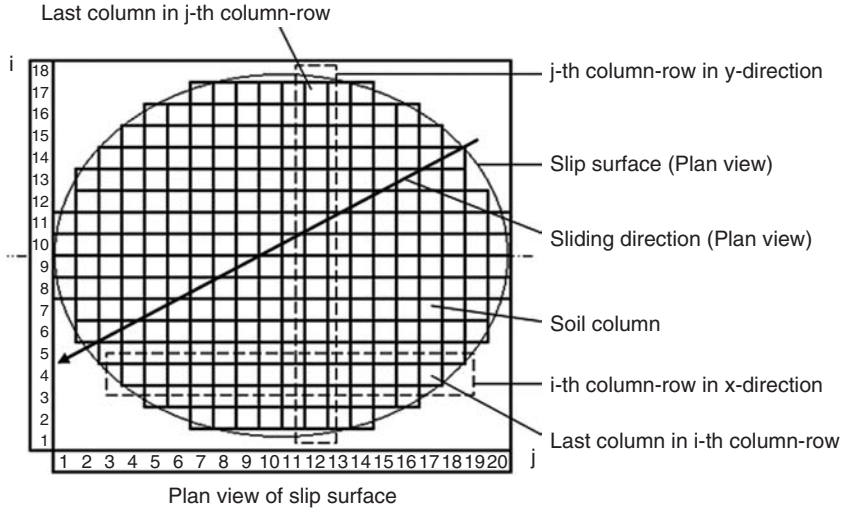

Figure 5.16 Column–row within potential failure mass of slope for Example 1.

of sectional moment equilibrium is used in the analysis. In fact, cross-section force or moment equilibrium is a common problem in all 3D analysis methods. To investigate the importance of the cross-section equilibrium, Example 5 shown in Figure 5.12 with one half of the soil mass loaded with a surcharge as shown in Figure 5.16 is considered with $\lambda_{xy} = 0$ in the analysis and the results are shown in Figures 5.17–5.20. In these figures, it can be seen that net forces/moments on each section exist and are fluctuating about 'zero' even though the global equilibrium for moment and force is satisfied.

As sectional force and moment equilibrium conditions have not been enforced in the 3D Morgenstern–Price method, force and moment equilibrium in each cross-section cannot be automatically achieved unless the following additional assumptions are used:

1 λ_x or λ_y is a function of y or x.
2 The safety factor is considered as different in different cross-sections, and it is subjected to the *force and moment equilibrium* on each cross-section in x and y directions.

For the first assumption, Hungr (1994) has a similar suggestion but Lam and Fredlund (1994) pointed out that these λ values should be considered as percentages of the inter-column shear forces used in the analysis and suggested that this value should be a constant rather than a function. As there is no theoretical background to determine the functions for λ_x or λ_y, and the number of

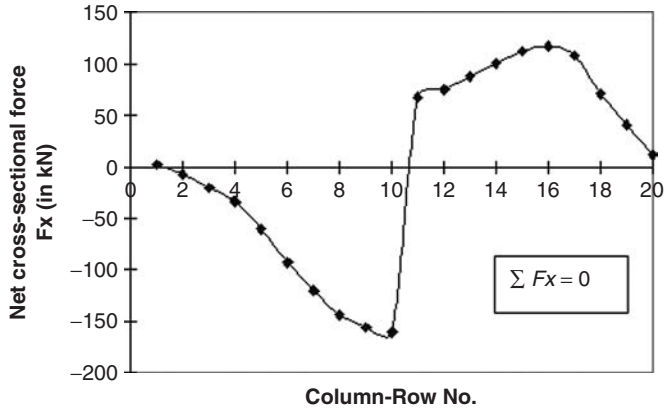

Figure 5.17 Cross-section force equilibrium condition in *x* direction.

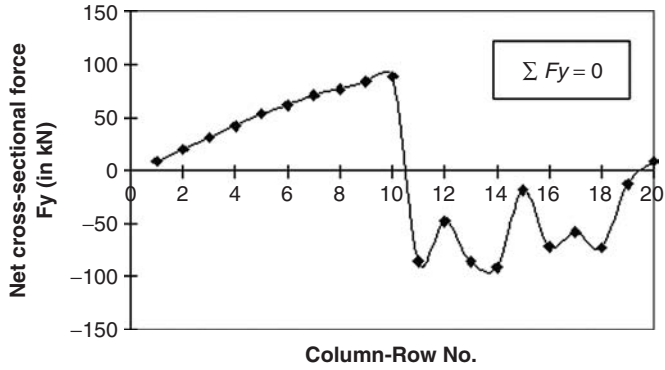

Figure 5.18 Cross-section force equilibrium condition in *y* direction.

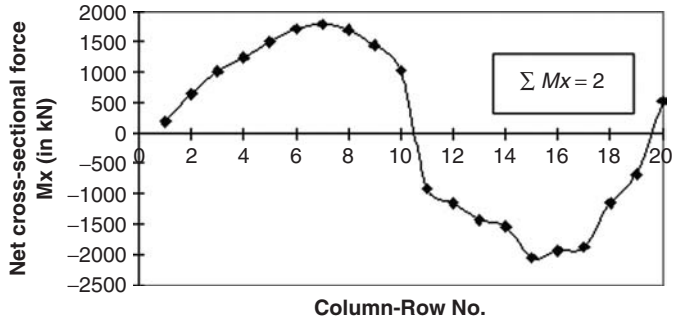

Figure 5.19 Cross-section moment equilibrium condition in *x* direction.

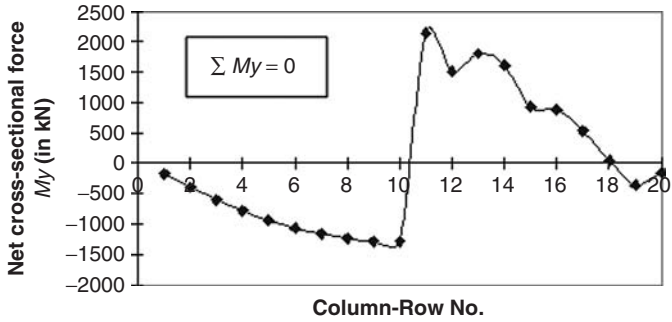

Figure 5.20 Cross-section moment equilibrium condition in *y* direction.

iterations required for a solution is extremely high for such a formulation, this formulation has not been used in any existing 3D slope analysis model. For the second assumption, a huge number of iterations is also required. Additional assumptions about the distribution of the safety factors are also required for analysis. Besides these limitations, it is also difficult to define the overall safety condition of a slope with different directional safety factors. Also, at the failure stage, the failure mode should be 'whole rigid mass movement' which will be in conflict with the requirement of different safety factors at different sections.

To ensure cross-section horizontal force equilibrium, Cheng and Yip (2007) propose that the base shear and normal forces on the last (or first) column in each section can be determined by using eqs. (5.9) and (5.10) for the *x* direction and eqs. (5.9) and (5.11) for the *y* direction. By solving eqs. (5.9) and (5.10) and (5.9) and (5.11) based on sectional force equilibrium, the base normal force on the last column can be expressed as eq. (5.29) for the *x* direction and eq. (5.30) for the *y* direction, respectively, as follows:

$$N_i = \frac{1}{g_{3i} \times \left(1 + \dfrac{g_{1i} \times f_{3i}}{f_{1i} \times g_{3i}}\right)} \times [(-Xx_i - Xy_i + W_i + P_{vi}) - \frac{f_{3i}}{f_{1i}} \times (-Ex_i - Hx_{i+1} + Hx_i)] \tag{5.29}$$

$$N_i = \frac{1}{g_{3i} \times \left(1 + \dfrac{g_{2i} \times f_{3i}}{f_{2i} \times g_{3i}}\right)} \times [(-Xx_i - Xy_i + W_i + P_{vi}) - \frac{f_{3i}}{f_{2i}} \times (-Ey_i - Hy_{i+1} + Hy_i)] \tag{5.30}$$

Table 5.6 Comparison between the overall equilibrium method and cross-sectional equilibrium method using the 3D Morgenstern–Price method for Example 5

Q (kPa)	*Method*	*FOS*	*SD*	*x*	*y*
300	1	0.616	10.99°	0.894	–0.1835
	2	0.619	10.93°	0.9195	0.2886
200	1	0.649	9.39°	0.8361	–0.1512
	2	0.651	9.33°	0.8941	0.2586
100	1	0.704	6.54°	0.708	–0.0857
	2	0.706	6.48°	0.8451	0.1944

Note: Method 1 = overall equilibrium method; Method 2 = cross-sectional equilibrium method.

In the present formulation, the inter-column normal and shear forces are calculated based on the adjoining column of the last column by using eqs. (5.9), (5.10) and (5.11); the base shear and normal force can then be found in the iteration process. The use of eqs. (5.29) and (5.30) is equivalent to enforcing cross-sectional horizontal force equilibrium in the last column of each section; hence, cross-sectional force equilibrium can be achieved. If eq. (5.29) or (5.30) is used, sectional force equilibrium can be achieved in either direction only and equilibrium along both *x* and *y* sections cannot be maintained *simultaneously*. For 2D analysis, the base normal forces for the last one or two slices may be negative if the cohesive strength is high (Abramson *et al.*, 2002). If the base force for the last column is not realistic, unrealistic numerical results may be introduced in the back calculation of the base and inter-column forces from the last column. After carrying out the computational analysis, it is found that the iteration process is more difficult to converge with the use of eq. (5.29) or (5.30). This situation is not surprising, as eqs. (5.29) and (5.30) become additional constraints to the convergence. The more constraints to a problem, the more difficult it will be for the analysis to get converged. For those problems where the cross-section force equilibrium can be achieved with converged results, the safety factors are virtually the same as those where the cross-section force equilibrium is not enforced and the results are shown in Table 5.6. In general, Cheng and Yip (2007) do not suggest the enforcement of the cross-section force equilibrium in the analysis, as convergence is usually more difficult to be achieved. If the cross-section horizontal force equilibrium is not enforced in the analysis, there will be overall unbalanced moment about the *z* axis. It appears that it is not possible to achieve better convergence and eliminate unbalanced moment about the *z* axis unless additional assumptions are introduced in the solution.

5.2.7 Discussion on λ_{xy} for Morgenstern–Price analysis

To examine the effect of λ_{xy} on the safety factor, a uniform distributed pressure of 300 kPa is applied to half of the failure mass for the problem shown

Table 5.7 Effect of λ_{xy} on the safety factor and sliding direction for Example 5 (292 columns)

λ_{xy}	*0*	*0.05*	*0.1*	*0.15*	*0.2*	*0.25*
F	0.6186	0.6187	0.6188	0.6188	Fail	Fail
SD	10.929°	10.920°	10.911°	10.902°	Fail	Fail
λ_x	0.9195	0.926	0.9325	0.9384	Fail	Fail
λ_y	0.289	0.289	0.289	0.289	Fail	Fail

in Figure 5.12 and the results are shown in Table 5.7. It can be seen that λ_{xy} is not sensitive to the analysis. This situation is not surprising, as the vertical shear forces Xx_i and Xy_i (with same direction as weight of soil) will be more important than the horizontal shear forces Hx_i and Hy_i in the present problem. However, if λ_{xy} becomes greater than 0.2, the iteration process tends to fail to converge (unless a relatively large tolerance is adopted).

Huang *et al*. (2002) believe that the disturbing force induced by the torque due to *Hx/Hy* is minor and *Hy* is actually taken as 0 in their formulation, which is in conflict with the concept of a complementary shear. Actually, no additional equation is available to determine λ_{xy}. Cheng and Yip (2007) have considered the use of moment equilibrium about the *z* axis to determine λ_{xy}, but unbalanced moment ΣMz can actually come from the sectional force equilibrium problem as mentioned before. If sectional equilibrium is enforced, ΣMz will actually be 0 so that λ_{xy} will be indeterminate. To avoid the introduction of an additional assumption in determining λ_{xy}, λ_{xy} is suggested to be prescribed by the engineer in the present formulation. Alternatively, Cheng and Yip suggest that λ_{xy} can be determined from the minimization of the FOS with respect to λ_{xy}. Because λ_{xy} is not a major factor in the analysis, λ_{xy} can be prescribed to be 0 for most cases without a major problem.

5.2.8 Discussion on the 3D stability formulation

In this chapter, new 3D slope stability methods are developed that are based on force/moment equilibrium. Fundamental principles of limit equilibrium are used with an extension of either the 2D Bishop simplified method, the Janbu simplified method or the Morgenstern–Price method. The new formulations possess several important advantages that are as follows:

1 simple extension of the corresponding 2D formulation;
2 a unique sliding direction can be determined;
3 better convergence that is not affected by the initial choice of a_i;
4 the results from the present study are comparable to those by other researchers for some well-known cases;
5 applicable to highly non-symmetric problems with transverse load.

By using this new formulation, the unique sliding direction can be determined with the corresponding safety factor. The limitations of Huang and Tsai's (2000) method are overcome by the new formulations as proposed while the assumption of a plane of symmetry can be eliminated in the analysis of 3D slopes. Cheng and Yip (2007) have tried more than 100 cases for 3D Bishop and Janbu analysis using Huang and Tsai's formulation and the present formulation for both symmetric and asymmetric problems. The factors of safety and sliding directions from all these examples are extremely close between these two formulations and the differences are small and negligible for all these cases. It can be viewed that for a normal problem with no transverse load, the present formulation and Huang and Tsai's formulation are practically the same.

The transverse earthquake load has not been considered in the past due to the lack of a suitable 3D analysis model. The present study on transverse earthquake load has demonstrated the limitation of Huang and Tsai's method, as transverse loads greatly affect the spread of the sliding directions and hence the convergence. Huang and Tsai's method faces difficulty in convergence with transverse load, as the sliding direction is not unique. For the present formulation, the sliding direction is unique and only two convergent criteria have to be met for directional safety factors to be determined. Convergence is hence greatly improved under the present formulation.

In the numerical examples, the present formulation is found to be reasonable in the determination of the safety factor and sliding direction of a 3D slope. In particular, the analytical results for the wedge-type failure in Examples 3 and 4 are exactly the same as those obtained by the present formulations. In Examples 1 and 2, Huang and Tsai's (2000) method gives results similar to those from the present formulation. However, the sliding direction from Huang and Tsai's analysis is based on the average sliding directions of all the columns. Conceptually, this is a major limitation as the spread of the individual sliding direction can be major if the problem is highly asymmetric. In fact, there is another fundamental problem in taking the average individual sliding direction. If there is a major variation in the sizes of columns, it is not clear whether the size of the column should be considered in the averaging process or not. Finally, if the sliding direction is not unique, some of the columns could be separating from each other and the summation of the overturning and restoring moment/force process is strictly not applicable. In view of all these limitations, the requirement on unique sliding direction appears to be important for 3D analysis and this has been solved effectively by the present formulation.

Cheng and Yip (2007) have demonstrated that the present formulation is equivalent to Yamagami and Jiang's (1996, 1997) formulation but is more convenient to be used for general conditions. No rotation of axes is required to determine the FOS and there is a significant reduction of work for the location of critical failure surfaces where thousands of trials are required.

In general, the behaviour of the present formulation is similar to the corresponding 2D formulation in most cases. For example, based on limited

case studies, it is found that the FOS is usually not sensitive to $f(x, y)$ ($f(x) = \sin(x, y)$ has been tried) in most cases. Although the 3D Janbu and Bishop methods suffer from the limitation of incomplete equilibrium conditions the 3D Morgenstern–Price method suffers from the limitation that exists only for 3D analysis. Overall force and moment equilibrium can be maintained under the Morgenstern–Price formulation while the cross-section equilibrium will be violated unless eqs. (5.29) and (5.30) are used, and cross-sectional equilibrium in both directions cannot be maintained simultaneously. As there are more equations than unknowns (more serious than the 2D condition), convergence with the Morgenstern–Price method is also more difficult as compared with the corresponding 2D condition. Due to the indeterminacy of the system, Cheng and Yip (2007) view that it is not possible to maintain overall and local equilibrium without additional assumptions in general 3D analysis. In the present formulation, enforcement of cross-section horizontal and moment equilibrium may affect convergence of the solution, and Cheng and Yip suggest that it is not worth imposing these constraints in analysis.

In spite of the limitations in the 3D Morgenstern–Price formulation, the applicability of the proposed 3D asymmetrical analysis has been demonstrated by several examples, where the results from the 3D Morgenstern–Price method are similar to those from the 3D Bishop simplified method and 3D Janbu simplified method. The proposed formulation can also predict the exact sliding directions and safety factors for the simple sliding wedge in Examples 3 and 4, which is a support to the applicability of the present formulation.

5.3 3D limit analysis

The extensions of the upper-bound technique to 3D geotechnical problems are being investigated. Michalowski (1989) presented a 3D slope stability method for drained frictional-cohesive material based on the upper-bound technique of limit analysis. The slip surface was approximated by a number of planar surfaces, whose lines of intersection were perpendicular to the plane of symmetry, in combination with so-called end surfaces that extended to the slope top or the slope surface. A typical failure mechanism used in the method consists of rigid-motion blocks separated by planar velocity discontinuity surfaces. The limit load involved in an energy balance equation was found directly. The minimum of the FOS or the limit load was obtained by searching all kinematically admissible mechanisms of failure. The simplification regarding the geometry of a slip surface and the surface of a slope made in the method limited the application to practical problems. Although the approach proposed by Michalowski was limited to homogeneous slopes, more recently Farzaneh and Askari (2003) modified and extended Michalowski's approach to deal with inhomogeneous symmetrical cases.

Chen *et al.* (2001a, 2001b) presented another 3D method based on the upper-bound theorem, in which an assumption of a so-called 'neutral plane' is needed so that the failure surface is generated by elliptical lines based on

the slip surface in the neutral plane and extended in the direction perpendicular to the neutral plane. Wang (2001) demonstrated its applications to several large-scale hydropower projects.

The common features for the upper-bound methods proposed by Michalowski (1989) and Chen *et al.* (2001a, 2001b) are that they both employ the column techniques in 3D limit equilibrium methods to construct the kinematically admissible velocity field, and have exactly the same theoretical background and numerical algorithm that involves a process of minimizing the FOS. The only difference is that Michalowski (1989) and Farzaneh and Askari (2003) use vertical columns, whereas Chen *et al.* (2001a, 2001b) and Wang (2001) use non-vertical columns, allowing flexibility in handling relatively complicated geometry and layered rocks and soils.

Lyamin and Sloan (2002b) presented a new upper-bound limit analysis using linear finite elements and nonlinear programming. The formulation permitted kinematically admissible velocity discontinuities at all inter-element boundaries and furnished a kinematically admissible velocity field by solving a nonlinear programming problem. The objective corresponded to the dissipated power (which was minimized) and the unknowns were subject to linear equality constraints as well as linear and nonlinear inequality constraints. The optimization problem could be solved very efficiently using an interior point, two-stage, quasi-Newton algorithm.

As an illustration, a landslide that occurred in Hong Kong is considered by the 3D rigid element method (Chen, 2004). During the morning of 23 July 1994, a minor landslide occurred at a cut slope at milestone 14 $\frac{1}{2}$, Castle Peak Road, New Territories, Hong Kong (Figure 5.21). In the afternoon on the same day, a second landslide occurred. On 7 August 1994, a further landslide took place at the same slope. This landslide caused 1 man to be killed and 17 other people taken to hospital. Due to the limited available information on the first and second landslides, only the third landslide, called the Castle Peak Road landslide herein, is analysed in this section. This landslide is of typical three dimensions and encompassed approximately 300 m^3 of soil and rock.

Site investigation showed that the ground at the location of the landslides generally comprised partially weathered fine-grained and medium-grained granite, which was a soil of silty sand. Rock of medium-grained granite (slightly to moderately decomposed) was exposed in the cut slope at the western edge of the landslide scar. The partially weathered granite exhibited a well-developed, black-stained relict joint structure. Results of laboratory tests on undisturbed samples of the weathered granite have shown that the strength of soil at this site is akin to that of similar material found in other parts of Hong Kong.

The granite at the site was intruded by a number of sub-vertical basalt dykes, which ran in a northeast direction. Two completely decomposed basalt dykes approximately 800 mm thick were exposed within the landslide scar. Field assessment and laboratory tests have revealed that the completely decomposed

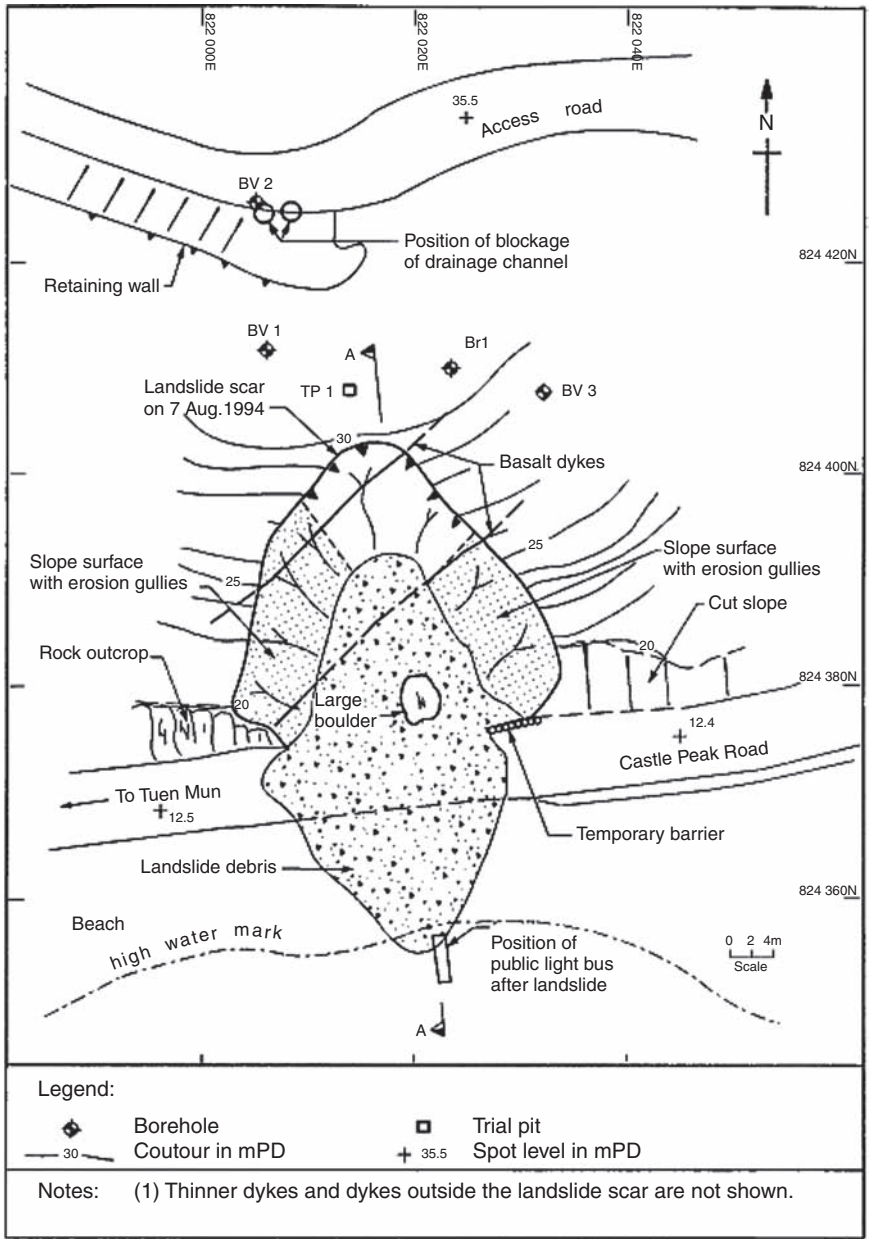

Figure 5.21 A plan view of a landslide in Hong Kong.

basalt dykes were much less permeable than the partially weathered granite. Therefore, the dykes acted as barriers to water (Pun and Yeo, 1995).

Before the landslide on 7 August, on 6 August rain was heavy in the area along Castle Peak Road, with a total of about 287 mm of rain being recorded. Water seepage was observed in the landslide scar on the uphill side of the two decomposed basalt dykes for a period of at least 1 week after the landslide on 7 August, indicating that the groundwater level was high behind the dykes. In addition, inspection of the access road on the hillside above the landslide scar found that a drainage channel along the edge of the road was completely blocked. This indicates, to a certain degree, the groundwater level in front of the dykes flowed along the ground surface. However, no measured data for the exact value of the groundwater level behind the basalt dykes are available. A parametric study of the different groundwater levels is to be conducted to reveal the essential influence of the groundwater level in the landslide mass on the stability of the slope.

A 3D slope stability analysis was conducted for the landslide on 7 August shown in Figure 5.21. The unit weight of the landslide material was taken to be 20.6 kN/m^3. The peak strength parameters were measured to be $c' = 6.7$ kPa and $\phi' = 35.5°$. The groundwater level in the sliding mass plays an important role on the stability of the landslide. Four different cases were therefore investigated in the 3D slope stability analyses, that is, (1) no groundwater involved in the failure mass, (2) water level at 5.50 m, (3) water level at 6.15 m and (4) water level at 6.80 m.

Because the slip surface of the landslide exhibits apparent 3D characteristics, the 3D upper-bound method is suitable for the analysis. Figure 5.22(a) illustrates how to generate the slip body in a slope model; Figure 5.22(b) shows the geometry model. The mesh generated for the slip body is shown in Figure 5.22(d). When the groundwater table is at the toe of the landslide (Case 1), the 3D FOS is 1.463, which indicates that the slope is stable if no water is infiltrated into the sliding mass. However, while the groundwater level increases gradually, the 3D FOS decreases accordingly. At the level of the groundwater 5.50 m over the base line (Case 2), the 3D FOS is 1.108. While the level of groundwater is 6.15 m (Case 3), the FOS calculated is 1.002, which is close to 1.0. It indicates that the slope has arrived in the limit state and the slope would collapse at the level of the groundwater at 6.15 m. When groundwater relative to the base line is 6.92 m (Case 4), the 3D FOS is 0.922, which is less than unity and the slope has collapsed.

5.4 Location of the general critical non-spherical 3D failure surface

Up to present, there is only limited research in determining the critical 3D slip surface due to the difficulties in performing large-scale global optimization analysis of the N-P type function. Searching for the 3D critical slip surface can be classified into two major groups: (a) the first assumes a slip surface to have

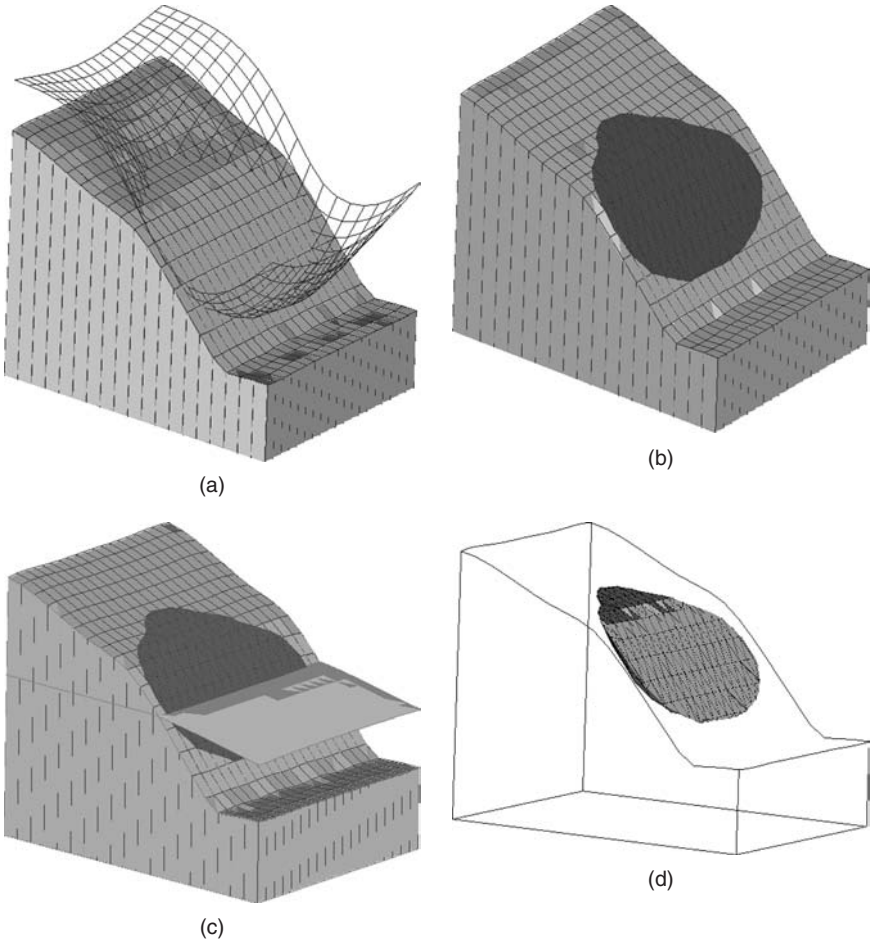

Figure 5.22 3D slope model: (a) Schematic diagram of generation of slip body; (b) Geometry model; (c) Schematic diagram of groundwater; and (d) Mesh generation for slip body.

a particular shape, for example, an extended circular arc (Baligh and Azzouz, 1975), a cylindrical surface (Ugai, 1985) or an ellipsoidal surface (Zhang, 1988); and (b) the second is valid for an arbitrary slip surface. When the analysis of slope stability is carried out by the first group of methods, the slip surface can be expressed analytically and the critical slip surface can be found easily through simple numerical computations.

Based on the methods that were valid for the slip surface of an arbitrary shape, however, it was quite difficult to search for the critical surface because possible slip surfaces exist infinitely. Thomaz and Lovell (1988) recommend a

procedure for 3D slope stability analysis using the method of random generation of surfaces. It has been indicated that the critical slip surface determined using the method was probably not the most critical one because the convergence criterion for solutions with the required precision did not exist.

Leshchinsky *et al.* (1985) and Leshchinsky and Baker (1986) presented a mathematical approach based on the limit equilibrium and variational calculus for 3D slope stability analysis. Solving the variational limit equilibrium equations made it possible to obtain the minimum FOS and the associated critical surface at the same time. However, the method based on the variational analysis has not yet been applied to practical problems because of the required mathematical format.

Yamagami and Jiang (1997) proposed an approach based on dynamic programming and random number generation. The approach could determine the location and shape of the 3D critical slip surface as well as the associated FOS for a slope of arbitrary shape, including layered soils and/or the phreatic surface. The random number generation was employed to generate states and thus transformed the 3D dynamic programming problem into a 2D one while 3D slope stability analysis could not directly be performed using a dynamic programming algorithm only. The dynamic programming approach by Yamagami and Jiang is generally applicable for simple problems, but there is no mechanism behind the dynamic programming method to escape from the local minimum during the optimization. The problem of the local minimum for some complicated 2D problems has been studied by Cheng (2003) and this is a difficult problem for the arbitrary slope problem. For complicated problems where the presence of the local minimum may be a critical factor in the search for the global minimum, the solution will be a difficult N-P type optimization problem for both 2D and 3D problems.

5.4.1 3D NURBS surfaces

The success of 3D global optimization requires the description of a general 3D surface using limited control variables but is able to model arbitrary geometry. This is extremely difficult, and there is no simple way to ensure a very special shape can be generated for an arbitrary solution domain. However, for most of the normal cases, a relatively smooth function may be good enough to model the 3D surface. NURBS or Non-Uniform Rational B-Splines (Les and Wayne, 1997; David, 2001) are now commonly adopted for describing and modelling curves and surfaces in solid modelling, computer aided design and computer graphics. It has a great ability to represent a regular surface such as flat planes and quadric surfaces as well as complex fully sculptured surfaces with only few local and global controls. A NURBS surface is a special case of a general rational B-spline surface that uses a particular form of knot vector. For a NURBS surface, the knot vector has a multiplicity of duplicate knot values equal to the order of the basis function at the ends, that is, a NURBS surface uses an open knot vector. The knot vector may or may not have uniform internal knot points and this can be

controlled by the user easily. Non-uniform spaced knot points are important for slope stability analysis as the critical failure surface may have its arbitrary extent controlled by the topography, and the use of the non-uniform spaced knot point is necessary for general problems.

A Cartesian product of the rational B-spline surface in a four-dimensional homogeneous coordinate space is given by (Les and Wayne, 1997; David, 2001)

$$Q(u,w)=\sum_{i=1}^{n+1}\sum_{j=1}^{m+1}B_{i,j}^{h}N_{i,k}(u)M_{j,l}(w), \tag{5.31}$$

where $B_{i,j}^{h}$ s are the four-dimensional homogeneous polygonal control vertices (3D coordinates and coordinate weight factor which are stored in the matrix NURBS surface as discussed later) and $N_{i,k}(u)$ and $M_{j,l}(w)$ are the non-rational B-spline basis functions in the x and y directions, respectively, given in eq. (5.32):

$$N_{i,1}(u)=\begin{cases}1 & \text{if } x_i\le u<x_{i+1}\\ 0 & \text{otherwise}\end{cases} \tag{5.32a}$$

$$N_{i,k}(u)=\frac{(u-x_i)N_{i,k-1}(u)}{x_{i+k-1}-x_i}+\frac{(x_{i+k}-u)N_{i+1,k-1}(u)}{x_{i+k}-x_{i+1}}$$
$$u_{\min}\le u<u_{\max},\ 2\le k\le n+1, \tag{5.32b}$$

$$M_{j,1}(w)=\begin{cases}1 & \text{if } y_j\le w<y_{j+1}\\ 0 & \text{otherwise}\end{cases} \tag{5.32c}$$

$$\text{and}\quad M_{j,l}(w)=\frac{(w-y_j)M_{j,l-1}(w)}{y_{j+l-1}-y_j}+\frac{(y_{j+l}-w)M_{j+1,l-1}(w)}{y_{j+l}-y_{j+1}}$$
$$w_{\min}\le w<w_{\max},\ 2\le l\le m+1. \tag{5.32d}$$

Projecting back into the 3D space by dividing with the homogeneous coordinate gives the rational B-spline surface as

$$Q(u,w)=\frac{\sum_{i=1}^{n+1}\sum_{j=1}^{m+1}h_{i,j}B_{i,j}N_{i,k}(u)M_{j,l}(w)}{\sum_{i=1}^{n+1}\sum_{j=1}^{m+1}h_{i,j}N_{i,k}(u)M_{j,l}(w)}=\sum_{i=1}^{n+1}\sum_{j=1}^{m+1}B_{i,j}S_{i,j}(u,w), \tag{5.33}$$

where $B_{i,j}$ s are the 3D control net vertices (3D coordinates which are a submatrix of the matrix NURBS surface) and $S_{i,j}(u,w)$ are the bivariate rational B-spline surface basis functions given by

$$S_{i,j}(u,w)=\frac{h_{i,j}N_{i,k}(u)M_{j,l}(w)}{\sum_{i1=1}^{n+1}\sum_{j1=1}^{m+1}h_{i1,j1}N_{i1,k}(u)M_{j1,l}(w)}=\frac{h_{i,j}N_{i,k}(u)M_{j,l}(w)}{\Sigma(u,w)}, \tag{5.34}$$

where $\Sigma(u,w) = \sum_{i1=1}^{n+1} \sum_{j1=1}^{m+1} h_{i1,j1} N_{i1,k}(u) M_{j1,l}(w)$.

It is convenient, though not necessary, to assume $h_{i,j} \geq 0$ for all i,j. The smooth NURBS surface will be controlled by the coordinates of the control points but will not pass through the control points exactly. The greater the values of $h_{i,j}$, the closer will be the NURBS surface to the control points.

In the above-mentioned formulas, the symbols are as follows:
u, w – the NURBS surface's transverse and longitudinal directions, being similar to the x and y axes;
n, m – the numbers of control net vertices in the u, w direction;
k, l – order in the u, w directions;
$b()$ – array containing the control net vertex:
$b(,1)$ contains the x component of the vertex,
$b(,2)$ contains the y component of the vertex,
$b(,3)$ contains the z component of the vertex,
$b(,4)$ contains the homogeneous coordinate weighting factor, h;
$B_{i,j}$ – are the 3D control net vertices. $B_{i,j} = b\ (n \times m, 1 \sim 3)$;
$B^h_{i,j}$ – are the 4D homogeneous polygonal controls. $B^h_{i,j} = b\ (n \times m, 1 \sim 4)$.

When eqs. (5.31) to (5.34) are used, the number of control net vertices must be equal to $n \times m$. However, for slope stability analysis, it is not always practical to have $n \times m$ control net vertices. In the optimization analysis, the coordinates of the control nodes will be changing and a $n \times m$ net vertices regular grid cannot be adopted. If the control net vertices are not arranged regularly to form a regular grid, the NURBS surface may twist seriously (cusps). A cusp is highly unlikely to occur in a real situation and should be avoided in the generation of a non-spherical failure surface. In fact, restraining forces will be provided by the cusp (if present) and this situation can be eliminated in the generation of non-spherical failure surfaces. Excessive unacceptable failure surfaces generated from the NURBS points will greatly reduce the efficiency of analysis and this has been experienced by Cheng *et al.* (2005) in the preliminary study, and a simple method is proposed to generate a NURBS surface that can avoid this problem.

First, four extreme fixed corners (net vertices) will define a domain similar to a net of $n \times m$ points (see Figure 5.23). The z ordinates of these four extreme fixed corners can change during the optimization analysis and they are the control variables. In general, the user should define a solution domain large enough to cover all possible failure mechanisms and this is usually not difficult. To eliminate the formation of a cusp, a NURBS surface can be viewed as a net stretched tightly within the plane force. Second, each control node should affect the net in order in forming the 3D sliding surface. The coordinates of every point on the regular grid are controlled by the control node. This approach is equivalent to putting a stone on a net stretched tightly and every

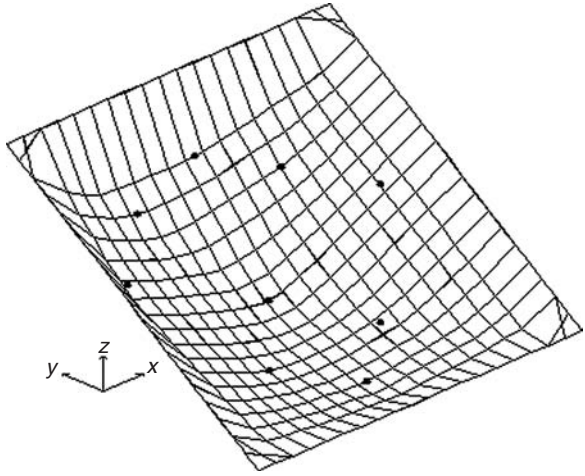

Figure 5.23 The NURBS surface with nine control nodes.

net point sinks with the stone. A NURBS surface with no kink will then be generated even if the control points are not spaced regularly. Obviously, the more control nodes used for modelling, the better will be the quality of the the NURBS surface. Third, the shape of the NURBS surface will change with the coordinates and weighting factors of control nodes. The greater the weight factor of a control node, the closer the NURBS net is to the control node. It is easy to modify the shape of the NURBS surface by changing the weighting factors.

During the simulated annealing analysis, each control variable will vary sequentially and Cheng (2003) has proposed a simple trick to avoid generating an unacceptable 2D failure surface by changing the requirement of 'kinematically acceptable mechanism' to 'dynamic boundaries' of control variables. Such a technique has been used by Cheng *et al.* (2005) for 3D analysis. That means that the shape of the trial failure surfaces will be examined in longitudinal as well as transverse directions so that the boundaries of the control variables will be modified, which is effectively Cheng's (2003) approach applied in two directions. Using this technique, most of the failure surfaces generated will be kinematically acceptable. By using the concept of the stretched net and the requirement of a 'kinematically acceptable mechanism', most of the failure surfaces as generated from NURBS functions will be suitable for optimization analysis.

5.4.2 Spherical and ellipsoidal surfaces

For simple problems, the use of spherical and ellipsoidal failure surfaces may be sufficiently good in application. For a spherical failure surface, it is simple

to operate and the number of control variables are four: (xc, yc, zc, r), where (xc, yc, zc) are the coordinates of the centre of the sphere and r is the radius of the sphere. For an ellipsoidal failure surface defined by global axes x, y, z, the equation will be

$$\frac{(x-xc)^2}{a^2}+\frac{(y-yc)^2}{b^2}+\frac{(z-zc)^2}{c^2}=1. \tag{5.35}$$

The ellipsoid can be defined in terms of the rotated axes x', y' and z' so that two more additional control variables for the rotation of the axes are required in the optimization process. The number of control variables are hence eight: (xc, yc, zc, a, b, c, θx, θy), where (xc, yc, zc) is the centre of the ellipsoid, a, b, c are the axes lengths of the ellipsoidal and θx and θy are the rotation of the xy and yz planes, respectively. The use of an ellipsoidal failure surface is attractive in that the number of control variables is not great and the solution time is acceptable for an ordinary design. Every ellipsoid is convex in shape and includes the spherical shape as a special case so that it is suitable for ordinary problems. Example 3 in Section 5.5 will illustrate the advantage of using the ellipsoid in analysis.

5.4.3 Selection of sliding surfaces

For 3D limit equilibrium analysis, the potential failure mass of a slope is divided into the number of columns. The NURBS/spherical or ellipsoidal surface intersects with the ground profile and generates soil columns and a sliding mass. For the 3D failure surfaces as generated, some surfaces are not unacceptable and should be removed from the analysis. The following failure surfaces should be eliminated in the optimization analysis:

1 The number of columns formed is too small. Cheng *et al.* (2005) have found that if the number of columns used for stability analysis is too small, the results on the safety factor will be greatly affected. This kind of problem may come up if the size of each column is too large (see Figure 5.24a). Generally, this problem can be avoided by a good pre-processing of the mesh for generating the soil columns and is only a minor problem.
2 The sliding surface is not a complete concave surface. Most sliding surfaces are completely concave. Any sliding surface that is composed of concave and convex portions can be eliminated in the analysis (see Figure 5.24b). This case is absent for spherical and ellipsoidal failure surfaces and is also not commonly found as the concave portion will induce additional restraining forces and is not critical in general. However, the user should be given the choice that this type of composite failure surface can be accepted in the optimization process. Based on the present proposal on the use of dynamic domains to the control variables in longitudinal and transverse directions, this situation is practically eliminated.

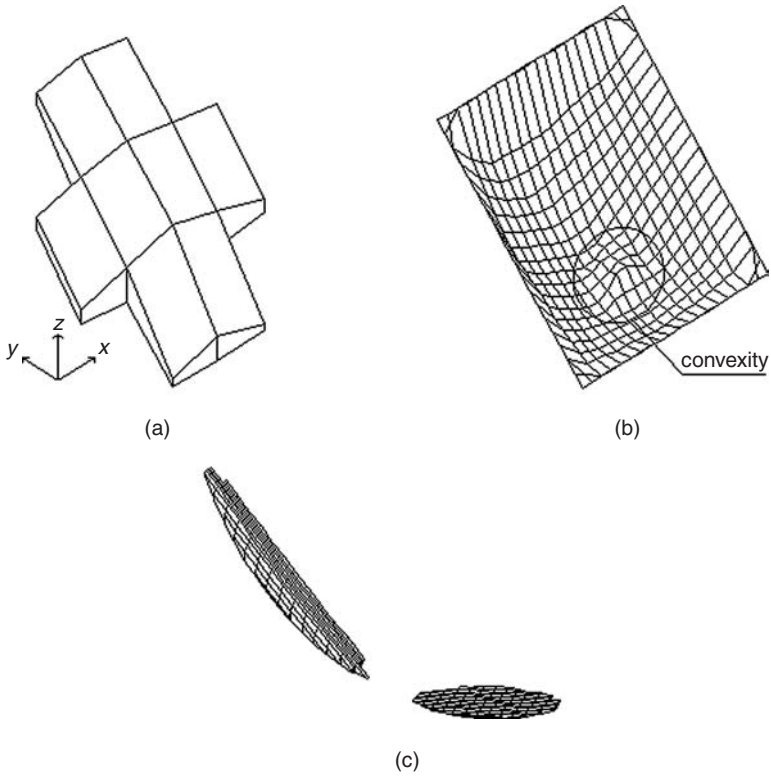

Figure 5.24 Three cases should be considered.

3 If the failure mass is divided into several unconnected parts as shown in Figure 5.24c, the failure surface will not be accepted. For the case shown in Figure 5.24c, only the larger failure mass will be considered as acceptable in the analysis, whereas the smaller failure zone is not considered.

A typical valid failure surface is shown in Figure 5.25.

5.4.4 Optimization analysis of the NURBS surface

The critical failure surface corresponds to the global minimum of the FOS function over the solution domain that can be determined from the heuristic optimization methods discussed in Chapter 3. For a spherical failure surface, the x, y, z coordinates of the centre of rotation and the radius of sliding sphere are the multidimensional variables and there are in total four control variables. The x, y, z coordinates of nodes on the NURBS surface are the multidimensional variables but the number of control variables will be much greater than the

corresponding spherical failure surface. The x, y, z coordinates of the control nodes are the control variables and upper and lower bounds to these control variables are required to be defined by the user. For the upper and lower bounds of z ordinates of the control variables, the upper bound will be dynamic in that the upper bound should not exceed the ground level based on the current x and y ordinates. To achieve this requirement, the order of the control variables must be in the form of (x, y, z, . . .) or (y, x, z, . . .) in simulated annealing analysis. The order of x and y are not important in the analysis but the order of z must follow (x, y) or (y, x) to control the upper bound of z by the updated x and y ordinates. The restraints as provided to the control variables are basically similar to the 2D optimization method as proposed by Cheng (2003) but are applied in both longitudinal and transverse directions so as to impose a kinematically acceptable mechanism in the failure surface generation.

5.5 Case studies in 3D limit equilibrium global optimization analysis

Based on the discussion in the previous section, Cheng *et al.* (2005) have developed a program, SLOPE3D, that is designed for a general asymmetric slope with arbitrary geometry and arbitrary external load in longitudinal and transverse directions. After generating an acceptable sliding surface based on the simulated annealing rule, the FOS will be calculated by the 3D Bishop, Janbu or Morgenstern–Price methods by Cheng and Yip (2007). The numerical examples in this section can illustrate the effectiveness of the proposed NURBS function in the optimization analysis.

Example 1:
To validate the applicability of the NURBS function in the location of the non-spherical failure surface, a simple problem where the exact solution is known is chosen for the study. The problem under consideration has only one type of soil where the unit weight, cohesion and internal friction angle are 20 kN/m^3, 0 kPa and 36°, respectively. Slope angles for 30°, 45° and 60°, respectively, are considered in the analysis. Theoretically, the critical failure surface is a very shallow symmetrical failure surface parallel to the slope surface and the FOS is equal to $\tan\phi/\tan\theta$. The minimum factors of safety after the optimization calculation are shown in Table 5.8.

In the present example, 17 control nodes are used to generate the NURBS failure surface and very good results are obtained from the analysis. All the critical failure surfaces are very shallow-type surfaces parallel to the ground surface, which is in accordance with classical soil mechanics theory. The small differences between the optimized values and the theoretical values can be considered to be acceptable in view of the discretization required for computation. These results have demonstrated the effectiveness of the NURBS function under this simple condition. For the present problem, the results are practically independent of the number of control points (unless the number is

Table 5.8 The minimum factors of safety after the optimization calculation

Factors of safety \ *Slope degree*	*30°*	*45°*	*60°*
Bishop[a]	1.25747	0.72625	0.41998
Janbu	1.25749	0.72627	0.42002
Morgenstern–Price	1.25755	0.72575	0.41905
Theoretical value: $F = \frac{\tan\phi}{\tan\theta}$	$\frac{\tan 36^\circ}{\tan 30^\circ} = 1.25841$	$\frac{\tan 36^\circ}{\tan 45^\circ} = 0.72654$	$\frac{\tan 36^\circ}{\tan 60^\circ} = 0.41947$

Note

a A spherical search is applied to the Bishop method, whereas the NURBS function simulated annealing search is used for the Janbu and Morgenstern–Price methods.

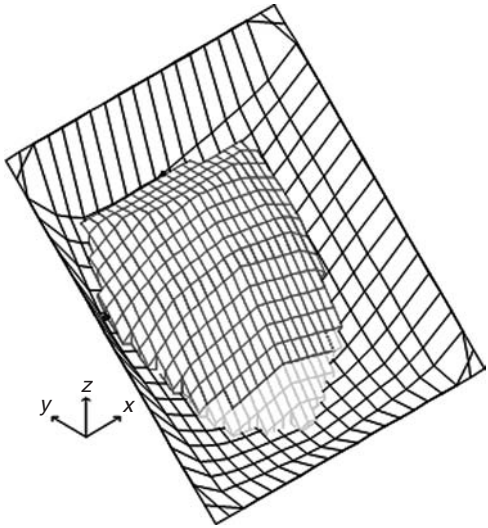

Figure 5.25 Sliding columns intersected by the NURBS sliding surface.

very small) as the critical failure surface is a very shallow surface. As long as the control points are near to the ground surface, a good shallow failure surface practically parallel to the ground surface will be generated. For the two following examples where the critical failure surfaces are not parallel to the ground surface, the results are more sensitive to the number of control points.

Example 2:
To illustrate the differences between the minimum factors of safety from spherical and NURBS failure surfaces, a special problem is devised with 3D Janbu analysis. The geometry of the slope is shown in Figure 5.26. There are two kinds of soils with a groundwater table. The geological profile remains constant in the direction normal to the figure. The cohesion of upper soil is much less than the lower soil so that the critical failure surface will be controlled by the boundary between the two layers of soil. First, the critical spherical sliding surface is evaluated by a simulated annealing algorithm. After 11,521 calculation steps, a minimum FOS of 0.6134 is obtained for the 3D Janbu analysis. The x, y, z coordinates of the centre of rotation and the radius of the spherical sliding surface with the minimum FOS are (0.0000, –0.3462, 8.5384) and 6.1879 m, respectively. The spherical critical failure surface shown in Figure 5.27(b) is tangential to the boundary between Layer 1 and Layer 2 at 1 point (geometry requirement).

Second, a NURBS sliding surface is constructed with 17 nodes. The dimension of the control net SS′T ′T shown in Figure 5.27c is 8 m × 6 m, and there are in total 361 columns used for analysis. After 78,943 calculation steps, a

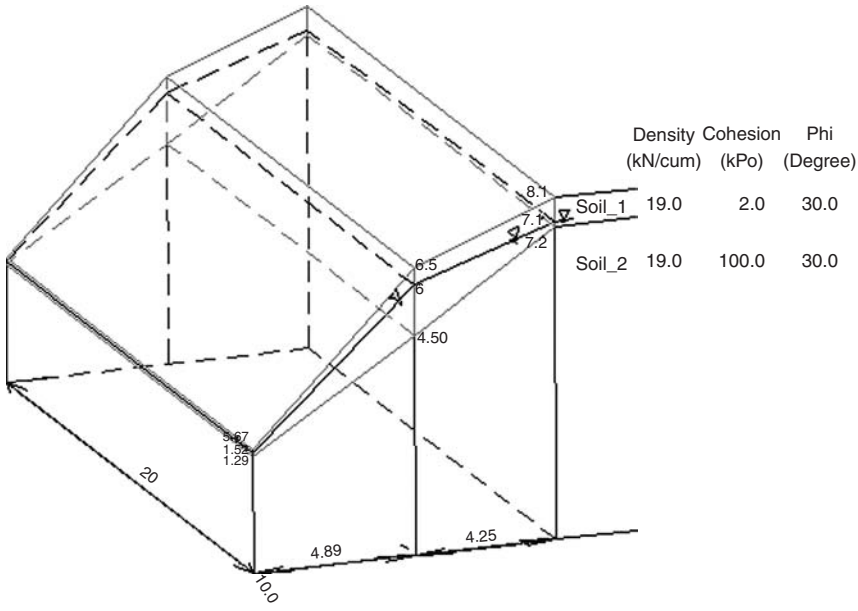

Figure 5.26 Slope geometry for Example 2.

minimum FOS of 0.5937 that is smaller than that by the spherical failure surface search is attained. The finer mesh shown in Figure 5.27c is the failure surface and the greater mesh is the NURBS grids as discussed before. The critical symmetrical NURBS failure surface formed by the control net SS′T′T and the NURBS surface is tangential to the boundary between Layers 1 and 2 over a region instead of just a single point touch, which is the expected solution. In Figure 5.27d, the failure mass is the lower part of the complete NURBS surface formed by the control net. This example has illustrated the importance of the non-spherical search for the critical 3D failure surface under the general condition. For 5 NURBS points, the minimum factors of safety and number of trials are 0.751 and 46,082, respectively, from the optimization search, whereas the corresponding figures for 10 NURBS points are 0.647 and 65,090. It is also found that the minimum FOS is practically insensitive to the number of NURBS points if the number is 15 or above. Unlike the previous case which is practically a planar failure mode, the present critical failure surface requires 15 or more NURBS points for a good description of the 3D failure surfaces.

Example 3:
In this example, a typical slope in Hong Kong with a soft band is considered. As shown in Figure 5.28, there are three kinds of soils and no groundwater table. The unit weight, cohesion and internal friction angle of the first layer

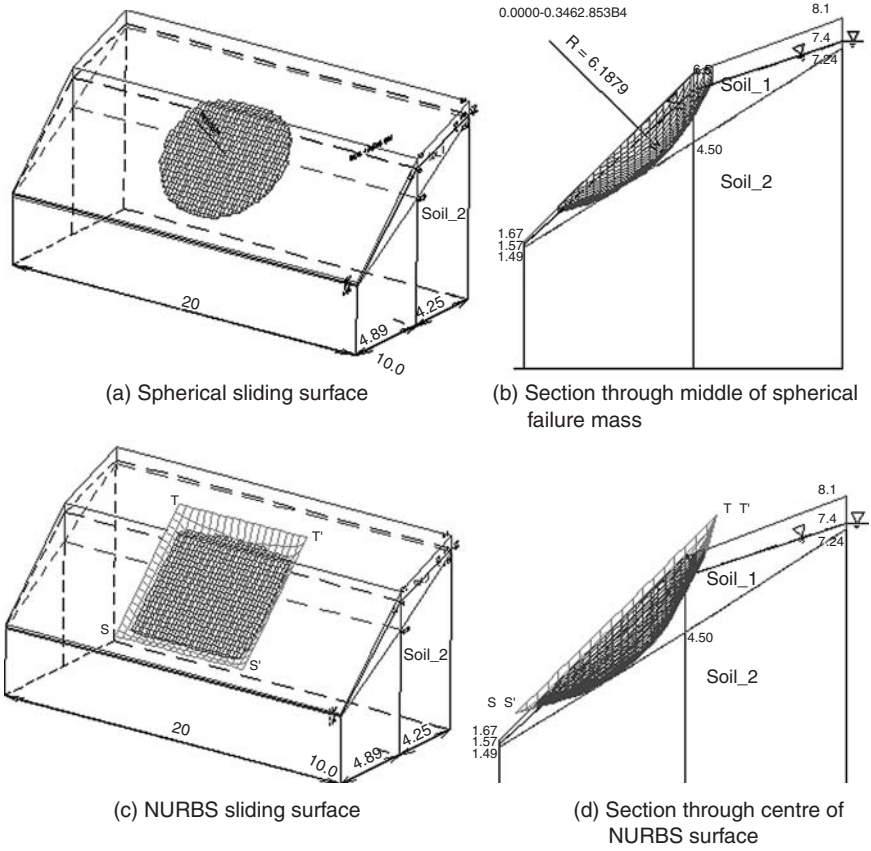

Figure 5.27 Sliding surface with the minimum FOS for Example 2.

of soil are 18 kN/m^3, 10 kPa and 30°, respectively. The soil parameters for the second layer, which is thin in thickness, are 18.5 kN/m^3, 2.0 kPa and 5°, respectively. The soil parameters for the third layer are 19 kN/m^3, 20 kPa and 25°, respectively. Actually, this is a slope with a soft band soil and each soil boundary surface is an irregular surface fluctuating in 3D space. Because the soil parameters for the second layer of soil are low, a major portion of the failure surface will lie within Layer 2, which is thin in thickness, and a spherical surface will not be adequate for the optimization analysis.

For the critical spherical asymmetric failure search that is obtained after 7488 calculation steps, the minimum FOS is 0.6177 from 3D Janbu analysis. The x, y, z coordinates of the centre of rotation and the radius of the spherical sliding surface with the minimum FOS are (59.8299, 52.8347, 42.2479) and

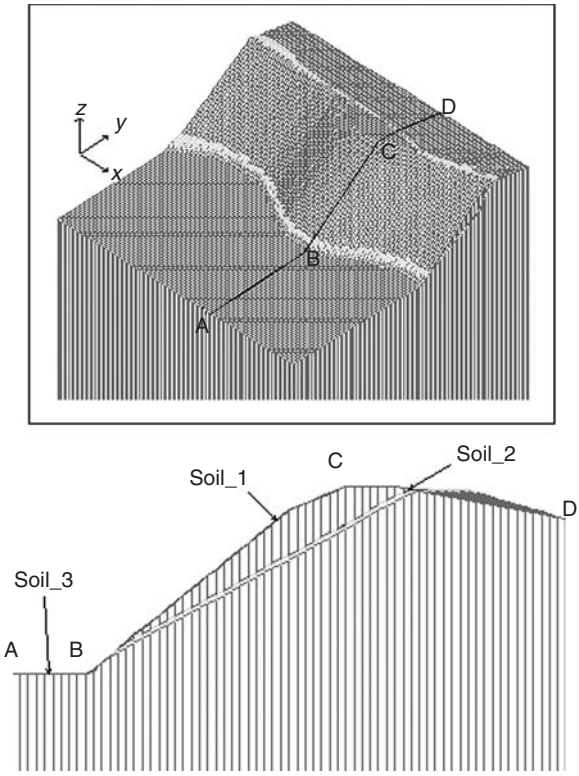

Figure 5.28 Slope geometry of Example 3.

20.4227, respectively, and is shown in Figure 5.29a and b. For the critical spherical surface, the middle part of the failure surface lies within Soil 3, whereas the outer part lies within Soil 2.

For the NURBS sliding surface search, 15 nodes are used to form the NURBS surface. The dimension of the control net SS′T′T is 54.8 m × 34.4 m with 361 columns. In the present analysis, Cheng *et al.* (2005) have tried two options for the initial failure surface:

1 Fifteen nodes are used based on the most critical spherical failure surface and this initial solution is far from the critical solution (63,507 trials).
2 Fifteen nodes are chosen within the second layer of soil so that the initial NURBS surface is close to the critical solution (53,424 trials).

Under both cases, the minimum FOS of 0.517 is obtained which is much smaller than the spherical search result of 0.6177. As shown in Figure 5.29e,

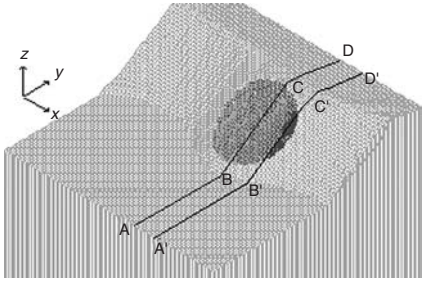

(a) Spherical sliding surface

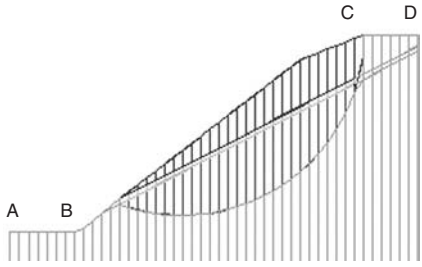

(b) Section along A–D for spherical search

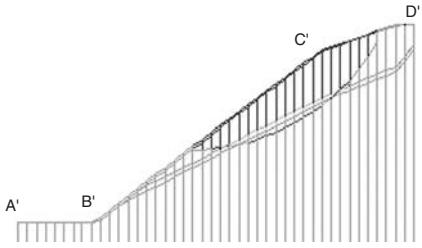

(c) Section along A'–D' for spherical search

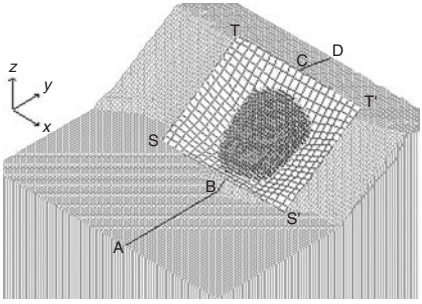

(d) NURBS sliding surface

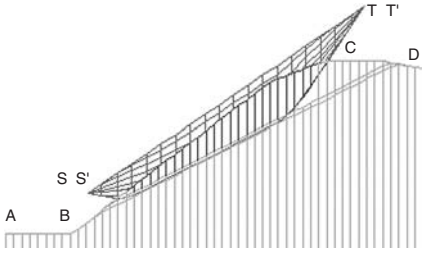

(e) Section along A–D for 15 points

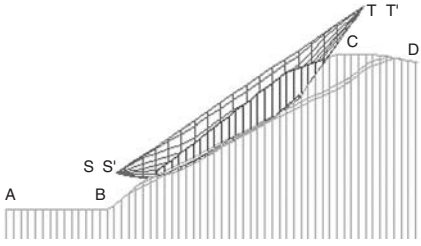

(f) Section along middle for 10 points

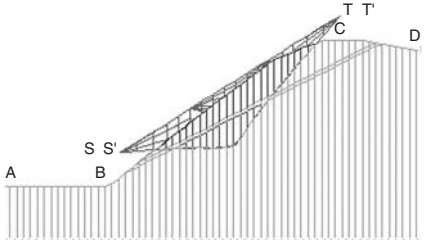

(g) Section along middle for 5 points

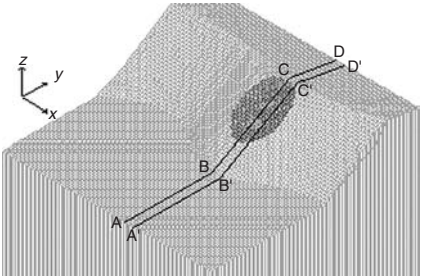

(h) Ellipsoid sliding surface

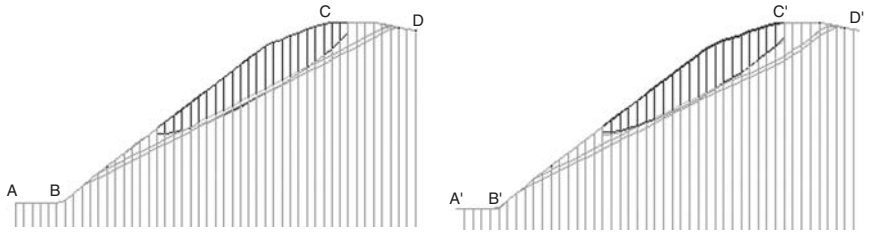

(i) Section along ABCD for ellipsoid search (j) Section along A'B'C'D' for ellipsoidal search

Figure 5.29 Sliding surfaces with the minimum FOS: (a) Spherical sliding surface; (b) Section along A–D for spherical search; (c) Section along A′–D′ for spherical search; (d) NURBS sliding surface; (e) Section along A–D for 15 points; (f) Section along middle for 10 points; (g) Section along middle for 5 points; (h) Ellipsoid sliding surface; (i) Section along ABCD for ellipsoid search; (j) Section along A′B′C′D′ for ellipsoid search.

a major portion of the critical failure surface lies within Soil 2, which is the expected result. The failure mass is the region formed by the NURBS surface from the control net SS′T′T and the ground profile shown in Figure 5.29e. This study has also demonstrated the advantage of using the simulated annealing technique in the global optimization search as the global minimum is practically independent of the initial solution. It is true that, for relatively regular geometry or soil conditions, other global optimization methods may work faster than the simulated annealing method that is also found by Cheng (2003). For a difficult problem where a good initial solution is hard to find, the simulated annealing method has the advantage of being insensitive to the initial solution and escaping from the local minimum during the search in its basic formulation.

The mesh shown in Figure 5.29d is the grid for computation of the NURBS surface while the centre portion within the grid is the actual failure mass. From Figure 5.29e, it is noticed that the shape of the critical asymmetric NURBS failure surface is greatly different from the critical spherical failure surface. The majority of the sliding surface is located in the second layer of soil which is as expected.

For the present problem, the FOS and the number of trials to achieve the critical solution are 0.9345 and 8425, respectively, for 5 NURBS points, and 0.5611 and 63,611, respectively, for 10 NURBS points. As shown in Figure 5.29f, the critical failure surface by 10 points is basically acceptable except that the extent of the failure surface within Soil 2 is not sufficient, which is the limitation of using the insufficient NURBS point to form the critical failure surface. For the critical failure surface shown in Figure 5.29g, the number of NURBS points is too small so that only the outer edge of the critical failure surface lies within Soil 2. It is also found that the critical solution is

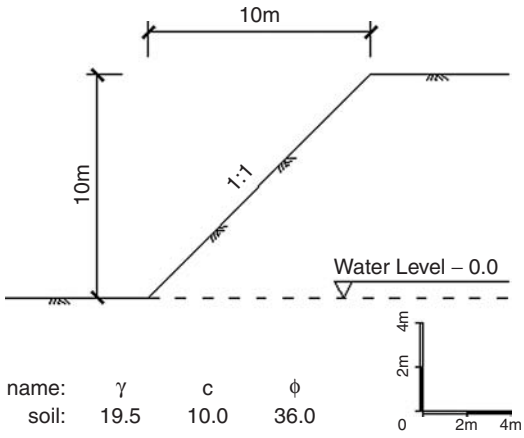

Figure 5.30 A simple slope with curvature.

practically not sensitive to the number of NURBS points if the number exceeds 15 and this is similar to the situation for the second case.

For the critical ellipsoidal failure surface, the results are shown in Figure 5.29h–j. The minimum FOS is 0.521 and the number of trials is 10,605. *Xc*, *yc* and *zc* in eq. (5.35) for the critical ellipsoidal failure surface are (57.72, 63.96, 36.21), whereas *a*, *b*, *c* are 2.41 m, 15.1 m and 5.27 m, respectively. This critical ellipsoidal failure surface is greatly different from the critical spherical failure surface and this is obvious. The FOS from the ellipsoidal search is very close to that by the NURBS search but the number of trials in the optimization analysis can be greatly reduced. It appears that, for a normal problem, an ellipsoidal search will be sufficiently good for the design purpose. It should be noted that there are noticeable differences in the critical NURBS surface and the ellipsoidal surface even though the factors of safety from these surfaces are close to each other.

5.6 Effect of curvature on the FOS

Many highway slopes have curvatures that can affect the stability of slopes but this problem is seldom considered in the past. Xing (1988) has considered the case of a concave slope and has demonstrated that curvature can play an important part in the stability of the slope. In the present study, the effect of curvature is investigated in more detail. Consider a simple slope with a typical section in Figure 5.30.

The typical section of the slope is shown in Figure 5.30, whereas the 3D view of the slope is shown in Figure 5.31 for clarity. For the present problem, the curvature at the bottom of the slope and the corresponding factors

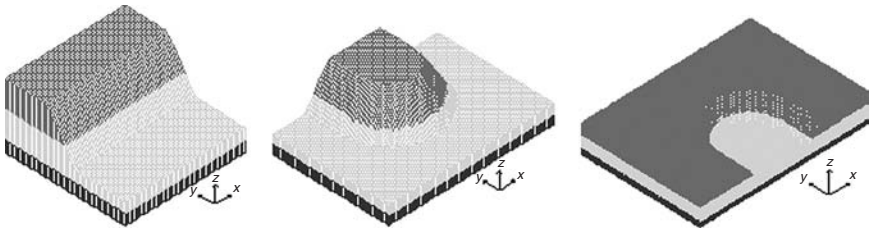

Figure 5.31 Layout of concave and convex slopes.

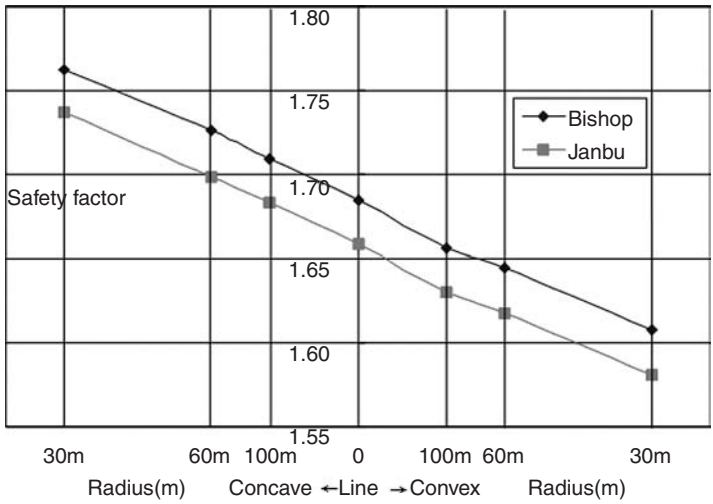

Figure 5.32 Effect of curvature on stability of the simple slope in Figure 5.30.

of safety for Bishop and Janbu analyses using spherical failure surfaces are shown in Figure 5.32. Conceptually, a concave slope should possess the greatest FOS, whereas a convex slope should possess the smallest FOS, and such results are given in Figure 5.32. It is found that curvature has played a major part in the FOS determination. These results are reasonable as a concave slope will provide more confinement from the two ends of a failure mass, whereas a convex slope has no confinement from the two ends. Xing (1988) has obtained the results for a concave slope with similar behaviour that is further extended for a convex slope. Interestingly, the relation of FOS and the radius of curvature of a slope appear to be approximately linear for the present problem.

6 Site implementation of some new stabilization measures

6.1 Introduction

When the British first occupied Hong Kong in the 1840s, they immediately put into place a network of military roads on Hong Kong Island. A road required the formation of a corridor by cut and fill. Both the resulting cut and fill slopes were designed using a rule-of-thumb, namely 10 on 6 for a cut soil slope and 1 on 1.5 for a fill slope (HK Government, 1972). The fill slope of the course was formed by end-tipping and not compacted. This practice would allow the roads to be built quickly and it was accepted that some of the slopes might fail from time to time. Corridors and platforms for other developments were also created in a similar fashion. As Hong Kong developed and grew, such slopes would become too hazardous for civilian use. One of the first engineered cut slopes in Hong Kong was the aviation chequerboard at Kai Tak airport and was analysed using the Bishop method of slices in the 1960s.

Two disastrous landslides that took place on 18 June 1972 following 653 mm of rainfall from 16–18 June were to fundamentally change the control of design and implementation of engineered slopes in Hong Kong. The first landslide was in Sau Mau Ping in eastern Kowloon, killing 71 people, and the second one occurred at Kotewall Road in Mid-levels, Hong Kong Island, killing 67 people. On the afternoon of 18 June 1972, an earth embankment failed, leaving tonnes of landslide debris in the resettlement area in Sau Mau Ping. By nightfall, on Hong Kong Island, landslide debris originating from Po Shan Road completely destroyed the 12-storey Kotewall Court and a 6-storey house, partially damaging an unoccupied block in its way. The Hong Kong Government then decided to start controlling all man-made cut slopes. This was not the case, however, for loose fill slopes where the relatively gentle slope angle gave the false impression that the slope was safe – loose fill is meta-stable and when shear may collapse and thus compact. If the soil is fully saturated, the slope may generate sufficient pore water pressure to liquefy. On 25 August 1976, a loose fill slope 40 m away from the previous landslide failed. The rainstorm associated with tropical storm ‘Ellen’ triggered many landslides across the territory, but the worst failure was in Sau Mau Ping. At

around 9 a.m. on 25 August 1976, the fill slope behind Block 9 of the Sau Mau Ping Estate in Kwun Tong collapsed, killing 18 people and injuring 24. A comprehensive report on these landslides can be found in the Civil Engineering Development Department publication (CEDD, 2005). After major landslides at Po Shan Road in 1972 for cut slopes and Sau Mau Ping in 1976 for fill slopes in Hong Kong, an extensive programme of rehabilitating and upgrading the man-made slopes to meet modern safety standards was put in place.

It is of note that, because soil nailing first became popular in the late 1980s, there have been no significant failures of permanently nailed cut slopes. Apart from a few exceptional cases, for example Ching Cheung Road, most cut slopes were upgraded by soil nailing. It can be concluded that soil nailing is a cost-effective and robust means to stabilize an over-steepened cut slope and, in so doing, also maintain the stability of the more deep-seated overall failure mode of a slope.

There are, however, a number of aspects for which a critical review of existing practice is in order. First is the uncontrolled grouting pressure of the soil nails and, second, the soil nail head design. The first problem arises from the configuration and arrangement of the soil nail, that is, a nail and grout tube within a hole. In the soil nailing design, it had been assumed that the bond strength between the grout and the ground is a function of the overburden pressure only (Watkins and Powell, 1992). However, recent researches have suggested that it is actually dependent on the grout pressure and not the overburden pressure (Yeung *et al.*, 2007). If we step back from the problem for a while and ask ourselves what the best method to pressure grout the ground is, the tube-a-manchette would immediately come to mind. And the response would be 'Why not?'. A tube-a-manchette would allow pressure grouting to be carried out at a particular location at a particular time. This flexibility would be most welcomed by practitioners. If we go back to the nail proper, there is no reason why the nail cannot be in the form of a pipe or for that matter constructed in either steel or another material such as fibre-reinforced plastic (FRP). If the nail is the form of a pipe, it can double up as a tube-a-manchette pipe and so grouting can be to a designed grouting pressure. Currently, the authors are considering the use of an FRP pipe as a possible new soil nail material. The FRP pipe is manufactured from a pultrusion process shown in Figures 6.3 to 6.6. As an example, an FRP nail can be grouted up to eight bars (Yeung *et al.*, 2005, 2007).

The other aspect that may be further improved is the nail head design. At the moment, it can either be through a bearing capacity-type calculation or prescriptive based on past experience (Pun and Shiu, 2007). Recent soil-nailed slope failure has suggested that the weak points of a nailed slope would be in the vicinity of the nail heads (Figure 6.1). This begs the second question: 'Why is local failure between soil nail heads not normally considered in a design at present?' With the advent of the high-tensile alloyed steel wire (3 mm

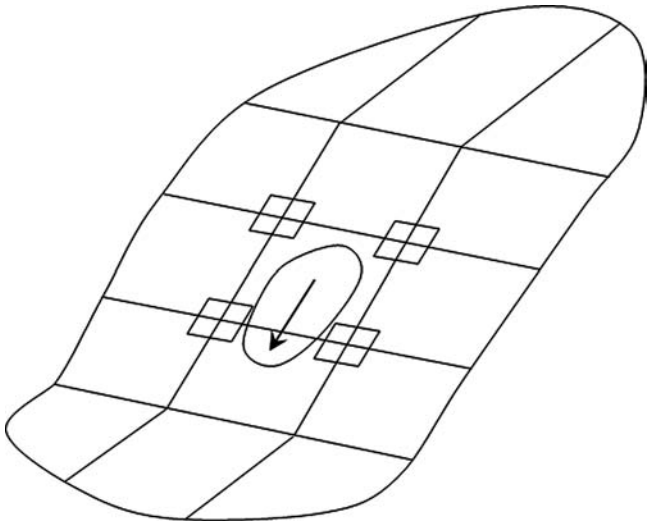

Figure 6.1 Failure of soil mass in between soil nail heads.

diameter, with a tensile strength of 1770 N/mm^2) and net weaving technology, there is no reason why local slip involving the soil body between soil nail heads should not be properly designed against failure. One of the solutions is to do away with the soil nail heads and replace them with a high-tensile alloyed steel wire mesh (Ruegger and Flum, 2001). One example is the TECCO system developed by Geobrugg. The system consists of a TECCO wire mesh, TECCO spike plates (facilitating force transmission from mesh to nails), TECCO compression claws (connecting mesh sheets and for fixing along the outer edges) and soil nails (grouted anchor bars) (Figure 6.2). What we are proposing here is that the practitioner should deal with local failure, shallow failure and global failure simultaneously.

6.2 The FRP nail

Corrosion protection is of paramount importance to the durability of steel soil nails installed in slopes. The provision of a 2 mm sacrificial steel thickness is the most widely used method of corrosion protection of soil nails in Hong Kong. Corrosion protection of a steel bar by hot-dip galvanizing or epoxy coating is also commonly adopted in Hong Kong in some corrosive conditions (Shiu and Cheung, 2003). Anyhow, there is a reduction of 4 mm in diameter for the tensile capacity of the soil nail. When the required stabilizing force is large, soil nails of 40 mm diameter steel reinforcement are often installed at very close spacing (1–1.5 m in Hong Kong). Such steel bars are

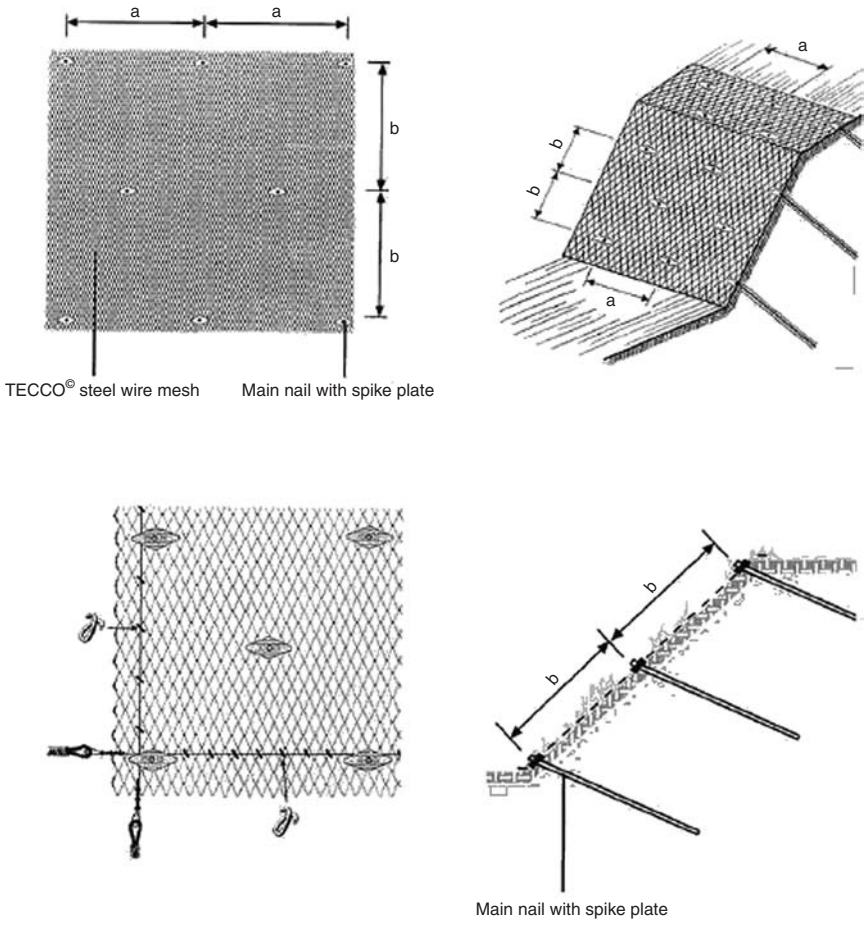

Figure 6.2 The TECCO system developed by Geobrugg.
Source: Reproduced by kind permission of Geobrugg AG.

heavy and thus difficult to manoeuvre on site. As a result, the zinc coating can be easily damaged. The length of each 40 mm diameter steel bar that can be handled on site is limited by its weight and individual site conditions and the typical length of each segment is approximately 3–5 m (due to lack of adequate working space in Hong Kong). Couplers are often used to connect bars to the required total length. When soil nails are required in aggressive ground, a double corrosion system similar to that for pre-stressed ground anchors is required, resulting in a significant increase in construction costs and time. The total cost of soil nail construction in Hong Kong, including the steel nails, couplers, handling and transportation costs, drilling and the corrosion protection system, is hence much higher than those in many other countries.

Usually, no pressure is applied during the grouting of conventional soil nails (gravity flow of grout) as the application of pressure with current soil nail systems is difficult to carry out. There are many reported cases in Hong Kong where the shrinkage of grout has resulted in a significant reduction in bond stress between cement grout and soil and remedial work has been required. Many engineers also have reservations on the bond stress transfer of soil nails within a loose fill slope. In particular, it is found that, even when good compaction has been carried out to loose fill, the compacted dry density of the fill will decrease with time, possibly due to the washout of fines by groundwater. In view of this concern, expensive and visually displeasing concrete grillage is commonly used in Hong Kong for loose fill slopes.

In view of the various problems associated with the use of reinforcement bars as soil nails, there is various research being carried out in Hong Kong, China and many other countries. The features that are required for the soil nails in Hong Kong include the following:

1 light weight and high strength;
2 the application of pressure to control the grouting zone, quality of grouting and bond strength;
3 resistance to corrosion;
4 acceptable cost;
5 ease of construction – handling, joining, cutting.

Recently, there have been rapid developments in the use of FRP for various structural purposes (Dolan, 1993; Dowling, 1999). The authors have carried out research works on the use of glass fibre reinforced polymer (GFRP) and carbon fibre reinforced polymer (CFRP) bars as soil nails for the project at the Sanatorium Hospital in Hong Kong, as bar-type FRP can be found easily on the market. From pilot studies carried out by the authors, the limitations of the GFRP bar are the following: (1) the pressure grouting system is complicated; (2) the joining of the bar is not easy; (3) low shear strength. The limitations of the CFRP bar are the following: (1) the pressure grouting is complicated; (2) the joining of the bar is not easy; (3) the cost is high. An innovative system of GFRP pipes has been devised by the Dae Won Soil Company Limited of Korea and is used for the present study. The system can fulfil the five criteria for a new soil nail system listed above and may be suitable for use in Hong Kong and other countries to improve the economy and constructability of soil nails.

GFRP is a material of light weight, high corrosion resistance and high strength. For the present system, a GFRP pipe of 37 mm internal diameter and 5 mm thick is used. It is fabricated by a pultrusion process, during which glass fibres are drawn through a die and bundled together through a resin matrix (Figure 6.3). The fibres are coated with sheeting and are pulled through a shaping die (Figure 6.4) to form the pipe. Pultrusion is a continuous moulding process using fibre reinforcement in polyester or other thermosetting resin matrices. Pre-selected reinforcements such as fibreglass, mat

Figure 6.3 Glass fibre drawn through a die and coated with epoxy.

Figure 6.4 Fibre drawn and coated with sheeting to form a pipe bonded with epoxy.

or cloth are drawn through a resin bath in which all materials are thoroughly impregnated with a liquid thermosetting resin. The wetted fibre is formed to the desired geometric shape and pulled through a heated steel die. The resin is cured inside the die by controlling the precise temperature of curing. The

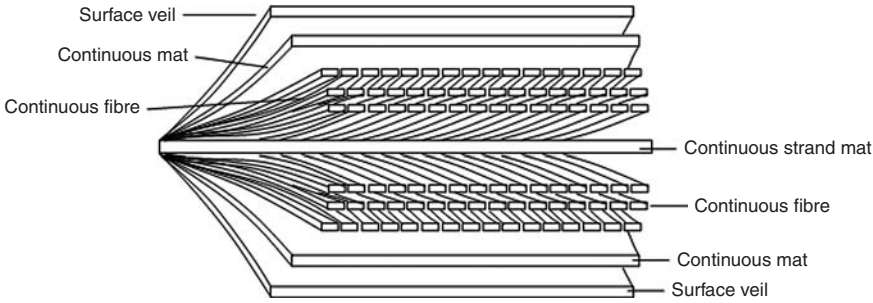

Figure 6.5 Lamination of FRP as produced from the pultrusion process.

laminates solidify to the shape of the die, and it is continuously but slowly pulled by the pultrusion machine. Typical FRP lamination formed by the pultrusion process is shown in Figure 6.5. This process of manufacturing has the advantage of forming various shapes suitable for different engineering uses. The mechanical properties and strengths of the laminates can be controlled easily through the use of different types of resin. For example, suitable filler, catalysts, ultra-violet inhibitors and pigments can be used to form the resin matrix, binding the fibres together and providing structural corrosion resistance as well as strength.

Field tests on the effect of the tube-a-manchette grouting technique have demonstrated a major beneficial improvement in the soil properties. The effective cohesive strength of soil can be greatly increased which is highly beneficial to the stability of a slope. Furthermore, the deformation and elastic modulus of soil are also greatly improved by the soil improvement process while the FRP pipe can act as the grouting tube as well as the reinforcement to the grouted soil mass. Because the quality of grouting is good due to the use of pressure grouting, this new material and grouting technique will be useful in loose fill where the bond stress is always a problem. The use of expensive and visually displeasing concrete grillage in loose fill slopes can also be avoided by the use of tube-a-manchette grouting and additional cost saving is possible.

The installation of the system in Hong Kong indicates there are no insurmountable installation difficulties encountered on site. The nail can be installed and grouted easily, and high strengths have been obtained from the pull out tests. The maximum test loads for the four pull out tests are all about 21.1 tonnes. Although the allowable tensile strength of an FRP pipe was set as 11.5 tonnes in design, it can be seen that the design value for the FRP pipe is quite safe and conservative.

Because there are doubts as to the transfer of bond stress from the soil nail in poor soil, a grillage system is also commonly adopted in conjunction with the use of soil nails for loose fill slopes or slopes with very poor quality soil

in Hong Kong, Taiwan and Japan. There are various possible methods to stabilize slopes in different kinds of soil, and only those systems commonly adopted in Hong Kong are covered in this book.

6.3 Drainage

Inadequate surface drainage design and detailing are quite common. This is mainly due to the local concentration of flow. It is commonly observed that while most of the storm drainage provisions for slopes in Hong Kong are adequate, some are under-designed by a wide margin. For example, drainage lines are something we have to take note of and ensure that, if present, they are properly accounted for in the drainage system design. Such concentrated flow may also have an impact on the slope groundwater table level if not diverted from the recharge zones where open discontinuities are present. Horizontal drains and sub-soil drains are useful in drawing down the groundwater table and relieving artesian water pressure.

In Hong Kong, a slope normally tends to have a lower hydraulic conductivity as it gets deeper. When there are zones with a large difference in hydraulic conductivity such as colluvium on top of Grade V granite, perched water may develop. A rise in transient perched and regional groundwater levels should be taken into account in the design. Persistent clay layers and kaolin-infilled discontinuities may also have an adverse impact on the design groundwater table assumptions. Ideally, an accurate hydrogeological model should be set up. Failing this, sensitivity analysis on the groundwater regime assumptions should be carried out, and, where necessary, more pessimistic assumptions should be used in the design.

6.4 Construction difficulties

Difficulties during the installation of soil nails should also be addressed. Certain geological features may also cause construction difficulties during the installation of the soil nails. For example, volcanic tuff is very hard to drill through, resulting in excessive wear and tear to the drill bits. The presence of core stones may catch the drill bit and stop it from being withdrawn easily. These may slow down the drilling process and cause drill hole collapse. The presence of a network of soil pipes may result in an excessive loss of grout during the grouting stage. All such problems can be overcome if identified early on. Examples are the following: (1) to use a drill bit with harder cutting beads; (2) to use the odex (or under-reaming) drilling system where a temporary casing can be introduced to avoid drill hole collapse; and (3) drilling and grouting can be carried out in two stages. After first-stage drilling, a quick-set cement grout should be injected followed by second-stage drilling before the second and final stage grouting. Such steps should be able to avoid excessive grout loss in most cases.

Appendix

General introduction to SLOPE 2000

The 2D and 3D formulations as well as the optimization search outlined in this book have been coded into two general purpose programs: SLOPE 2000 and SLOPE3D. SLOPE3D is under development and a relatively nice 3D interface has been completed recently. It can be obtained from Cheng for testing and evaluation. SLOPE 2000 is a mature 2D program with the support of some simple 3D cases. Most of the examples in this book were carried out using versions 2.1 and 2.2 of this program. This program has been used for many projects in different countries, and the latest English and Chinese versions can be downloaded from Cheng's web site at http://www.cse.polyu.edu.hk/~ceymcheng/download.htm. This program (version 1.8) is also incorporated into the Geo-Suite delivered by Vianova Finland System Oy. SLOPE 2000 has many important and useful features which include:

1 The location of a critical failure surface with evaluation of the global minimum factor of safety for both circular as well as non-circular failure surfaces under general conditions. Very difficult problems with multiple soft band problems have also been tested with satisfaction. The verification examples in the user guide have demonstrated the power of the modern optimization methods in SLOPE 2000 as compared with other slope stability programs.
2 The generation of graphics files in the form of Autocad DXF, bitmap BMP, postscript, HP plotter format or vector format (CGM and Lotus PIC) for incorporation into other programs. For the Windows version, clipboard and Windows print manager are also supported.
3 Bishop simplified, Fellenius, Swedish, Janbu simplified and Janbu rigorous, China load factor (including the simplified version required by some China codes), Sarma, Morgenstern–Price, Corps of Engineers, Lowe–Karafiath and GLE methods and extremum principles are implemented under the 2D analysis (12 methods). For 3D analysis, the load factor, extremum and GLE methods are not implemented while all the other corresponding 2D analyses are extended to 3D analyses. A true 3D slope stability analysis for spherical and non-spherical failure surfaces is covered by a separate program, SLOPE3D, by Cheng.

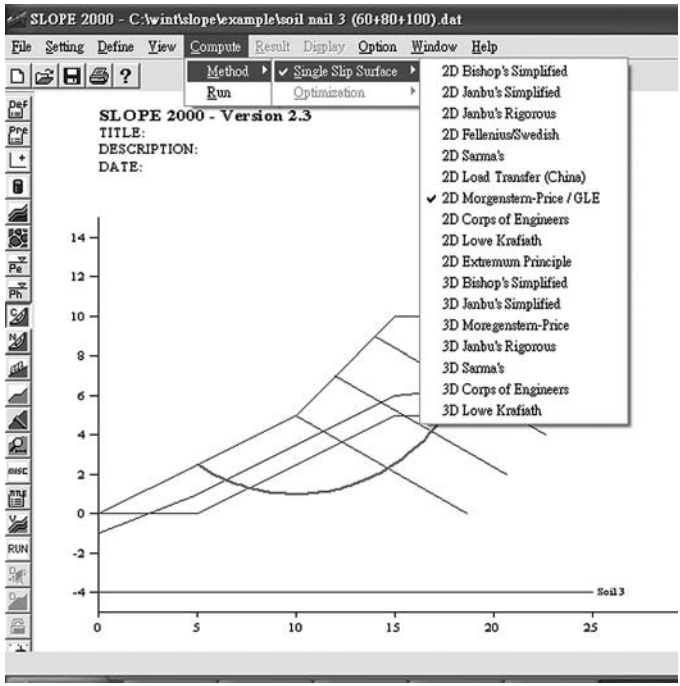

Figure A1 Various types of stability methods available for analysis in SLOPE 2000.

4 f_0 for the Janbu simplified method is incorporated into the program (optional) so that the user need not determine it from the design graph by Janbu.
5 The China load factor method is available.
6 The Janbu rigorous method and Sarma method (2D and 3D) are available which are not present in many commercial programs.
7 Windows and Linux versions are available. For the older version of SLOPE 2000, DOS and other platforms are available as well.
8 Water tables, pore pressure coefficients, perch water tables and excess pore pressure contours can all be defined.
9 Earthquake loading in the form of horizontal/vertical acceleration can be accepted by this program.
10 It is able to accept vertical surcharge and horizontal loads with the presence of a rock boundary. Loading can be applied on or below ground level.
11 Many options are available for soil nail modelling which is shown in Figure A2. Nail loads can be controlled by the tensile strength of the nail, the bond length proportional to the effective zone or the bond stress from vertical overburden stress (unique). The bond stress from overburden

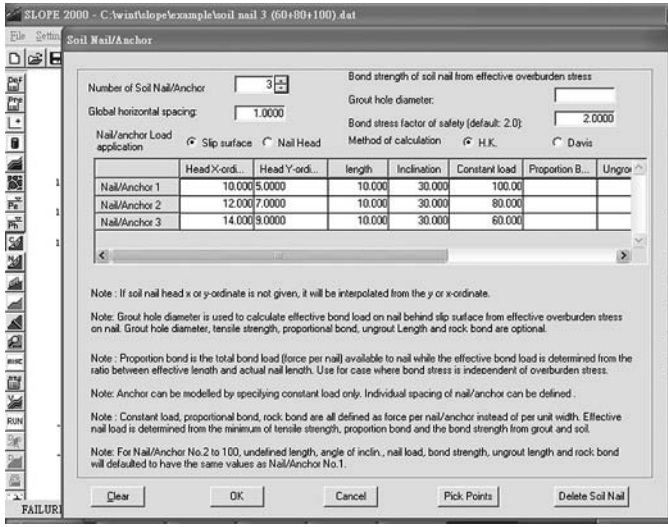

Figure A2 Extensive options for modelling soil nails.

stress can be determined from Hong Kong practice or the US Davis method. Furthermore, the nail horizontal spacing can be controlled for individual rows which is also unique among other similar programs. The nail load can be applied to the failure surface by default or to the nail head if necessary. If part of the nail is not grouted or the end of the nail is socketed into rock, these options can also be modelled by SLOPE 2000.

12 Cheng (2003) has formulated the slope stability problem in a matrix approach and the factor of safety can be determined directly from a complex double QR matrix method. The special advantage of this double QR method is that the factor of safety and internal forces for 'rigorous' methods can be determined directly from the matrix equation and no initial factor of safety is required. Cheng has proved that there are N factors of safety for a problem with N slices. In this new approach, all the N factors of safety are determined directly from the tedious matrix equation without using any iteration, and the factors of safety can be classified into three groups: imaginary numbers, negative numbers and positive numbers.

If all the factors of safety are either imaginary or negative, the problem under consideration has no physically acceptable answer by nature. Otherwise, the positive number (usually 1–2 positive numbers left) will be examined for the physical acceptability of the corresponding internal forces and the final answer will be then obtained. Under this new formulation, the fundamental nature of the problem is fully determined.

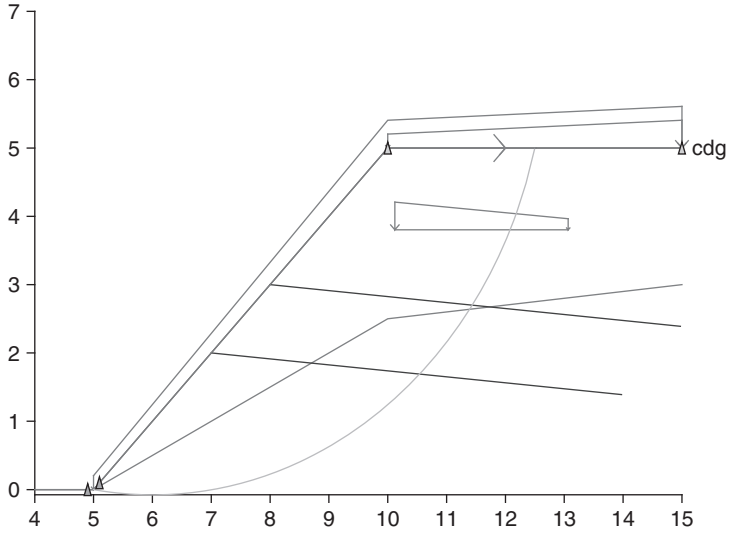

Figure A3 A simple slope with 2 soil nails, 3 surface loads, 1 underground trapezoidal vertical load and a water table.

If a physically acceptable answer exists for a specific problem, it will be determined by this double QR method. If no physically acceptable answer exists for the double QR method (all are imaginary or negative numbers), the problem under consideration has no answer by nature and the problem can be classified as 'failure to converge' under the assumption of the specific method of analysis. The authors have found that many problems which fail to converge with the classical iteration method actually possess meaningful answers by the double QR method. That means that the phenomenon of 'failure to converge' which comes out from the use of the iteration method of analysis may be a false phenomenon in some cases. The authors have also found that many failure surfaces which fail to converge are normal in shape and should not be neglected in ordinary analysis and design.

13 China's earthquake code for dam design is available. The coefficient varies with height according to the formula $a_h \xi a_i$ which is different between different slices.

14 Ponded water (water table above ground) can be modelled automatically.

15 The interslice force function $f(x)$ can be determined from the lower bound/extremum principle. This is unique among all existing slope stability programs.

16 Soil parameters can vary with depth from ground surface or from contour lines.

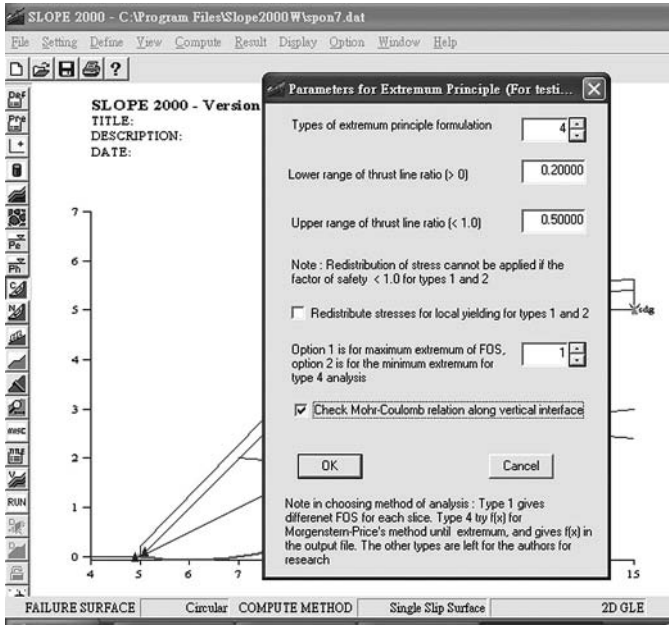

Figure A4 Parameters for extremum principle.

Illustration

For the slope as shown in Figure A3, the bond load on the soil nail is defined by the overburden stress acting on the soil nail according to Hong Kong practice. To perform the analysis, choose extremum principle from the method of analysis and select the parameters as shown in Figure A4. Choose type 4 extremum formulation and select option 1 for type 4 formulation (maximum extremum). Click the checkbox for checking the Mohr–Coulomb relation along the interfaces and then perform the analysis.

The factor of safety from the lower bound theorem/extremum principle is 1.558 while $\lambda = 0.134$. The complete output with the interslice force function $f(x)$ for this case from SLOPE 2000 is shown below:

```
SLOPE 2000 ver. 2.3 by Dr. Y.M. Cheng
Dept. of Civil and Structural Engineering
Hong Kong Polytechnic University
**********************************
*          SINGLE SLIP SURFACE          *
**********************************

=====================
=     Basic Data     =
=====================
```

Density of water : 9.81 (kNm^{-3})
Tolerance in analysis : 0.00050
Slip surface is : circular
No. of slice is : 10

****

FOS for Bishop method = 1.5298
FOS for Janbu simplified method = 1.4514
FOS for Swedish method = 1.3020
FOS for Load factor method = 1.6211
FOS for Sarma method = 1.6471
FOS for Morgenstern–Price method = 1.4982

* Factor of safety and internal forces for chosen method of analysis *
****

Method of analysis = 2D extremum principle
Factor of safety = 1.5576
Max. extremum factor of safety
Lambda = .134E+01

Material type = 0

** Soil Properties **

Soil name	*Density (kNm^{-3})*	*Cohesion (kNm^{-2})*	*Phi (°)*	*Saturated density*	*Delta C*	*Delta Phi*
CDG	18.00	5.00	36.00	20.00	0.00	0.00

==========
= Soil Profile Co-ordinates =
==========

X/Y Coor (m)	*4.00*	*5.00*	*10.00*	*15.00*
CDG	0.00	0.00	5.00	5.00
Water (m)	0.00	0.00	2.50	3.00

==========
== Slip Surface Co-ordinates ==
==========

No.	*X (m)*	*Y (m)*	*Line of thrust (m)*
1	5.000	0.000	0.000
2	5.625	–0.066	–0.066

(Continued overleaf)

3	6.250	–0.073	0.945
4	6.875	–0.021	1.352
5	7.500	0.091	1.580
6	8.125	0.266	1.808
7	8.750	0.510	2.043
8	9.375	0.831	2.290
9	10.000	1.243	2.571
10	11.250	2.455	3.459
11	12.500	5.000	5.000

Centre of circle (X,Y) = (6.011, 6.608)
Radius of circle = 6.685

==========
= Surface Load =
==========

No.	*StartX (m)*	*EndX (m)*	*VPress (kN/m²)*	*VPress2 (kN/m²)*	*HPress (kN/m²)*	*HPress2 (kN/m²)*	*Depth1 (m)*	*Depth2 (m)*
1	5.000	15.000	5.000	15.000	0.000	0.000		
2	10.000	15.000	5.000	10.000	0.000	0.000		
3	12.000	12.000	0.000	0.000	10.000	20.000		
4	10.120	13.068	10.000	4.000	0.000	0.000	3.802	3.802

==========
= Soil Nail Information =
==========

Diameter of grout hole = 0.07500
Soil/Grout Bond stress factor of safety = 2.000
Bond load determined from Hong Kong Practice by the overburden stresses

No. of rows of Soil Nails : 2
Soil nail horizontal spacing : 1.000
All the loads are defined per nail

No.	*Nail head coordinates*		*Nail angle (degree)*	*Bond strength (kN)*	*Length (m)*	*Tensile strength (kN)*	*Actual load (kN)*
	X (m)	*Y (m)*					
1	7.000	2.000	5.00		7.00		12.24
2	8.000	3.000	5.00		7.00		10.40

No.	*Nail/slip coordinates*		*Ungrout length*	*Bond length*	*Nail spacing*
	X (m)	*Y (m)*	*(m)*	*(m)*	*(m)*
1	10.467	1.697	0.00	3.519	1.000
2	11.373	2.705	0.00	3.615	1.000

Nail load applied at the ground surface

==========

Slice details

==========

No.	*Weight (kN)*	*Surchage load (kN)*	*Horiz load (kN)*	*Base angle (deg)*	*Base length (m)*	*Base pore p. (kPa)*	*Base frict. tan(phi)*	*Base cohe (kPa)*
1	4.12	3.32	0.00	–6.01	0.628	1.86	0.727	5.000
2	12.00	3.71	0.00	–0.63	0.625	5.28	0.727	5.000
3	19.14	4.10	0.00	4.73	0.627	8.12	0.727	5.000
4	25.54	4.49	0.00	10.15	0.635	10.39	0.727	5.000
5	31.17	4.88	0.00	15.65	0.649	12.04	0.727	5.000
6	35.97	5.27	0.00	21.31	0.671	13.06	0.727	5.000
7	39.86	5.66	0.00	27.20	0.703	13.35	0.727	5.000
8	42.70	6.05	0.00	33.42	0.749	12.82	0.727	5.000
9	72.67	30.32	0.00	44.11	1.741	7.00	0.727	5.000
10	28.64	28.09	0.00	63.84	2.835	0.06	0.727	5.000

No.	*Base normal (kN)*	*Base shear (kN)*
1	52.455	25.941
2	11.536	5.849
3	7.892	3.318
4	17.313	7.038
5	67.494	29.920
6	–2.152	–2.936
7	70.049	30.555
8	21.101	7.770
9	101.881	47.430
10	46.455	30.693

Nail	*Nail loads at slice*	
slice	*Hori. (kN)*	*Vert. (kN)*
1	0.00	0.00
2	0.00	0.00

(*Continued overleaf*)

(Continued)

3	0.00	0.00
4	12.19	1.07
5	10.36	0.91
6	0.00	0.00
7	0.00	0.00
8	0.00	0.00
9	0.00	0.00
10	0.00	0.00

Interface No.	*Interface length l(i,i+1) (m)*	*Interface friction tan(phi)*	*Interface cohesion c(i,i+1) (kPa)*	*Interface normal force E(i,i+1) (kN)*	*Interface shear force X(i,i+1) (kN)*	*f(x)*
1	0.69	0.73	5.00	31.29	–42.01	1.000
2	1.32	0.73	5.00	37.26	–37.77	0.755
3	1.90	0.73	5.00	39.92	–22.67	0.423
4	2.41	0.73	5.00	55.99	–9.85	0.131
5	2.86	0.73	5.00	76.96	–45.96	0.445
6	3.24	0.73	5.00	75.01	–1.64	0.016
7	3.54	0.73	5.00	70.17	–32.39	0.344
8	3.76	0.73	5.00	65.03	–5.52	0.063
9	2.54	0.73	5.00	28.16	–8.70	0.230

Total weight of the soil mass = 311.81

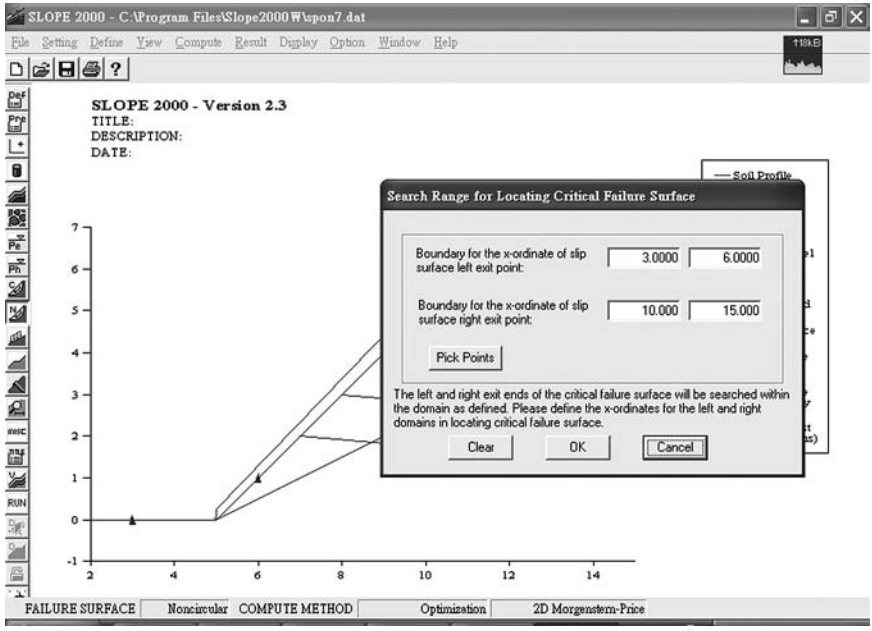

Figure A5 Defining the search range for optimization analysis.

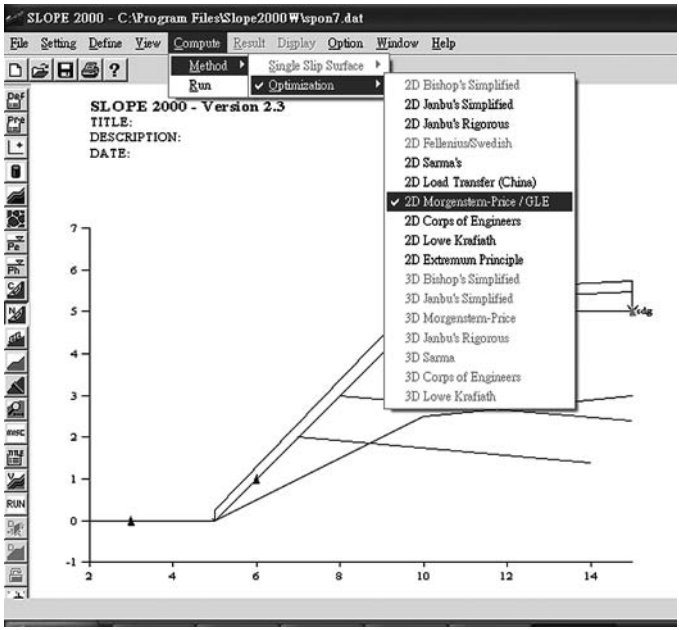

Figure A6 Choose the stability method for optimization analysis.

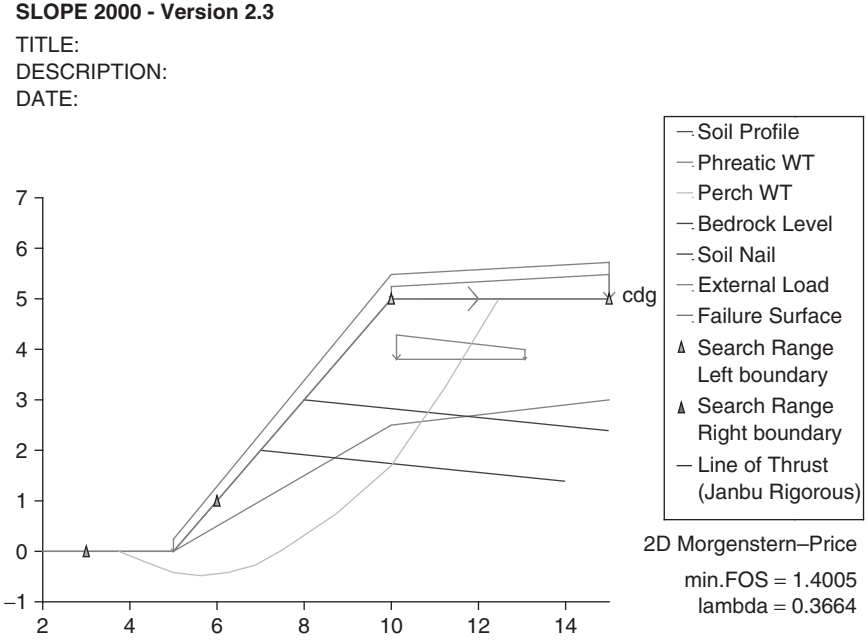

Figure A7 The critical failure surface with the minimum factor of safety corresponding to Figure A6.

To search for the critical failure surface corresponding to the problem in Figure A3, define the left and right search range as (4.0,6.0) and (10.0,15.0) as shown in Figure A5. That means that the left exit end will be controlled within (4.0,6.0) and the right exit end will be controlled within (10.0,15.0). Choose the shape of the failure surface from the Failure Surface option under the Define menu (default to non-circular in SLOPE 2000), then proceed to the selection of the method of analysis as shown in Figure A6. The minimum factor of safety of 1.4 for the Spencer method is obtained as shown in Figure A7, and the default tolerance in locating the critical failure surface is 0.0001, which can be adjusted in the default if necessary. SLOPE 2000 is the only program at present for which a tolerance in the optimization search can be defined.

SLOPE 2000 is robust and has been used in many countries (Hong Kong, Taiwan, China, Italy, United States, Finland, Syria, Argentina). This program has been used in China for many major national projects and a simplified Chinese version is available. The interface is completely the same as the English one except the words are all simplified in to Chinese language.

References

Abramson L.W., Lee T.S., Sharma S. and Boyce G.M. (2002), *Slope Stability and Stabilization Methods*, 2nd edition, John Wiley.

ACADS (1989), *Soil Slope Stability Programs Reviews*, Publication No. U255, ACADS, Melbourne.

AGS-HK (2004), Ground Investigation Guidelines 04.5 – Landslides, *Association of Geotechnical and Geoenvironmental Specialists* (Hong Kong).

Anderheggen E. and Knopfel H. (1972), Finite element limit analysis using linear programming, *International Journal of Solids and Structures*, 8(12), 1413–1431.

Arai K. and Tagyo K. (1985), Determination of noncircular slip surfaces giving the minimum factor of safety in slope stability analysis, *Soils and Foundations*, 25, 43–51.

Assadi A. and Sloan S.W. (1990), Undrained stability of shallow square tunnel, *Journal of the Geotechnical Engineering Division*, *ASCE*, 117(8), 1152–1173.

Ausilio E., Conte E. and Dente G. (2001), Stability analysis of slopes reinforced with piles, *Computers and Geotechnics*, 28(8), 591–611.

Azzouz A.S. and Baligh M.M. (1983), Loaded areas on cohesive slopes, *Journal of Geotechnical Engineering*, *ASCE*, 709–729.

Baker R. (1980), Determination of the critical slip surface in slope stability computations, *International Journal of Numerical and Analytical Methods in Geomechanics*, 4, 333–359.

Baker R. and Garber M. (1977), *Variational Approach to Slope Stability*, Proceedings of the 9th International Conference on Soil Mechanics and Foundations Engineering, Tokyo, Vol. 2, pp. 9–12.

Baker R. and Garber M. (1978), Theoretical analysis of the stability of slopes, *Geotechnique*, 28, 395–411.

Baker R. and Frydman S. (1983), Upper bound limit analysis of soil with nonlinear failure criterion, *Soils and Foundations*, 23, 35–42.

Baker R. and Leshchinsky D. (1987), Stability analysis of conical heaps, *Soils and Foundations*, 27(4), 99–110.

Baker R. and Leshchinsky D. (2001), Spatial distribution of safety factors, *Journal of Geotechnical and Geoenvironmental Engineering*, 127(2), 135–145.

Baligh M.M. and Azzouz A.S. (1975), End effects on the stability of cohesive soils, *Journal of the Geotechnical Engineering Division*, *ASCE*, 101(GT11), 1105–1117.

Belegundu A.D. and Chandrupatla T.R. (1999), *Optimization Concepts and Applications in Engineering*, Upper Saddle River, NJ: Prentice Hall.

Bishop A.W. (1954), The use of pore pressure coefficients in practice, *Geotechnique*, 4(4), 148–152.

Bishop A.W. (1955), The use of the slip circle in the stability analysis of earth slopes, *Geotechnique*, 5(1), 7–17.

Bishop A.W. (1972), Shear strength parameters for undisturbed and remoulded soils specimens, in: R.H.G. Parry (ed.), *Stress–Strain Behaviour of Soils*, pp. 3–58, London: Foulis.

Bishop A.W. and Morgenstern N. (1960), Stability coefficients for earth slopes, *Geotechnique*, 10(4), 129–150.

Bjerrum L. (1967), Progressive failure in slopes of overconsolidated plastic clay and clay shades. The 3rd Terzaghi Lecture, *Journal of the Soil Mechanics and Foundations Division*, Proceedings of the American Society of Civil Engineers, Vol. 93, pp. 1–49.

Bolton M.D. and Lau C.K. (1993), Vertical bearing capacity factors for circular and strip footings on a Mohr–Coulomb soil, *Canadian Geotechnical Journal*, 30(6), 1024–1033.

Bolton H.P.J., Heymann G. and Groenwold A. (2003), Global search for critical failure surface in slope stability analysis, *Engineering Optimization*, 35(1), 51–65.

Bottero A., Negre R., Pastor J. and Turgeman S. (1980), Finite element method and limit analysis theory for soil mechanics problems, *Computer Methods in Applied Mechanics and Engineering*, 22, 131–149.

Boutrup E. and Lovell C.W. (1980), Searching techniques in slope stability analysis, *Engineering Geology*, 16(1–2), 51–61.

Brent R.P. (1973), *Algorithms for Minimization Without Derivatives*, Englewood Cliffs, NJ: Prentice-Hall.

Brinkgreve R.B.J. and Bakker H.L. (1991), *Non-Linear Finite Element Analysis of Safety Factors*, Proceedings of the Seventh International Conference on Computer Methods and Advances in Geomechanics, Cairns, Australia, 6–10 May 1991, 1117–1122.

Bromhead E.N. (1992), *The Stability of Slopes*, 2nd edition, London: Blackie Academic & Professional.

Brunsden D. and Piror D.B. (eds.) (1984), *Slope Instability*, Chichester, UK: John Wiley & Sons Ltd.

Cai F., Ugai K., Wakai A. and Li Q. (1998), Effects of horizontal drains on slope stability under rainfall by three-dimensional finite element analysis. *Computers and Geotechnics*, 23(4), 255–275.

Castilo E. and Luceno A. (1980), Evaluation of variational methods in slope analysis. *Proceedings of International Symposium on Landslides*, New-Delhi, India, Vol. 1, pp. 255–258.

Castilo E. and Luceno A. (1982), A critical analysis of some variational methods in slope stability analysis. *International Journal for Numerical and Analytical Methods in Geomechanics*, *6*, 195–209.

Cavounidis S. (1987), On the ratio of factors of safety in slope stability analyses, *Geotechnique*, 37(2), 207–210.

Celestino T.B. and Duncan J.M. (1981), *Simplified Search for Non-Circular Slip Surface*, Proceedings of 10th International Conference on Soil Mechanics and Foundation Engineering, Stockholm, Sweden, pp. 391–394.

Chang M. (2002), A 3D slope stability analysis method assuming parallel lines of intersection and differential straining of block contacts, *Canadian Geotechnical Journal*, 39(4), 799–811.

Chatterjee A. and Siarry P. (2006), Nonlinear inertia weight variation for dynamic adaptation in particle swarm optimization, *Computers and Operations Research*, 33, 859–871.

Chen J. (2004), *Slope Stability Analysis Using Rigid Elements*, PhD thesis, Hong Kong Polytechnic University.

Chen R.H. and Chameau J.L. (1982), Three-dimensional limit equilibrium analysis of slopes, *Geotechnique*, 32(1), 31–40.

Chen W.F. (1975), *Limit Analysis and Soil Plasticity*, USA: Elsevier.

Chen W.F. and Giger M.W. (1971), Limit analysis of stability of slopes. *Journal of the Soil Mechanics and Foundations Division*, Proceedings of the American Society of Civil Engineers, Vol. 97, pp. 19–26.

Chen Z. (1992), Random trials used in determining global minimum factors of safety of slopes, *Canadian Geotechnical Journal*, 29(2), 225–233.

Chen Z. (1998), On Pan's principles of rock and soil stability analysis, *Journal of Tsinghua University (Sci & Tech)*, 38, 1–4 (in Chinese).

Chen, Z.Y. (1999), The limit analysis for slopes: theory, methods and applications, in: Yagi, Yamagami and Jiang (eds.), *Slope Stability Engineering*, pp. 15–29, Balkema: Rotterdam.

Chen Z. and Morgenstern N.R. (1983), Extensions to generalized method of slices for stability analysis, *Canadian Geotechnical Journal*, 20(1), 104–109.

Chen Z. and Shao C. (1988), Evaluation of minimum factor of safety in slope stability analysis, *Canadian Geotechnical Journal*, 25(4), 735–748.

Chen Z.Y., Wang X.G., Haberfield C., Yin J.H. and Wang Y.J. (2001a), A three-dimensional slope stability analysis method using the upper bound theorem. Part I: Theory and methods. *International Journal of Rock Mechanics and Mining Sciences*, 38(3), 369–378.

Chen Z.Y., Wang J., Wang Y.J., Yin J.H. and Haberfield C. (2001b), A three-dimensional slope stability analysis method using the upper bound theorem. Part II: Numerical approaches, applications and extensions. *International Journal of Rock Mechanics and Mining Sciences*, 38(3), 379–397.

Cheng Y.M. (1998), Advancement and improvement in discontinuous deformation analysis, *Computers and Geotechnics*, 22(2), 153–163.

Cheng Y.M. (2003), Locations of critical failure surface and some further studies on slope stability analysis, *Computers and Geotechnics*, 30(3), 255–267.

Cheng Y.M. (2007), Global optimization analysis of slope stability by simulated annealing with dynamic bounds and Dirac function, *Engineering Optimization*, 39(1), 17–32.

Cheng Y.M. and Zhang Y.H. (2000), Rigid body rotation and internal block discretization in DDA analysis, *International Journal for Numerical and Analytical Methods in Geomechanics*, 24, 567–578.

Cheng Y.M. and Zhang Y.H. (2002), Coupling of FEM and DDA methods, *International Journal of Geomechanics*, 2(4), 503–517.

Cheng Y.M. and Zhu L.J. (2005), Unified formulation for two dimensional slope stability analysis and limitations in factor of safety determination, *Soils and Foundations*, 44(6), 121–128.

Cheng Y.M. and Yip C.J. (2007), Three-dimensional asymmetrical slope stability analysis – Extension of Bishop's, Janbu's, and Morgenstern–Price's techniques, *Journal of Geotechnical and Geoenvironmental Engineering*, 133(12), 1544–1555.

Cheng Y.M., Liu H.T., Wei W.B. and Au S.K. (2005), Location of critical three-dimensional non-spherical failure surface by NURBS functions and ellipsoid with applications to highway slopes, *Computers and Geotechnics*, 32(6), 387–399.

Cheng Y.M., Lansivaara T. and Wei W.B. (2007a), Two-dimensional slope stability analysis by limit equilibrium and strength reduction methods, *Computers and Geotechnics*, 34, 137–150.

Cheng Y.M., Li L. and Chi S.C. (2007b), Studies on six heuristic global optimization methods in the location of critical slip surface for soil slopes, *Computers and Geotechnics*, 34(6), 462–484.

Cheng Y.M., Li L. and Lansivaara T. (2007c), Slope stability analysis by dual extremum principle with a mixed optimization algorithm, *Journal of Geotechnical and Geoenvironmental Engineering* (under review).

Cheng Y.M., Zhao Z.H. and Li L. (2007d), Determination of the bounds to the factor of safety and the evaluation of $f(x)$ in slope stability analysis by lower bound method, *International Journal for Numerical and Analytical Methods in Geomechanics* (under review).

Cheng Y.M., Li L., Chi S.C. and Wei W.B. (2007e), Particle swarm optimization algorithm for location of a critical non-circular failure surface in two-dimensional slope stability analysis, *Computers and Geotechnics*, 34(2), 92–103.

Cheng Y.M., Li L., Lansivaara T., Chi S.C. and Sun Y.J. (2007f), Minimization of factor of safety using different slip surface generation methods and an improved harmony search minimization algorithm, *Engineering Optimization* (accepted for publication).

Cheng Y.M., Lansivaara T. and Siu J. (2008a), Impact of convergence on slope stability analysis and design, *Computers and Geotechnics*, 35(1), 105–113.

Cheng Y.M., Liang L., Chi S.C. and Wei W.B. (2008b), Determination of the critical slip surface using artificial fish swarms algorithm, *Journal of Geotechnical and Geoenvironmental Engineering*, 134(2), 244–251.

Chowdhury R.N. (1987), *Slope Analysis*, New York: Elsevier.

Chun R.H. and Chameau J.L. (1982), Three-dimensional limit equilibrium analysis of slopes, *Geotechnique*, 32(1), 31–40.

Chugh A.K. (1986), Variable factor of safety in slope stability analysis. *Geotechnique*, 36, 57–64.

Civil Engineering Development Department (CEDD) (2005), *When Hillsides Collapse – A Century of Landslides in Hong Kong*, CEDD, Hong Kong SAR Government.

Clouterre (1991), Soil nailing recommendations 1991 for design, calculating, constructing and inspecting earth support system using soil nailing, *Recommendations Clouterre*.

Collin A. (1846), *Recherches Expérimentales sur les Glissements Spontanés des Terrains Argileux, accompagnées de Considerations sur Quelques Principes de la Méchanique Terrestre*. Carilian-Goeury and Dalmont, Paris.

Collins I.F. (1974), A note on the interpretation of Coulomb's analysis of the thrust on a rough retaining wall in terms of the limit theorems of limit plasticity, *Geotechnique*, 24, 106–108.

Cox A.D. (1962), Axially-symmetric plastic deformation in soils – II, Indentation of ponderable soils, *International Journal of Mechanical Sciences*, 4, 371–380.

Cundall P.A. and Strack O.D.L. (1979), A discrete numerical model for granular assemblies, *Geotechnique*, 29(1), 47–65.

David F.R. (2001), *An Introduction to NURBS: With Historical Perspective*, CA, USA: Morgan Kaufmann Publishers.

Dawson E.M., Roth W.H. and Drescher A. (1999), Slope stability analysis by strength reduction. *Geotechnique*, 49(6), 835–840.

Dawson E., Motamed F., Nesarajah S. and Roth W. (2000), *Geotechnical Stability Analysis by Strength Reduction. Slope Stability 2000*, Proceedings of Sessions of Geo-Denver 2000, August 5–8, 2000, Denver, Colorado, pp. 99–113.

De Josseline De Jong G. (1980), Application of calculus of variation to the vertical cut-off in cohesive frictionless soil, *Geotechnique*, 30(1), 1–16.

De Josseline De Jong G. (1981), Variational fallacy, *Geotechnique*, 31(4), 289–290.

Department of the Navy (1982), *Design Manual 7*, NAVFAC DM, USA.

Desai C.S. (1977), Drawdown analysis of slopes by numerical method, *Journal of the Geotechnical Engineering Division*, *ASCE*, 98(11), 1143–1162.

Dolan C.W. (1993), FRP development in the United States, in: A. Nanni (ed.), *Fiber-Reinforced Plastic (FRP) Reinforcement for Concrete Structures: Properties and Applications*, pp. 129–163, Amsterdam, the Netherlands: Elsevier.

Donald I. and Chen Z.Y. (1997), Slope stability analysis by the upper bound approach: fundamentals and methods, *Canadian Geotechnical Journal*, 34(6), 853–862.

Donald I.B. and Giam S.K. (1988), *Application of the Nodal Displacement Method to Slope Stability Analysis*, Proceedings of the 5th Australia–New Zealand Conference on Geomechanics, Sydney, Australia, pp. 456–460.

Dorigo M. (1992), Optimization, learning and natural algorithms, PhD thesis, Department of Electronics, Politecnico di Milano, Italy.

Dowling N.E. (1999), *Mechanical Behavior of Materials: Engineering Methods for Deformation, Fracture and Fatigue*, 2nd edition, Upper Saddle River, NJ: Prentice-Hall.

Drescher A. and Christopoulos C. (1988), Limit analysis slope stability with non-linear yield condition, *International Journal for Numerical and Analytical Methods in Geomechanics*, 12(3), 341–345.

Drescher A. and Detournay E. (1993), Limit load in translational failure mechanisms for associative and non-associative materials. *Geotechnique*, 43(3), 443–456.

Drucker D.C. and Prager W. (1952), Soil mechanics and plastic analysis or limit design, *Quarterly of Applied Mathematics*, 10, 157–165.

Drucker, D.C., Greenberg, W. and Prager, W. (1951), The safety factor of an elastic plastic body in plane strain, *Transactions of the ASME, Journal of Applied Mechanics*, 73, 371.

Duncan J.M. (1996), State of the art: Limit equilibrium and finite element analysis of slopes, *Journal of Geotechnical Engineering*, *ASCE*, 122(7), 577–596.

Duncan J.M. and Wright S.G. (2005), *Soil Strength and Slope Stability*, Hoboken, NJ: John Wiley.

Elias V. and Juran I. (1991), *Soil Nailing for Stabilization of Highway Slopes and Excavations*, FHWA-RD-89-198, United States Federal Highway Administration.

Espinoza R.D. and Bourdeau P.L. (1994), Unified formulation for analysis of slopes with general slip surface, *Journal of Geotechnical Engineering*, *ASCE*, 120(7), 1185–1204.

Fan K., Fredlund D.G. and Wilson G.W. (1986), An interslice force function for limit equilibrium slope stability analysis, *Canadian Geotechnical Journal*, 23(3), 287–296.

Farzaneh O. and Askari F. (2003), Three-dimensional analysis of nonhomogeneous slopes, *Journal of Geotechnical and Geoenvironmental Engineering*, 129(2), 137–145.

Fellenius W. (1918), Kaj-och jordrasen i Goteborg, *Teknisk Tidskrift V.U.*, 48, 17–19.

Fellenius W. (1927), *Erdstatische Berechnungen mit Reibung und Kohasion* (in German), Berlin: Ernst.

Fellenius W. (1936), Calculation of the stability of earth dams, *Transactions of the 2nd Congress on Large Dams*, *International Commission on Large Dams of the World Power Conference*, 4, 445–462.

Feng S.R., Feng D.X., Ge X.R. and Gu X.R. (1999), 3D limit equilibrium method for slope stability and its application, *Chinese Journal of Geotechnical Engineering* (in Chinese), 21(6), 657–661.

Feng Z.Q., Joli P. and Seguy N. (2004), FER/Mech – a software with interactive graphics for dynamic analysis of multibody system, *Advances in Engineering Software*, 35(1), 1–8.

Fisher R.A. and Yates F. (1963), *Statistical Tables for Biological, Agricultural and Medical Reasearch, 6th edition*, Edinburgh: Oliver and Boyd.

Fredlund D.G. and Krahn J. (1977), Comparison of slope stability methods of analysis, *Canadian Geotechnical Journal*, 14(3), 429–439.

Fredlund D.G. and Krahn J. (1984), Analytical methods for slope analysis, *International Symposium on Landslides*, pp. 229–250.

Fredlund D.G., Zhang Z.M. and Lam L. (1992), Effect of axis on moment equilibrium in slope stability analysis, *Canadian Geotechnical Journal*, 29(3), 456–465.

Frohlich O.K. (1953), *The Factor of Safety with Respect to Sliding of a Mass of Soil Along the Arc of a Logarithmic Spiral*, Proceedings of the 3rd International Conference on Soil Mechanics and Foundation Engineering, Switzerland, Vol. 2, pp. 230–233.

Frydman S. and Beasley D.H. (1976), Centrifugal modeling of riverbank failure, *Journal of the Geotechnical Engineering Division*, Proceedings of the American Society of Civil Engineers, 102, 395–409.

Geem Z.W. (2006), Optimal cost design of water distribution networks using harmony search, *Engineering Optimization*, 38, 259–280.

Geem Z.W., Kim J.H. and Loganathan G.V. (2001), A new heuristic optimization algorithm: Harmony search, *Simulation*, 76(2), 60–68.

Geotechnical Engineering Office (1977), *Report on the Slope Failures at Sau Mau Ping*, August, Hong Kong Government.

Geotechnical Engineering Office (1984), *Geotechnical Manual of Slopes, Hong Kong Government*, the HKSAR Government.

Geotechnical Engineering Office (1994), *Report on the Kwun Lung Lau Landslide of 23 July 1994*, the HKSAR Government.

Geotechnical Engineering Office (1996a), *Report on the Fei Tsui Road Landslide of 13 August 1995*, the HKSAR Government.

Geotechnical Engineering Office (1996b), *Report on the Shum Wan Road Landslide of 13 August 1995*, the HKSAR Government.

Geotechnical Engineering Office (1996c), *GEO Report No. 52: Investigation of Some Major Slope Failures between 1992 and 1995*, the HKSAR Government.

Geotechnical Engineering Office (1998), *GEO Report No. 78: Report on the Ching Cheung Road Landslide of 3 August 1997*, the HKSAR Government.

Geotechnical Engineering Office (2007), *GEO Publication No. 1/2007 – Engineering Geological Practice in Hong Kong*, the HKSAR Government.

Glover F. (1989), Tabu search – Part I, *ORSA Journal on Computing*, 1(3), 190–206.

Glover F. (1990), Tabu search – Part II, *ORSA Journal on Computing*, 2(1), 4–32.

Goh A.T.C. (1999), Genetic algorithm search for critical slip surface in multiple-wedge stability analysis, *Canadian Geotechnical Journal*, 36(2), 382–391.

Graham J. (1984), *Slope Instability*, John Wiley & Sons.

Greco V.R. (1996), Efficient Monte Carlo technique for locating critical slip surface, *Journal of Geotechnical Engineering*, *ASCE*, 122, 517–525.

Greenwood J.R. (1987), *Effective Stress Stability Analysis*. Discussion in 9th European Conference on Soil Mechanics and Foundations, Dublin, September 1987, Vol. 3, Post Conference Proceedings, Balkema, 1989, pp. 1082–1108.

Griffiths D.V. and Lane P.A. (1999), Slope stability analysis by finite elements, *Geotechnique*, 49(3), 387–403.

Haefeli R. (1948), *The Stability of Slopes Acted Upon by Parallel Seepage*, Proceedings of the Second International Conference on Soil Mechanics and Foundation Engineering, Rotterdam, Vol. 1, pp. 57–62.

Hoek E. and Bray J.W. (1977), *Rock Slope Engineering*, 2nd edition, London: The Institute of Mining and Metallurgy.

Holland John H. (1975), *Adaptation in Natural and Artificial Systems*, Ann Arbor: University of Michigan Press.

Hong Kong Government (1972), *Final Report of the Commission of Enquiry into the Rainstorm Disasters.*

Hong Kong Government (1977), *Report on the Slope Failures at Sau Mau Ping, August*, Hong Kong Government Printer.

Hovland H.J. (1977), Three-dimensional slope stability analysis method, *Journal of the Geotechnical Engineering Division*, *ASCE*, 103(GT9), 971–986.

Huang C.C. and Tsai C.C. (2000), New method for 3D and asymmetrical slope stability analysis, *Journal of Geotechnical and Geoenvironmental Engineering*, *ASCE*, 126(10), 917–927.

Huang C.C., Tsai C.C. and Chen Y.H. (2002), Generalized method for three-dimensional slope stability analysis, *Journal of Geotechnical and Geoenvironmental Engineering*, *ASCE*, 128(10), 836–848.

Hungr O. (1987), An extension of Bishop's simplified method of slope stability analysis to three dimensions, *Geotechnique*, 37(1), 113–117.

Hungr O. (1994), A general limit equilibrium model for three-dimensional slope stability analysis: Discussion, *Canadian Geotechnical Journal*, 31(5), 793–795.

Hungr O. (1997), Slope stability analysis, keynote paper, *Proceedings of 2nd Pan American Symposium on Landslides*, Rio de Janeiro, International Society for Soil Mechanics and Geotechnical Engineering, 3, 123–136.

Hungr O., Salgado F.M. and Byrne P.M. (1989), Evaluation of a three-dimensional method of slope stability analysis, *Canadian Geotechnical Journal*, 26(4), 679–686.

Izbicki R.J. (1981), Limit plasticity approach to slope stability problems, *Journal of the Geotechnical Engineering Division*, Proceedings of the American Society of Civil Engineers, 107, 228–233.

Janbu N. (1973), Slope stability computations, in: R.C. Hirschfield and S.J. Poulos (eds.), *Embankment-Dam Engineering*, pp. 47–86, John Wiley.

Janbu N., Bjerrum L. and Kjaernsli B. (1956), *Soil Mechanics Applied to Some Engineering Problems*, Norwegian Geotechnical Institute, Publ. No. 16.

Jiang J.C. and Yamagami T. (1999), *Determination of the Sliding Direction in Three-Dimensional Slope Stability Analysis*, Proceedings of 44th Symposium on Geotechnical Engineering, pp. 193–200.

Jiao J.J., Ding G.P. and Leung C.M. (2006), Confined groundwater near the rockhead in igneous rocks in the Mid-Levels area, Hong Kong, China, *Engineering Geology*, 84(3–4), 207–219.

Karel K. (1977a), Application of energy method, *Journal of the Geotechnical Engineering Division*, Proceedings of the American Society of Civil Engineers, 103, 381–397.

Karel K. (1977b), Energy method for soil stability analyses, *Journal of the Geotechnical Engineering Division*, Proceedings of the American Society of Civil Engineers, 103, 431–445.

Kawai T. (1977), New discrete structural models and generalization of the method of limit analysis, in: P.G. Bergan *et al.* (eds.), *Finite Elements in Nonlinear Mechanics*, pp. 885–906, Trondheim: NIT.

Kennedy J. and Eberhart R. (1995), *Particle Swarm Optimization*, Proceedings of the IEEE International Conference on Neural Networks, Perth, Australia, pp. 1942–1948.

Kim J., Salgado R. and Yu H.S. (1999), Limit analysis of soil slopes subjected to pore-water pressures, *Journal of Geotechnical Engineering*, *ASCE*, 125(1), 49–58.

King G.J.W. (1989), Revision of effective stress method of slices, *Geotechnique*, 39(3), 497–502.

Kirkpatrick S., Gelatt Jr. C.D. and Vecchi M.P. (1983), Optimization by simulated annealing, *Science*, *220*, 671–680.

Krahn J. (2003), The 2001 R.M. Hardy Lecture: The limits of limit equilibrium analyses, *Canadian Geotechnical Journal*, 40(3), 643–660.

Kwong J.S.M. (1991), *Shaft Stability*, PhD thesis, King's College London.

Lam L. and Fredlund D.G. (1993), A general limit equilibrium model for three-dimensional slope stability analysis, *Canadian Geotechnical Journal*, 30(6), 905–919.

Lam L. and Fredlund D.G. (1994), A general limit equilibrium model for three-dimensional slope stability analysis: Reply, *Canadian Geotechnical Journal*, 31(5), 795–796.

Lam L., Fredlund D.G. and Barbour S.L. (1987), Transient seepage model for saturated–unsaturated soil systems: A geotechnical engineering approach, *Canadian Geotechnical Journal*, 24(4), 565–580.

Lau J.C.W. and Lau C.K. (1998), *Risk Management in Design-and-Build in Foundation Works*, Half-day Seminar on Foundation Design and Construction in Difficult Ground, jointly organized by the Building and Geotechnical Divisions, HKIE, 20 February.

Law K.T. and Lumb P. (1978), A limit equilibrium analysis of progressive failure in the stability of slopes. *Canadian Geotechnical Journal*, 15(1), 113–122.

Lee K.S. and Geem Z.W. (2005), A new meta-heuristic algorithm for continuous engineering optimization: Harmony search theory and practice, *Computer Methods in Applied Mechanics and Engineering*, 194, 3902–3933.

Les P. and Wayne T. (1997), *The NURBS Book*, 2nd edition, Springer Verlag.

Leshchinsky D. and Huang C.C. (1992), Generalized three-dimensional slope stability analysis, *Journal of Geotechnical Engineering*, *ASCE*, 118, 1559–1576.

Leshchinsky D., Baker R. and Silver M.L. (1985), Three-dimensional analysis of slope stability, *International Journal for Numerical and Analytical Methods in Geomechanics*, 9(3), 199–223.

Li K.S. and White W. (1986), *Rapid Evaluation of the Critical Slip Surface in Slope Stability Analysis, Report No. 9*, University College, Australian Defence Force Army, University of New South Wales.

Li L., Chi S.C. and Lin G. (2005), The genetic algorithm incorporating harmony procedure and its application to the search for the non-circular critical slip surface for soil slopes, *Journal of Hydraulic Engineering*, 36, 913–918 (in Chinese).

Li X.L., Shao Z.J. and Qian J.X. (2002), An optimization method based on autonomous: Fish swarm algorithm, *Theories and Practice of Systems Engineering*, pp. 32–37.

Low B.K., Gilbert R.B. and Wright S.G. (1998), Slope reliability analysis using generalized method of slices, *Journal of Geotechnical and Geoenvironmental Engineering*, 124(4), 350–362.

Lowe J. and Karafiath L. (1960), *Stability of Earth Dams Upon Drawdown*, Proceedings of the 1st Pan-American Conference on Soil Mechanics and Foundation Engineering, Mexico City, Vol. 2, pp. 537–552.

Lyamin A.V. (1999), Three-dimensional lower bound limit analysis using nonlinear programming, PhD thesis, Department of Civil, Surveying and Environmental Engineering, University of Newcastle, Australia.

Lyamin A.V. and Sloan S.W. (1997), A comparison of linear and nonlinear programming formulations for lower bound limit analysis, in: S. Pietruszczak and G.N. Pande (eds.), *Proceedings of the 6th International Symposium on Numerical Models in Geomechanics*, pp. 367–373, Balkema, Rotterdam.

Lyamin A.V. and Sloan S.W. (2002a), Lower bound limit analysis using nonlinear programming, *International Journal for Numerical Methods in Engineering*, 55(5), 573–611.

Lyamin A.V. and Sloan S.W. (2002b), Upper bound limit analysis using linear finite elements and non-linear programming, *International Journal for Numerical and Analytical Methods in Geomechanics*, 26(2), 181–216.

Lysmer J. (1970), Limit analysis of plane problems in soil mechanics, *Journal of the Soil Mechanics and Foundations Division*, Proceedings of the American Society of Civil Engineering, 96, 1311–1334.

Malkawi A.I.H, Hassan W.F. and Sarma S.K. (2001), Global search method for locating general slip surface using Monte Carlo techniques, *Journal of Geotechnical and Geoenvironmental Engineering*, 127, 688–698.

Martin R.P. (2000), Geological input to slope engineering in Hong Kong, *Engineering Geology HK*, November, IMM (HK Branch), 117–138.

Matsui T. and San K.C. (1992), Finite element slope stability analysis by shear strength reduction technique, *Soils and Foundations*, 32(1), 59–70.

Mencl V. (1966), Mechanics of landslides with non-circular slip surfaces with special reference to the Vaiont slide, *Geotechnique*, 16(4), 329–337.

Michalowski R.L. (1989), Three-dimensional analysis of locally loaded slopes, *Geotechnique*, 39(1), 27–38.

Michalowski R.L. (1995), Slope stability analysis: A kinematical approach, *Geotechnique*, 45(2), 283–293.

Miller T.W. and Hamilton J.H. (1989), A new analysis procedure to explain a slope failure at the Martin Lake mine, *Geotechnique*, 39(1), 107–123.

Morgenstern N.R. (1992), The Evaluation of Slope Stability – A 25-Year Perspective, Stability and Performance of Slopes and Embankments – II, *Geotechnical Special Publication No. 31*, *ASCE*.

Morgenstern N.R. and Price V.E. (1965), The analysis of stability of general slip surface, *Geotechnique*, 15(1), 79–93.

Morrison I.M. and Greenwood J.R. (1989), Assumptions in simplified slope stability analysis by the method of slices, *Geotechnique*, 39(3), 503–509.

Mroz Z. and Drescher A. (1969), Limit plasticity approach to some cases of flow of bulk solids, *Journal of Engineering for Industry*, *Transactions of the American Society of Mechanical Engineers*, 51, 357–364.

Nash D. (1987), A comparative review of limit equilibrium methods of stability analysis, in: M.G. Anderson and K.S. Richards (eds.), *Slope Stability*, pp. 11–75, New York: John Wiley & Sons.

Naylor D.J. (1982), Finite elements and slope stability, in: *Numerical Methods in Geomechanics, Proceedings of the NATO Advanced Study Institute*, Lisbon, Portugal, 1981, pp. 229–244.

Nguyen V.U. (1985), Determination of critical slope failure surfaces, *Journal of Geotechnical Engineering*, *ASCE*, 111(2), 238–250.

Otten R.H.J.M. and Ginneken L.P.P.P. (1989), *The Annealing Algorithm*, Boston: Kluwer Academic Publishers.

Ourique C.O., Biscaia E.C. and Pinto J.C. (2002), The use of particle swarm optimization for dynamical analysis in chemical processes, *Computers and Chemical Engineering*, 26(12), 1783–1793.

Pan Jiazheng (1980), *Analysis of Stability and Landslide for Structures*, Hydraulic Press, Beijing, pp. 25–28 (in Chinese).

Petterson K.E. (1955), The early history of circular sliding surfaces, *Geotechnique*, 5, 275–296.

Pham D.T. and Karaboga D. (2000), *Intelligent Optimisation Techniques*, Germany: Springer Verlag.

Pham H.T.V. and Fredlund D.G. (2003), The application of dynamic programming to slope stability analysis, *Canadian Geotechnical Journal*, 40(4), 830–847.

Pun W.K. and Yeo K.C. (1995), *Report on the Investigation of the 23 July and 7 August 1994 Landslides at Milestone 14½ Castle Peak Road*, GEO Report No. 52, Geotechnical Engineering Office, Hong Kong, pp. 83–97.

Pun W.K. and Shiu Y.K. (2007), Design Practice and Technical Developments of Soil Nailing in Hong Kong, *HKIE Geotechnical Division Annual Seminar*, pp. 192–212.

Qian L.X. and Zhang X. (1995), Rigid finite element method and its applications in engineering, *Acta Mechanica Sinica* (English edition), 11(1), 44–50.

Rao S.S. (1996), *Engineering Optimization*, 3rd edition, New York: John Wiley.

Revilla J. and Castillo E. (1977), The calculus of variations applied to stability of slopes, *Geotechnique*, 27, 1–11.

Ruegger R. and Flum D. (2001), *Slope Stabilization with High-performance Steel Wire Meshes in Combination with Nails and Anchors*, International Symposium, Earth Reinforcement, IS Kyushu, Fukuoka, Japan, November, pp. 14–16.

Saeterbo Glamen M.G., Nordal S. and Emdal A. (2004), Slope stability evaluations using the finite element method, NGM 2004, XIV Nordic Geotechnical Meeting. Vol. 1, pp. A49–A61.

Sait S.M. and Youssef H. (1999), *Iterative Computer Algorithms with Applications in Engineering*, CA: IEEE Computer Society.

Salman A., Ahmad I. and Madani S.A. (2002), Particle swarm optimization for task assignment problem, *Microprocessors and Microsystems*, 26, 363–371.

Sarma S.K. (1973), Stability analysis of embankments and slopes, *Geotechnique* 23(3), 423–433.

Sarma S.K. (1979), Stability analysis of embankments and slopes, *Journal of the Soil Mechanics and Foundations Division*, 105(GT12), 1511–1522.

Sarma S.K. (1987), A note on the stability of slopes, *Geotechnique*, 37(1), 107–111.

Sarma S.K. and Tan D. (2006), Determination of critical slip surface in slope analysis, *Geotechnique*, 56(8), 539–550.

Seed H.B. and Sultan H.A. (1967), Stability analysis for a sloping core embankment, *Journal of the Soil Mechanics and Foundations Division*, 93, 69–83.

Shi G.H. (1996), *Manifold Method*, Proceedings of 1st International Forum on DDA and Simulations of Discontinuous Media, Berkeley, CA, USA, pp. 52–204.

Shield R.T. (1955), On the plastic flow of metals under conditions of axial symmetry, *Proceedings of the Royal Society of London Series A*, 233, 267–287.

Shiu Y.K. and Cheung W.M. (2003), *Long-Term Durability of Steel Soil Nails*, GEO Report No. 135, Geotechnical Engineering Office, Civil Engineering and Development Department, the Government of Hong Kong Special Administrative Region, China.

Shukha R. and Baker R. (2003), Mesh geometry effects on slope stability calculation by FLAC strength reduction method – linear and non-linear failure criteria, 3rd International Conference on FLAC and Numerical Modeling in Geomechanics, Sudbury, Ontario, Canada, 109–116.

Sloan S.W. (1988a), Lower bound limit analysis using finite elements and linear programming. *International Journal for Numerical and Analytical Methods in Geomechanics*, 12(1), 61–77.

Sloan S.W. (1988b), A steepest edge active set algorithm for solving sparse linear programming problem, *International Journal for Numerical Methods in Engineering*, 26(12), 2671–2685.

Sloan S.W. (1989), Upper bound limit analysis using finite elements and linear programming, *International Journal for Numerical and Analytical Methods in Geomechanics*, 13(3), 263–282.

Sloan S.W. and Kleeman P.W. (1995), Upper bound limit analysis using discontinuous velocity fields, *Computer Methods in Applied Mechanics and Engineering*, 127(1–4), 293–314.

Slope 2000, *User Guide*, 2007, http://www.cse.polyu.edu.hk/~ceymcheng/

Sokolovskii V.V. (1960), *Statics of Soil Media* (translated by D.H. Jones and A.N. Scholfield), London: Butterworths Scientific.

Song E. (1997), Finite element analysis of safety factor for soil structures, *Chinese Journal of Geotechnical Engineering*, 19(2), 1–7 (in Chinese).

Spencer E. (1967), A method of analysis of the stability of embankments assuming parallel inter-slice forces, *Geotechnique*, 17, 11–26.

Sridevi B. and Deep K. (1991), Application of global optimization technique to slope stability analysis, *Proceedings of 6th International Symposium on Landslides*, 573–578.

Stark T.D. and Eid H.T. (1998), Performance of three-dimensional slope stability methods in practice, *Journal of Geotechnical and Geoenvironmental Engineering, ASCE*, 124(11), 1049–1060.

Taylor D.W. (1937), Stability of earth slopes, *Journal of the Boston Society of Civil Engineers*, 24, 197–246.

Taylor D.W. (1948), *Fundamentals of Soil Mechanics*, New York: John Wiley.

Thomaz J.E. and Lovell C.W. (1988), *Three-dimensional Slope Stability Analysis with Random Generation of Surfaces*, Proceedings of the 5th International Symposium on Landslides, Vol. 1, pp. 777–781.

Ting Z. and Donald I.B. (1994), *Safety Factor Evaluation Difficulties in Multi-Wedge Slope Stability Analysis*, International Conference on Computational Methods in Structural and Geotechnical Engineering, Hong Kong.

Ugai K. (1985), Three-dimensional stability analysis of vertical cohesive slopes, *Soils and Foundations*, 25, 41–48.

Ugai K. (1988), *3-D Slope Stability Analysis by Slice Methods*, Proceedings of the 6th International Conference on Numerical Methods in Geomechanics, Innsbruck, Austria, pp. 1369–1374.

Ugai K. and Leshchinsky D. (1995), Three-dimensional limit equilibrium and finite element analysis: a comparison of results. *Soils and Foundations*, 35(4), 1–7.

Wang Y.J. (2001), Stability analysis of slopes and footings considering different dilation angles of geomaterial. Ph.D. thesis, Department of Civil and Structural Engineering, Hong Kong Polytechnic University.

Watkins A.T. and Powell G.E. (1992), Soil nailing to existing slopes as landslip preventive works, *Hong Kong Engineer*, 20(3), 20–27.

Wei W.B., Cheng Y.M. and Li L. (under review), Three-dimensional slope failure by strength reduction and limit equilibrium methods, *Computers and Geotechnics*.

Whitman R.V. and Bailey W.A. (1967), Use of computers for slope stability analyses, *Journal of the Soil Mechanics and Foundation Division, ASCE*, 93(4), 475–498.

Wong H.N. (2001), *Recent Advances in Slope Engineering in Hong Kong*, Proceedings of the 14th Southeast Asian Geotechnical Conference, Hong Kong, Vol. 1, pp. 641–659.

Xing Z. (1988), Three-dimensional stability analysis of concave slopes in plan view, *Journal of Geotechnical Engineering, ASCE*, 114(6), 658–671.

Yamagami T. and Ueta Y. (1988), Search for noncircular slip surfaces by the Morgenstern–Price method, *Proceedings of the 6th International Conference on Numerical Methods in Geomechanics*, pp. 1219–1223.

Yamagami T. and Jiang J.C. (1996), *Determination of the Sliding Direction in Three-Dimensional Slope Stability Analysis*, Proceedings of the 2nd International Conference on Soft Soil Engineering, Vol. 1, pp. 567–572, Nanjing, May.

Yamagami T. and Jiang J.C. (1997), A search for the critical slip surface in three-dimensional slope stability analysis, *Soils and Foundations*, 37(3), 1–16.

Yeung A.T., Cheng Y.M., Lau C.K., Mak L.M., Yu R.S.M., Choi Y.K. and Kim J.H. (2005), An innovative Korean system of pressure-grouted soil nailing as a slope stabilization measure, HKIE Geotechnical Division, 25th Annual Seminar, 4 May, pp. 43–49.

Yeung A.T., Cheng Y.M., Tham L.G., Au A.S.K., So S.T.C. and Choi Y.K. (2007), Field evaluation of a glass-fiber soil reinforcement system, *Journal of Performance of Constructed Facilities, ASCE*, 21(1), 26–34.

Yin J.H., Ding X.L., Yang Y.W., Lau C.K., Huang D.F. and Chen Y.Q. (2002), *An Integrated System for Slope Monitoring and Warning in Hong Kong*, Proceedings of Advanced Building Technology 2002, 4–6 December, Hong Kong.

Yin P.Y. (2004), A discrete particle swarm algorithm for optimal polygonal approximation of digital curves, *Journal of Visual Communication and Image Representation*, 15(2), 241–260.

Yu H.S., Sloan S.W. and Kleeman P.W. (1994), A quadratic element for upper bound limit analysis, *Engineering Computations*, 11, 195–212.

Yu H.S., Salgado R., Sloan S.W. and Kim J.M. (1998), Limit analysis versus limit equilibrium for slope stability, *Journal of Geotechnical and Geoenvironmental Engineering, ASCE*, 124(1), 1–11.

Zhang X. (1988), Three-dimensional stability analysis of concave slopes in plan view, *Journal of Geotechnical Engineering*, 114, 658–671.

Zhang X. (1999), Slope stability analysis based on the rigid finite element method, *Geotechnique*, 49(5), 585–593.

Zhang X.J. and Chen W.F. (1987), Stability analysis of slopes with general nonlinear failure criterion, *International Journal for Numerical and Analytical Methods in Geomechanics*, 11(1), 33–50.

Zhang X. and Qian L.X. (1993), Rigid finite element and limit analysis, *Acta Mechanica Sinica* (English Edition), 9(2), 156–162.

Zheng Y.R., Zhao S.Y., Kong W.X. and Deng C.J. (2005), Geotechnical engineering limit analysis using finite element method, *Rock and Soil Mechanics*, 26(1), 163–168.

Zhu D.Y., Lee C.F., Qian Q.H., Zou Z.S. and Sun F. (2001), A new procedure for computing the factor of safety using the Morgenstern–Price's method, *Canadian Geotechnical Journal*, 38(4), 882–888.

Zhu D.Y., Lee C.F., Qian Q.H. and Chen G.R. (2005), A concise algorithm for computing the factor of safety using the Morgenstern–Price method, *Canadian Geotechnical Journal*, 42(1), 272–278.

Zhuo J.S. and Zhang Q. (2000), *Interface Element Method for Discontinuous Mechanics Problems* (in Chinese), Beijing: Science Press.

Zienkiewicz O.C., Humpheson C. and Lewis R.W. (1975), Associated and non-associated visco-plasticity and plasticity in soil mechanics. *Geotechnique*, 25(4), 671–689.

Zolfaghari A.R., Heath A.C. and McCombie P.F. (2005), Simple genetic algorithm search for critical non-circular failure surface in slope stability analysis, *Computers and Geotechnics*, 32(3), 139–152.

Index